Evaluation, Local Calibration, and Validation of Performance Prediction Models in AASHTOWare^{TM} Pavement ME Design Software Using NCAT Test Track Data

by

Xiaolong Guo

A dissertation submitted to the Graduate Faculty of
Auburn University
in partial fulfillment of the
requirements for the Degree of
Doctor of Philosophy

Auburn, Alabama
May 6, 2017

Keywords: Pavement ME Design, Local Calibration, Input Level 1

Approved by

David H. Timm, Chair, Brasfield & Gorrie Professor
Randy West, Director of National Center for Asphalt Technology
Nam Tran, Associate Research Professor
Rod E. Turochy, Associate Professor of Civil Engineering

Abstract

The AASHTOWare^{TM} Pavement ME Design software was adopted by the American Association of State Highway and Transportation Officials (AASHTO) for structural pavement designs. The performance prediction models in the software were only calibrated based on a national database of pavement sections in the U.S. and Canada. These models may not apply to local pavement designs due to insufficient adequacy. The National Center for Asphalt Technology (NCAT), equipped with a full-scale accelerated pavement Test Track and asphalt materials laboratory, supported this study on evaluation, local calibration, and validation of the rutting, bottom-up fatigue cracking, and IRI models. The NCAT database was developed with research-grade detail and accuracy and was locally-based regarding the information of materials, traffic, and climate, and field performance. In the process of local calibration, automation was used during software runs and data compiling to minimize human interaction with the computer. Considerable labor savings (100% reduction) and time savings (nearly 35% reduction) were gained. As for evaluation results, over-predictions by the nationally-calibrated rutting and bottom-up fatigue cracking model were seen for a majority of experimental sections, and local calibration reduced bias and standard error of the estimate. The IRI prediction by the nationally-calibrated model was only accurate between 35 in./mile to 65 in./mile, and local calibration insignificantly improved the IRI prediction accuracy. The improvement of model accuracy was adequately validated for the locally-calibrated rutting and bottom-up fatigue cracking model, but not for the locally-calibrated IRI model, using independent local datasets. The recommended calibration coefficients should be evaluated based on a local database if they are intended for other design conditions. The automation method is recommended for future calibration studies since benefits in saving time and labor cost.

Acknowledgments

I would like to thank my academic advisor Dr. David H. Timm for his guidance on my Ph.D. program. His rigorousness, patience, and expectation motivated me to reach deeper and be more involved in the research of pavement engineering. I not only learned a wealth of knowledge and skills in the field of pavement design and asphalt technology, but also formed my habit of independent thinking and trained myself with professionalism, reasonability, and a sense of sympathy. It is his advice that strengthens my confidence to insist on the study until a completion of this program.

I would like to thank Dr. Randy West for taking the time to advise me about my work and participate as one of my committee members. I am also truly grateful to Dr. Nam Tran and Dr. Rod Turochy for their time and endeavor to guide and inspire my study. I would like to thank Dr. Daniela Marghitu for taking the time to serve as a university reader for my dissertation.

I am thankful to Dr. Robbins, Dr. Powell, Dr. Rodezno, Jason Nelson, Adam Taylor, and Dr. Heitzman for their assistance in carrying out research and experiments. I would like to thank Xiao Zhao, Zhenyu Wang, Hao Wu, Michael Vrtis, Bing Han, Wangyu Ma as well as other students of the civil engineering program here for their kind help in my life.

Finally, I would like to thank my parents for their selfless care and encouragement during my study. I would like to thank my relatives and friends in China for their support during my study.

Table of Contents

List of Figures

List of Tables

Chapter 1 Introduction

1.1 Background

Since the 1950's, structural pavement design has evolved to ensure appropriate and cost-effective solutions for building roads of the time. Advanced materials, new conditions of traffic loading, and ever-changing climate become convincing reasons to reexamine and improve pavement design. The modern design approach, mechanistic-empirical (M-E) design, has been adopted by AASHTO (AASHTO, 2004), and it has significant advantages over traditional approaches (i.e., empirically-based approaches) to account for recent changes in design needs. Now, the challenge exists in the implementation of M-E design approaches into practice.

As of July 2013, the AASHTOWare™ Pavement ME Design software became commercially available to the pavement design community. The commercialized version has replaced the Mechanistic-Empirical Pavement Design Guide (MEPDG) whose development began in 1998 with multiple beta versions available between 2004 and 2012. Although there are no significant changes in algorithms among software versions, the implementation of the software still calls for evaluation and local calibration of performance prediction models. The M-E approach mechanistically calculates pavement responses to loads, and then empirically relates responses to distress and ride quality by performance prediction models. These models have been only nationally-calibrated based on the Long Term Pavement Performance (LTPP) database (ARA, 2004), so they reflect a general and somewhat broad relationship between pavement responses and long-term performance. If these models are locally used for a pavement design, the most appropriate designs might not be delivered by the M-E approach. For example, the cost of pavement turns out to be more expensive than necessary (over-designed). The worse is that the service pavement shows failure sooner than the time that a design life warrants (under-designed), which would put road users into higher risks of traffic accidents. The latter is more serious in high speed roadways, and much likely associated with higher health care cost (Shen and Neyens, 2015).

Half of the U.S. states expect to implement an M-E approach within the next two years (Pierce and McGovern, 2014). Three states (i.e., Indiana, Oregon, and Missouri) have completed the implementation, and some have already obtained significant benefits. According to Indiana's experience (Nantung, 2010), a savings of $3,024,954 was successfully achieved for five completed projects. They mentioned that much-needed cost savings had been gained by using the M-E guide instead of the AASHTO 1993 method (Nantung, 2010). Recently, more and more state agencies have realized the necessity of M-E implementation. However, they yet need to evaluate and locally calibrate the performance prediction models. A big challenge was that the effectiveness of local calibration was limited by the database in term of many aspects of data, such as representativeness, the level of detail, availability and accuracy, and compatibility and consistency (Guo and Timm, 2016). The state agencies focus on sections mainly from LTPP or the state pavement management system (PMS) to conduct model evaluation, local calibration, and validation. Unfortunately, the sections from LTPP are representative of conventional pavements from earlier decades, which account little for recent technology innovations. The sections from PMS are known to have data issues regarding detail, consistency, and accuracy (Guo and Timm, 2016). Given the existing limitations of calibration data, a study using a database that has research-grade detail and accuracy is warranted for model evaluation, local calibration, and validation.

Moreover, local calibration is a time-consuming and labor-intensive process. Researchers often need to create reliable design project files, run design software simulations with varied calibration coefficients, and compile unordered data for analysis. A previous study (ARA, 2004) documented a task of 4,896 MEPDG runs, with each run taking 30 minutes. Guo and Timm (2015) executed more than 172 MEPDG runs in their preliminary investigation. To address these problems, pavement engineers sought ways for minimizing the human interaction with the design software. Fortunately, computer automation technology has been successfully adopted by a few (e.g., Schram and Abdelrahman, 2010; Jadoun and Kim, 2012; Guo, 2013) to facilitate software runs and data compiling.

A previous study by Guo and Timm (2015) performed a preliminary evaluation and local calibration on performance models with selected test sections from the NCAT Test Track. Though preliminary findings were achieved, the study results have not been very comprehensive due to a very limited number of investigated pavement sections. The purpose of this study is to use more test sections to conduct a comprehensive evaluation, local calibration, and validation of the performance models in the Pavement ME Design.

1.2 Objectives

Based on the discussion, there are four main objectives as follows:

1. Evaluate the accuracy of nationally-calibrated performance models in the AASHTOWare^{TM} ME software using the NCAT Test Track data.
2. Locally-calibrate the performance models to the Test Track condition.
3. Validate the locally-calibrated performance models using the NCAT Test Track data.
4. Develop an automation method to facilitate software runs and data compiling.

1.3 Scope of work

To meet the first three objectives, 31 asphalt pavement sections from the Test Track were investigated as experimental sections. These sections were built with a range of materials and technologies as selected by sponsoring state Departments of Transportation and corporations. Each section was subjected to two years of traffic loads (amounting to 10 million equivalent single axle loads (ESALs)) and weathering by the local environment. The performance of all these sections was monitored throughout the testing phase. The performance of the sections was predicted through simulations by the AASHTOWare^{TM} Pavement ME Design software. A large number of trial calibration coefficients were conducted to arrive at an optimal set of calibration coefficients that minimize the error between measured and predicted performance. To accomplish the fourth objective, an automation program named Automation Anywhere® was used to interact with the Pavement ME design software that greatly reduced the time and labor cost.

The dissertation is organized as follows: Chapter 2 covers a literature review to identify key topics for an M-E design calibration study and gather useful background information. Chapter 3 addresses the key topics for this study and explains the dataset and methodology adopted. Chapter 4 summarizes and discusses the results of the study. Chapter 5 introduces the concept of automation. Also included is an evaluation of time savings by automation against human maneuver. Considering that this dissertation is a follow-up study for the author's Master's thesis, Chapter 6 summarizes the comparison between the thesis and dissertation research. Chapter 7 presents conclusions and recommendations. Finally, references and appendixes are presented.

Chapter 2 Literature Review

To complete this study, relevant literature was reviewed and used as a reference. In this chapter, an overview of the AASHTOWare^{TM} Pavement ME design software is first provided. Next, the performance prediction models in the software are presented. Then, the recommended procedure for local calibration is introduced. Further, historical studies were reviewed, and recent relevant studies were carefully examined and compared. Useful information about the methodological framework and experimental methods are collected in this step. Lastly, studies that mention automation are reviewed and summarized.

2.1 Overview of the Pavement M-E Design software

The AASHTOWare^{TM} Pavement ME design is the current version of the M-E based software for a replacement of the MEPDG which was recommended by the AASHTO. It is delivered by the NCHRP 1-37A and NCHRP 1-40D projects as the companion software of the new guide for the M-E design and analysis. The AASHTOWare^{TM} software became commercialized in July 2013. Table 2.1 summarizes former versions of the AASHTOWare^{TM} software and the associated updates. The AASHTOWare^{TM} Pavement ME Design v2.0 was used in this study.

Table 2.1 Former versions of Pavement ME Design software

Software Name and Version	Release Date	Major Updates	Reference Materials
MEPDG v0.9	Beta-version	ESALs calculation, climate model (EICM), thermal cracking model, reliability	Documentation (Darter et al., 2006; Li et al., 2011)
MEPDG v1.0	April 2007	Not clearly listed	Documentation (AASHTO, 2008; Li et al., 2011)
MEPDG v1.1	September 2009	Portland Cement Concrete (PCC) pavement modules	Documentation (*Release Notes for MEPDG Version 1.1 – September 2009*)
Darwin ME	2011	Interface, running time, sensitivity, thickness optimization	Presentation (Clark, 2010)
AASHTOWare™ Pavement ME Design v1.0	July 2013	Educational version, fixing defects	Documentation (ARA, 2013)
AASHTOWare™ Pavement ME Design v2.0	January 2014	Bugs removal, user feature	Documentation (ARA, 2014)

The AASHTOWare™ Pavement ME Design v2.0 was the most updated version at the time when this study was conducted. Though many updates exist between these versions, the nature of the M-E approach (Figure 2.1) remained unaltered in these versions. "Mechanistic" refers to the application of the principles of engineering mechanics, which leads to a rational design process (ARA, 2004). "Empirical" refers to the characterization of material properties, traffic, environment, field performance data used to correlate to accumulated damage, or other inputs to the design process (ARA, 2004). The transfer function, namely performance prediction models, relates the theoretical computation of "damage" (which is a function of pavement deflection, strain, or stress responses) at some critical location with measured distress, completing the full mechanistic-empirical loop of the pavement design (ARA, 2004).

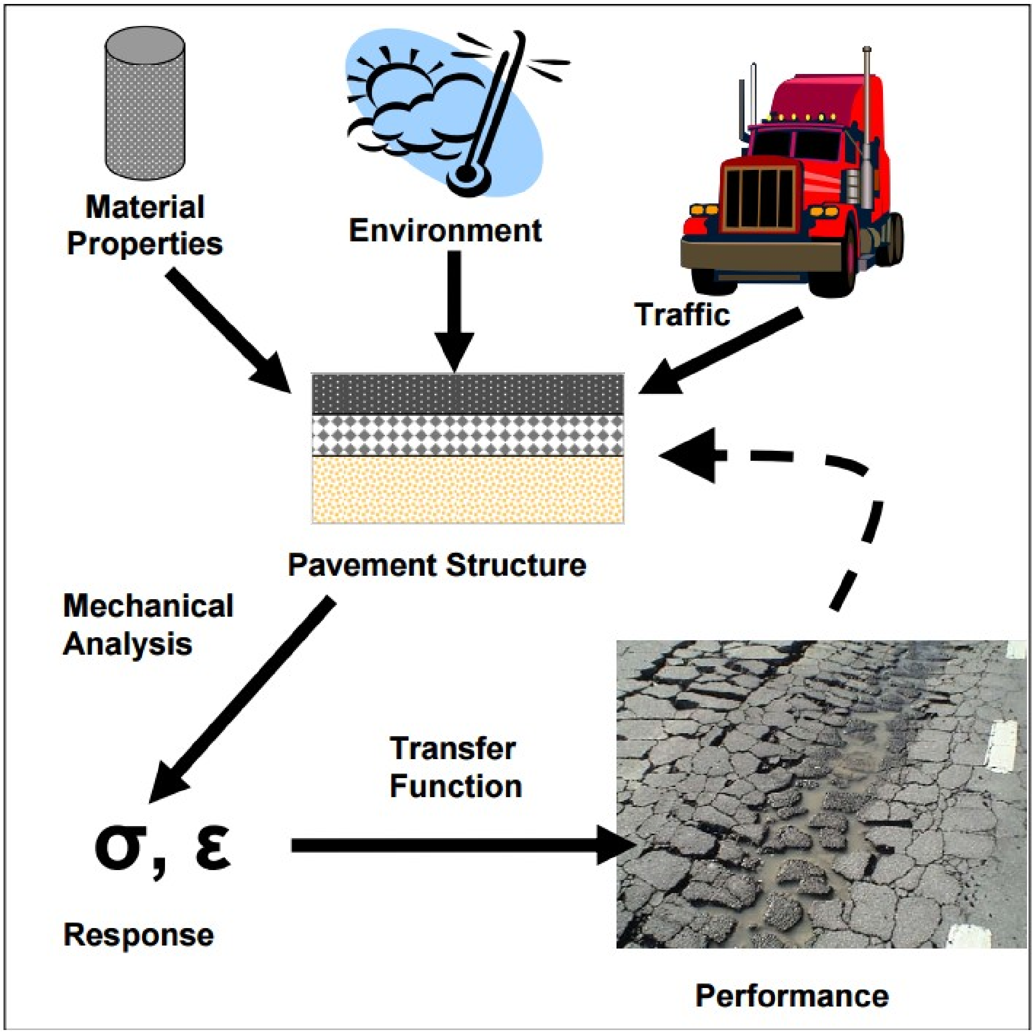

Figure 2.1 M-E design schematic (Priest and Timm, 2006)

The major advantages of the M-E approach are realistic input characterization and specific distress prediction, enabling users to set failure criteria and generate cost-effective structural designs. For the Pavement ME design software, inputs can be entered at one of three different levels: level 1 (i.e., measured directly, site- or project-specific), level 2 (i.e., estimated from correlations or regression equations), and level 3 (i.e., default values). On the other hand, a disadvantage of the approach is that additional data and analysis for the models is considered necessary including: conducting input sensitivity analyses, developing input libraries, locally calibrating transfer functions, and user training (Timm et al., 2014). As the MEPDG documentation (ARA, 2004) states, "Without calibration, the results of mechanistic calculations cannot be used to predict rutting, fatigue cracking, and thermal cracking with any degree of confidence."

2.2 Performance prediction models

Three performance prediction models (i.e., rutting, bottom-up fatigue cracking, and International Roughness Index (IRI) models) were investigated in this study since the corresponding distresses are prevalent at the Test Track. As mentioned in Chapter 1, these models were nationally-calibrated based on the LTPP database, revealing a general and somewhat broad relationship between pavement responses and long-term performance. They represent a national rather than region-specific perspective. ARA (2004) briefly mentioned that the input level for materials was at level 2 or 3 in the national calibration. Table 2.2 summarizes some statistical results for the national calibration of these models. The standard error of the estimate (SEE) is the standard deviation of the residual error between the model-predicted and field-measured values, which is a measure of model accuracy. The R^2 represents the proportion of total variation explained by the model, which is a measure of model efficiency.

TABLE 2.2 Statistical summary of national calibration results (Schwartz and Carvalho, 2007)

	Fatigue Cracking	Rutting			IRI
		Asphalt Concrete (AC)	base/ subbase	subgrade	
SEE	6.2%	0.055 in.	0.014 in.	0.056 in.	0.387 m/km
R^2	N/A	0.643	0.62	0.19	0.62
Number of LTPP Sections	82	88			>350

2.2.1 Rutting model

Rutting is a load-induced distress caused by vertical consolidation and/or plastic deformation often at moderate to high temperatures. Because rutting occurs in each layer of pavement structure, the rutting model accounted for rutting in both asphalt concrete (AC) layers and unbound materials (i.e., base and subgrade materials). For the AC layers, the rutting model was initially based on Leahy's model, modified by Ayres, and lastly by Kaloush (ARA, 2004).

To predict the AC rutting, the AC layer is subdivided into thinner sublayers in performance calculation. For each sublayer, the pavement response (e.g., vertical resilient strain ε_r) is computed by mechanistic model, and it is used to predict vertical plastic strain (i.e., ε_p) by equation (1). Then, the predicted rutting of the sublayer i can be derived by a product of vertical plastic strain and the sublayer i thickness. The predicted rutting of the entire AC layer can be achieved by summing up the rutting of each sublayer.

$$\frac{\varepsilon_p}{\varepsilon_r} = \beta_{r1} * 10^{-3.35412} * T^{1.5606*\beta_{r2}} * N^{0.4791*\beta_{r3}} \tag{1}$$

where:

β_{r1}, β_{r2}, β_{r3} = local calibration coefficients for AC rutting model (national values or defaults = 1)

ε_p = vertical permanent strain at mid-thickness of the sublayer i under a given load

ε_r = vertical resilient strain at mid-thickness of the sublayer i under a given load (derived from the Layered Elastic Analysis program, JULEA, which was the built in the AASHTOWare™ Pavement ME Design software (ARA, 2004))

T = AC temperature of sublayer i, °F

N = number of repetitions of a given magnitude of load

For unbound materials, the model was first derived by Tseng and Lytton, which was modified by Ayres and later by El-Basyouny and Witczak (ARA, 2004). The unbound material is divided into sublayers, and the rut depth of the material is the summation of rutting occurred in each of its sublayers. The rutting deformation (i.e., δ_i) appeared in a given sublayer is computed by equation (2) (ARA, 2004). In fact, the approach to predict rutting for the unbound materials is similar to the approach to predict rutting for the AC. The ratio $\varepsilon_0/\varepsilon_r$ in the unbound material model plays a similar role as the ratio in the AC rutting model. The exponential term is to account for effects of traffic loading and water on rutting. The right side of equation (2) is simply a product of model-fitting parameters (i.e., β_1 and k_1), a ratio $\varepsilon_0/\varepsilon_r$ adjusted by an exponential term, vertical resilient strain ε_v, and sub-layer thickness h_i.

$$\delta_i = \beta_1 * k_1 * (\frac{\varepsilon_0}{\varepsilon_r}) * e^{-(\frac{\rho}{N})^{\beta}} * \varepsilon_v * h_i \qquad (2)$$

where:

β_1 = local calibration coefficient for unbound materials rutting model, i.e. noted as β_b for granular base and β_s for subgrade (default = 1)

δ_i = rut deformation in the sublayer i, in.

k_1 = regression model coefficient (2.03 for base and 1.35 for subgrade as default)

$\varepsilon_r/\varepsilon_0$ = laboratory-determined or estimated based on the type of material investigated (granular or subgrade soil)

β, ρ = unbound material properties (dependent on water content)

N = number of load applications under a given magnitude of load

ε_v = vertical resilient strain of the sublayer i under a given load (derived from the program JULEA)

h_i = thickness of the sub-layer i, in.

2.2.2 Bottom-up fatigue cracking model

Fatigue cracking is another load-induced distress and caused by repetitive flexing of pavements. It usually initiates from the pavement surface or the bottom of the AC. The bottom-up fatigue cracking model accounts for fatigue cracking that initializes from the bottom of the AC and propagates to the road surface. The metric of cracking is the percentage of the cracked surface area over the total lane area, which is a commonly-used measure of cracking range. To predict this percentage, there are two steps in computation: fatigue accumulation and cracking conversion. When calculating fatigue accumulation, the allowable repetition number was first calculated based on the Asphalt Institute equation, which was derived by modifications to constant stress laboratory fatigue criteria (ARA, 2004). The equation was nationally calibrated to the following equation (3) (ARA, 2004). The fatigue accumulated at a given magnitude of load is equal to the ratio of an actual number of load repetitions to the allowable number of load repetitions. Then, the fatigue accumulated at different magnitudes of loads is summed up using the Miner's hypothesis (Equation (5)) for cracking conversion.

$$N_f = 0.00432 * C * \beta_{f_1} * \varepsilon_t^{-\beta_{f_2} * 3.9492} * E^{-\beta_{f_3} * 1.281} \tag{3}$$

where:

β_{f1}, β_{f2}, β_{f3} = local calibration coefficients for fatigue cracking model (national values or defaults = 1)

N_f = number of repetitions under a given magnitude of load to failure

ε_t = tensile strain at the critical location in the asphalt layer (derived from the JULEA program)

E = AC stiffness at a given temperature, psi

C = laboratory to field adjustment factor, $C = 10^M$

$$M = 4.84 * \left[\frac{V_{beff}}{V_a + V_{beff}} - 0.69 \right] \tag{4}$$

where:

V_{beff} = effective binder content, percent by volume

V_a = air voids, percent by volume

$$D = \sum \frac{n_k}{N_k} \tag{5}$$

Where:

D = accumulated damage, percent

n_k = actual number of load applications under a given magnitude of k

N_k = allowable number of load applications under a given magnitude of k

Once fatigue accumulation (i.e., D) is computed, it can be converted into the percentage of cracked area by the cracking conversion model (Equation (6)). The model, generated by determining the correlation between the amount of bottom-up fatigue cracking and damage, was nationally calibrated to the equation as follows (ARA, 2004):

$$FC = \left[\frac{C_4}{1 + e^{(C_1 * C_1' + C_2 * C_2' * \log(D))}} \right] * \left[\frac{1}{60} \right] \quad (6)$$

where:

FC = bottom-up fatigue cracking, percent

$$C_2' = -2.40874 - 39.748(1 + h_{AC})^{-2.856}$$

$$C_1' = -2 * C_2'$$

C_1, C_2 = local calibration coefficients for bottom-up cracking conversion model (national values or defaults = 1)

C_4 = local calibration coefficient for bottom-up cracking conversion model (default = 6000)

D = accumulated damage, percent

h_{AC} = total thickness of the AC layer, in.

2.2.3 IRI model

IRI is an index to represent surface roughness of the pavement. The IRI model was developed based on the assumption that IRI is related to various pavement surface distresses. The IRI model for new flexible pavement is shown below (Equation (7)). It can be seen that calibration coefficients relate rutting, fatigue cracking, transverse cracking, and site factors to the IRI prediction in a linear relationship (AASHTO, 2008).

$$IRI = IRI_0 + C_1 * RD + C_2 * FC_{total} + C_3 * TC + C_4 * SF \quad (7)$$

where:

IRI_0 = initial IRI value before traffic loading

C_1, C_2, C_3, C_4 = local calibration coefficients (national values or defaults: C_1=40, C_2=0.4, C_3=0.008, C_4=0.015)

RD = average rut depth, in.

FC_{total} = total area of load-related cracking (combined bottom-up, top-down, and reflection cracking in the wheel path), percent

TC = total length of transverse cracks, ft/mile

SF = site factor

2.3 Recommended local calibration procedures

As described in Chapter 1, evaluation, local calibration, and validation are necessary during the implementation of the M-E design approach. Evaluation is to examine the adequacy of the nationally-calibrated models in a local design scenario. Local calibration is required when the predicted results from the models poorly match the measured results. This calibration process (Figure 2.2) aims to eliminate the bias and residual error between the predicted results from the models and the measured results from the real world (AASHTO, 2010). Validation is to examine whether the locally-calibrated models correctly predict the performance of local pavements. The dataset used for validation should be different from the one for local calibration to keep the independence of validation.

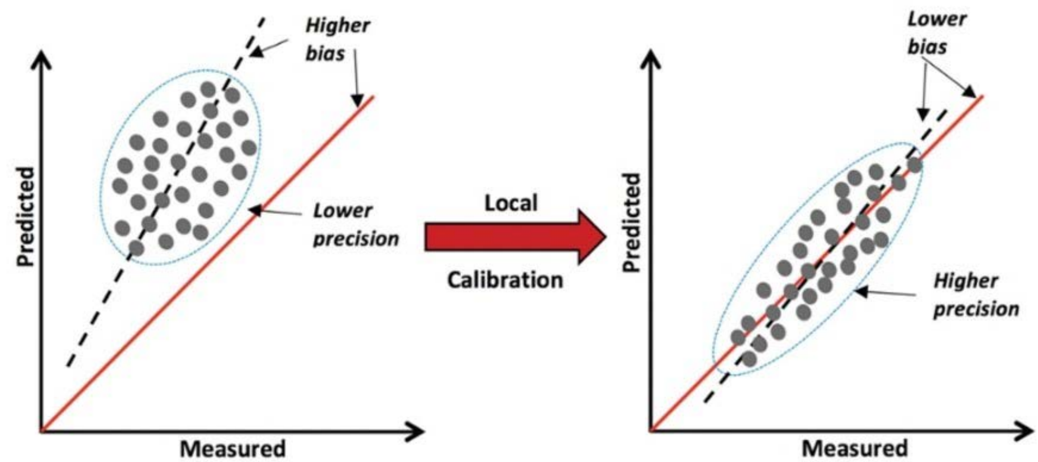

Figure 2.2 Reduction of bias and improvement of precision ("Summary of ME Design," 2016)

In the documentation (AASHTO, 2010), there is a systematic guidance for performing local calibration of the MEPDG. The flow chart of the procedure (Figure 2.3 and Figure 2.4) and steps suggested for local calibration are provided as follows. Eleven steps are needed for adapting the MEPDG to local conditions (AASHTO, 2010):

1. Select hierarchical input level for each input parameter

The step is to select hierarchical input level (either level 1, 2, and 3) for the inputs that are to be used in the Pavement ME design software for design and analysis. This step can be important because the input level can have a significant impact on the standard error of each distress prediction model (AASHTO, 2010). The selection of input level should be based on the typical practice by an agency for pavement design (AASHTO, 2010).

2. Develop local experimental plan and sampling template

This step is to develop an experimental plan or a sampling template to refine the calibration of the performance prediction models. The sampling template is a matrix developed based on local conditions, policies, and materials. Each cell of the matrix is assigned multiple pavement sections. This step is performed to evaluate the effect of pavement type, local conditions, and materials on reducing the bias and standard error term.

3. Estimate sample size for specific distress prediction models

This step is to estimate the sample size or number of pavement sections for the evaluation and local calibration. In each cell of the sampling template, the number of pavement sections (i.e., N) should be higher than a minimum that depends on the confidence interval (i.e., α) and tolerable bias (i.e., e_t) (AASHTO, 2010).

$$N \geq \left(\frac{Z_{\alpha/2} * S_y}{e_t}\right)^2 \tag{8}$$

where:

$Z_{\alpha/2}$ = a statistical term corresponding to the desired confidence level α

S_y = the standard deviation of the values of investigated variable “y”

4. Select roadway segments

This step is used to select pavement sections to obtain the most information and keep sampling and testing cost to a minimum. The selection of pavement sections can be performed for a specific distress or multiple distresses for efficiency. For Accelerated Pavement Testing (APT) facilities, the evaluation and calibration results are independent of climatic-related factors and time-dependent properties of the pavement materials (AASHTO, 2010). Therefore, fewer tests are needed to determine the effect of selected factors than non-APT facilities (AASHTO, 2010). Also, APT pavement sections should not be used to determine the standard error of the estimate since the use of APT will result in much lower standard errors of the estimate (AASHTO, 2010). This is because traffic and climate parameters are highly controlled, and time-dependent properties are excluded from these short-term loading conditions (AASHTO, 2010).

5. Extract and evaluate distress and project data

This step is to collect all data and identify any missing data elements that are needed to execute the AASHTOWare™ Pavement ME Design software (AASHTO, 2010). It is imperative to keep a consistent definition and measurement protocol of surface distress throughout the evaluation and calibration process (AASHTO, 2010). Also, it is important to check if the maximum measured distress values exceed the design criteria (or the trigger value) used by the agency. If not, the accuracy and bias of the prediction model may not be well evaluated at the values that trigger rehabilitation (AASHTO, 2010). Moreover, the measured distress data for all pavement sections should be evaluated and checked for anomalies and outliers – observations that have irrational trends in the distress data (AASHTO, 2010).

6. Conduct field and forensic investigations

This step is to develop a sampling and testing plan for materials properties for pavement sections and to perform forensic investigations (e.g., trenching or coring) for cracking types (i.e., top-down, bottom-up cracking, or others) or the assumption for layer rutting (AASHTO, 2010). The plan can have a significant impact on costs and time to conduct field investigation (AASHTO, 2010).

7. Assess local bias: validation of global calibration values to local conditions, policies, and materials

The validation of global calibration values (or evaluation of national calibration values) is to compare the predicted performance with the measured values. The bias and SEE should be determined for each distress prediction model (AASHTO, 2010). Also, the Student's t-test can be used to determine if there is a significant difference between the sets of predicted and measured distresses or IRI values (AASHTO, 2010). If there is no bias, the standard error of the estimate should be compared with the global calibration data set – proceed to Step 9.

8. Eliminate local bias of distress and IRI predictions models

This step is to eliminate the local bias. It requires adjusting the local calibration values (AASHTO, 2010). This step requires some runs or iterations of the Pavement ME design software.

9. Assess the standard error of the estimate

This step is to compare the local SEE with that from the global (or national) data set. If the difference between SEEs is small, the local calibration coefficients can be used for pavement design – proceed to Step 11.

10. Reduce standard error of the estimate

This step is to further eliminate the SEE. This step can be complicated and will probably require external revisions to the local calibration coefficients (AASHTO, 2010). This step also requires some runs or iterations of the Pavement ME design software.

11. Interpretation of results, deciding on adequacy of calibration parameters

This step is to evaluate the SEEs for distress and IRI models to determine their impact on the resulting designs at different reliability levels (AASHTO, 2010). An agency should review the expected pavement/rehabilitation design life within each cell of the sampling template (AASHTO, 2010).

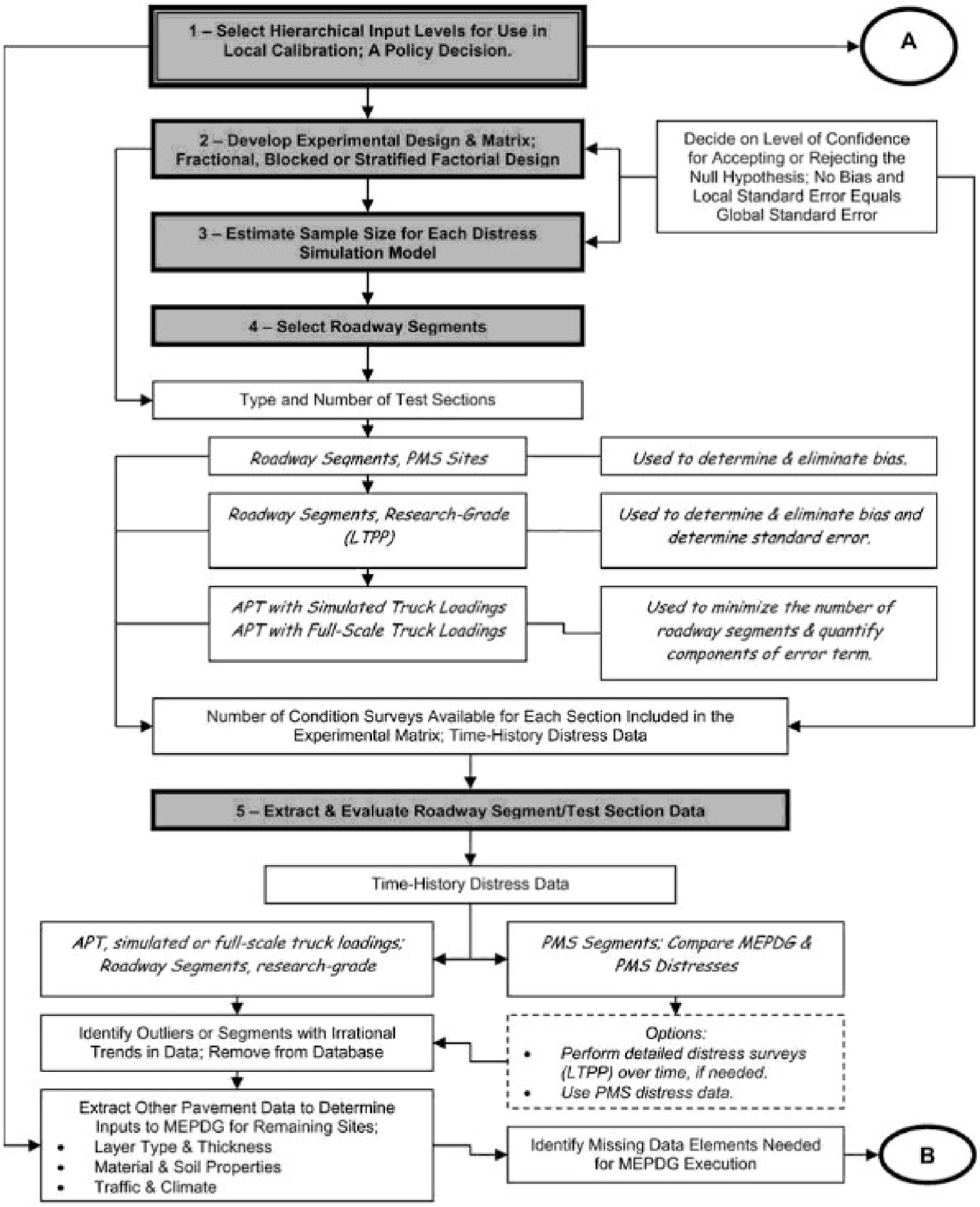

Figure 2.3 Flow chart of the procedure and steps suggested for local calibration; Steps 1 through 5 (AASHTO, 2010)

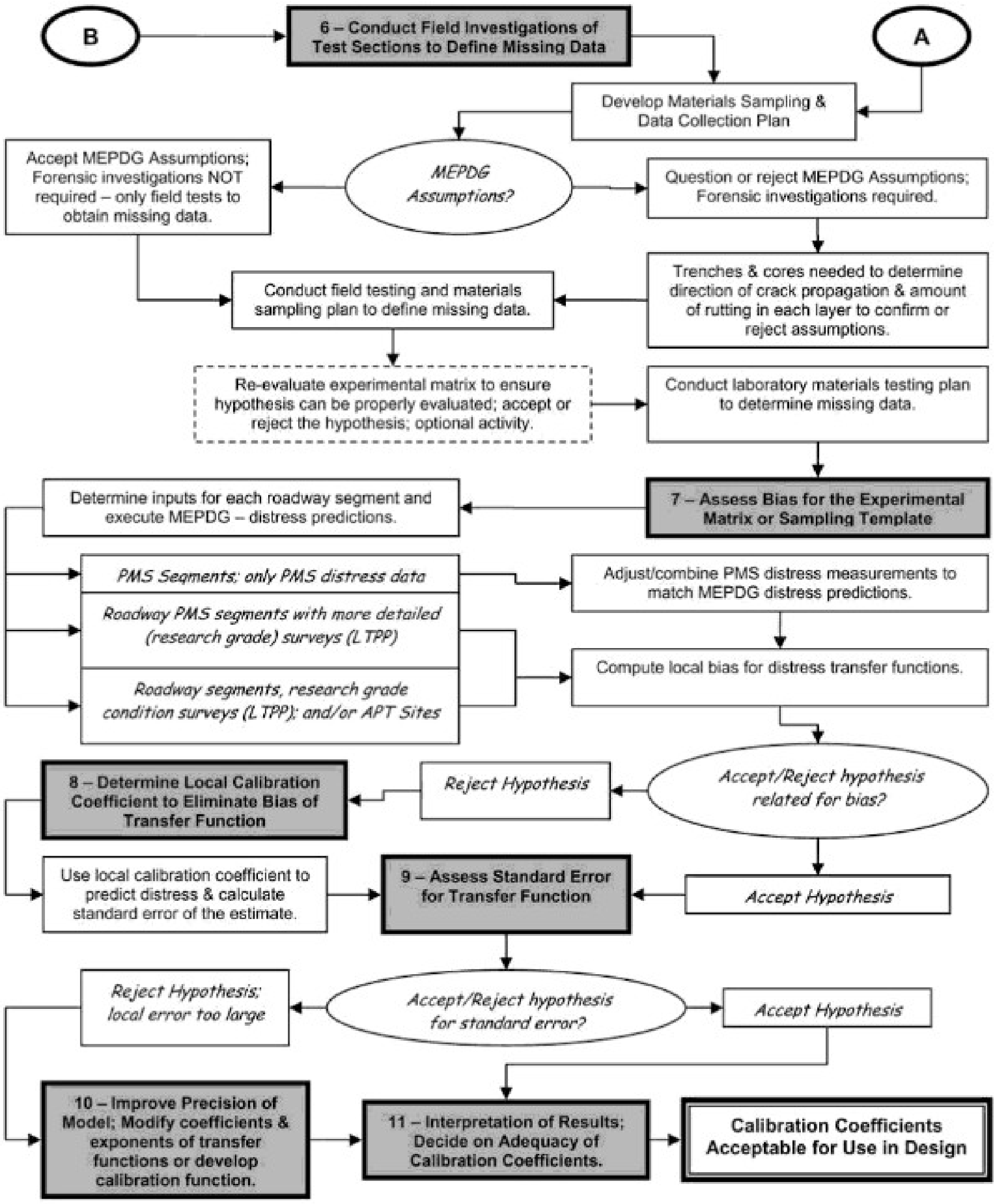

Figure 2.4 Flow chart of the procedure and steps suggested for local calibration; Steps 6 through 11 (AASHTO, 2010)

2.4 Previous efforts of local calibration

Many state highway agencies, collaborating with research institutes, have carried out necessary tasks of M-E implementation, including local calibration studies. The studies (i.e., Saeed and Hall, 2003; Schram and Abdelrahman, 2006; Li et al., 2009; Hoegh et al., 2010; Hossain et al., 2011; Jadoun and Kim, 2012; Hall and Beam, 2005; Tran and Hall, 2007; Wang et al., 2008; Hall et al., 2011), discussed a variety of issues and emphasized some aspects of concern for MEPDG evaluation and calibration. The documentation of their work was reviewed to understand the general background and identify key topics for an M-E design calibration study.

Saeed and Hall (2003) proposed a Phase-I MEPDG implementation plan for the Mississippi DOT. The plan mainly covered MEPDG familiarization, calibration preparation, and budget. This document outlined a stepwise plan to implement the M-E design guide. Some ideas of local calibration were described, though no actual calibration work had been carried out. Calibration preparation explained the processes of establishing pavement types, designing a factorial experiment, and selecting experimental sections. To design a factorial experiment, they listed a variety of contributing factors for prevalent distresses and ride quality, and defined the levels of these factors. Worthy to mention, the LTPP sections located in the state were recommended to be investigated experimental sections because of diverse pavement types and reliable data. Also, the Phase-II plan was mentioned to cover a detailed review of design factors and inputs, an initial sensitivity analysis, a comparison with current design procedures, and a guide to field and laboratory testing. However, this document did not elaborate the actual work and experiment results.

Schram and Abdelrahman (2006) performed a study of MEPDG local calibration using Nebraska data. The main goal was to calibrate the IRI model for jointed plain concrete pavement (JPCP) and HMA overlay pavements. One unique approach was that the IRI prediction, as a function of several specific distresses, was calibrated directly based on the distresses measured from the field, rather than the distresses predicted by the MEPDG. Thus, IRI model coefficients (explained earlier in Chapter 2) were derived to fit the relationship between the in-field IRI values and in-field distress values. The effectiveness of this calibration approach is debatable because the model coefficients may not apply to the MEPDG. The MEPDG predicts IRI based on model predicted values of several distresses, which may not reflect the in-field values as assumed. Further, the calibration was performed using three calibration datasets: in-state LTPP sections for national calibration (default level), state highway sections (statewide level), and a subset of state highway sections. The division of calibration dataset is illustrated in Figure 2.5. The subset of state highway sections was categorized and grouped by Average Daily Truck Traffic (ADTT) and surface layer thickness. For the subset data, the coefficients were sought using the software Pavement Condition Assessment and Rehabilitation Effectiveness (PaveCARE).

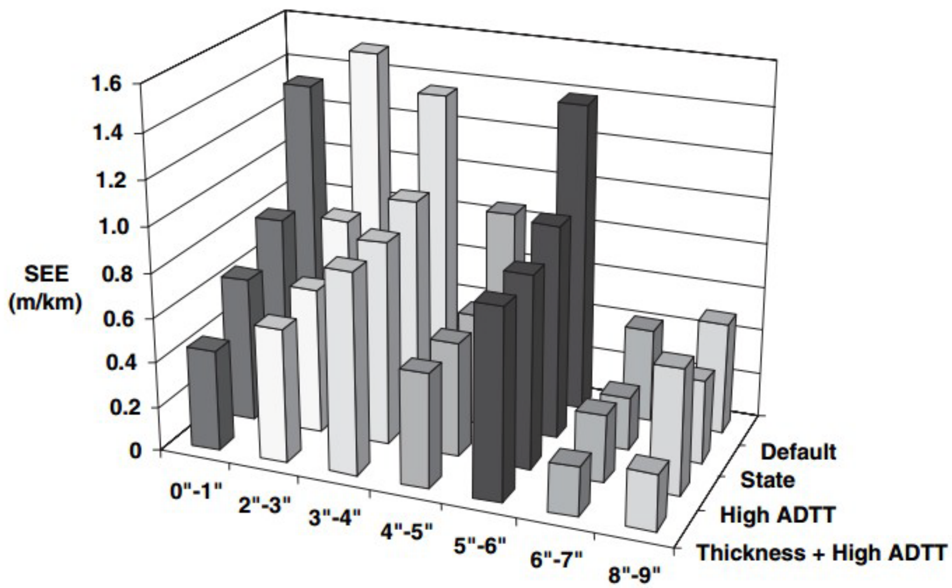

Figure 2.5 HMA overlay IRI model: SEE for high ADTT level (Schram and Abdelrahman, 2006)

Then, a separate dataset of state highway sections was used to validate the accuracy of the calibrated models. The statistical validation (i.e., two-sample Student's t-test) was used to analyze the results in addition to graphical validation (i.e., scatter plots of predicted against measured IRI values). In conclusion, Schram and Abdelrahman (2006) stated that local calibration attempted to harness the range of local area conditions and use them to improve prediction accuracy, but each project boasted unique local elements that could not be tamed with a systematic model. Also, Schram and Abdelrahman (2006) suggested that the challenge of applying focus calibrations to M-E models lies in the amount of time required to complete the calibrations, however, the improvement in prediction accuracy may justify the effort. The suggestion indicated that a considerable amount of time and effort was needed to justify the value of focus calibration on database subsets of particular design interests.

Jadoun and Kim (2012) targeted two main goals in their local calibration study for North Carolina conditions. The first goal was to determine k-values model for twelve HMA mixtures used by the state. The coefficient k in the rutting prediction models (i.e., transfer function) was for the rutting accumulation patterns under loads, and it was assumed that the determination of k-values was worthy of efforts before applying local calibration. The k-values were determined from the triaxial repeated load permanent deformation (TRLPD) tests. The second goal was to locally calibrate the rutting and bottom-up fatigue cracking models based on the LTPP database and state DOT data. Both models were calibrated using two methods for comparison: the Generalized Reduced Gradient (GRG) Optimization method and Genetic Algorithm (GA) method. The GRG method was applied by using macro recorder software, Workspace Macro Pro, to populate calibration coefficients in the software, while the GA method was applied by using MATLAB to optimize calibration coefficients. Figure 2.6 shows a comparison between measured vs. predicted rut depth and fatigue cracking by the default model, GRG-calibrated model, and GA-calibrated model, respectively.

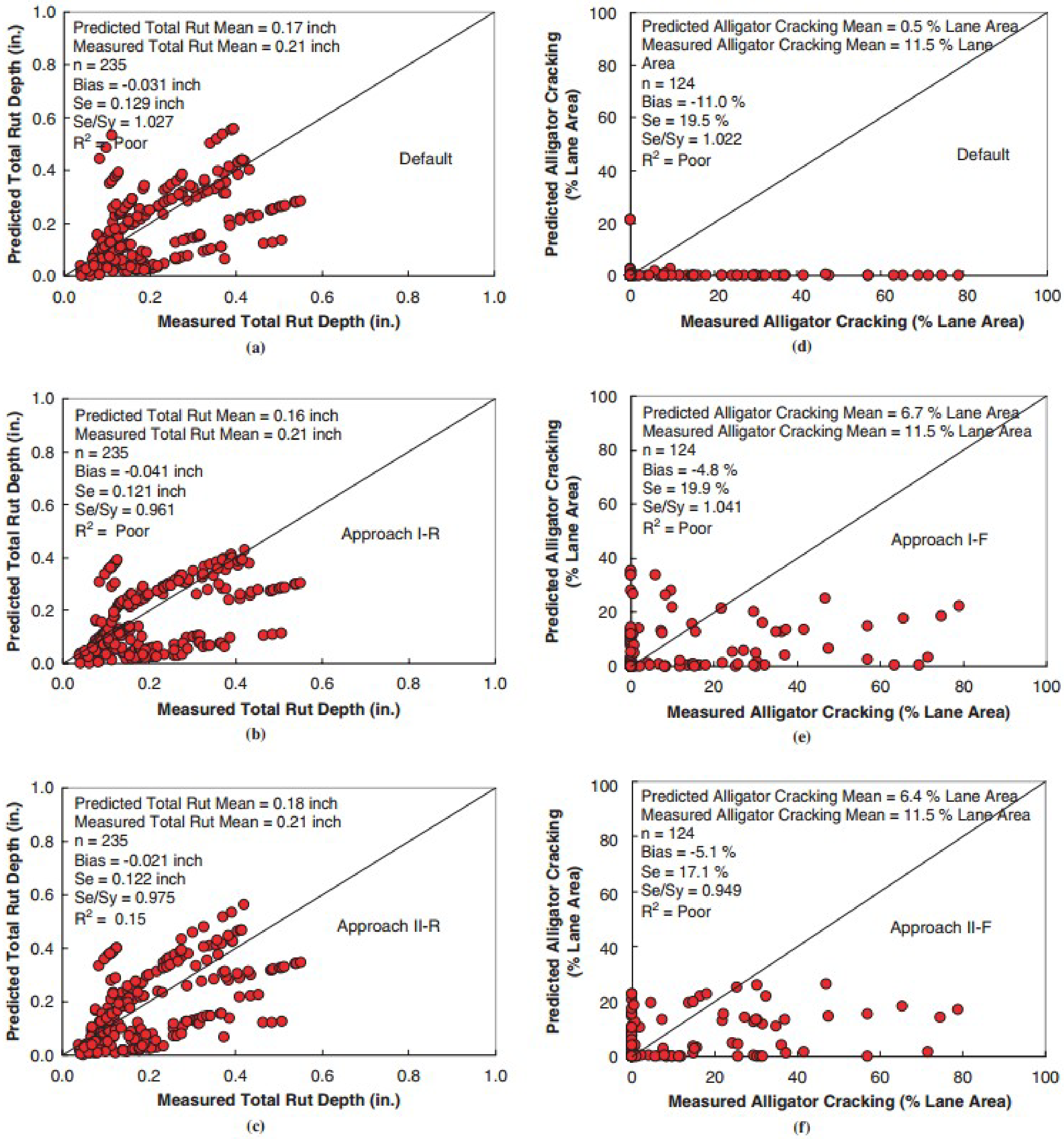

Figure 2.6 Comparison of measured versus predicted calibration results: total rut depth values from (a) default, (b) Approach GRG-R, and (c) Approach GA-R; and fatigue cracking values from (d) default, (e) Approach GRG-F, and (f) Approach GA-F (Jadoun and Kim, 2012)

The study concluded that the nationally calibrated model under-predicted the total rut depth and fatigue cracking. The local calibration improved the model accuracy to some degree. The researchers suggested that reliable distress data are highly important for successful calibration. Field and forensic investigation should be performed to identify the amount of rutting accumulated in each pavement layer, and it is also necessary to differentiate bottom-up cracking from the top-down cracking.

Three studies briefly described above exemplify three state agencies' M-E local calibration work, each of which had a state-specific focus. Indeed, the progress and focus of M-E calibrations were different depending on state's early preparation (i.e. budget plan, database, research teams, and so on) and M-E implementation plan. For instance, the calibration work of Arkansas was carried out in a strategic order (i.e., sensitivity studies, traffic data, database support, and model calibration), which can be traced back through available published documents (Hall and Beam, 2005; Tran and Hall, 2007; Wang et al., 2008; Hall et al., 2011). Although the three studies had different focuses, they had some common concerns, such as the source and use of calibration datasets. Saeed and Hall (2003) emphasized the selection of calibration database and design of the factorial experiment. Schram and Abdelrahman (2006) described the use of separate datasets for calibration and validation and discussed the effect of dataset ranges. Jadoun and Kim (2012) claimed that their dataset included the LTPP data as well as state DOT laboratory data and field inspections of pavement sections. To summarize, eight recent studies (i.e., Muthadi and Kim, 2008; Mallela et al., 2009; Li et al., 2009; Hoegh et al., 2010; Hall et al., 2011; Rahman, 2014; Darter et al., 2014; Haider et al., 2016) were carefully examined.

Muthadi and Kim (2008) used LTPP sections and North Carolina Department of Transportation databases to locally calibrate the alligator cracking model and permanent deformation models for HMA and unbound materials. Their local calibration process included three steps: verification, calibration, and validation. The verification performed software runs on the pavement sections using nationally-calibrated models. The calibration varied the appropriate model calibration coefficients to eliminate the bias and reduce the standard error between the predicted and measured distresses, if any exists. During the calibration, the Microsoft Excel Solver program was used to optimize the model coefficients β_b and β_s (in the rutting model), and C_1 and C_2 (in the bottom-up cracking model). The validation performed software runs on the additional pavement sections using the locally-calibrated models for a check of the reasonableness of performance predictions. Figure 2.7 presents both measured and predicted for rutting and alligator cracking (before and after calibration).

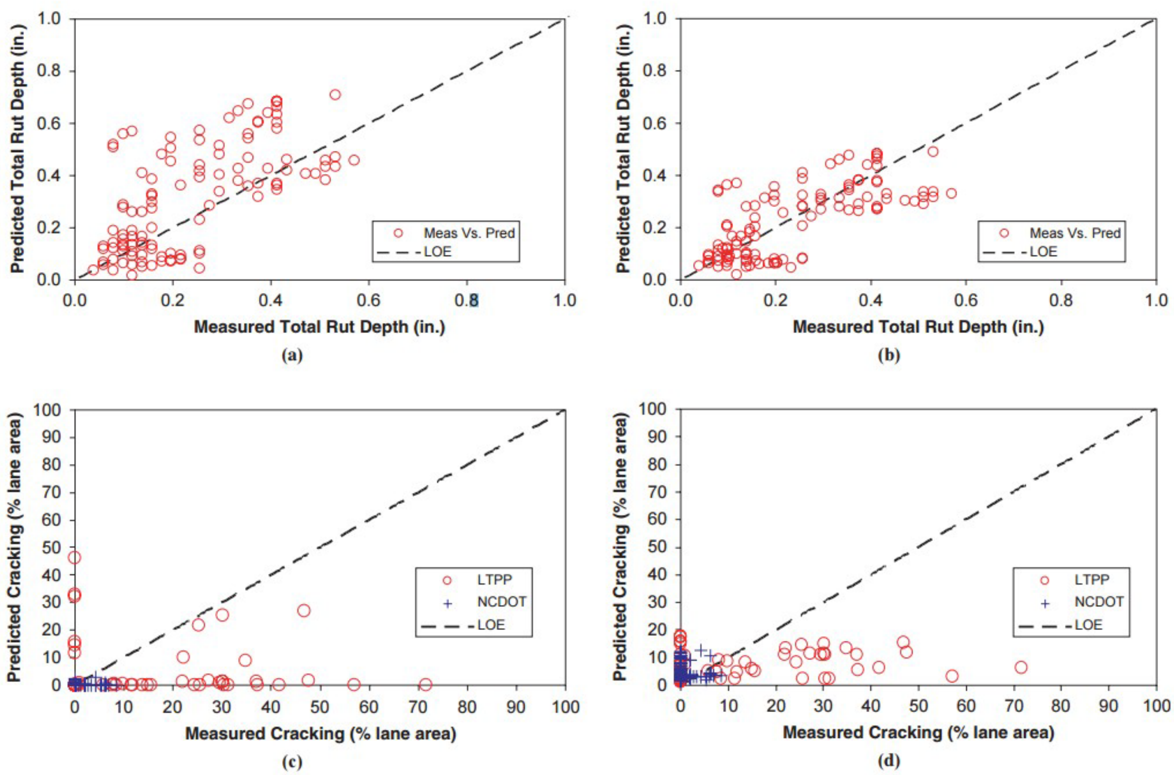

Figure 2.7 Measured versus predicted distresses before and after calibration: (a) total rut depth before calibration, (b) total rut depth after calibration, (c) alligator cracking before calibration, and (d) alligator cracking after calibration (Muthadi and Kim, 2008)

The overall conclusion was that the calibration effort significantly reduced bias (from -0.0771 to 0 for rutting, from 3.67 to 0 for fatigue cracking) and the standard error (from 0.154 to 0.109 for rutting, and 6.02 to 3.64 for fatigue cracking). The main recommendation was that field investigation (e.g., trenching and coring) should be performed. A more robust calibration should be carried out with an increased number of sections and more detailed inputs of a higher detail.

Mallela et al. (2009) conducted a comprehensive study of MEPDG model validation and calibration for the Missouri Department of Transportation (MoDOT). The investigated models included: alligator cracking, transverse cracking, and rutting models for three types of pavements (i.e., new HMA, HMA over HMA, and HMA over PCC pavements), and transverse slab cracking, transverse joint faulting, and IRI model for the new JPCP pavements. They identified and assessed suitable pavement sections from MoDOT and LTPP databases to conduct the experiment design based on several factors, such as HMA thickness and mix type for HMA, and lane width, shoulder type, dowel diameter, and thickness for PCC. The framework for MEPDG model validation and recalibration included four parts: 1. assembling of all relevant data; 2. processing assembled data to develop MEPDG input files and time series pavement performance data; 3. validation of nationally-calibrated models by evaluating goodness of fit and bias in Missouri conditions; 4. recalibration of national-calibrated models that were found to be inadequate. The study found that a majority of the paired measured and predicted alligator cracking points fell within a cracking group of 0 to 2 percent total lane area, which could not fairly account for the model predictions at higher percentages of cracking. The nationally-calibrated MEPDG rutting model was shown to be inadequate but after local calibration the model was deemed reasonable (Figure 2.8 and Figure 2.9);

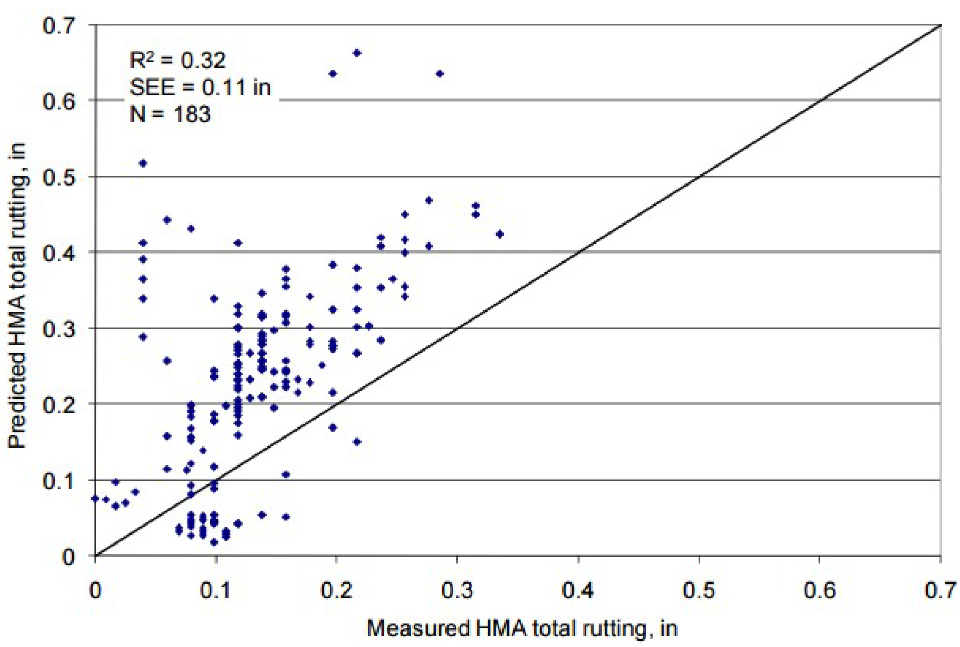

Figure 2.8 Plot of measured versus MEPDG nationally-calibrated model predicted new HMA pavement total rutting (Mallela et al., 2009)

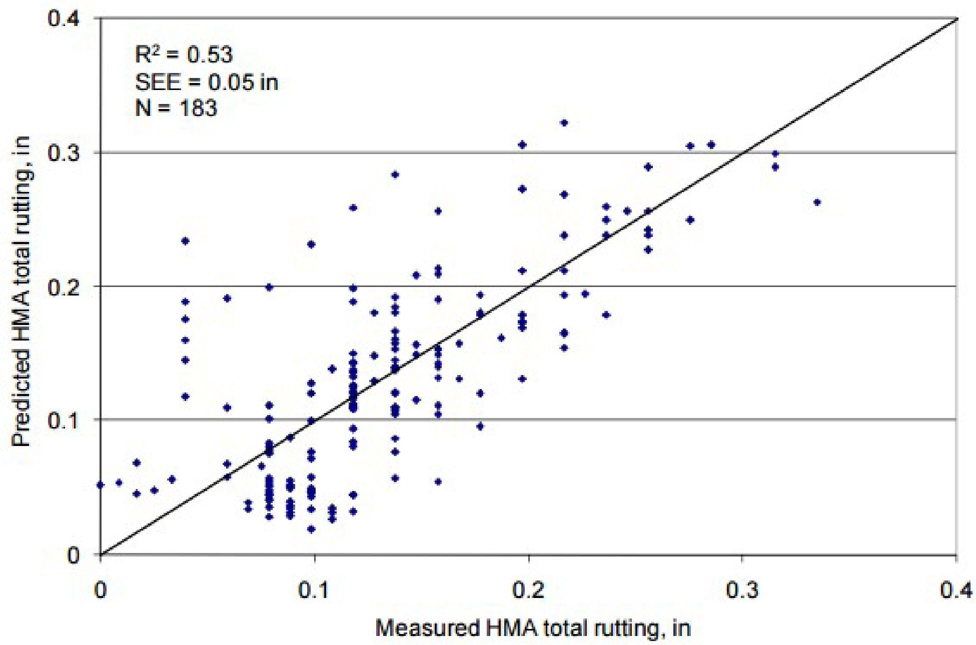

Figure 2.9 Plot of measured versus locally calibrated model predicted new HMA pavement total rutting (Mallela et al., 2009)

The researchers also found that the nationally-calibrated IRI model for new HMA and HMA over HMA pavements was inadequate for Missouri conditions. The local calibration barely improved the model predictions (Figure 2.10 and Figure 2.11). The study concluded that nationally-calibrated IRI model for HMA over JPCP pavements was reasonable for Missouri conditions (Figure 2.12).

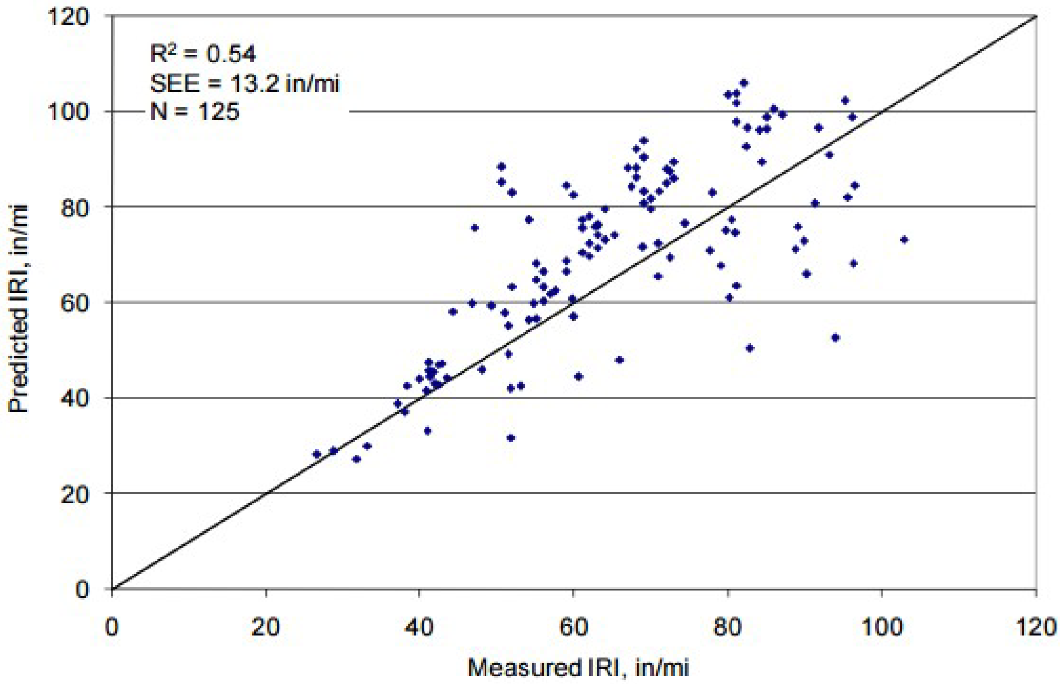

Figure 2.10 Plot of measured versus MEPDG predicted IRI (nationally calibrated) for new HMA and HMA overlays of existing HMA pavements (Mallela et al., 2009)

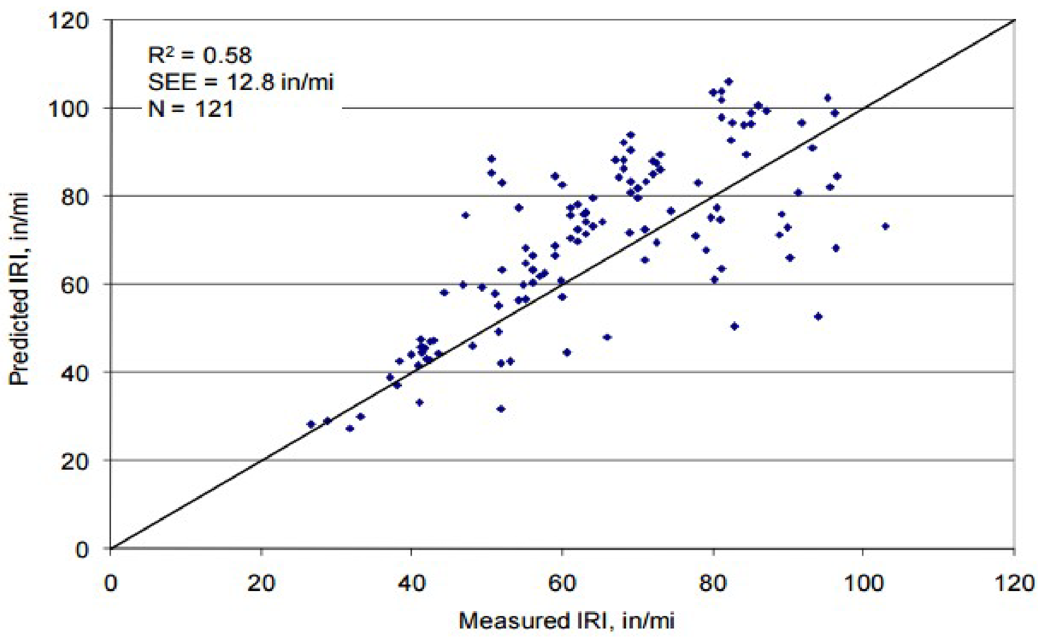

Figure 2.11 Plot of measured versus MEPDG predicted IRI (locally calibrated) for new HMA and HMA overlays of existing HMA pavements (Mallela et al., 2009)

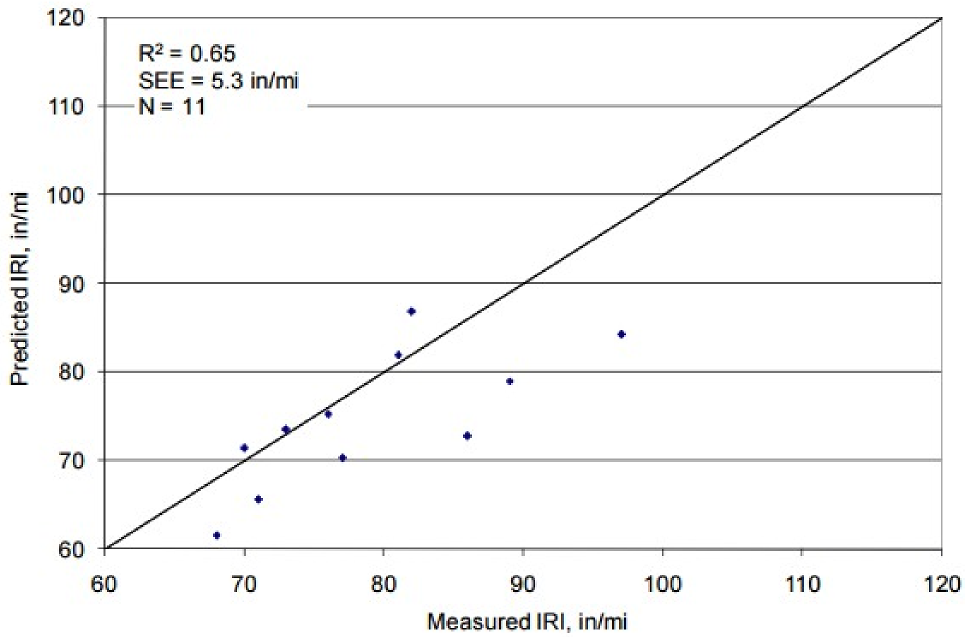

Figure 2.12 Plot of measured versus MEPDG predicted IRI (nationally calibrated) for flexible and composite pavements (Mallela et al., 2009)

Li et al. (2009) worked on the evaluation and calibration of MEPDG flexible pavement distress models for Washington State Department of Transportation (WSDOT). The calibration data was primarily from the Washington State Pavement Management System (WSPMS) database. Before performing calibration, bench testing was used to check input sensitivity and calibration necessity. It suggested that nationally-calibrated models tended to under-predict longitudinal cracking, alligator cracking, and rutting (Figure 2.13, Figure 2.14, and Figure 2.15). Local calibration improved the model predictions for longitudinal cracking, alligator cracking, transverse cracking, and rutting (Figure 2.13, Figure 2.14, and Figure 2.15).

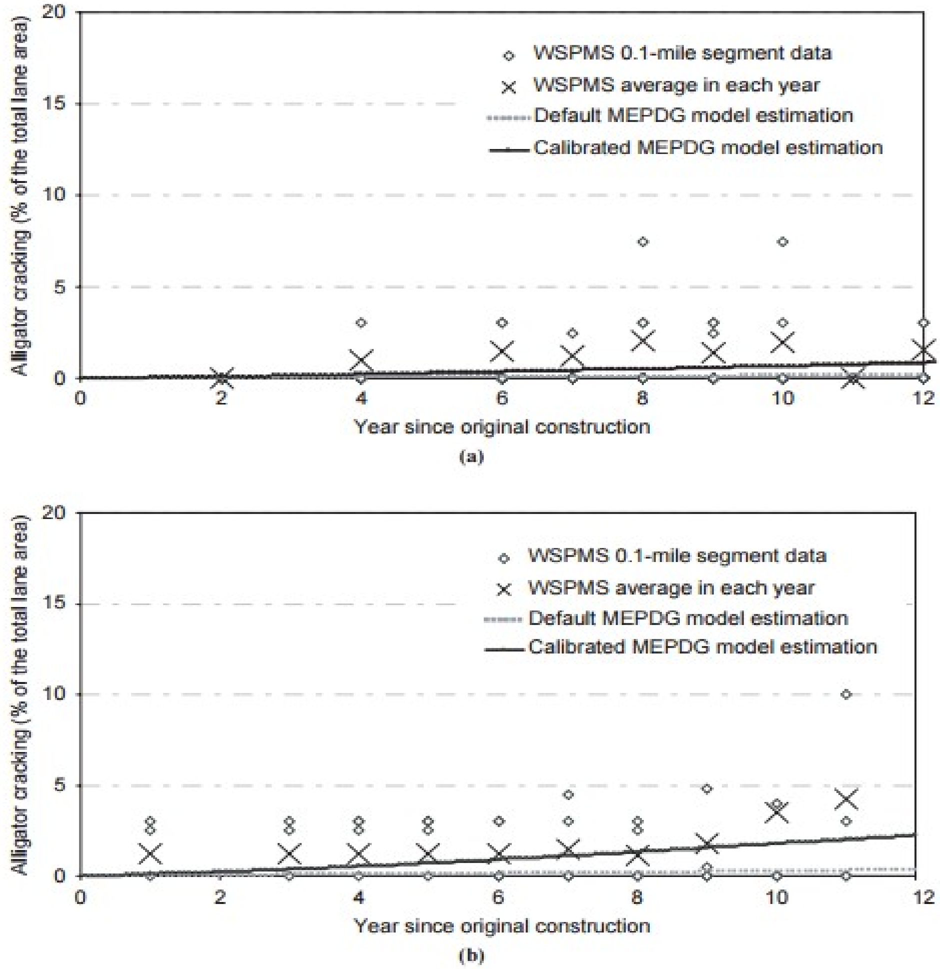

FIGURE 1 Alligator cracking (*a*) in western Washington and (*b*) in eastern Washington.

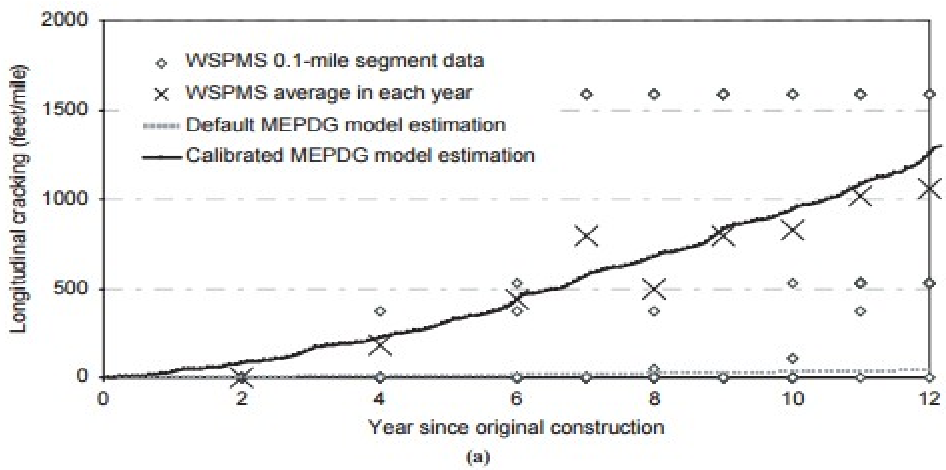

FIGURE 2 Longitudinal cracking (*a*) in western Washington.

(continued on next page)

Figure 2.13 Predicted versus measured performance in western and eastern Washington (1) (Li et al., 2009)

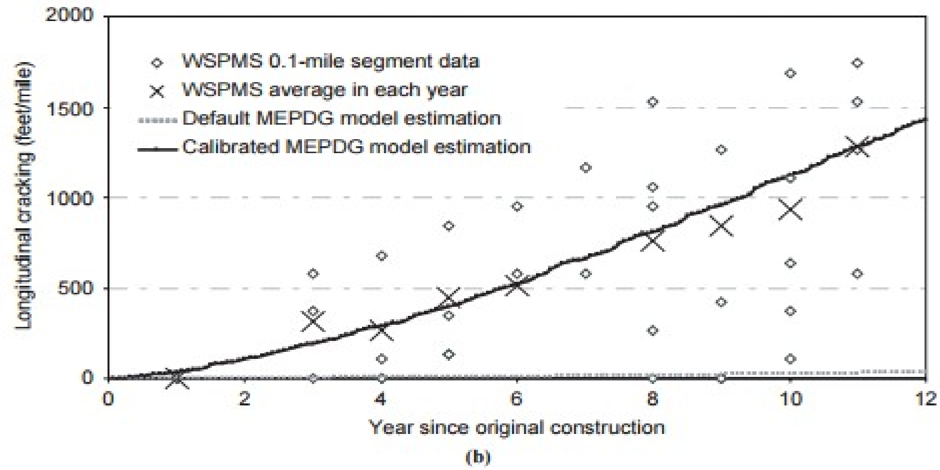

FIGURE 2 *(continued)* Longitudinal cracking (*b*) in eastern Washington.

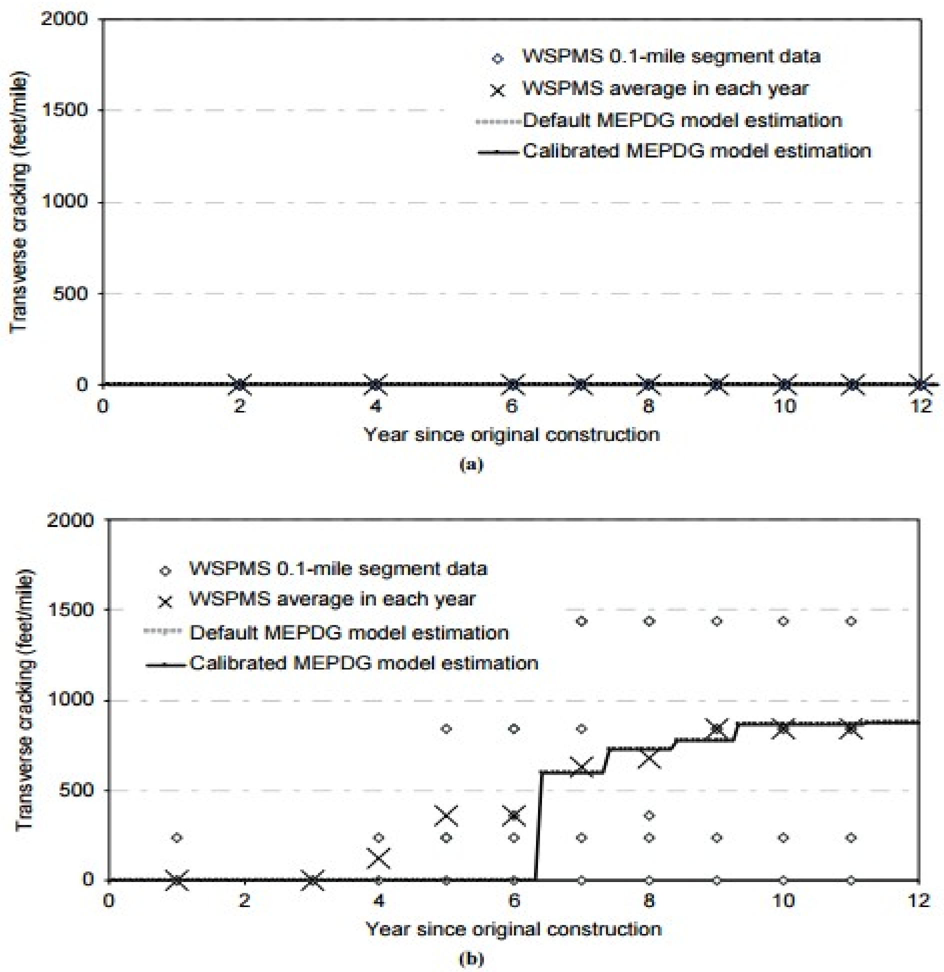

FIGURE 3 Transverse cracking (*a*) in western Washington and (*b*) in eastern Washington.

Figure 2.14 Predicted versus measured performance in western and eastern Washington (2) (Li et al., 2009)

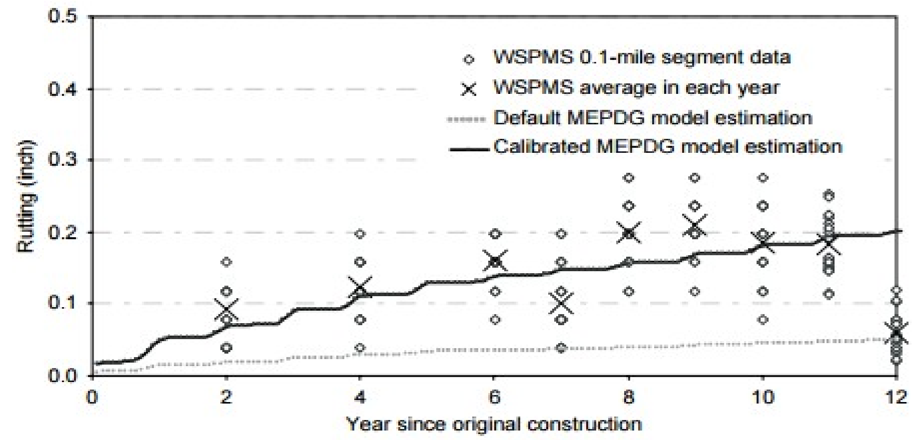

(a)

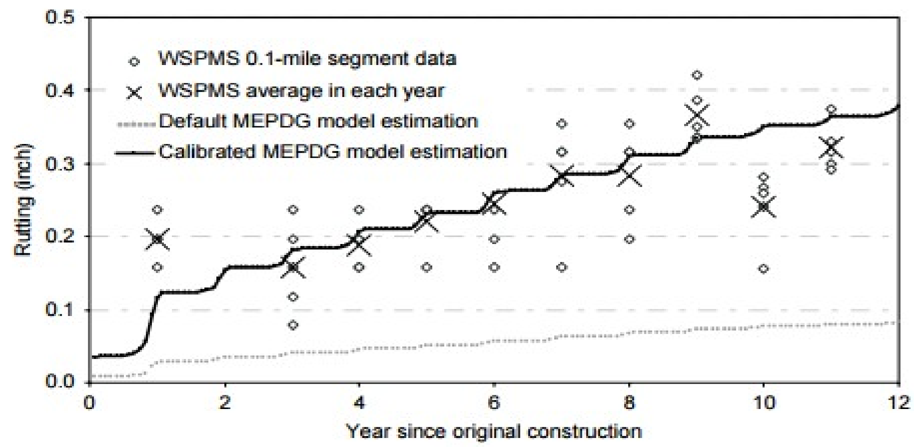

(b)

FIGURE 4 Rutting (*a*) in western Washington and (*b*) in eastern Washington.

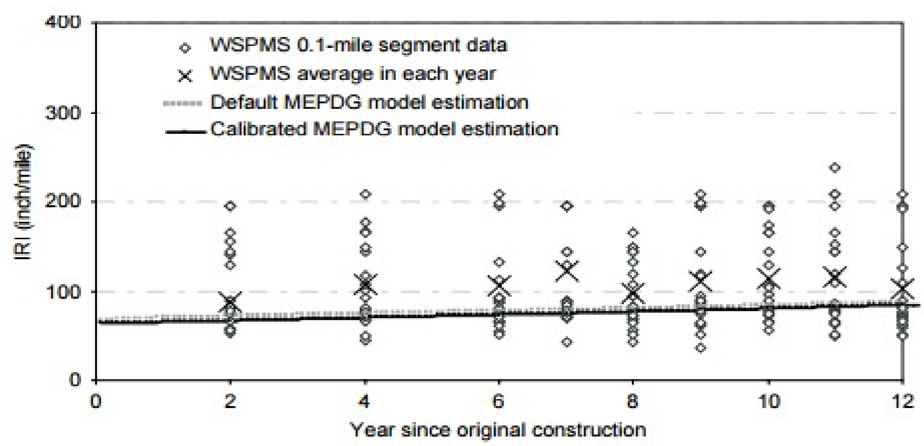

(a)

FIGURE 5 IRI (*a*) in western Washington (calibrated MEPDG estimation uses calibrated cracking and rutting outputs with default IRI model calibration factors).

(continued on next page)

Figure 2.15 Predicted versus measured performance in western and eastern Washington (3) (Li et al., 2009)

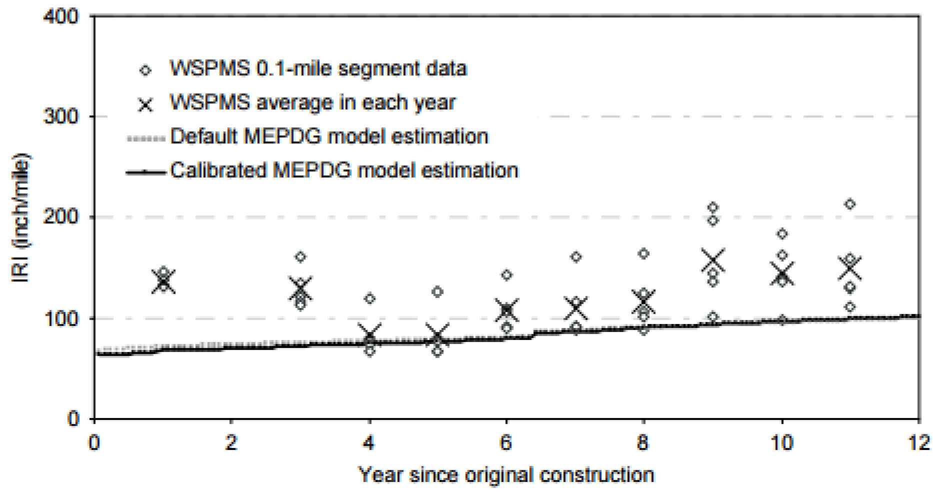

(b)

FIGURE 5 *(continued)* IRI (*b*) in eastern Washington (calibrated MEPDG estimation uses calibrated cracking and rutting outputs with default IRI model calibration factors).

Figure 2.16 Predicted versus measured performance in western and eastern Washington (4) (Li et al., 2009)

An "elasticity analysis" mentioned in the study was conducted to describe the effects of those calibration factors on the pavement distress models. Based on analysis results, the calibration factors were adjusted in order of high to low elasticity. Two calibration sections were carefully selected to represent typical design parameters and pavement condition data for WSDOT's new flexible pavements. A variety of sections (totally 13 sections), independent of the two for calibration, were used to validate the calibration results. The main conclusion was that calibration applies to more than 90% of all WSDOT flexible pavements. It was recommended that local roadway agencies need to balance the accuracy of inputs and costs, and they should further examine MEPDG models. The calibration results will benefit agencies that are, or will be, involved with MEPDG.

Hoegh et al. (2010) utilized the time history rutting performance data from Minnesota Road Research Project (MnRoad) to evaluate and locally-calibrate the MEPDG rutting model. Other forms of pavement distress were not evaluated. 12 asphalt sections, part of westbound Interstate 94, were used for this investigation. These sections, though built according to various designs (i.e., thickness, mix design, base type, etc.), were subjected to the same environmental and traffic loading condition. The local calibration did not involve an adjustment of the calibration coefficients. Instead, it was achieved with a subtraction of initial base and subgrade rutting jump (i.e., the first month's prediction). Trenches were cut for two-thirds of the asphalt sections, which indicated the majority of rutting occurred in the upper lifts of the HMA, with the granular base and subgrade mostly unaffected. This suggested that the nationally-calibrated rutting model over-predicted rutting for the MnRoad conditions because of an initial over-prediction of base and subgrade rutting (Figure 2.17). The conclusion indicated that local calibration was successful in improving rutting predictions.

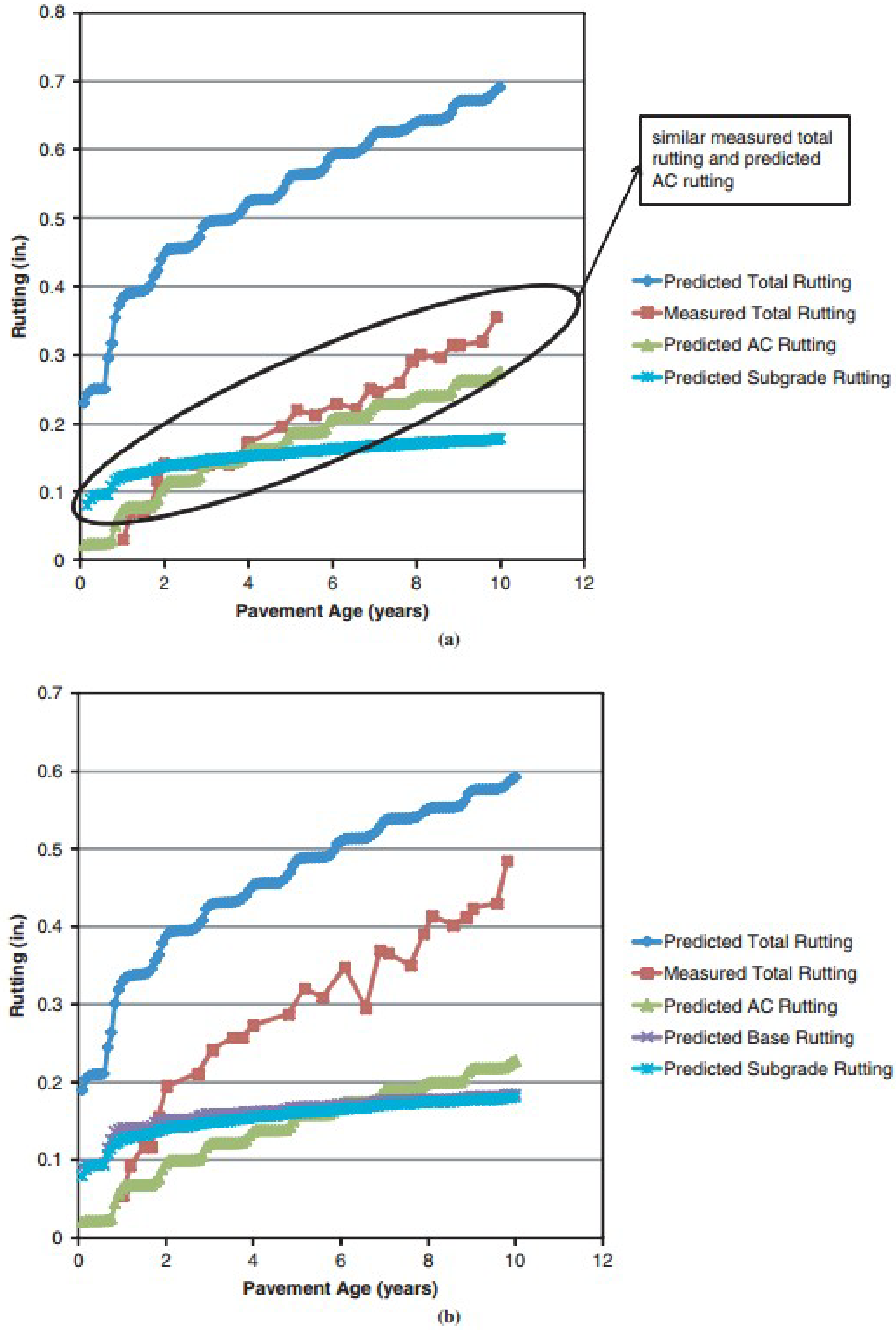

Figure 2.17 Results: (a) measured and predicted rutting over the pavement age for Section 1 and (b) measured and predicted rutting over the pavement age for Section 2 (Hoegh et al., 2010)

Hall et al. (2011) performed the initial local calibration of flexible pavement models in the MEPDG for Arkansas. Data from LTPP database and local pavement management system (PMS) was used for the study. Three parts of work were presented: verification, calibration, and validation. The verification showed that predicted distresses (longitudinal cracking, transverse cracking, rutting, and IRI) did not match well with measured distresses (Figure 2.18).

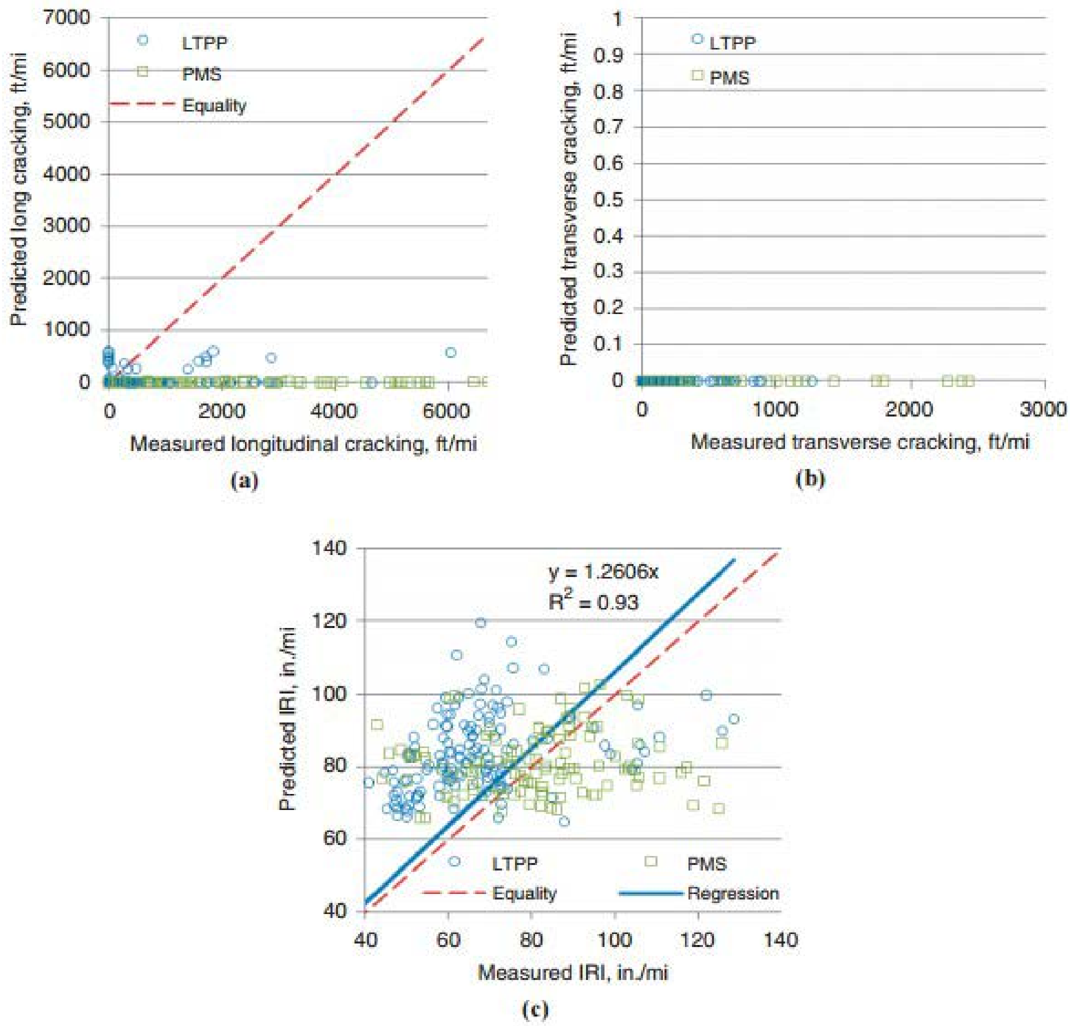

Figure 2.18 Verification of nationally calibrated model: (a) longitudinal cracking, (b) transverse cracking, and (c) IRI (Hall et al., 2011)

For the calibration effort, the longitudinal and transverse cracking models were not calibrated due to a lack of full understanding of cracking mechanism. The IRI model was not calibrated because the predicted IRI is a function of other predicted distresses. The Solver function in Microsoft Excel was used to optimize the coefficients in the alligator cracking model. Iterative runs of the MEPDG were used to optimize the rutting model. The validation effort indicated that the adjusted calibration coefficients improved the model predictions. The study concluded that alligator cracking and rutting models were improved by local calibration (Figure 2.19). In terms of the alligator cracking, the average of cracking predictions was increased from 0.5512% to 2.0070%, as compared to the average of measurements 2.0688%. The standard deviation of cracking predictions was reduced from 2.0661% to 1.4456%, as compared to the average of measurements 4.9029%. As for the rutting, the average of predictions was reduced from 0.2586 in. to 0.1852 in., as compared to the average of measurements 0.1945 in.. The standard deviation of rutting predictions was reduced from 0.0885 in. to 0.0628 in., as compared to the average of measurements of 0.0670 in.. The availability and quality of design, materials, construction, and performance data are crucial for local calibration. It was recommended that data from additional sites be added to future calibration efforts.

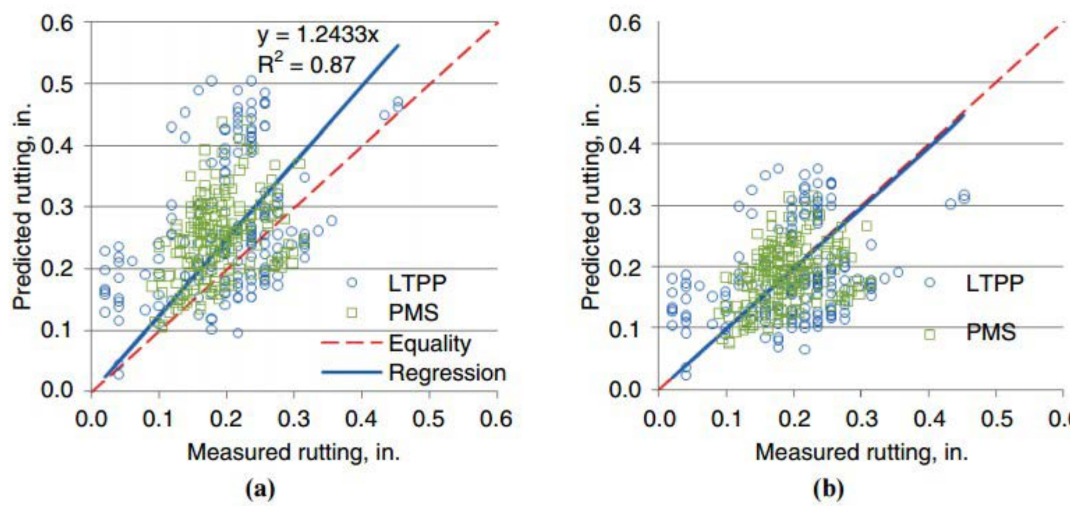

Figure 2.19 Rutting models: (a) verification of national calibration and (b) local calibration (Hall et al., 2011)

Rahman (2014) conducted a study on the MEPDG models based on Oregon rehabilitated roadways. 38 pavement sections throughout Oregon were included in this calibration study. A detailed comparison of predicted and measured distresses suggested that MEPDG prediction models (for rutting, alligator cracking, longitudinal cracking, and thermal cracking) did not accurately reflect measured distresses. Therefore, a local calibration was warranted. The local calibration improved the model accuracy for rutting (SEE: from 1.443 to 0.457), alligator cracking (SEE: from 3.384 to 2.144), and longitudinal cracking (SEE: from 682 m/km to 486 m/km) by adjusting calibration coefficients (Figure 2.20, Figure 2.21, Figure 2.22, and Figure 2.23).

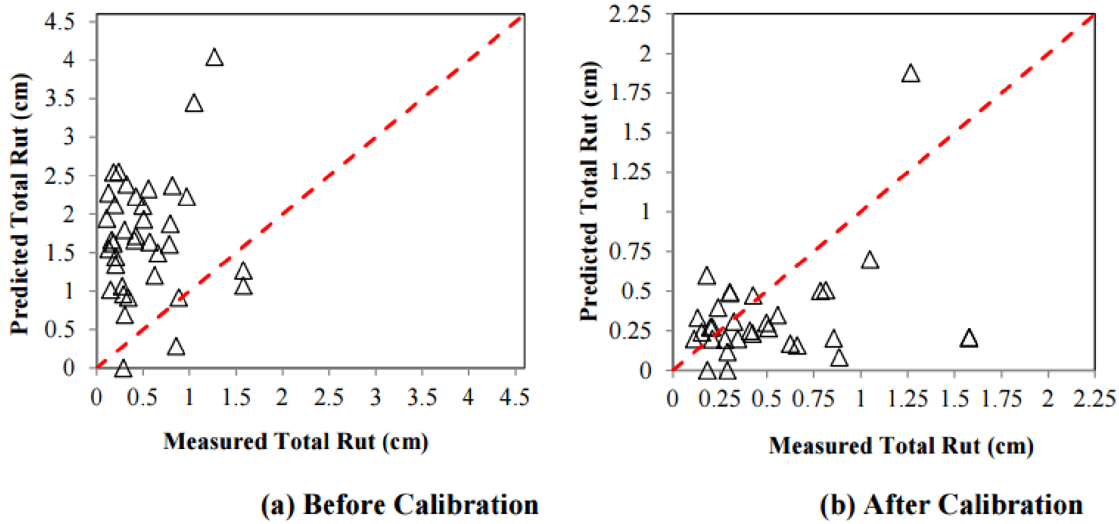

Figure 2.20 Comparison of predicted and measured rutting (a) before calibration and (b) after calibration (Rahman, 2014)

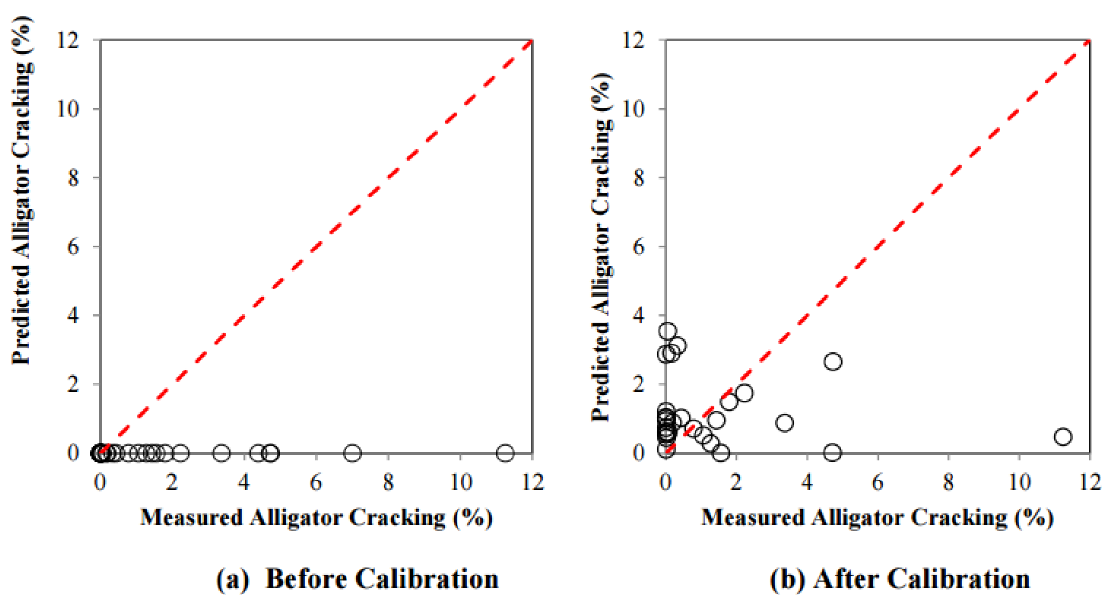

Figure 2.21 Comparison of predicted and measured alligator cracking (a) before calibration and (b) after calibration (Rahman, 2014)

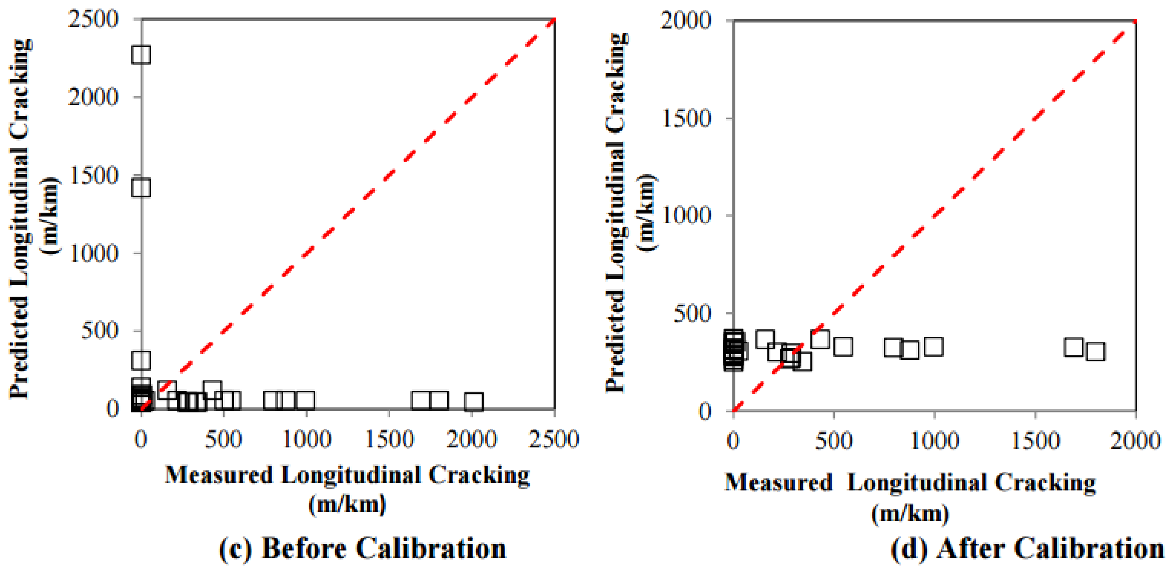

Figure 2.22 Comparison of predicted and measured longitudinal cracking (a) before calibration and (b) after calibration (Rahman, 2014)

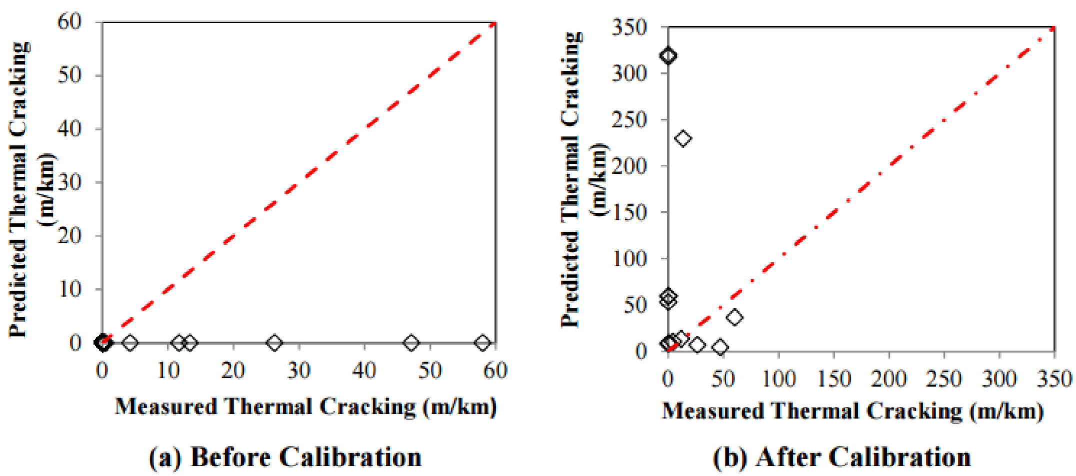

Figure 2.23 Comparison of predicted and measured thermal cracking (a) before calibration and (b) after calibration (Rahman, 2014)

However, there was still a high degree of variability between predicted and measured distresses. The researchers believed that the calibrated models of rutting and alligator cracking could be implemented. They suggested that future effort should be spent on further calibration using additional sites and using more detailed inputs.

Darter et al. (2014) took efforts to implement DARWin-ME pavement design guide for Arizona DOT. Implementation focused on several tasks: identifying the desired pavement design application, characterizing materials, determining traffic loadings, collecting and assembling input data, calibrating prediction models, and training Arizona DOT staff. A variety of pavements were investigated: new HMA pavement, AC over AC, etc. 42 LTPP and 16 ADOT sections were used to locally calibrate the alligator cracking, rutting, transverse cracking, and IRI models. For alligator cracking, it was recognized that the SEE was about the same after the local calibration. However, the predictions (at higher levels of fatigue damage) were obviously improved. Therefore, it was overall believed that the alligator cracking model was improved. It was concluded that the local calibration effort improved the accuracy of the rutting and IRI models (Figure 2.24, Figure 2.25, Figure 2.26, Figure 2.27, Figure 2.28, and Figure 2.29).

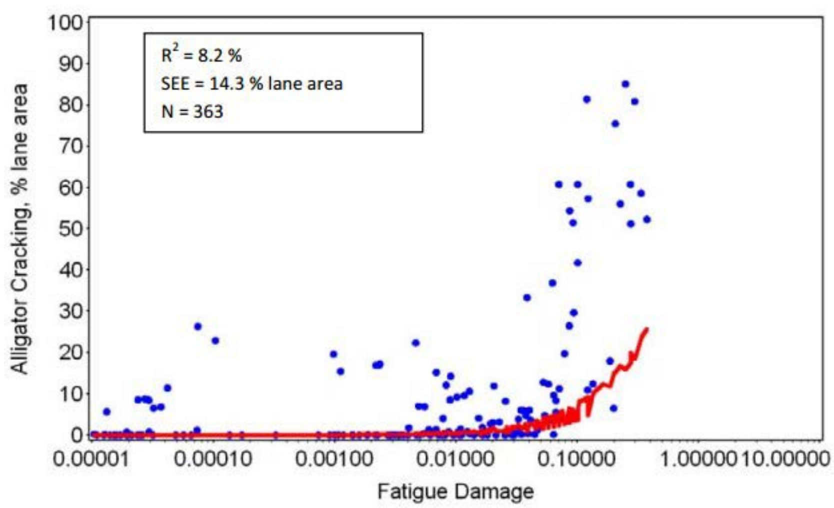

Figure 2.24 Initial verification of the HMA alligator fatigue cracking models with global coefficients using Arizona performance data (Darter et al., 2014)

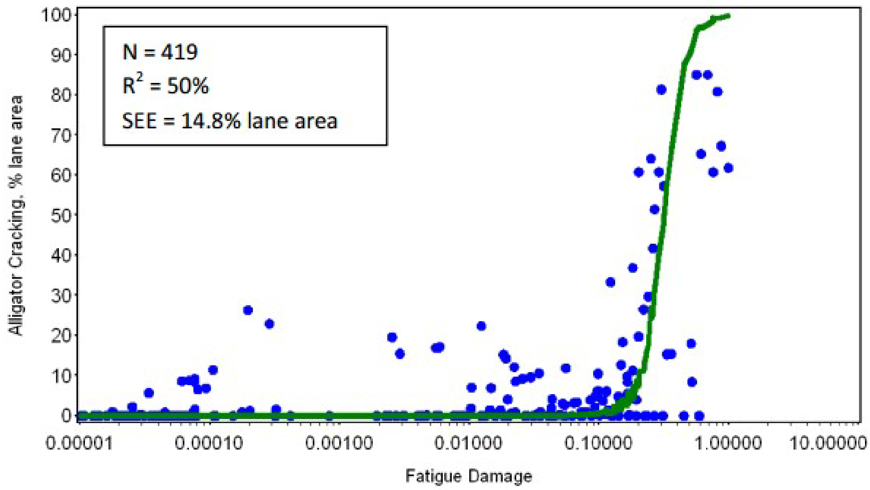

Figure 2.25 Measured and predicted alligator cracking versus cumulated fatigue damage for the locally calibrated alligator cracking submodels data (Darter et al., 2014)

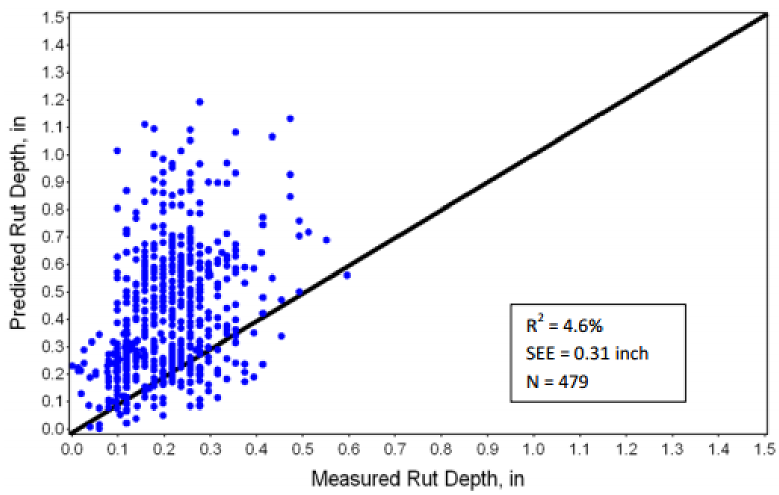

Figure 2.26 Predicted total rutting using global coefficients and Arizona HMA pavement performance data (Darter et al., 2014)

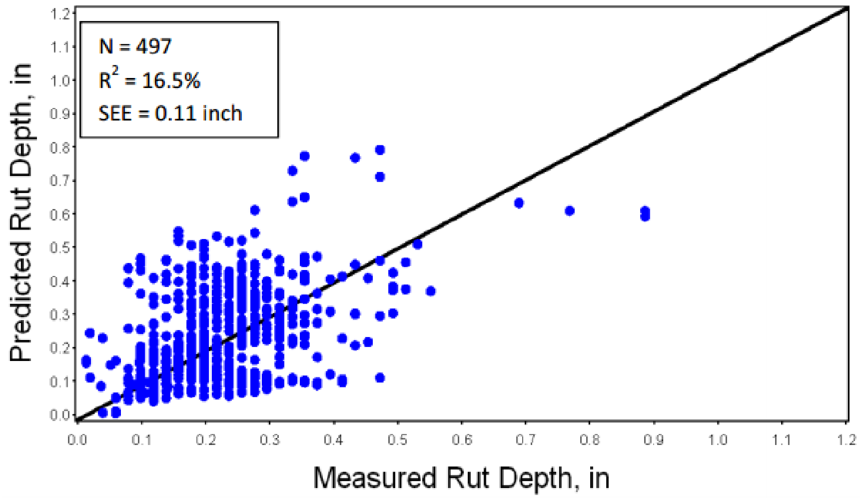

Figure 2.27 Predicted total rutting using local coefficients and Arizona HMA pavement performance data (Darter et al., 2014)

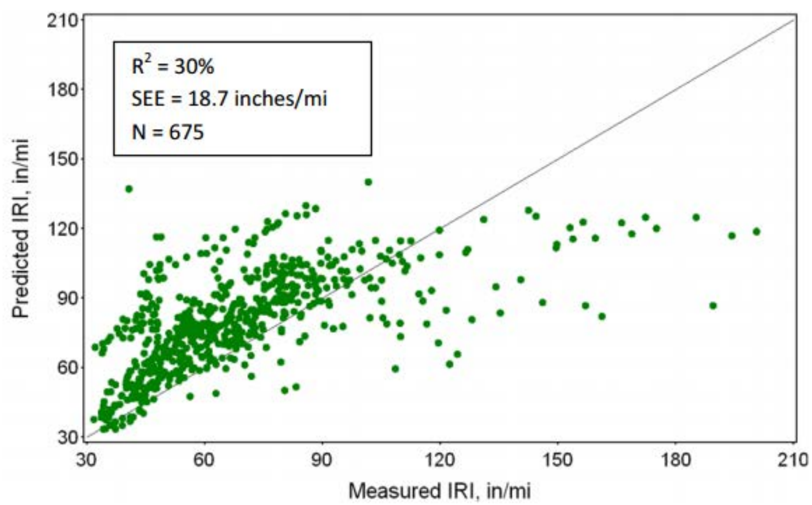

Figure 2.28 Predicted versus measured IRI using global coefficients (Darter et al., 2014)

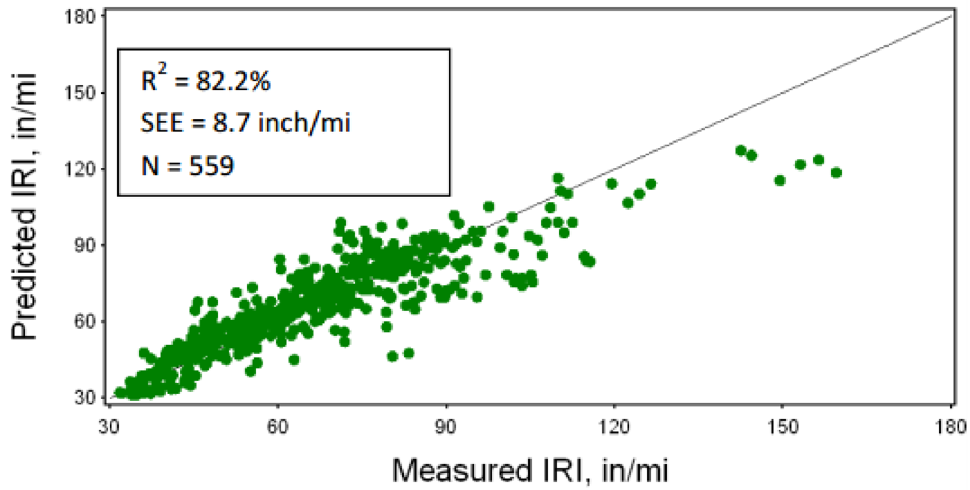

Figure 2.29 Predicted versus measured IRI using local coefficients (Darter et al., 2014)

The study gave some recommendations on generating binder and mixtures data library, evaluating the transverse cracking model, and collecting more traffic data.

Haider et al. (2016) undertook the local calibration of the Pavement-ME flexible pavement performance models for Michigan conditions. Rutting and transverse cracking models were calibrated in this study. Traditional split sampling (70% for calibration and 30% for validation), as well as bootstrapping, was used as resampling strategies when data was limited. Traditional split sampling was to randomly select subsets of individuals within a statistical population to estimate characteristics of the whole population. The bootstrapping relies on random sampling with replacement, and this can be implemented by constructing a number of resamples with replacement of the observed dataset. These strategies were to quantify the variability associated with the model predictions and parameters. The models were improved with the local calibration effort (Figure 2.30). The main conclusion was that these resampling strategies would help in reducing the SEE and bias for the calibrated model.

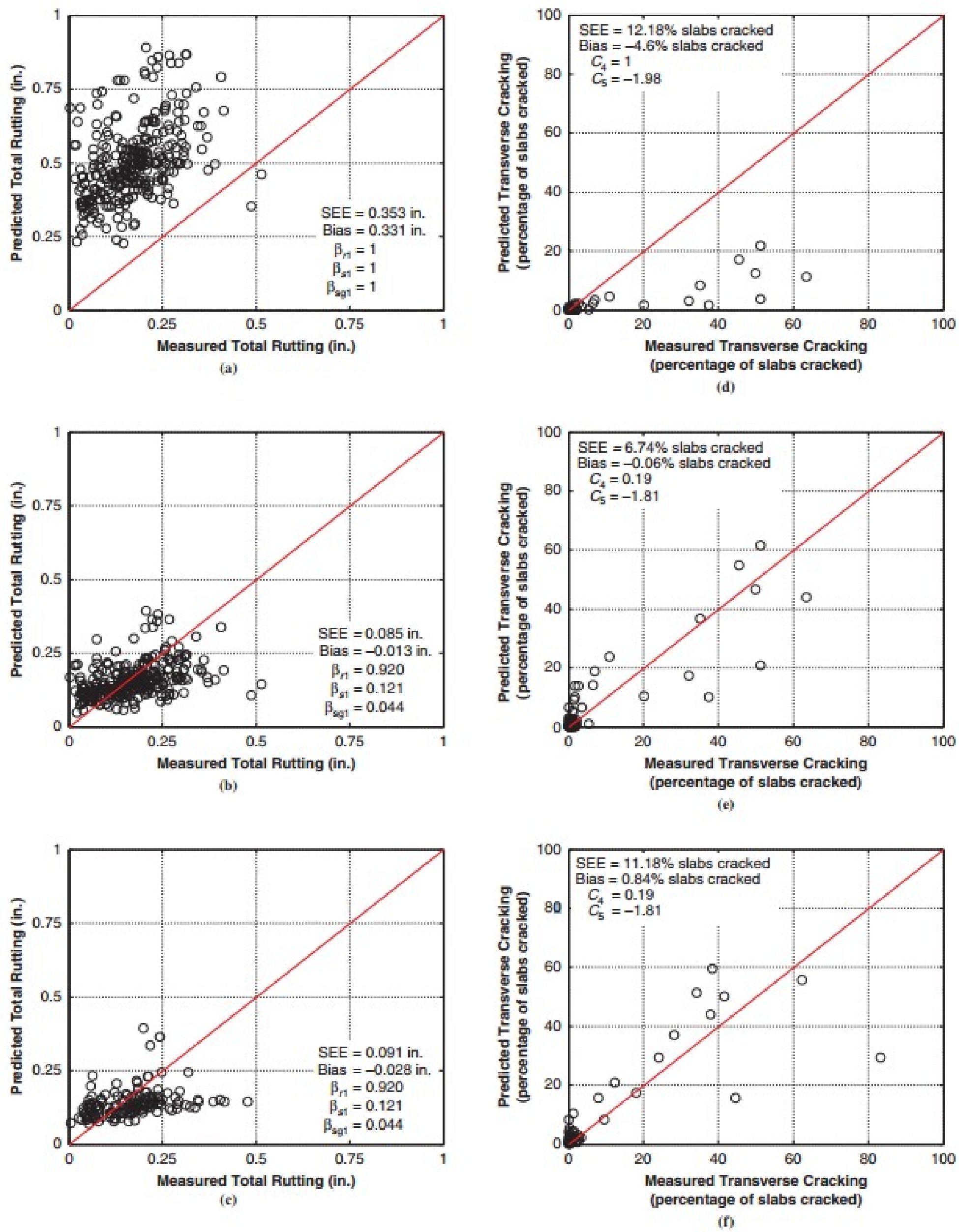

FIGURE 7 Split-sampling local calibration results: (a) global model, total rutting; (b) local model, total rutting; (c) validation for total rutting; (d) global model, transverse cracking; (e) local model, transverse cracking; and (f) validation for transverse cracking.

Figure 2.30 Split-sampling local calibration results: (a) global model, total rutting; (b) local model, total rutting; (c) validation for total rutting; (d) global model, transverse cracking; (e) local model, transverse cracking; and (f) validation for transverse cracking (Haider et al., 2016)

After examing the eight studies, a synthesis was made to identify common concerns and gather relevant information from each study. Table 2.3 present common concerns (i.e., data source, input level, the number of calibration and validation sections, and experimental factors) for the eight calibration studies. A summary of Table 2.3 is provided after that.

Table 2.3 Common concerns of recent studies

Author (Year)	State	Data Source (Traffic, Climate, Material, and Performance)	Input Level (Traffic, Climate, Material, and Performance)	The Number of Calibration and Validation Sections	Experimental Factors
Muthadi and Kim(2008)	North Carolina	State traffic unit, geotechnical unit, state pavement management unit, pavement management unit	Traffic (Level 1), others not specified	30 LTPP sections and 23 NCDOT sections. 80% for calibration and 20% for validation	Pavement type, HMA thickness, mix type, materials
Mallela et al. (2009)	Missouri	State WIM sites, interpolation of data from local weather stations, state DOT and LTPP database, state DOT, and LTPP database	Traffic (Level 1 and 3), climate (Level 1), material (Level 1, 2, and 3)	40 LTPP sections and 39 MoDOT sections. Split ratio was not mentioned	Supporting layer, HMA thickness, HMA mix type
Li et al. (2009)	Washington State	Representative axle load spectra, software-provided weather station, WSPMS and state specifications, WSPMS	Level 2 preferred	2 representative sections for calibration, 13 sections for validation	Traffic level, soil type, climate
Hoegh et al. (2010)	Minnesota	MnRoad database	Material (Level 3)	12 MnRoad sections. Split ratio was not mentioned	N/A
Hall et al. (2011)	Arkansas	LTPP database and state research, MEPDG database, LTPP database and state specifications, LTPP database, and state yearly distress survey	Traffic (Level 2 and 3), climate (Level 1), material (Level 1, 2, and 3)	A total of 38 LTPP sections and PMS sections. 80% for calibration and 20% for validation	Base type, HMA thickness
Rahman (2014)	Oregon	State DOT data, MEPDG database, state DOT data, ODOT field condition survey	Material (Level 3), others not specified	38 pavement sections. Split ratio is was not mentioned	Traffic, pavement performance, region
Darter et al. (2014)	Arizona	ADOT project report, MEPDG database, ADOT project report, LTPP database and ADOT PMS/research project	Traffic (Level 2 and 3), climate (Level 1), material (Level 1, 2, and 3)	42 LTPP sections and 16 Arizona PMS sections. 90% for calibration and 10% for validation	HMA thickness, granular base thickness, subgrade type
Haider et al. (2016)	Michigan	MDOT traffic study, closest available climate station, project record and MDOT study, PMS database	Traffic (Level 1, 2, and 3), climate (Level 1), material (Level 1, 2, and 3)	121 PMS sections. 80% for calibration and 20% for validation	Site factor, traffic, surface layer thickness, permanent age

N/A means “not applicable or not included in the documentation.”

Summary of Table 2.3:

- Data Source: most of these studies used LTPP sections and PMS sections as calibration database, while Hoegh et al. (2010) used data from the Mn/Road full-scale pavement testing facility.
- Input Level: of eight studies reviewed, most studies selected the level of input detail based on data availability. None used level 1 inputs for all of the modules (i.e., traffic, climate, and material).
- The Number of Calibration and Validation Sections: all studies except Li et al. (2009) and Hoegh et al. (2010) adopted more than 30 calibration sections, which satisfied the AASHTO guidance for calibrating rutting (i.e. more than 20) and load-related cracking model (i.e., more than 30) (AASHTO, 2010).
- Experimental Factors for Calibration Sections: all eight studies reviewed except Hoegh et al. (2010) had a factorial design. Hoegh et al. (2010) used only a small number of MnRoad sections, which may have prevented the researchers from considering experimental factors.

The following tables present the other three common concerns (i.e., optimization approach, local calibration coefficients, and assessment of improved accuracy). These common concerns are presented respectively for each of distress prediction models: rutting (Table 2.4), bottom-up fatigue cracking (Table 2.5), and IRI models (Table 2.6). A summary is provided for each.

Table 2.4 Common concerns of recent studies on rutting model calibration

Author (Year)	Muthadi and Kim (2008)	Mallela et al. (2009)	Li et al. (2009)	Hoegh et al. (2010)	Hall et al. (2011)	Rah-man (2014)	Darter et al. (2014)	Haider et al. (2016)
Optimization Approach	Excel solver	Statistical software, varying coefficients	Varying coefficients	Prediction modification	Varying coefficients	N/A	Optimization using linear and non-linear regression techniques	Varying coefficients
Local Calibration Coefficients	βr1 = 1.02, βr2 = 1, βr3 = 1; βb = 1.5803; βs = 1.10491	βr1 = 1.07, βr2 = 1, βr3 = 1; βb = 0.01; βs = 0.4375	βr1 = 1.05, βr2 =1.109, βr3 = 1.1; βb = N/A; βs = 0	N/A	βr1 = 1.2, βr2 = 1, βr3 = 0.8; βb = 1; βs = 0.5	N/A	βr1 = 0.69, βr2 = 1, βr3 = 1; βb = 0.14; βs = 0.37	βr1 = 0.948, βr2 = 1.3, βr3 = 0.7; βb = 0.094; βs = 0.037
Assessment of Improved Accuracy	Graphic validation (i.e., predicted vs. measured plot), statistics (i.e., mean, R^2, and SSE), and statistical analysis (i.e., t-test and Chi-test)	Graphic validation (i.e., predicted vs. measured plot) and statistical analysis (i.e., paired t-test)	Graphic validation (i.e., distress vs. time plot)	Graphic validation (i.e., predicted vs. measured plot and distress vs. time plot)	Graphic validation (i.e., predicted vs. measured plot), and statistical analysis (i.e., t-test and F-test)	N/A	Graphic validation (i.e., predicted vs. measured plot), comparison of statistics (i.e., mean, R^2, and SEE), and statistical analysis (i.e., linear regression analysis and paired t-test)	Graphic validation (i.e., predicted vs. measured plot), comparison of statistics (i.e., bias and SEE), and statistical analysis (i.e., paired t-test)

N/A means "not applicable or not included in the documentation."

Summary of Table 2.4:

- Optimization Approach: the studies used different types of approaches: varying coefficients, Excel solver, statistical software, optimization using regression techniques, and prediction modification. Varying coefficients is a trial and error process based on attempting various coefficient values to obtain improved correlation of measured and predicted outcomes. Excel solver, statistical software, and optimization using regression techniques are model regression tools that were used to adjust calibration factors. The details of these tools and the criteria for evaluating coefficients were not documented. These tools were employed to optimize coefficients β_{r1}, β_b, and β_s (i.e., Muthadi and Kim, 2008, Mallela et al., 2009, and Darter et al., 2014). The coefficients β_{r1}, β_b, and β_s were regarded as constant multipliers, which accounted for a proportion of rutting assigned to each layer (i.e., AC, base, and subgrade rutting). Prediction modification (Hoegh et al., 2010) is a method which does not require varying calibration coefficients. It can be simply based on arithmetic operations (e.g., adding or subtracting a term) on existing predictions to reach the best match with field performance. Among these studies, the varying coefficients approach was used the most.

- Recommended Results: some similarities were found for those studies which provided relevant information. The values of calibration coefficients β_{r1}, β_{r2}, and β_{r3} ranged from 0 to 2, fairly close to the default value (i.e., 1). The values of coefficients β_b and β_s were smaller than 1, except for the study by Muthadi and Kim (2008). Since the coefficients β_b and β_s were regarded as constant multipliers, a value of less-than-one indicates that the calibrated models provided a reduction of rutting prediction compared to default prediction.
- Assessment of Improved Accuracy: a common practice was found among those studies: the improved model accuracy was assessed by graphic validation (i.e., scatter plots of predicted against measured rutting values) and statistical analysis (i.e., statistics or the Student's t-test). The statistics include the mean, bias, sum of squared error (SSE), R^2, or standard error of the estimate (SEE). The Student's t-test was to evaluate the difference between model predictions and in-field measurements.

Table 2.5 Common concerns of recent studies on bottom-up fatigue model calibration

Author (Year)	Muthadi and Kim (2008)	Mallela et al. (2009)	Li et al. (2009)	Hoegh et al. (2010)	Hall et al. (2011)	Rahman (2014)	Darter et al. (2014)	Haider et al. (2016)
Optimization Approach	Excel Solver	N/A	varying coefficients	N/A	Excel Solver	N/A	Optimization using linear and non-linear regression techniques	Varying coefficients
Local Calibration Coefficients	βf1 = 1, βf2 = 1, βf3 = 1; C1 = 0.437199, C2 = 0.150494, C4 = N/A	N/A	βf1 = 0.96, βf2 = 0.97, βf3 = 1.03; C1 = 1.071, C2 = 1, C4 = 6000	N/A	βf1 = N/A, βf2 = N/A, βf3 = N/A; C1 = 0.688, C2 = 0.294, C4 = 6000	N/A	βf1 = 249.009, βf2 = 1, βf3 = 1.233; C1 = 1, C2 = 4.5, C4 = 6000	βf1 = N/A, βf2 = N/A, βf3 = N/A; C1 = 0.5, C2 = 0.56, C4 = 6000
Assessment of Improved Accuracy	Graphic validation (i.e., predicted vs. measured plot), statistics (i.e., mean, R^2, and SSE), and statistical analysis (i.e., t-test and Chi-squared test)	N/A	Graphic validation (i.e., distress vs. time plot)	N/A	Graphic validation (i.e., predicted vs. measured plot), and statistical analysis (i.e., t-test and F-test)	N/A	Graphic validation (i.e., predicted vs. measured plot), comparison of statistics (i.e., mean, R^2, and SEE), and statistical analysis (i.e., linear regression analysis and paired t-test)	Graphic validation (i.e., predicted vs. measured plot), comparison of statistics (i.e., bias and SEE), and statistical analysis (i.e., paired t-test)

N/A means "not applicable or not included in the documentation."

Summary of Table 2.5:

- Optimization Approach: these studies used a range of types: Excel solver, optimization using regression techniques, and varying coefficients. However, the details of these tools and the criteria of evaluating coefficients were not documented.
- Recommended Results: some similarities were found among those studies which provided relevant information. The values of calibration coefficients β_{f1}, β_{f2} and $\beta_{f3,}$ were fairly close to the default value (i.e., 1) except the result (i.e., β_{f1} = 249.009) from Darter et al. (2014). The values of calibration coefficients C_1 and C_2 were fairly close to the default value (i.e., 1) except the result (i.e., C_2 = 4.5) from Darter et al. (2014). The default value of C_4 for all studies was not changed from 6000.

- Assessment of Improved Accuracy: a common practice was to illustrate improved model accuracy by graphic validation (i.e., scatter plots of predicted against measured bottom-up fatigue cracking values) and statistical analysis (i.e., statistics or the Student's t-test).

Table 2.6 Common concerns of recent studies on IRI model calibration

Author (Year)	Muthadi and Kim (2008)	Mallela et al. (2009)	Li et al. (2009)	Hoegh et al. (2010)	Hall et al. (2011)	Rahman (2014)	Darter et al. (2014)	Haider et al. (2016)
Optimization Approach	N/A	Statistical software, varying coefficients	N/A	N/A	N/A	N/A	Optimization using linear and non-linear regression techniques	Non-linear optimization
Local Calibration Coefficients	N/A	C1 = 17.7, C2 = 0.975, C3 = 0.008, C4 = 0.01	N/A	N/A	N/A	N/A	C1 = 1.2281, C2 = 0.1175, C3 = 0.008, C4 = 0.028	C1 = 32.3, C2 = 0.404, C3 = 0.006, C4 = 0.016
Assessment of Improved Accuracy	N/A	Graphic validation (i.e., predicted vs. measured plot) and statistical analysis (i.e., paired t-test)	N/A	N/A	N/A	N/A	Graphic validation (i.e., predicted vs. measured plot), comparison of statistics (i.e., mean, R^2, and SEE), and statistical analysis (i.e., linear regression analysis and paired t-test)	Graphic validation (i.e., predicted vs. measured plot), comparison of statistics (i.e., bias and SEE), and statistical analysis (i.e., paired t-test)

N/A means "not applicable or not included in the documentation."

Summary of Table 2.6:

- Optimization Approach: three types of approaches were adopted among studies which provided relevant information: statistical software and varying coefficients, optimization using regression techniques, and non-linear optimization. However, the detail of how to use these tools and the criteria of evaluating coefficients were not documented.
- Recommended Results: little similarity was found among studies which provided relevant information. The value of C_3 for all studies was fairly close to the default value (i.e., 0.008).

- Assessment of Improved Accuracy: the studies illustrated the improved model accuracy by graphic validation (i.e., scatter plots of predicted against measured IRI values) and/or statistical analysis (i.e., statistics or the Student's t-test).

Among the eight recent studies, local calibration on the three investigated models (i.e., rutting, bottom-up cracking, and IRI) was found and examined. A summary of the models attempted and improved is shown in Table 2.7.

Table 2.7 Model improvement through local calibration

Author (Year)	Muthadi and Kim (2008)	Mallela et al. (2009)	Li et al. (2009)	Hoegh et al. (2010)	Hall et al. (2011)	Rahman (2014)	Darter et al. (2014)	Haider et al. (2016)
Models Attempted	Rutting and Cracking	Rutting and IRI	Rutting and Cracking	Rutting	Rutting and Cracking	N/A	Rutting, Cracking, and IRI	Rutting
Models Improved	Rutting and bottom-up cracking	Rutting and IRI	Rutting and bottom-up cracking	Rutting	Rutting and bottom-up cracking	N/A	Rutting, Cracking, and IRI	Rutting
Before Calibration	Rutting: SEE_{before} = 0.154 in.; Cracking: SEE_{before} = 6.02%	Rutting: SEE_{before} = 0.11 in., IRI: SEE_{before} = 13.2 in./mile	N/A	N/A	N/A	N/A	Rutting: SEE_{before} = 0.31 in.; Cracking: SEE_{before} = 14.3 %; IRI: SEE_{before} = 18.7 in./mile	SEE_{before} = 0.353 in.
After Calibration	Rutting: SEE_{after} = 0.109 in.; Cracking: SEE_{after} = 3.64%	Rutting: SEE_{after} = 0.05 in., IRI: SEE_{after} = 12.8 in./mile	N/A	N/A	N/A	N/A	Rutting: SEE_{after} = 0.11 in.; Cracking: SEE_{after} = 14.8 %; IRI: SEE_{after} = 8.7 in./mile	SEE_{after} = 0.085 in.

N/A means "not applicable or not included in the documentation."

To summarize, there were seven common concerns among the eight studies briefed.

1. Data source

2. Input level

3. Number of calibration and validation sections

4. Experimental factors

5. Optimization approach

6. Recommended results

7. Assessment of improved accuracy

These concerns are crucial for a M-E design calibration study. The data source indicates much information about calibration data, regarding representativeness, consistency, and compatibility. The input level suggests the level of detail and certainty of data. The number of calibration and validation sections quantifies the size of calibration dataset. The experimental factors explain the division of experimental sections into groups to account for various design conditions. The optimization approach refers to the method of calibration coefficient “trial-and-error” process, which governs the complexity of the process and the robustness of optimal calibration coefficients. The recommended results summarize the recommended calibration coefficients. The assessment of improved accuracy explains how the study measures the improvement in model accuracy.

2.5 Automation

The automation concept was very little documented in pavement research literature. Historically, the term “automation” was not widely used until 1947 when General Motors established automation department. The term was to represent control systems for operating equipment with minimal or reduced human intervention. The benefits of automation are 1. increased productivity. 2. extended working hours. 3. labor, energy, and materials savings. 4. improved quality, accuracy, and precision.

For pavement researchers, local calibration studies are labor-intensive and time-consuming as many human interactions are needed to populate the software with trial calibration coefficients and extract performance predictions after software simulations. For example, say an experiment has six levels for full factorial fatigue calibration. Then, there would be totally 216 (6 x 6 x 6) sets of coefficients for trial simulation runs. For 30 experimental sections, there would be 6,480 simulation runs in total. If 10 minutes of human interaction is needed per run, there would be at least 45 days of human interaction needed. In addition to human interaction, the software simulation itself takes a large amount of time for each run. A 20-year pavement design takes about 20 minutes for the software to perform simulation, amounting to 90 days of software running. It would take longer than 90 days if software runs are not operated on a continuous basis. The investment in human interaction and frequent software run is a big problem. Table 2.8 summarizes software runs demanded by some previous studies.

Table 2.8 Time investment for software runs in calibration studies

Investigators	Number of MEPDG Runs	Estimated Execution Time per Run	Total Execution Time Required	Automation Tool
Velasquez et al. (2009)	> 202,664	N/A	N/A	N/A
ARA (2004)	4,896	30 minutes /run	102 days	N/A
Guo and Timm (2015)	> 172	3 minutes /run	> 22 days	Macro Recorder Software

N/A means "not applicable or not included in the documentation."

Some researchers have thought of some ideas to minimize the human interaction with the design software and facilitate software runs. Some used computer programs to automate repetitive interactions with the software and the process of compiling prediction results. Schram and Abdelrahman (2010) suggested that macro software may be used for reading data from a spreadsheet and entering the data into the correct MEPDG menu. Excel macros can be easily adapted to retrieve the performance predictions for each distress and store them in a single spreadsheet automatically. Jadoun and Kim (2012) mentioned the use of macro recorder software and MATLAB to avoid repetitive manual running of MEPDG analysis. Guo (2013) implemented the concept of automation in local calibration, which utilized macros to populate the software with trial calibration coefficients and execute repetitive software running automatically. In this study, an automation method was adopted to interact with the AASHTOWare^{TM} Pavement ME Design software.

In summary, this chapter reviewed literature. The Pavement ME Design software and the performance prediction model were explained. The seven common concerns (i.e., data source, input level, the number of calibration and validation sections, experimental factors, optimization approach, recommend results, and assessment of improved accuracy) were recognized as key topics for an M-E design calibration study. The automation concept was introduced and previous relevant studies were reviewed.

Chapter 3 Methodology

Based on the literature review, the methodology for this study was devised. The seven key topics identified in Chapter 2 are firstly addressed for this study. Then, the dataset from NCAT is described regarding materials, traffic, climate, and measured data. The specific inputs to the AASHTOWare^{TM} Pavement ME software are compiled in Appendix A. Next, the evaluation and calibration process is described.

The seven key topics are addressed in Table 3.1 for this study, thereby illustrating the methodology. 31 newly-constructed flexible pavements were investigated: 80% were used for both the evaluation and local calibration, and the remaining 20% for the validation. No experimental factors were considered due to the simplicity of the local scenario (i.e., single traffic and single environment condition).

Table 3.1 Seven key topics addressed for this study

Data Source	Input Level	Number of Calibration and Validation Sections	Experimental Factors	Optimization Approach	Recommended Results	Assessment of Improved Accuracy
NCAT database (Test Track and laboratory)	Material (AC: level 1; unbound materials: level 3); traffic (level 1); climate (locally determined)	A total of 31 sections. 80% for calibration and 20% for validation	N/A	Varying coefficients, Excel Solver, and automation software	Included in Chapter 4	Graphic validation (i.e., predicted vs. measured plot), comparison of statistics (i.e., bias, standard error of the estimate (SEE) and SSE), and statistical analysis (i.e., Student's t-test)

N/A means "not applicable or not included in the documentation."

3.1 NCAT database

The NCAT database was obtained from testing performed at the Test Track and in the laboratory. The Test Track is a 1.7-mile full-scale pavement testing facility located in Opelika, Alabama. It is primarily devoted to asphalt pavement research since 2000, generating ample data with reliability and consistency. Divided into 46 sections, the track is designed and built to observe and evaluate innovative pavement technologies. Sections are sponsored on three-year cycles. In each cycle, sections are subject to approximately 10 million equivalent single-axle loads (ESALs) of traffic loading in two years; meanwhile, the pavement performance and environmental conditions are monitored throughout the traffic loading. Some of these sections are referred to as “structural sections,” and are instrumented with strain sensors and pressure plates to capture dynamic pavement response under loads (Timm, 2009). The structural sections from four research cycles (i.e., 2003, 2006, 2009, and 2012) were used as the experimental sections. The NCAT laboratory is a pavement material testing facility located in Auburn, Alabama. It is equipped to perform all routine mix design, quality control, and advanced materials characterization tests for asphalt binders and mixtures. Data from the Test Track and the laboratory were available to prepare software inputs (i.e., as-built materials characterization, traffic loading characterization, climate characterization) and distress measurements. Each category of program inputs is described and discussed in the following sections.

3.1.1 Material characterization

The 31 investigated experimental sections (summarized in Table 3.2) feature real-world pavement cross-sections with a range of advanced and conventional asphalt materials. Some sections contained unique base and subgrade materials.

Table 3.2 Investigated experimental sections

<table>
<tr><th></th><th>Number of Structural Sections</th><th>Number of Experimental Sections</th><th colspan="5">Sections Sustaining More Than One Cycle</th></tr>
<tr><td>2003 Cycle</td><td>8 (Figure 3.1)</td><td>8</td><td rowspan="3">Section N3 and N4</td><td rowspan="2">Section N5, N6, and N7</td><td></td><td></td><td></td></tr>
<tr><td>2006 Cycle</td><td>11 (Figure 3.2)</td><td>6</td><td rowspan="2">Section N1 and N2</td><td rowspan="3">Section N8 and N9</td><td></td></tr>
<tr><td>2009 Cycle</td><td>16 (Figure 3.3)</td><td>10</td><td></td><td rowspan="2">Section N7, N10, N11, S8 through S11</td></tr>
<tr><td>2012 Cycle</td><td>16 (Figure 3.4)</td><td>7</td><td></td><td></td><td></td></tr>
</table>

Eight of the 31 experimental sections were from the 2003 cycle (Figure 3.1) which had the same subgrade soil and 6-inch crushed aggregate base. The subgrade soil, commonly termed the “Track Soil,” was classified as an AASHTO A-4(0) soil (silt material). Their AC configurations are described as follows:

- N1 through N6 were built in a pairwise manner such that each pair had the same total AC thickness. However, one section within each pair was produced with a modified asphalt binder (i.e., Performance Grade (PG) 76-22) while the other was produced with an unmodified binder (i.e., PG 67-22).
- N7 was surfaced with a wearing layer made with PG 76-22 stone matrix asphalt (SMA).
- The N8 surface course was also a PG 76-22 SMA but had a PG 67-22 “rich bottom” layer with an additional 0.5% binder.

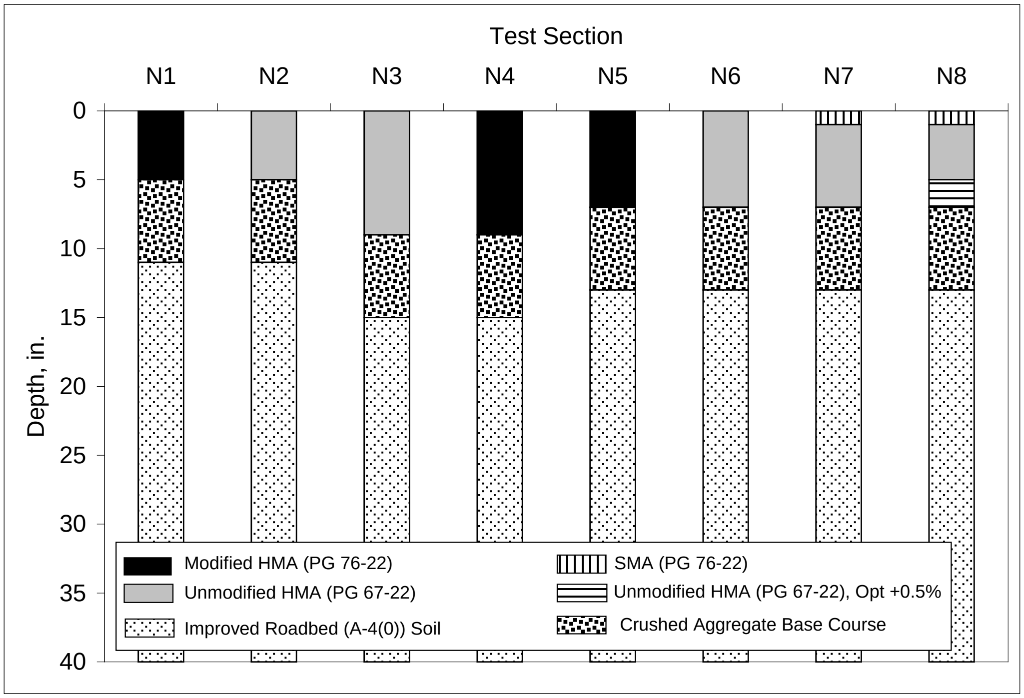

Figure 3.1 Cross-sections of 2003 structural sections (Timm and Priest, 2006)

Six of the 31 experimental sections were from the 2006 cycle (Figure 3.2). Though there were eleven structural sections in the 2006 cycle, five of them (i.e., N3 through N7) were structurally healthy by the end of the last cycle, so these five were given minor maintenance (i.e., milling and overlay) or just left-in-place for the next cycle (shown in Table 3.2). These five are not analyzed because of discontinuous traffic applications (i.e., two-year's loading and one-year's rest, followed by two-year's loading) that cannot be directly simulated in the Pavement ME Design software. The six newly-built structural sections are described as follows:

- N1 and N2 were pavement structures for the Florida DOT. N1 and N2 both used 10 inches of limerock, rather than crushed granite aggregate, as the base material. N1 had three lifts of AC with unmodified PG 67-22 binder, while the upper two lifts in N2 contained SBS-modified PG 76-22 binder.

- N8 and N9 featured two structures for the Oklahoma DOT. N8 included a surface course of PG 76-28 SMA, a lift of PG 76-28 AC, a lift of PG 64-22 AC, and a base lift of PG 64-22 AC. The base lift was designed at 2% air voids ("rich-bottom") to improve resistance to bottom-up fatigue cracking. N9 had the same set of materials as N8 but included an extra lift of PG 64-22 Superpave AC that increased the overall AC thickness.
- N10 was a pavement structure for the Missouri DOT. It was built with Missouri Type 5 aggregate base, which is a dolomitic limerock base material. The upper AC layers were one lift of PG 64-22 AC and two lifts of PG 70-22 AC.
- S11 was a pavement structure for the Alabama DOT. It consisted of two upper lifts with modified AC (i.e., PG 76-22) and two lower lifts with unmodified AC (i.e., PG 67-22).

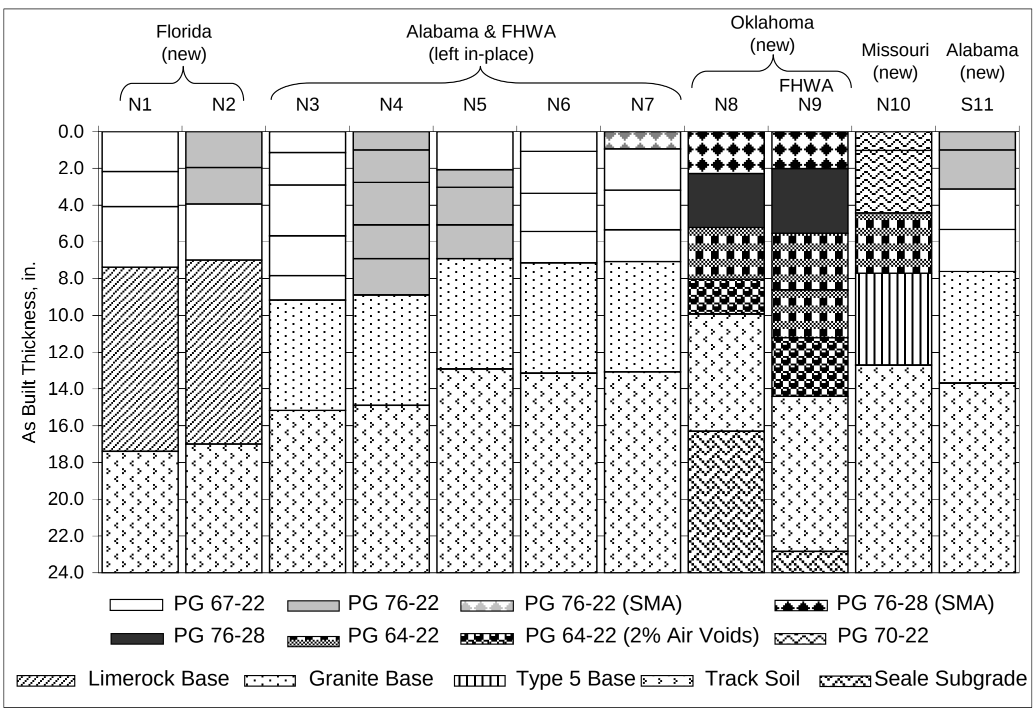

Figure 3.2 Cross-sections of 2006 structural sections (Timm, 2009)

Ten of the 31 experimental sections were from the 2009 cycle (Figure 3.3). Though there were sixteen structural sections in the 2009 cycle, two of them (i.e., N8 and N9) were from the 2006 cycle, and four of them (i.e., N1 through N4) were from the 2003 cycle (shown in Table 3.2). They were given minor maintenance or just left-in-place. Due to discontinuous traffic application, they were not analyzed. The ten newly-built structural sections had the same "Track Soil" as subgrade and 6-inch crushed aggregate as a base. Their AC configurations are described as follows:

- N5 and N6 both contained Thiopave® technology, a method of using sulfur as a binder replacement (Timm et al., 2012). N5 had 9 inches of AC, including a wearing course of PG 76-22 HMA, two lifts of 40% Thiopave® AC, and a bottom lift of 30% Thiopave mixture. N6 had 7 inches of AC layer that had the same set of materials as N5, but it had only one lift of 40% Thiopave® mixture.
- N7 had 6-inch AC including three lifts of highly polymer modified asphalt mixture sponsored by Kraton.
- The remaining sections were a comparative study between virgin AC and 50% reclaimed asphalt pavement (RAP) mixtures, Warm Mix Asphalt (WMA), and Open Graded Friction Course (OGFC). S9 was the virgin mixture control section. N10 and N11 used 50% RAP in all of the AC mixtures. However, N10 used HMA while N11 used WMA. S8 uniquely had a surface lift of OGFC, a base lift of PG 76-22 AC, and an intermediate lift of PG 67-22 AC. S10 and S11 both used WMA: S10 used a foam technique while S11 used chemical additives. S12 used 25% Trinidad Lake Asphalt (TLA) pellets in the AC layers. This section was sponsored by Lake Asphalt of Trinidad and Tobago Ltd.

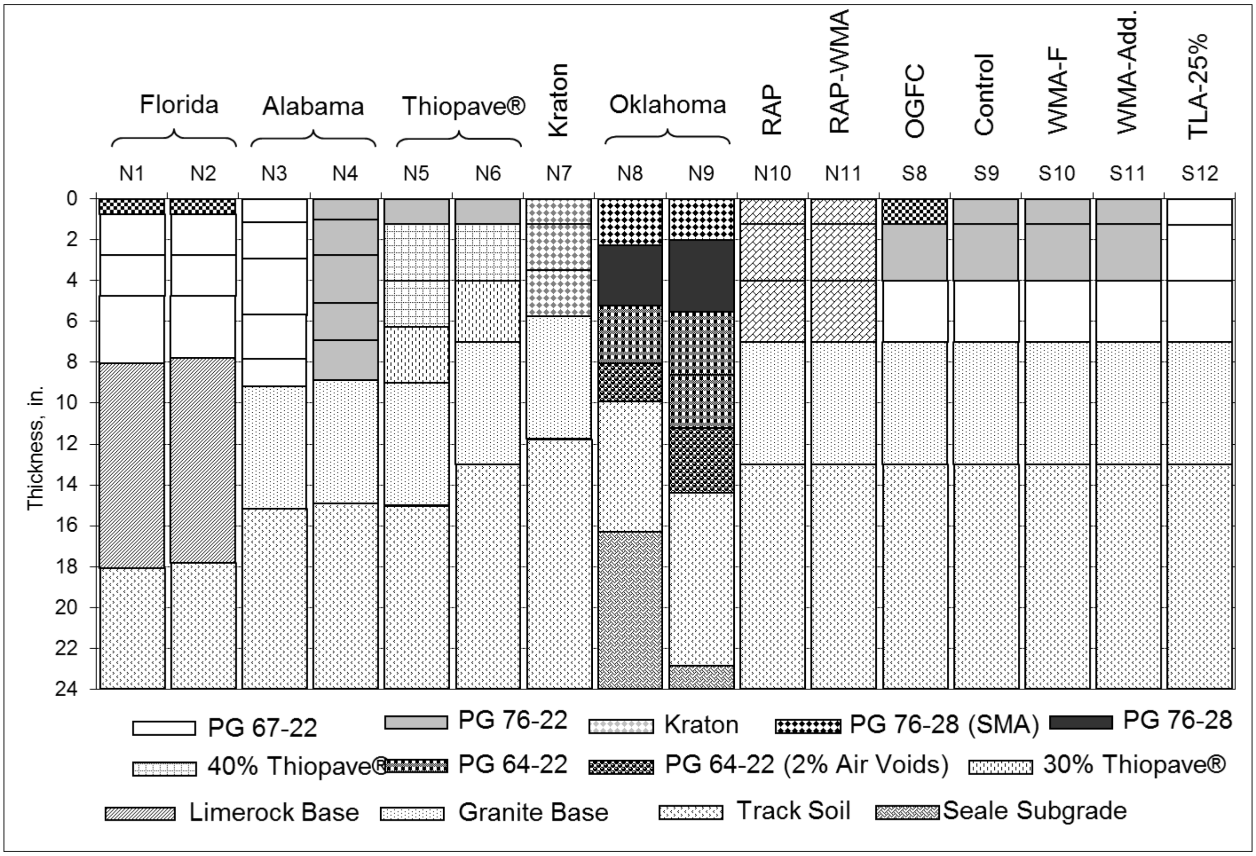

Figure 3.3 Cross-sections of 2009 structural sections (courtesy of David Timm)

Seven of the 31 structural sections were from the 2012 cycle (Figure 3.4). Though there were sixteen structural sections in the 2012 cycle, seven of them (i.e., N7, N10, N11, and S8 through S11) were from the 2009 cycle, and two of them (i.e., N8 and N9) were from the 2006 cycle (shown in Table 3.2). Due to discontinuous traffic application, they were not analyzed. The seven newly-built sections had the same "Track Soil" subgrade and crushed aggregate base. Their AC configurations are described as follows:

- N3, N4, and S12 used the cold-central-place recycling (CCPR) technology for the bottom lift of the AC pavement. N3 had a 6-inch granular base and four lifts of AC layers: a surface lift of SMA, two intermediate lifts of Superpave AC, and a bottom lift of CCPR with foamed asphalt. N4 had three AC lifts: a top lift of SMA, an intermediate lift of Superpave AC, and a bottom lift of CCPR with foamed asphalt. S12 had full depth reclamation (FDR) base and three AC lifts: a top lift of SMA, an intermediate lift of Superpave AC, and a bottom lift of foamed asphalt.

- N5, S5, S6, and S13 were named the "Green Group" sections due to the use of sustainable materials technologies. N5 consisted of three AC lifts: a surface lift of PG 67-22 AC (20% RAP), an intermediate lift of PG 67-22 AC (35% RAP), and a bottom lift of PG 67-22 AC (35% RAP). S5 had the same granular base and the same top lift of AC as N5. However, S5 has a top lift of PG 88-22 AC (25% RAP), and a bottom lift of PG 88-22 AC (35% RAP). S6 had three AC lifts: a top lift of PG 76-22 AC (25% RAP), an intermediate lift of PG 67-22 AC (35% RAP+5% RAS), and a bottom lift of PG 76-22 AC (25% RAP). S13 had three AC lifts: a top lift of SMA with ARB-12 (i.e., Ground Tire Rubber (GTR) accounted for 12% of the weight of asphalt), an intermediate lift of AC containing 35% RAP and ARB-12, and a bottom lift of AC with ARB-20.

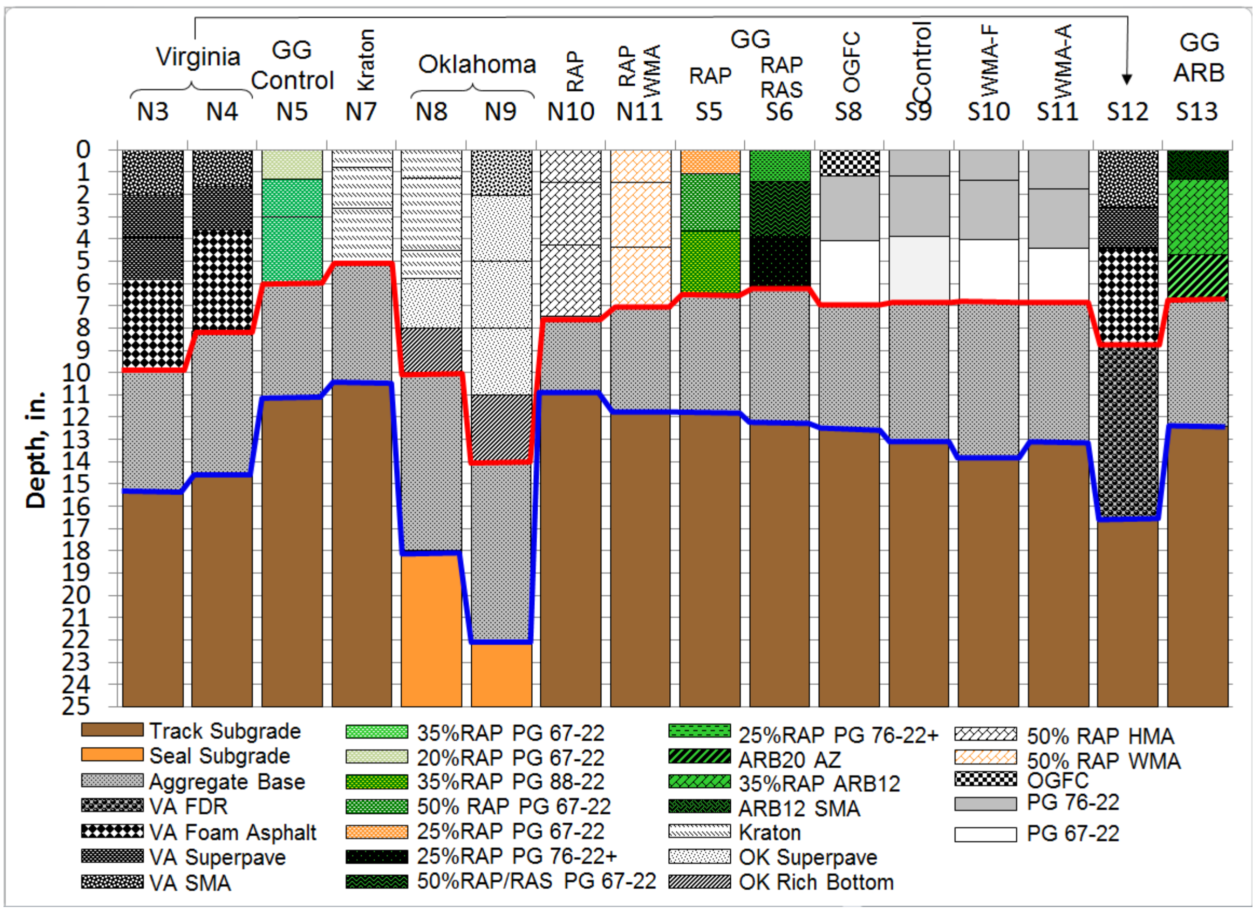

Figure 3.4 Cross-sections of 2012 structural sections (courtesy of David Timm)

The AC dynamic modulus of these experimental sections was determined in the laboratory by reheating and compacting plant-produced mixtures at the time of construction. Testing of dynamic modulus (E*) for the 2003 mixtures was conducted at Purdue University (Timm and Priest, 2006) while the 2006, 2009, and 2012 mixtures were tested at NCAT under the guidance of AASHTO TP 62-07 (Robbins, 2013). In both cases, the binder properties, characterized by the dynamic shear modulus (G*) and phase angle (δ), were determined by dynamic shear rheometer according to AASHTO T315-06. Also, the as-built volumetric properties were provided by construction records. The unbound materials resilient moduli were determined by the falling weight deflectometer (FWD) test data and theoretical calculation. The resilient moduli were only characterized at input level 3 defined by the software. Level 1 was not used because it required material properties to execute finite element analysis not measured in this investigation. Level 2 was not used because it relied on correlations from tests other than direct measurement of the modulus. For the 2003 sections, the resilient moduli were backcalculated based on the falling weight deflectometer (FWD) test data (Guo, 2013). For the 2006, 2009, and 2012 sections, the base and subgrade moduli were derived by theoretical calculation, which is to use measured vertical pressures in the base and subgrade layers combined with laboratory triaxial testing to establish representative moduli for each material (Taylor and Timm, 2009). More details about the theoretical calculation of resilient moduli can be found in the author's master's thesis (Guo, 2013). The inputs for the Pavement ME Design software are compiled in detail in Appendix A.

3.1.2 Traffic loading characterization

For each experimental section, traffic loading was applied to accumulate 10 million ESALs in a two-year phase. The truck fleet was run at an average speed of 45 mph, and operated 16 hours a day, five days a week. There were fluctuations in hourly traffic volume due to work shift changes, truck refuels, driver breaks, and maintenance stops (Guo, 2013). There was no significant fluctuation in daily traffic volume. There was no monthly and yearly growth in traffic volume. In the 2003 cycle, five of the trucks, termed “triple trailers”, consisted of a steering axle, a tandem axle, and five trailing single axles (Figure 3.5). The sixth truck, termed “box trailer”, consisted of a steer axle and two tandems (Figure 3.6). In the 2006, 2009, and 2012 cycle, only five triple trailers were used to apply traffic loads. The daily traffic volume was determined based on drivers’ logs. More details about traffic characterization can be found in the author’s master’s thesis (Guo, 2013). The inputs for the Pavement ME Design software are compiled in detail in Appendix A.

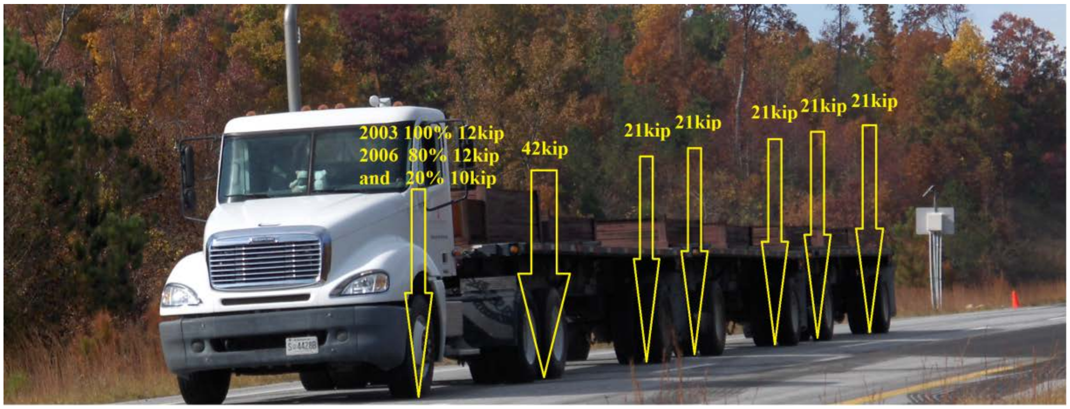

Figure 3.5 Triple trailer truck (Guo, 2013)

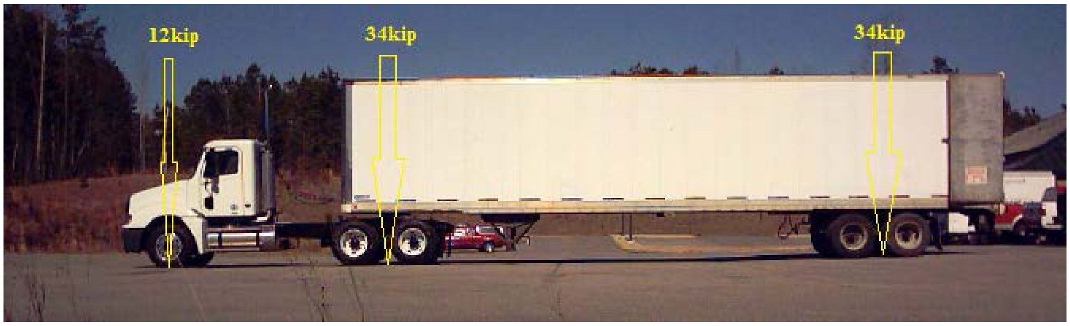

Figure 3.6 Box trailer truck (Guo, 2013)

3.1.3 Climate characterization

The Test Track is located in Opelika, Alabama, whose climate is classified as humid subtropical. This type of climate is marked by mild winters, early springs, long and hot summers, and warm autumns. The monthly average temperatures range from a high of 90°F to a low of 33°F in a year (“U.S. climate data,” 2017). The average yearly precipitation is 55 inches. The climate of Test Track can be seen as a representative of the climate of many Southeastern states. Table 3.3 provided general climate information of some Southeastern states.

Table 3.3 Climate information of southeastern states ("Alabama geography from Netstate," 2016)

State	Alabama	Arkansas	Mississippi	Georgia	South Carolina
Climate Type	humid subtropical	humid subtropical	humid subtropical	humid subtropical	humid subtropical
Monthly Average Temperatures Range	High: 91.5°F Low: 30.0°F	High: 93.6°F Low: 26.6°F	High: 92.5°F Low: 34.9°F	High: 92.2°F Low: 32.6°F	High: 91.9°F Low: 31.2°F
Average Yearly Precipitation Range	56 inches	From 40 to 60 inches	From 50 to 61 inches	From 45 to 75 inches	From 40 to 80 inches

The climate of the Test Track was monitored hourly by a weather station (Figure 3.7) installed near the track. The information (including time, temperature, wind speed, solar energy, precipitation, and relative humidity) was compiled into climate input files needed by the AASHTOWare Pavement ME software. The procedure of compiling input files was introduced in the author's master's thesis (Guo, 2013). The general climate information is compiled in Appendix A.

Figure 3.7 Test Track on-site weather stations (Guo, 2013)

3.1.4 Distress measurements

The test sections at the Test Track gradually deteriorated in structural integrity and rideability. The pavement surface was inspected weekly. Once a distress (i.e., rutting and cracking) was found, it was quantified. Rut depths of both inside and outside wheelpaths were measured by an Automatic Road Analyzer (ARAN) van. Only the total rutting was measured in the field. Crack maps were generated for each test section. The percentage of the cracking area over the total lane was computed. Limited coring or trenching was used to identify whether cracking was bottom-up or top-down (only the bottom-up cracking is investigated in this study). IRI was also measured by the ARAN van. The measurement data are compiled in detail in Appendix A.

3.2 Evaluation, calibration, and validation process

With the material, traffic, and climate inputs, a design project was created in the AASHTOWare™ Pavement ME Design software v2.0 for each experimental test section. Based on these design projects, the evaluation, local calibration, and validation were performed on the software models.

The initial evaluation compared software predictions using the nationally-calibrated models against in-situ distress measurements. 80% of 31 experimental sections are randomly selected for this purpose (refer to Appendix B). The differences between model predictions and measurements were quantified by computing statistics (e.g., Sum of Squared Error (SSE)) and performing paired two-sample student's t-test. The SSE was calculated using equation (9). Since evaluations were meant to examine predictions from the nationally-calibrated models, the calibration coefficients in these models were set as default.

$$SSE = \sum_{\mathrm{n}=1}^{\mathrm{B}} \sum_{m=1}^{A} (\text{predicted value} - \text{measured value})^2 \tag{9}$$

where,

m = the mth measurement (A is the total number of monthly measurements)

n = the nth experimental section (B is the total number of experimental sections)

The local calibration was meant to reduce the SSE between model predictions and measurements by optimizing or adjusting local calibration coefficients. The coefficient optimization of the SSE can result in the optimization of bias and SEE simultaneously. The optimization attempted a range of trial calibration coefficients that covered many possible values for each coefficient. The ranges of trial coefficients are presented below for the rutting, bottom-up fatigue cracking, and IRI models. The same dataset as the evaluation was used for this purpose.

3.2.1 Rutting model

For the rutting model, the calibration coefficients were the β_{r1}, $\beta_{r2,}$ and β_{r3} in the AC rutting model (Equation (1) in Chapter 2), β_b in the base rutting model (Equation (2) in Chapter 2), and β_s in the subgrade model (Equation (2) in Chapter 2). However, only coefficients β_{r2} and β_{r3} needed to be attempted for the Pavement ME Design software runs. The other coefficients, β_{r1}, $\beta_{b,}$ and β_s were regarded as constant multipliers, which assign weights to each component of pavement rutting: AC rutting, base rutting, and subgrade rutting. Thus, the calculation involving these coefficients is a known linear formula which does not require running the software. The optimization attempted a range of values for β_{r2} and β_{r3} for the software runs and subsequently calculated β_{r1}, $\beta_{b,}$ and β_s using Microsoft Solver. The trial values of β_{r2} and β_{r3} are shown in Table 3.4. There was an 8*8 matrix for the software runs. The upper and lower limits were tentatively set to cover the range of local calibration coefficients mentioned or the values recommended by previous studies (i.e., ARA, 2004; Muthadi and Kim, 2008; Li et al., 2009; Banerjee et al., 2009; Glover and Mallela, 2009; Hall et al., 2011; Rahman et al., 2013; Darter et al., 2014) and meanwhile, they were selected based on a principle mentioned in the following paragraph. The intervals for these trial values were selected to produce as many trial values as feasible. The optimal calibration coefficients were the set of coefficients that provided the highest SSE reduction. The SSE results from each set of coefficients are compiled in Appendix C.

Table 3.4 Trial values of coefficients (rutting)

β_{r2}	β_{r3}
0.05	0.05
0.1	0.1
0.25	0.25
0.5	0.5
1	1
2	2
4	4
8	8

8 (β_{r2}) * 8 (β_{r3}) = 64 sets of trial values

Since the searching of the optimal coefficients has no constraints theoretically, the selection of upper and lower limits of trial values can influence the effectiveness of coefficient optimization. According to the monotonic principle of rutting model (i.e., the prediction varies in a way that it either never increases or never decreases with the change of a calibration coefficient), it was assumed that the selected set of trial coefficients (β_{r2} = 0.05 and β_{r3} = 0.05) would produce the lowest rutting predictions if the remaining coefficients (i.e., $\beta_{r1,}$ $\beta_{b,}$ and β_s) were set as the default (see the rutting model in Chapter 2), whereas the set (β_{r2} = 8 and β_{r3} = 8) would produce the highest predicted rutting. The prediction results from the software runs were shown in Figure 3.8, verifying the assumption based on the monotonic principle. The two sets of trial coefficients (hitting the upper and lower limits) defined the boundary of searching. Although the two extreme cases do not lead to the optimal calibration coefficients, the locations of data points (indicating the distress level and density of data points) for the two extreme cases were set to roughly "bound" or "encompass" the equality line (i.e., the 45° line). The remaining coefficients (i.e., $\beta_{r1,}$ $\beta_{b,}$ and β_s) then had an easy chance to shift the locations of data points closer to the equality line due to their roles of "constant multipliers." Since it was expected that some set of coefficients between the two cases would be the optimal set of trial coefficients. Obviously, the appropriate selection of upper and lower limits increased the probability of successful searching for the optimal coefficients.

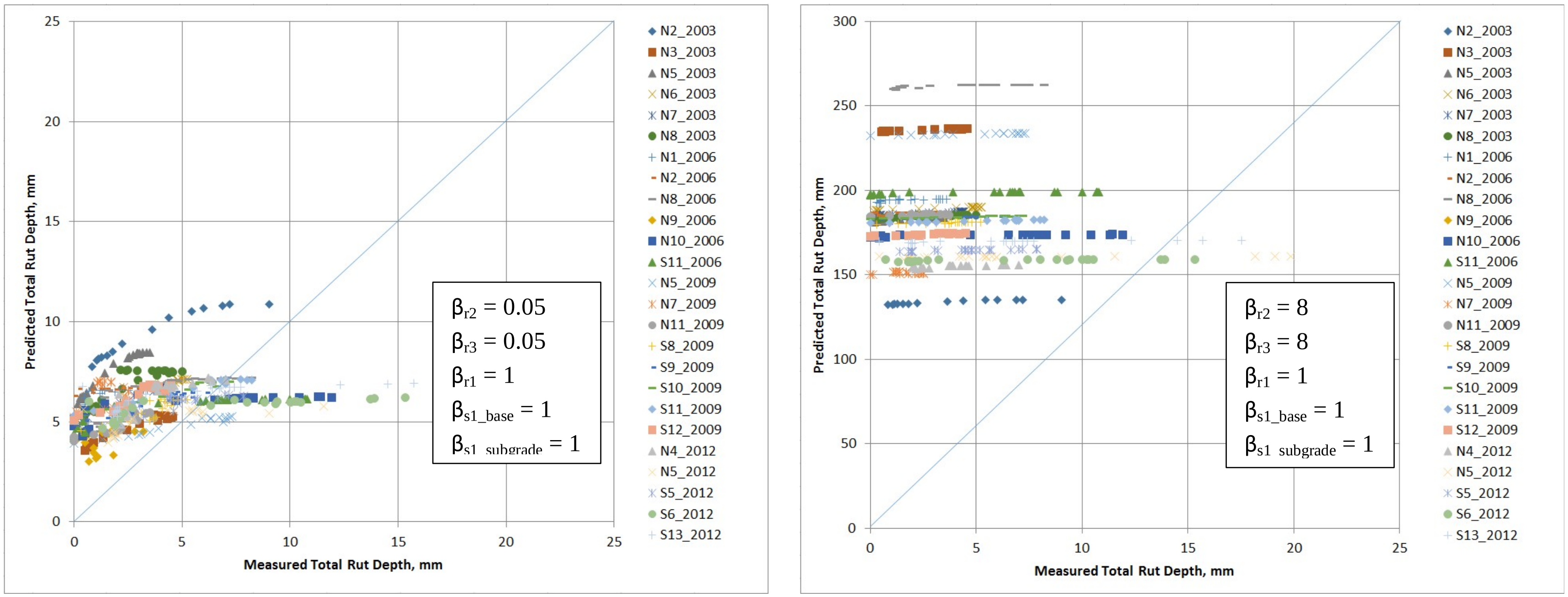

Figure 3.8 “Lowest and highest” prediction illustrations

3.2.2 Bottom-up fatigue cracking model

For the bottom-up fatigue cracking model, the calibration coefficients include β_{f1}, β_{f2}, and β_{f3} in the fatigue accumulation model (Equation (3) in Chapter 2), and C_1, C_2, and C_4 in the cracking conversion model (Equation (6) in Chapter 2). However, only coefficients β_{f1}, β_{f2}, and β_{f3} needed to be attempted for the software runs. The C_1, C_2, and C_4, were regarded as constant multipliers, just like β_{r1}, $\beta_{b,}$ and β_s in the rutting model. Therefore, the optimization attempted a range of values for β_{f1}, β_{f2}, and β_{f3} (phase_1), and then calculated C_1, C_2, and C_4 by Microsoft Solver (phase_2). The searching range could be very large for bottom-up fatigue cracking model considering that three coefficients needed to be attempted for the software runs, so the optimization should attempt a reasonable number of coefficient sets and adopt “pick the best from the attempted” strategy. Under this strategy, there were three rounds during optimization:

The first round aimed to reach the “boundary” or extreme cases (significant over-prediction and under-prediction). The optimal coefficients would be found within the “boundary.” In Figure 3.9, the left is an illustration of under-prediction (data points are dispersed near the line of “prediction = 0 %”), and the right is an illustration of over-prediction (data points are lined up on the line of “prediction = 100 %”).

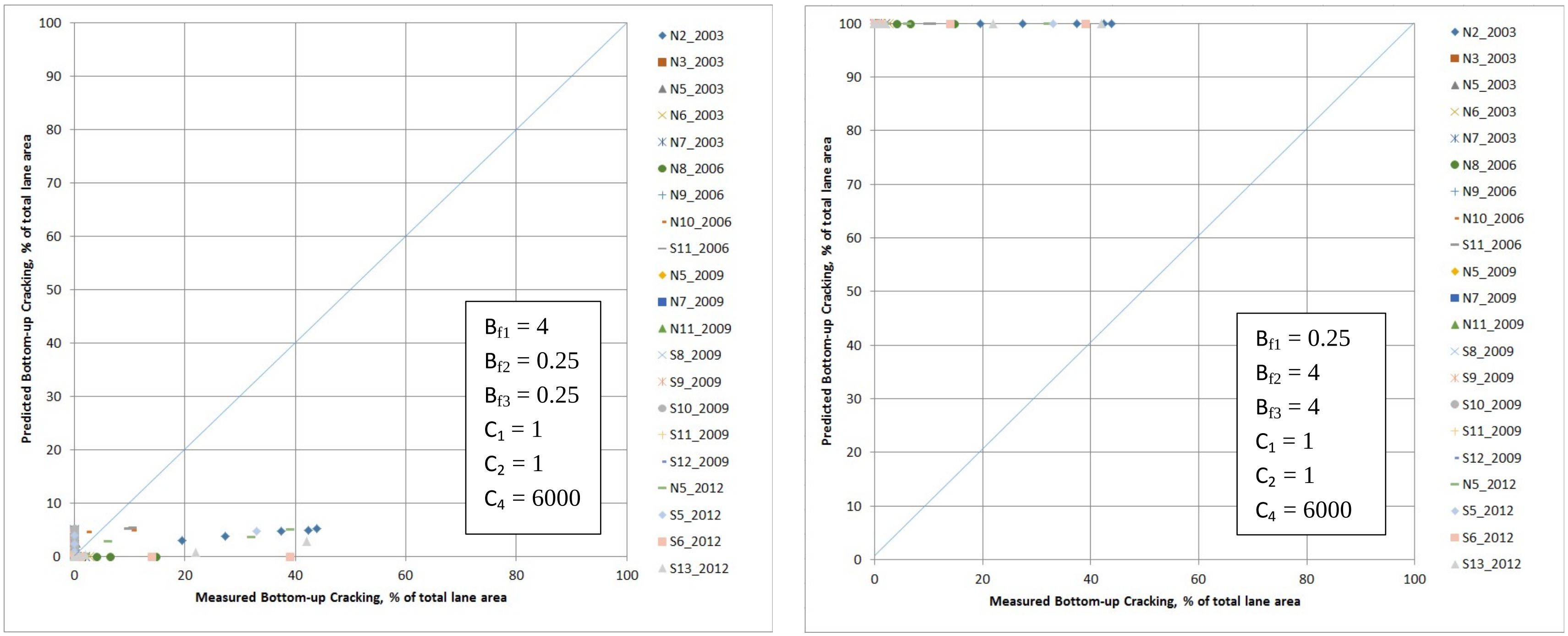

Figure 3.9 “Boundary” cases illustrations

The second round aimed to seek the "inflection point" within the boundary. The "inflection point" was a set of coefficients that produced the highest reduction of SSE. The upper and lower limit were tentatively selected to cover the range of local calibration coefficients recommended by many previous studies (i.e., ARA, 2004; Muthadi and Kim, 2008; Li et al., 2009; Hall et al., 2011; Rahman et al., 2013; Darter et al., 2014). Li et al. (2009) suggested that the SSE was more sensitive to a change of coefficients β_{f1} and β_{f2} than a change of β_{f3}, so the intervals for coefficients β_{f1} and β_{f2} were set to be smaller than β_{f3}. In this round, three matrices of trial coefficients (i.e., round 2 (a), (b), and (c)) were attempted for the software runs.

The third round sought sets of coefficients near the "inflection point" that lead to the higher SSE reduction. The optimal calibration coefficients were the set of coefficients that enabled the highest SSE reduction through these rounds of optimization.

Table 3.5 Trial values of coefficients – round 1 (bottom-up fatigue cracking)

β_{f1}	β_{f2}	β_{f3}
0.25	0.25	0.25
1	1	1
4	4	4

<u>3</u> (β_{f1}) * <u>3</u> (β_{f2}) * <u>3</u> (β_{f3}) = <u>27</u> sets of trial values

Table 3.6 Trial values of coefficients – round 2 (bottom-up fatigue cracking)

β_{f1}	β_{f2}	β_{f3}
0.5	0.5	0.5
0.7	0.7	0.9
0.9	0.9	1.3
1.1	1.1	1.7
1.3	1.3	2.1
1.5	1.5	2.5

Round 2 (a): <u>6</u> (β_{f1}) * <u>6</u> (β_{f2}) * <u>6</u> (β_{f3}) = <u>216</u> sets of trial values

β_{f1}	β_{f2}	β_{f3}
0.5	0.25	0.25
2	1	1
2.1	4	4
3		

Round 2 (b): <u>4</u> (β_{f1}) * <u>3</u> (β_{f2}) * <u>3</u> (β_{f3}) = <u>36</u> sets of trial values

β_{f1}	β_{f2}	β_{f3}
1.5	1	1
1.8		
2.2		
2.5		

Round 2 (c): 4 (β_{f1}) * 1 (β_{f2}) * 1 (β_{f3}) = 4 sets of trial values

Table 3.7 Trial values of coefficients – round 3 (bottom-up fatigue cracking)

β_{f1}	β_{f2}	β_{f3}
2.1	0.9	0.9
2.2	1	1
2.3	1.1	1.1

3 (β_{f1}) * 3 (β_{f2}) * 3 (β_{f3}) = 27 sets of trial values

3.3.3 IRI model

For the IRI model (Equation (7) in Chapter 2), the calibration coefficients included C_1, C_2, C_3, and C_4. These coefficients were regarded as constant multipliers. Each describes a linear correlation between pavement distress or site factor with the IRI prediction. Therefore, the optimization for these coefficients was obtained by through running Excel Solver. Since a positive linear correlation was widely seen in the IRI models for different material types (ARA, 2004), when running Excel Solver the lower limit for these coefficients was zero, and no upper limit was assigned.

In the final validation, the remaining 20% of 31 experimental sections were used (refer to Appendix B). The validation was meant to compare predictions from the nationally-calibrated models (using default values) and locally-calibrated models (using local values). The differences between model predictions and measurements were quantified by computing statistics (e.g., SSE) and performing paired two-sample student’s t-test. The results of local calibration and validation are summarized in Chapter 4.

Chapter 4 Results and Discussion

The chapter shows results of the study for three objectives: evaluation, local calibration, and validation. The evaluation and local calibration results were paralleled to contrast both the nationally-calibrated and locally-calibrated model predicted values with field-measured distress (rutting, bottom-up fatigue cracking, and IRI). The validation was conducted based on a different dataset from that of the evaluation and calibration to compare the nationally-calibrated and locally-calibrated model predicted values.

4.1 Rutting model (evaluation and local calibration)

Based on 25 selected experimental sections (explained in Appendix B), the predictions were obtained by the simulation runs in the Pavement ME Design software. The results of the initial evaluation revealed inadequate predictions by the nationally-calibrated model, and this warranted local calibration.
Figure 4.1 shows predictions versus measurements for the evaluation: the data points are scattered broadly, most of which are above the EL. It suggests that the nationally-calibrated rutting model tends to over-predict total rut depth from the start of traffic for most experimental sections. Exceptions include rutting growth of sections N10_2006, S11_2006, N5_2012, S6_2012, and S13_2012 which tend to level off, but still growing very slowly, around or higher than 6 mm of rut depth and pass through the EL. Discussion about this will be provided later.

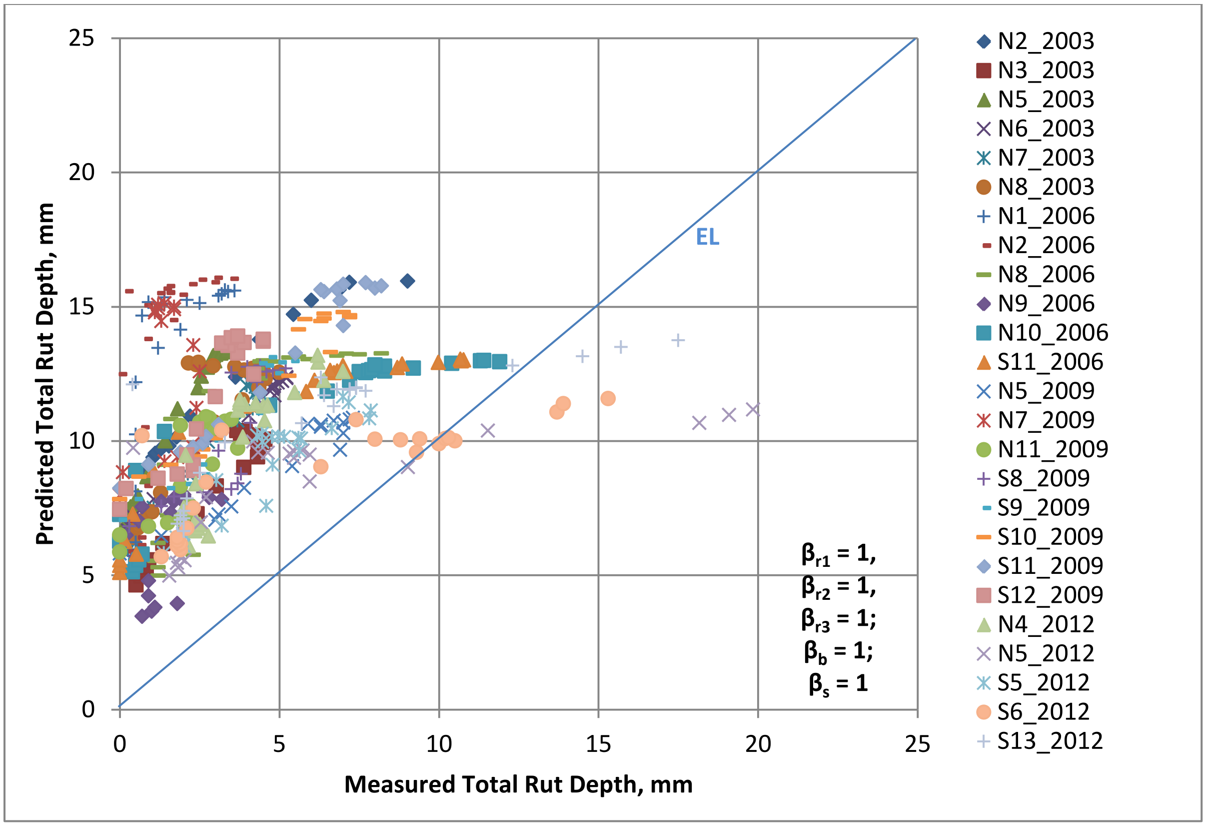

Figure 4.1 Predicted vs. measured rut depth (evaluation)

The local calibration process included attempting 64 sets of coefficients β_{r2} and β_{r3} with subsequent optimization of coefficients β_{r1}, β_{b}, and β_{s} (explained in Chapter 3). Figure 4.2 presents the derived SSE versus trial number during the calibration process. The trial #30 (i.e., $\beta_{r1} = 0.05$; $\beta_{r2} = 0.5$; $\beta_{r3} = 2$; $\beta_{b} = 0$; $\beta_{s} = 0$) is the optimal calibration coefficients. The SSE under the default (or national) calibration coefficients is 28371.89, and the SSE under the optimal calibration coefficients is 3139.15, which means an 89% reduction. The details of trial values of calibration coefficients versus SSE are tabulated in Appendix C.

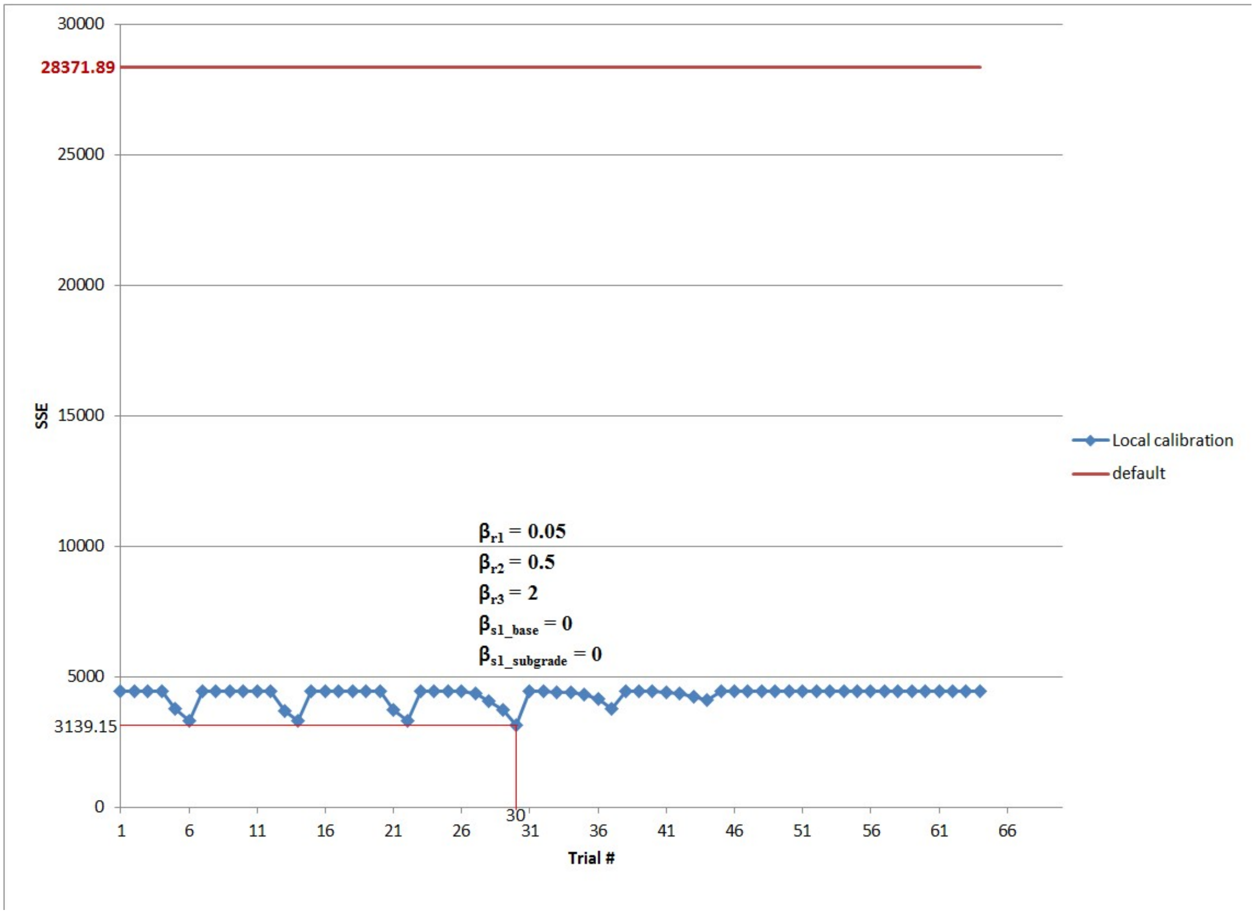

Figure 4.2 Rutting model calibration

Figure 4.3 shows predictions versus measurements for the local calibration: a majority of the data points are distributed near the EL. A small portion of the data points deviates from the EL and level off as rut depth increases. Compared with the spread of data points in Figure 4.1, most of the data points show a better convergence to the EL, which indicates an improvement in model accuracy. Curiously, the "level-off" trend of some data points (sections N10_2006, S11_2006, N5_2012, S6_2012, and S13_2012), also a sign of under-prediction, were again noticed after reaching a "significant" level (i.e., around or higher than 6 mm) of rut depth. This trend implies that the rutting accumulation predicted by the locally-calibrated model can no longer keep up with the pace of actual rutting accumulation after reaching a "significant" level. In other words, the actual rutting accumulation accelerates, which might not be accurately predicted by the model. Therefore, it was thought that the "level-off" trend reveals little on the predictability of rutting model. The “level off” trend should be explained by some factors other than the rutting model’s predictability. That only 6 of 25 experimental sections had the trend of “level-off” also suggested limited implications of the “level-off” trend caused by the locally-calibrated model for future pavement design.

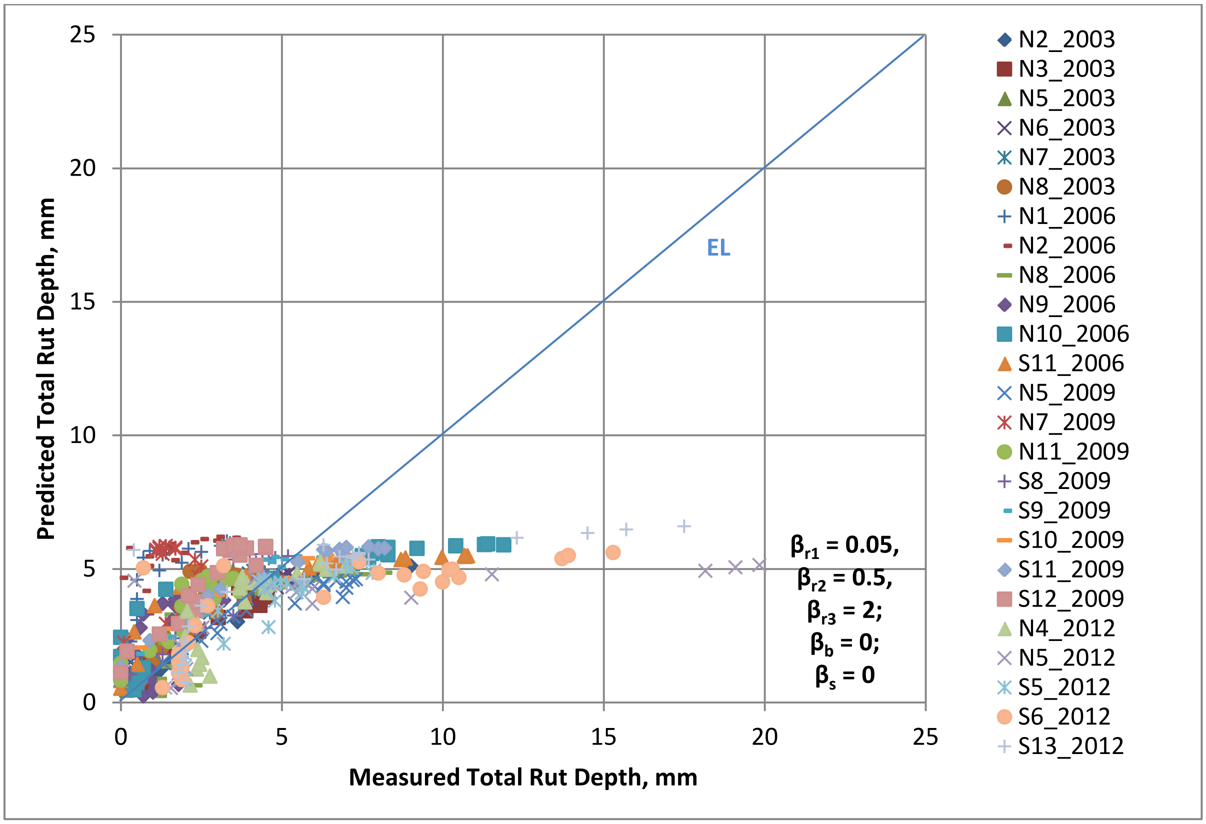

Figure 4.3 Predicted vs. measured rut depth (local calibration)

Table 4.1 exhibits statistical analysis for the evaluation and local calibration. A total of 526 data points (measurement data in Appendix A) was used as a basis to draw some inferences for the Test Track situation. The average rut depth decreased from 10.35 mm for predictions from the nationally-calibrated model to 3.79 mm for predictions from the locally-calibrated model, compared to an average of 3.70 mm for the measurements, which suggested a lower bias after the local calibration. The SSE and SEE decreased significantly after the local calibration was applied. These suggested that there was a significant increase in accuracy due to the local calibration. In light of the paired two-sample t-test, the model predictions were no longer statistically different from the measurements after the local calibration, and the locally-calibrated model predictions were statistically satisfactory because the p-value (0.40) is greater than 0.05.

Table 4.1 Statistical summary of evaluation and local calibration results (rutting)

	Nationally-Calibrated Model Predictions vs. Measurements	Locally-Calibrated Model Predictions vs. Measurements
Number of Data Points	526	
Average Rut Depth (Predicted vs. Measured)	10.35 mm vs. 3.70 mm	3.79 mm vs. 3.70 mm
Bias	6.65 mm	0.09 mm
SSE	28371.89	3139.15
SEE	2.65 mm	1.32 mm
P-value*	7.6E-197	0.40

*The p-value was derived from the two-tailed paired t-test (α=0.05) to compare nationally-calibrated/locally-calibrated model predictions with measurements.

4.2 Rutting model (validation)

Based on six selected experimental sections (explained in Appendix B), the validation was performed. Figure 4.4 shows nationally-calibrated predictions versus measurements: the data points of two sections (i.e., N1_2003 and N4_2003) are interspersed above the EL, and a portion of the data points emerge along the EL. It is suggested that the nationally-calibrated rutting model over-predicts total rut depth from the start of traffic for some sections (i.e., N1_2003 and N4_2003), which agrees with the findings from the initial evaluation. Meanwhile, the predictions for sections N6_2009, N3_2012, and S12_2012 were fairly accurate. The accuracy of the rutting model varies depending on which section the model is applied. As it is known, three factors (i.e., traffic loading, climate, and materials) are important determinants of distress prediction. In this investigation, the traffic loading and climate weathering condition were very similar for all experimental sections, but the materials were not. Thus, the reason for varied levels of model accuracy among the sections may largely rest on the factor materials: N1_2003 (5-in. of PG 76-22 with 6-in. granular base), N4_2003 (9-in. of PG 76-22 with 6-in. granular base), N6_2009 (7-in. of 30%-40% Thiopave® with 6-in. granular base), and S12_2012 (9-in. of SMA-foam-combined with 7.5-in. of FDR base). However, the material-specific effect on the nationally-calibrated model accuracy is frequently seen in the evaluation and out of the scope of this study. Therefore, it is left for future investigation.

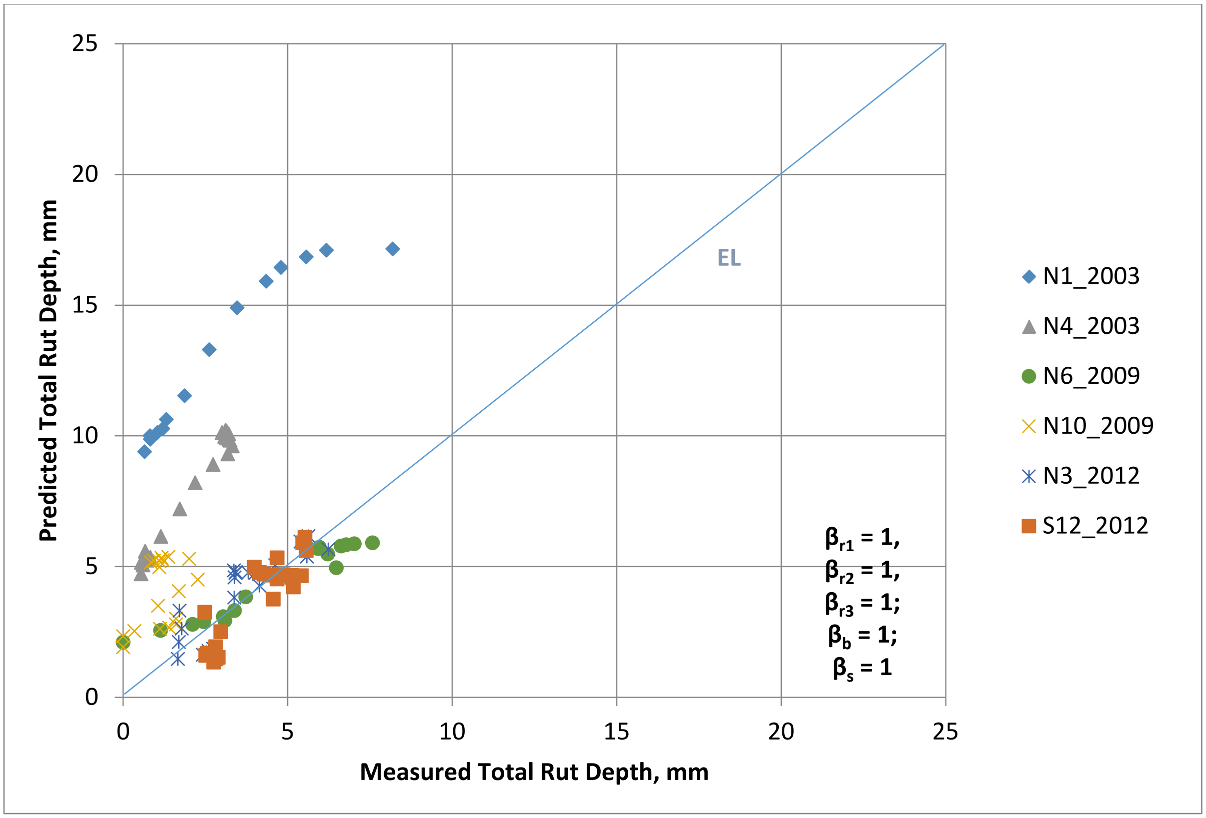

Figure 4.4 Predicted vs. measured rut depth (validation: nationally-calibrated model)

Figure 4.5 shows locally-calibrated predictions versus measurements: a majority of the data points are distributed near the EL with a small portion showing a tendency of deviation from the EL. Compared with the spread of data points in Figure 4.4, the data points of two sections (i.e., N1_2003 and N4_2003), which were recognized as over-predicted by the nationally-calibrated model, show a much better convergence to the EL. The other data points still converge to the EL, which indicates an overall improvement in model accuracy after the local calibration. The tendency of the “level-off” still exists for the locally-calibrated model around 6 mm of rut depth in the section N1_2003.

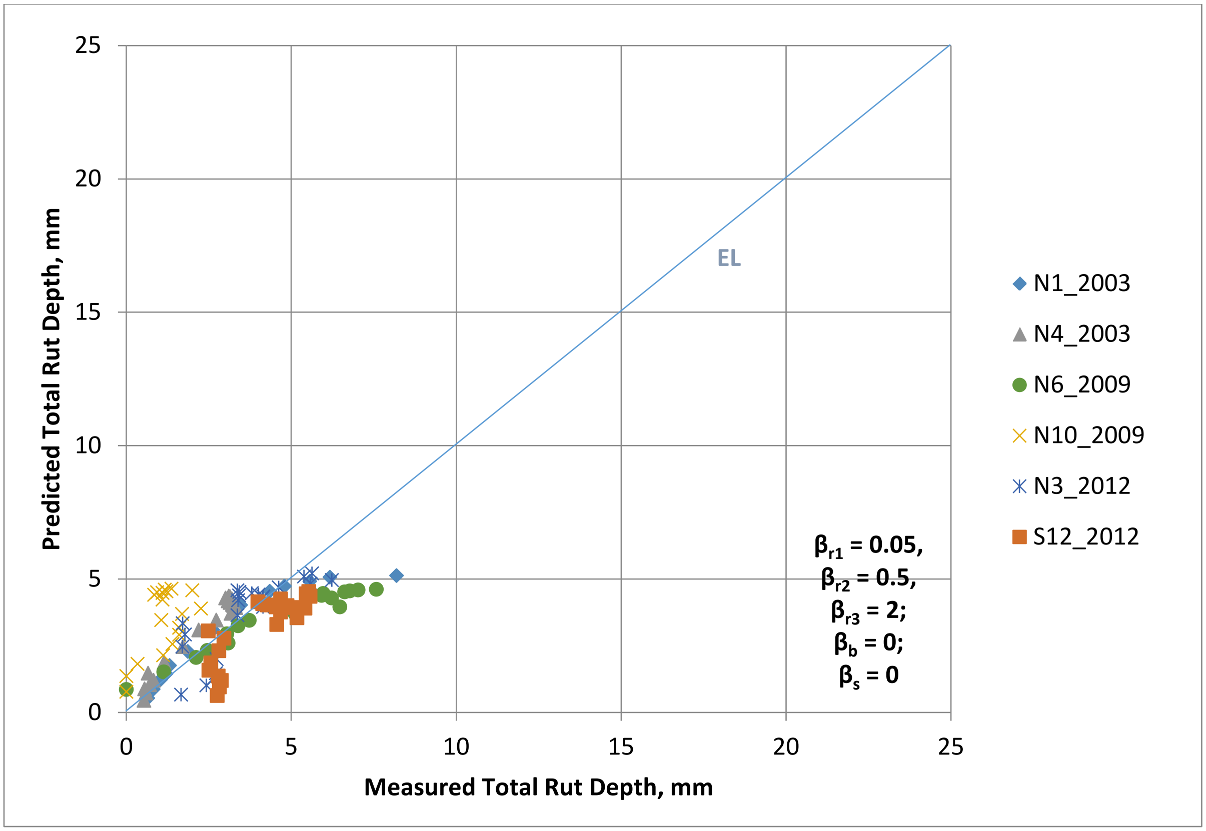

Figure 4.5 Predicted vs. measured rut depth (validation: locally-calibrated model)

The "level-off" around 6 mm of rut depth occurs in many experimental sections for both nationally-calibrated and locally-calibrated models. Therefore, the results for sections were reexamined. Interestingly, sections with actual cracks measured showed the "level-off" trend, however, sections without actual cracks measured did not show the "level-off" trend. Also, as shown in Table 4.2, the start time of the "level-off" coincides with the predicted initiation of bottom-up cracking. It is evident that the measured, rather than predicted, rutting accumulation is accelerated by the actual bottom-up cracking development. A hypothesis for this assumption is that surface cracking jeopardizes the integrity of pavement structures and allows water infiltration into the subgrade material. The water damage to the structure, especially in the rutted range (i.e., wheelpaths), would make the pavement more vulnerable to traffic loading and ultimately lead to an acceleration of rutting accumulation. Meanwhile, the surface cracking may change the evenness of nearby pavement surface, thereby affecting rutting measurements. The rutting model may need to be modified to factor in water damage when fatigue damage occurs.

Table 4.2 Start time of bottom-up cracking and "level-off" trend of rutting

Investigation Purpose	Section_Year	Initiation Time of Bottom-up Cracking at Surface	Start Time of "Level-off"	Rut Depth (Predicted vs. Measured) at start time of "Level-off"
Evaluation and Calibration	N8_2006	July 2008	July 2008	4.75 mm vs. 6.8 mm
Evaluation and Calibration	N10_2006	July 2008	July 2008	5.86 mm vs. 10.4 mm
Evaluation and Calibration	S11_2006	July 2008	July 2008	5.44 mm vs. 9.97 mm
Evaluation and Calibration	S11_2009	No cracking	Not evident	-
Evaluation and Calibration	N5_2012	April 2013	July 2013	3.69 mm vs. 5.95 mm
Evaluation and Calibration	S6_2012	September, 2013	August, 2013	4.52 mm vs. 10 mm
Evaluation and Calibration	S13_2012	June 2013	July 2013	4.62 mm vs. 5.7 mm
Validation	N1_2003	July 2004	October 2004	5.07 mm vs. 6.18 mm
Validation	N6_2009	No cracking	Not evident	-

Table 4.3 shows results of the statistical analysis for the validation. A total of 120 data points (measurement data in Appendix A) was used in the statistical analysis. The average rut depth decreased from 5.81 mm for the predictions from the nationally-calibrated model to 3.26 mm for the predictions from the locally-calibrated model, compared to an average of 3.15 mm for the measurements, indicating a lower bias after the local calibration. The SSE and SEE decreased significantly after the local calibration was applied. The statistics suggest that there was a significant increase in accuracy due to the local calibration. In light of the paired two-sample t-test, the model predictions were no longer statistically different from the measurements after the local calibration, and the locally-calibrated model predictions were statistically satisfactory because the p-value (0.36) is greater than 0.05.

Table 4.3 Statistical summary of validation results (rutting)

	Nationally-Calibrated Model Predictions vs. Measurements	Locally-Calibrated Model Predictions vs. Measurements
Number of Data Points	120	
Average Rut Depth (Predicted vs. Measured)	5.81 mm vs. 3.15 mm	3.26 mm vs. 3.15 mm
Bias	2.66 mm	0.11 mm
SSE	2444.94	230.53
SEE	3.54 mm	1.02 mm
P-value*	1.14E-12	0.36

*The p-value was derived from the two-tailed paired t-test (α=0.05) to compare nationally-calibrated/locally-calibrated model predictions with measurements.

4.3 Bottom-up fatigue cracking model (evaluation and local calibration)

The same 25 sections for the rutting model calibration were initially selected for bottom-up fatigue cracking model calibration. However, four of them were eliminated due to a few reasons, such as non-matching type of distress (e.g., top-down cracking) and insufficient measurement data. Thus, only 21 of the test sections were used.

Figure 4.6 shows predictions versus measurements for the initial evaluation: most of the data points were lined up on the Y-axis and very few on the X-axis, with some data points scattered around the equality line (EL). Data points on the X-axis mean that the actual surface cracking was found, but the model has not predicted its appearance, whereas data points on the Y-axis mean that no cracking was found, but the model predicted its appearance. The wide dispersion of data points suggests that the nationally-calibrated bottom-up fatigue cracking model does not predict fatigue cracking very well.

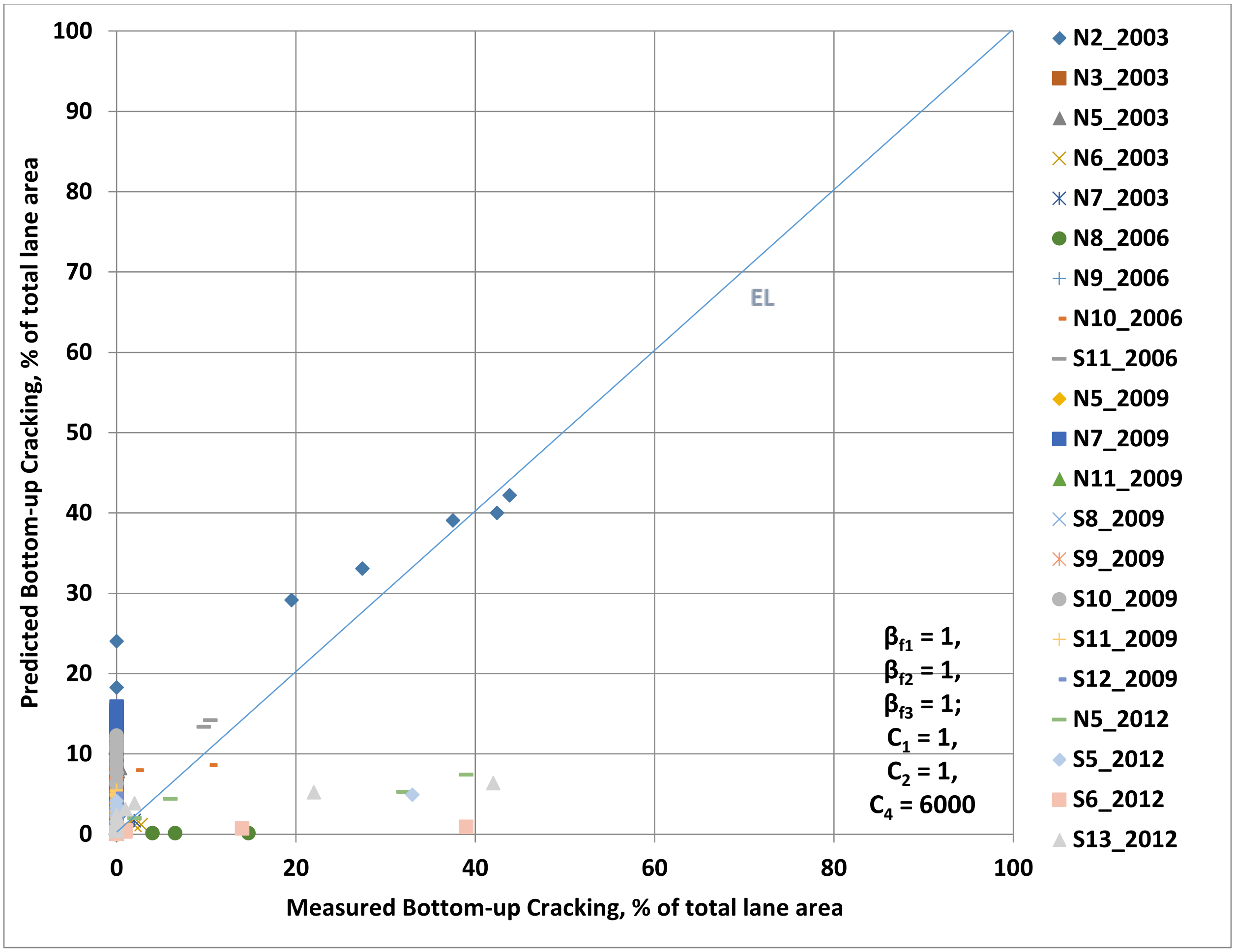

Figure 4.6 Predicted vs. measured bottom-up fatigue cracking (evaluation)

The local calibration process included attempting 310 sets of coefficients β_{f1}, β_{f2}, and β_{f3} (phase_1) with subsequent optimization for coefficients C_1, C_2, and C_4 (phase_2) (explained in Chapter 3). Figure 4.7 presents the derived SSE versus trial number during the calibration process. The trial #282 (i.e., $\beta_{f1} = 2.2$; $\beta_{f2} = 1$; $\beta_{f3} = 1$; $C_1 = 2.03$; $C_2 = 2.62$; $C_4 = 5729.28$) is the optimal calibration coefficients. The SSE under the default calibration coefficients is 15782.68, and the SSE under the optimal calibration coefficients is 8317.852, which means a 47.3% reduction. The details of trial values of calibration coefficients versus SSE are tabulated in Appendix C.

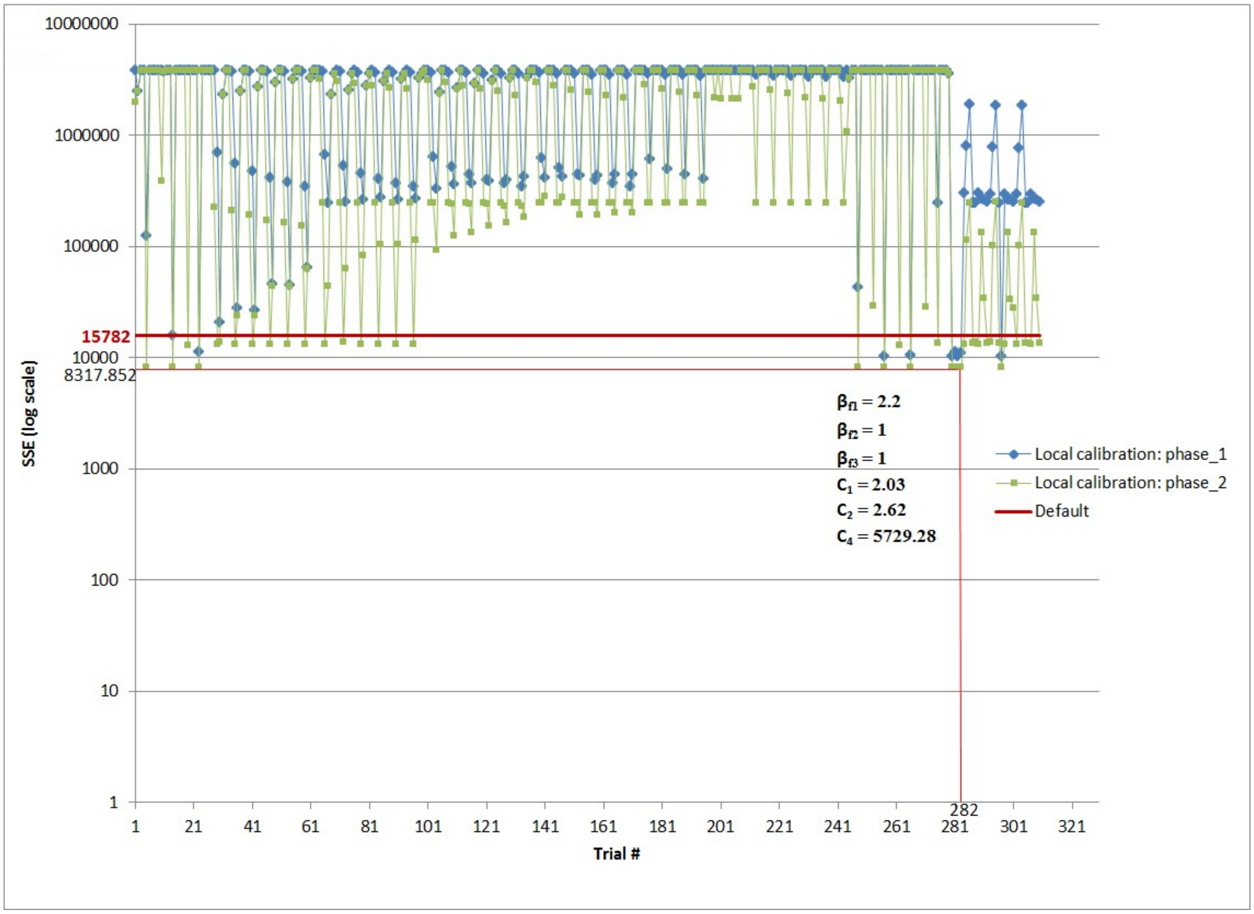

Figure 4.7 Bottom-up fatigue cracking model calibration

Figure 4.8 shows locally-calibrated predictions versus measurements: most of the data points are distributed near the origin of coordinates with a few scattered around the equality line (EL). Compared with the spread of data points in Figure 4.6, the majority of the data points, originally staying on the Y-axis, are shifted toward the origin of coordinates while a few are shifted to the X-axis. This shift toward the origin of coordinates indicates an overall improvement in prediction accuracy. Although there are still a few data points falling along on the x-axis, that only 6 of 21 experimental sections had this phenomenon suggested limited implications of the "data points on the x-axis" phenomenon caused by the locally-calibrated model for future pavement design.

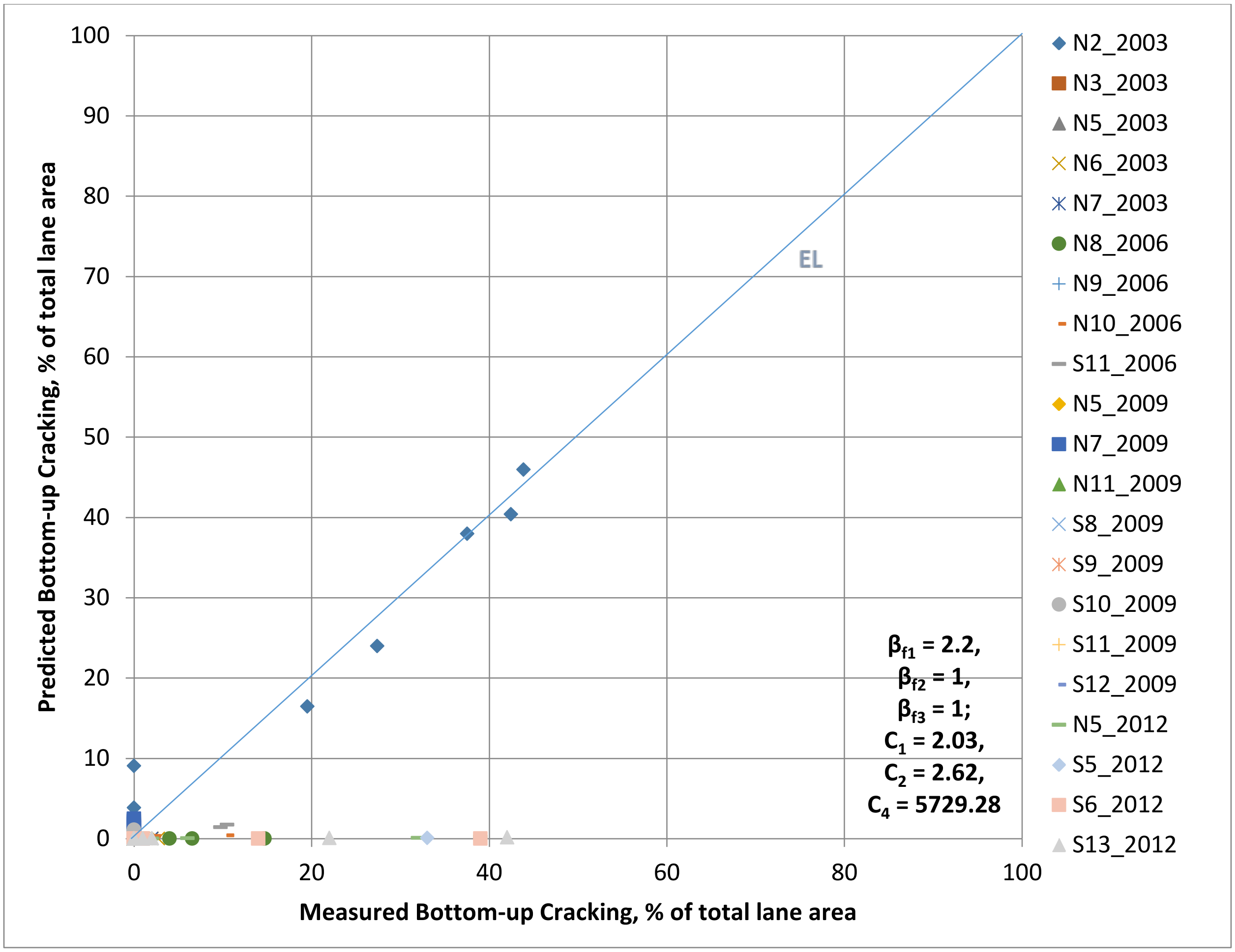

Figure 4.8 Predicted vs. measured bottom-up fatigue cracking (local calibration)

Table 4.4 exhibits statistical analysis for the evaluation and local calibration. A total of 394 data points (measurement data in Appendix A) was used for the analysis. The average of bottom-up cracking decreased from 3.80 % for the predictions from the nationally-calibrated model to 1.71 % for the predictions from the locally-calibrated model, compared to 1.20 % for the measurements, thus a lower bias was achieved with the local calibration. The SSE and SEE were also reduced by about half after the local calibration. These statistics suggest that there was an increase in accuracy due to the local calibration. In light of the paired two-sample t-test, the model predictions were no longer statistically different from the measurements after the local calibration, and the locally-calibrated model predictions were statistically satisfactory because the p-value (0.0503) is greater than 0.05.

Table 4.4 Statistical summary of evaluation and local calibration results (bottom-up fatigue cracking)

	Nationally-Calibrated Model Predictions vs. Measurements	Locally-Calibrated Model Predictions vs. Measurements
Number of Data Points	394	
Average Bottom-up Cracking (Predicted vs. Measured)	3.80 % vs. 1.20 %	1.71 % vs. 1.20 %
Bias	2.60 %	0.51 %
SSE	15782.68	8317.85
SEE	4.74 %	2.27 %
P-value*	1.91E-17	0.0503

*The p-value was derived from the two-tailed paired t-test (α=0.05) to compare nationally-calibrated/locally-calibrated model predictions with measurements.

4.4 Bottom-up Fatigue cracking model (validation)

There were originally six selected sections for bottom-up fatigue cracking model validation, but two of them were eliminated due to non-matching types of distress and insufficient measurement data. Thus, only four sections were used.

Based on the four experimental sections, the validation was performed. Figure 4.9 shows nationally-calibrated predictions versus measurements: most of the data points are lined up on the Y-axis, with a few scattered near the equality line (EL). This suggests that the nationally-calibrated bottom-up fatigue cracking model does not accurately predict the cracking for the experimental sections, which is consistent with the findings of the initial evaluation.

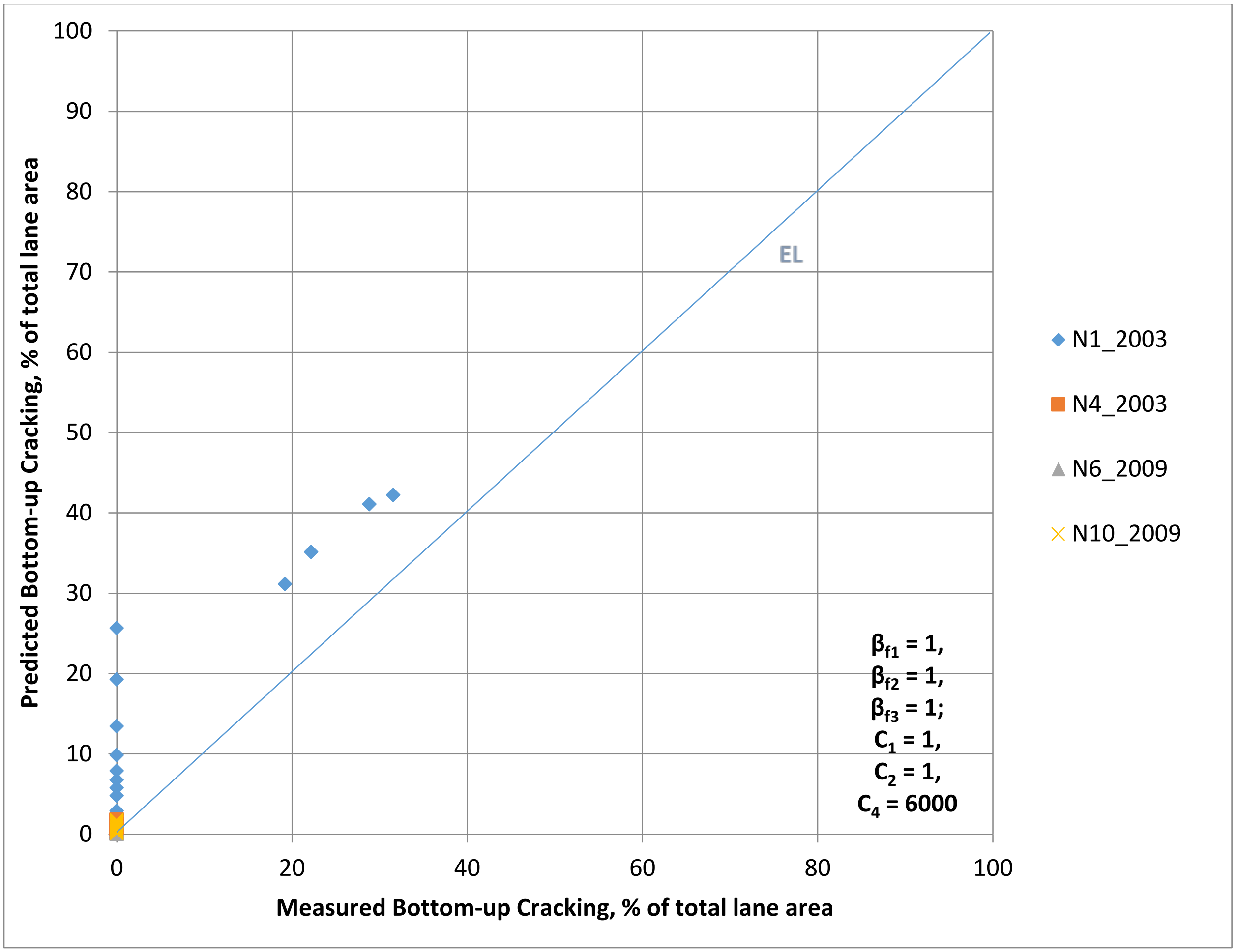

Figure 4.9 Predicted vs. measured bottom-up fatigue cracking (validation: nationally-calibrated model)

Figure 4.10 shows locally-calibrated bottom-up fatigue cracking predictions versus measurements: a majority of the data points are distributed near the origin, yet a small portion converge near the EL. Compared with Figure 4.9, the data points that are lying on the Y-axis shift towards the origin of coordinates, and the data points of the section N2_2003 converge toward the EL. The shift of data points towards the EL indicates there was an improvement in model accuracy.

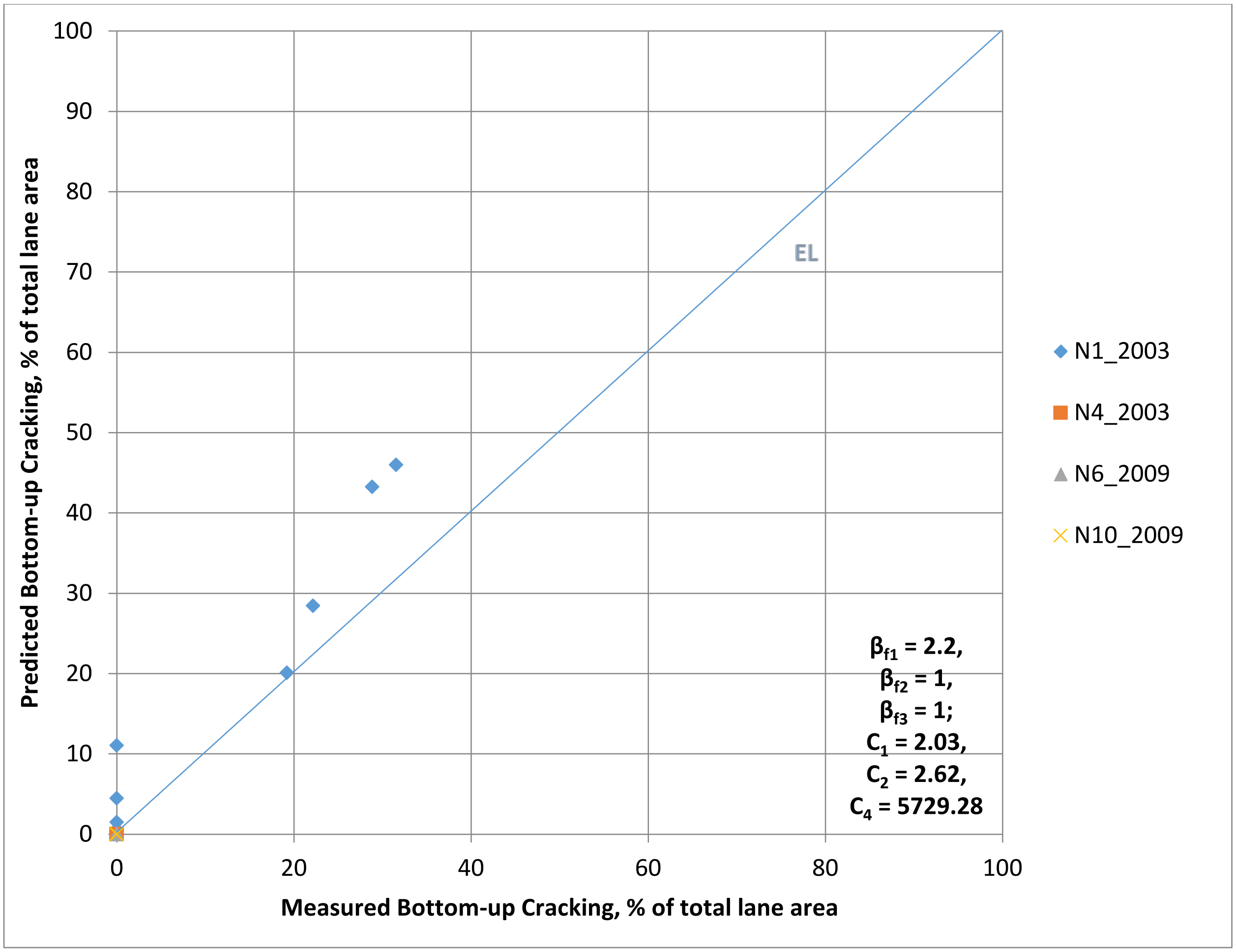

Figure 4.10 Predicted vs. measured bottom-up fatigue cracking (validation: locally-calibrated model)

Table 4.5 shows results of the statistical analysis for the validation. A total of 85 data points (measurement data in Appendix A) was used as a basis to make some inferences for the Test Track situation. The average bottom-up cracking decreased from 3.56 % for the predictions from the nationally-calibrated model to 1.71 % for the predictions from the locally-calibrated model, compared to an average of 1.20 % for the measurements, indicating a lower bias after the local calibration. The SSE and SEE decreased significantly after the local calibration. The statistics suggested that there was an increase in accuracy due to the local calibration. In light of the paired two-sample t-test, the model predictions were still statistically different from the measurements after the local calibration, but the locally-calibrated model predictions were almost statistically satisfactory because the p-value (0.048) is very close to 0.05.

Table 4.5 Statistical summary of validation results (bottom-up fatigue cracking)

	Nationally-Calibrated Model Predictions vs. Measurements	Locally-Calibrated Model Predictions vs. Measurements
Number of Data Points	85	
Average Bottom-up Cracking (Predicted vs. Measured)	3.56 % vs. 1.20 %	1.71 % vs. 1.20 %
Bias	2.36 %	0.51 %
SSE	2123.45	601.28
SEE	3.93 %	1.80 %
P-value*	4.39E-06	0.048

*The p-value was derived from the two-tailed paired t-test (α=0.05) to compare nationally-calibrated/locally-calibrated model predictions with measurements.

4.5 IRI model (evaluation and local calibration)

As noted earlier, 25 sections were used in the rutting model calibration, and 21 were later used in the bottom-up fatigue cracking model calibration. Considering that IRI predictions are impacted by rutting and cracking prediction, the sections for the IRI model calibration were the 21 sections used by both rutting and bottom-up fatigue cracking model calibrations.

Figure 4.11 shows predictions versus measurements for the evaluation: data points in the range of 35 in./mile to 65 in./mile were scattered along the EL but data points in the range of IRI (higher than 65 in./mile) were widely dispersed along the EL. The IRI data points of some sections (i.e., N10_2006, S11_2006, N5_2012, S6_2012, and S13_2012) tend to level off with the increase of IRI. These sections were found to have the same "level-off" trend as the rutting data. The IRI data points of section N8_2006 tend to level off as well. The reason for these inaccurate predictions might be related to rutting predictions. Moreover, some data points (sections S8_2009, S9_2009, S11_2009, S12_2009, and S5_2012) were over-predictions. No specific reason can be proposed since too many potential causes (rutting, cracking, site factors, or a combination of these). The accuracy of IRI prediction appears to be dependent on the level of IRI. It was believed that the nationally-calibrated model could predict the IRI performance between 35 in./mile to 65 in./mile. However, the model could not predict the IRI performance above 65 in./mile. In this regards, the locally-calibrated model could be of little value for future pavement design.

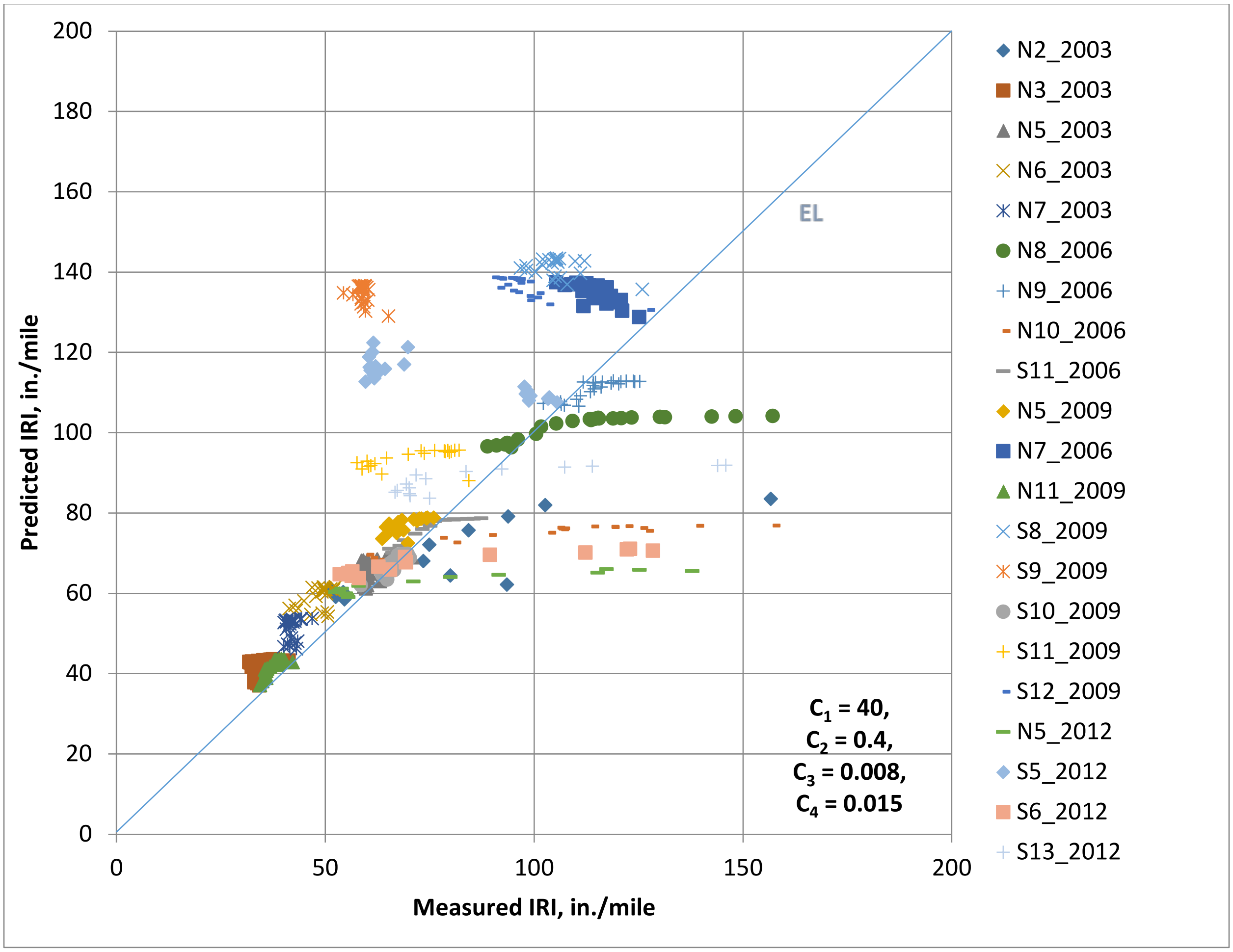

Figure 4.11 Predicted vs. measured IRI (evaluation)

The local calibration process includes the optimization for coefficients C_1, C_2, C_3, and C_4. The SSE under the default calibration coefficients is 347113.2. The SSE under the optimal calibration coefficients (i.e., $C_1 = 0$, $C_2 = 0$, $C_3 = 9730.12$, and $C_4 = 0$) is 296890.6, which means a 14.5% reduction.

Figure 4.12 shows locally-calibrated predictions versus measurements: the data points "form" many horizontal lines. Compared with Figure 4.11, the general locations of the data points are not changed, but the predicted values are essentially unchanged with time or traffic, which seems irrational. In this sense, the shift of data points does not cause a significant improvement in prediction accuracy.

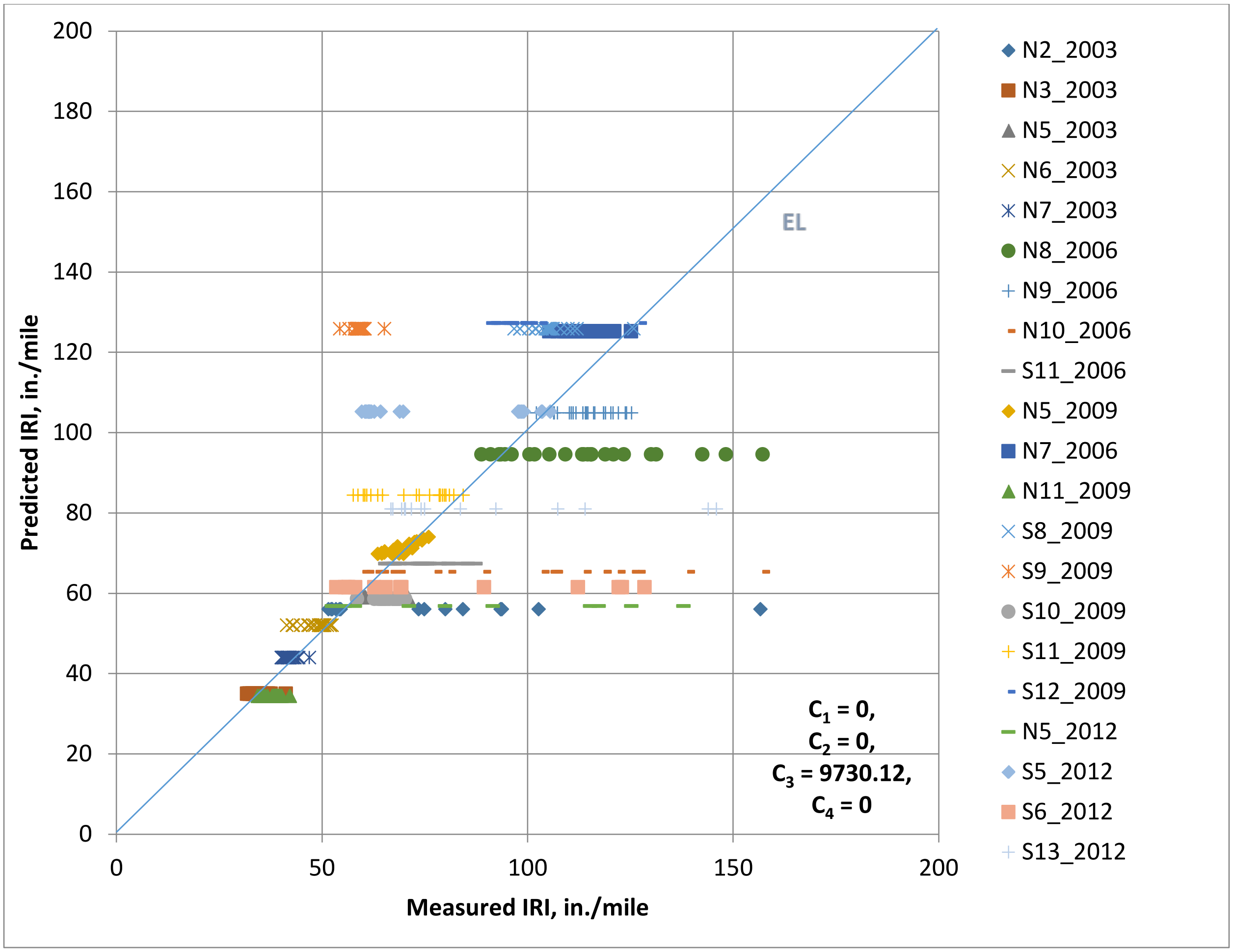

Figure 4.12 Predicted vs. measured IRI (local calibration)

Table 4.6 exhibits results of statistical analysis for the evaluation and local calibration. A total of 445 data points (measurement data in Appendix A) was used in this analysis. The average IRI decreased from 86.69 in./mile for the predictions from the nationally-calibrated model to 78.54 in./mile for the predictions from the locally-calibrated model, compared to an average of 76.20 in./mile for the measurements, indicating a slightly lower bias after the local calibration. The SSE and SEE were reduced slightly by the local calibration. The statistics suggested a slight increase in accuracy due to the local calibration. In light of the paired two-sample t-test, the model predictions were no longer statistically different from the measurements after the local calibration, and the locally-calibrated model predictions were statistically satisfactory because the p-value (0.056) is greater than 0.05.

Table 4.6 Statistical summary of evaluation and local calibration results (IRI)

	Nationally-Calibrated Model Predictions vs. Measurements	Locally-Calibrated Model Predictions vs. Measurements
Number of Data Points	445	
Average IRI (Predicted vs. Measured)	86.69 in./mile vs. 76.20 in./mile	78.54 in./mile vs. 76.20 in./mile
Bias	10.49 in./mile	2.34 in./mile
SSE	347113.2	296890.6
SEE	30.67 in./mile	29.62 in./mile
P-value*	2.17E-16	0.056

*The p-value was derived from the two-tailed paired t-test (α=0.05) to compare nationally-calibrated/locally-calibrated model predictions with measurements.

4.6 IRI model (validation)

In the previous discussion, six sections were used in the rutting model validation, and four of them were used in the bottom-up fatigue cracking model validation. Therefore, the sections for the IRI model validation were only the four sections used by both model validations.

Based on the four sections, the validation was performed. Figure 4.13 shows nationally-calibrated predictions versus measurements: data points in the range of IRI from 35 in./mile to 65 in./mile lay mostly along the EL but the predicted IRI for N1_2003 changed little even though the measured IRI change dramatically over time. The reason for inaccurate prediction by the nationally-calibrated model might be inaccurate rutting and fatigue cracking prediction or inadequate site factors.

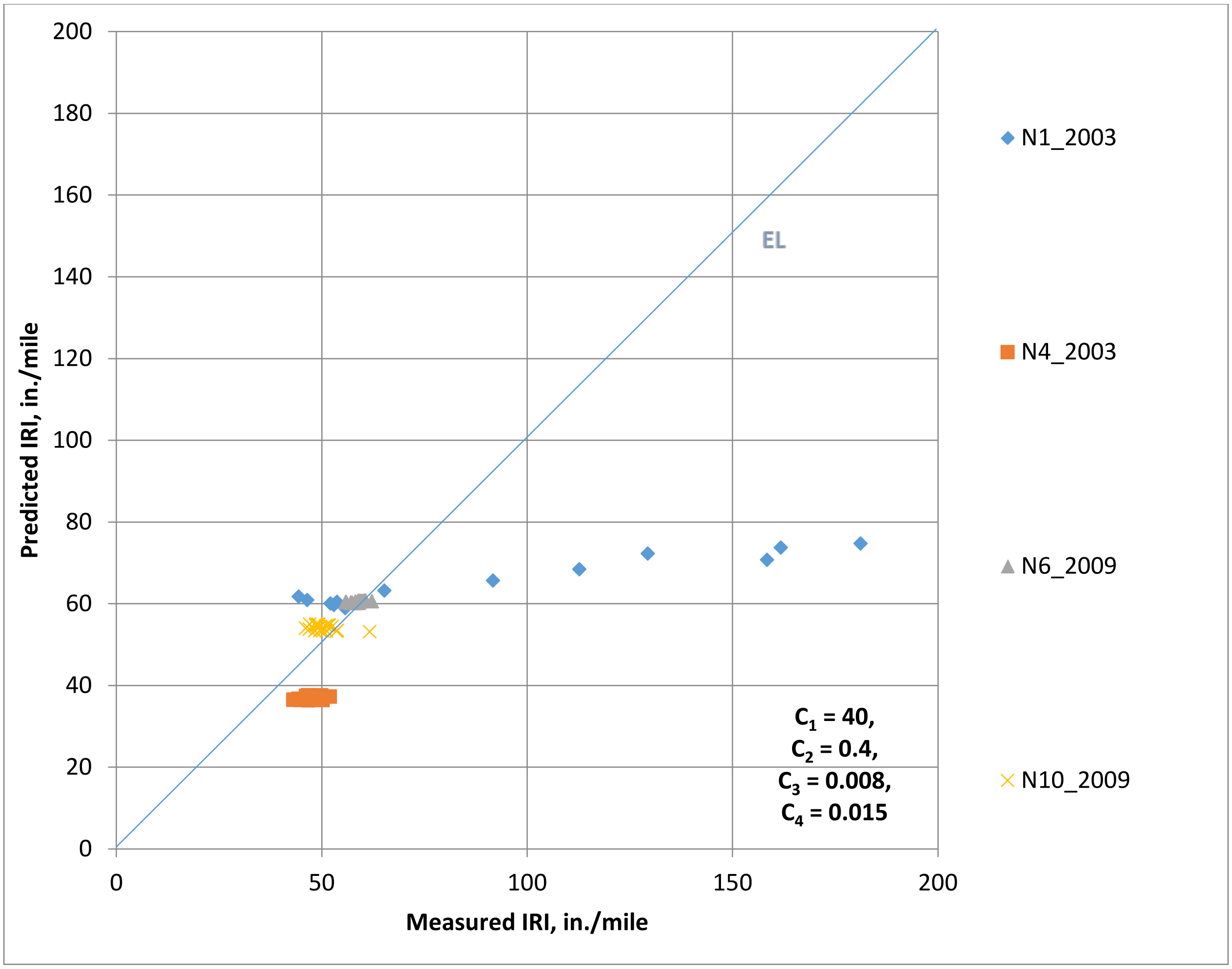

Figure 4.13 Predicted vs. measured IRI (validation: nationally-calibrated model)

Figure 4.14 shows locally-calibrated predictions versus measurements: the data points “form” four horizontal lines. Compared with Figure 4.13, the general positions of data points are not changed, but the predicted values for any section are essentially unchanged with time or traffic, which seems irrational. The finding agrees with the evaluation and local calibration. The IRI model locally-calibrated by Excel Solver (explained in Chapter 3) did remove the impact of rutting, fatigue cracking, and site factor (since the corresponding coefficients C_1, C_2, and C_4 all equal to 0). The calibrated model is only dependent on the effect of thermal cracking. However, the implication of this model is not consistent with our common knowledge that the IRI is affected by the development of rutting and cracking. Moreover, the change due to calibration does not cause a significant improvement in prediction accuracy.

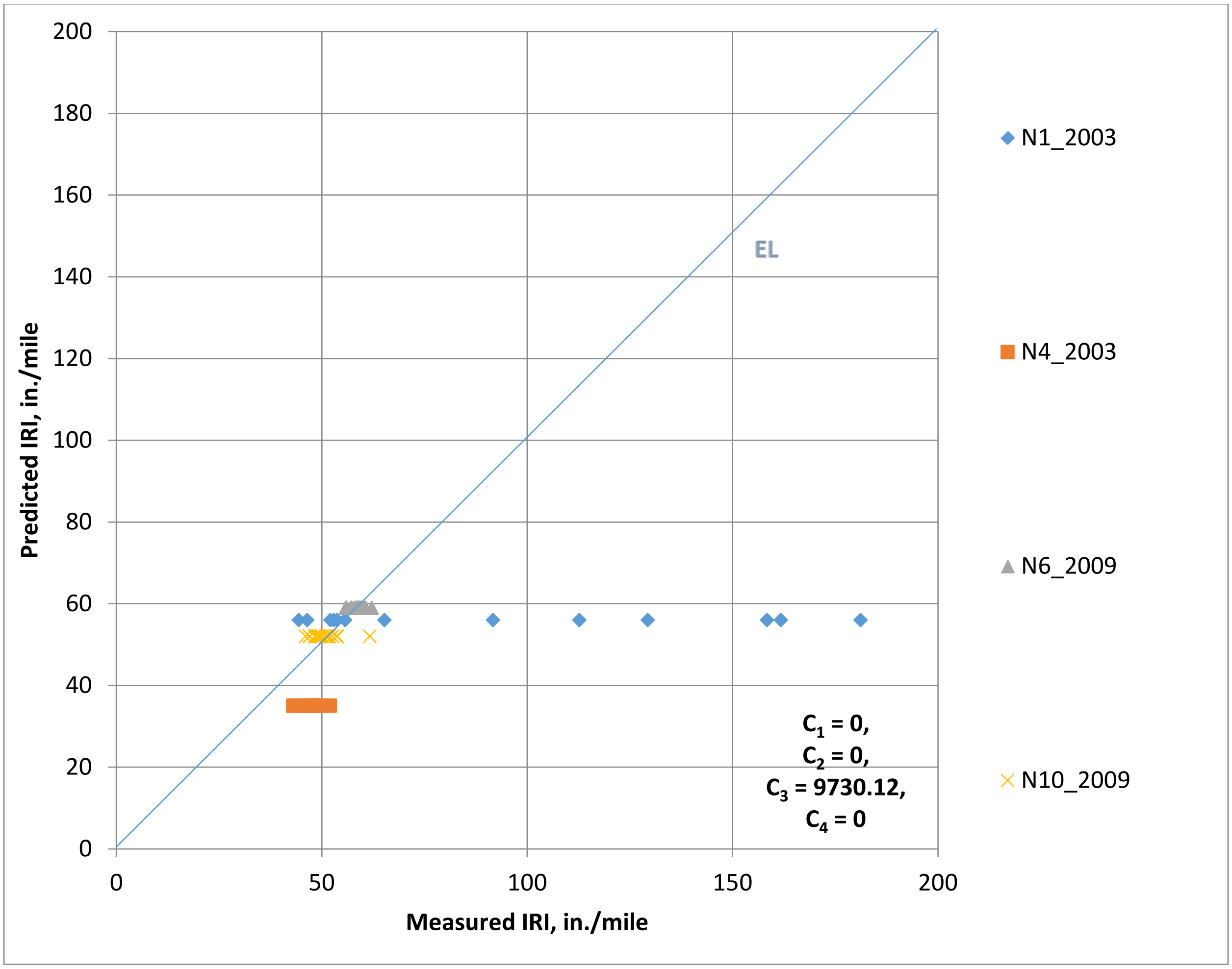

Figure 4.14 Predicted vs. measured IRI (validation: locally-calibrated model)

Table 4.7 shows results of the statistical analysis for the validation. A total of 83 data points (measurement data in Appendix A) is used as a basis to make some inferences for the Test Track situation. The average IRI decreased from 52.18 in./mile for the nationally-calibrated model to 49.66 in./mile for the locally-calibrated model, compared to an average of 67.61 in./mile for the measurements, indicating a higher bias after the local calibration. The SSE and SEE also increased after the local calibration, indicating that there was a lower accuracy due to the local calibration. In light of the paired two-sample t-test, the model predictions were statistically different from the measurements both before (p-value = 0.03 < 0.05) and after the local calibration (p-value = 0.009 < 0.05). In this regard, the locally-calibrated model prediction was not statistically satisfactory. The improvement in prediction accuracy was not verified in the validation.

Table 4.7 Statistical summary of validation results (IRI)

	Nationally-Calibrated Model Predictions vs. Measurements	Locally-Calibrated Model Predictions vs. Measurements
Number of Data Points	83	
Average IRI (Predicted vs. Measured)	53.18 in./mile vs. 67.61 in./mile	49.66 in./mile vs. 67.61 in./mile
Bias	-14.43 in./mile	-17.95 in./mile
SSE	202229.5	233228.3
SEE	45.82 in./mile	45.93 in./mile
P-value*	0.03	0.009

*The p-value was derived from the two-tailed paired t-test (α=0.05) to compare nationally-calibrated/locally-calibrated model predictions with measurements.

In summary, the prediction results of nationally-calibrated and locally-calibrated models on rutting, bottom-up fatigue cracking, and IRI were compared with the measured data gained from the Test Track. The results showed that: firstly, the nationally-calibrated rutting model over-predicted the performance of most experimental sections throughout their service life. However, the local calibration coefficients (shown in Table 4.8) reduced the rutting model bias by 98.6% and the SEE by 50.2%. The rutting model improvement was validated with 95.9% decrease in bias and 71.2% decrease in SEE using an independent local dataset. The local calibration was only limited to reach an agreement between the total rutting predictions with the total rutting measurements. It was found that rutting calibration coefficients for the Test Track impacts predictions in a similar way as coefficients from some studies (i.e., Mallela et al., 2009; Li et al., 2009; Darter et al., 2014; Haider et al., 2016). These coefficients eliminated the over-prediction of the unbound layer rutting to reach an agreement between total rutting predictions and the total rutting measurements.

Similarly, the nationally-calibrated fatigue bottom-up cracking model over-predicted bottom-up cracking for the majority of sections. The local calibration coefficients (shown in Table 4.8) reduced the bottom-up cracking model bias by 80.4% and the SEE by 52.1%. The bottom-up cracking model improvement was validated with 78.4% decrease in bias and 54.2% decrease in SEE. The fatigue cracking calibration coefficients for the Test Track were found different to reviewed studies (Muthadi and Kim, 2008; Li et al., 2009; Hall et al., 2011; Darter et al., 2014; Haider et al., 2016). This difference could only be roughly attributed to the difference in calibration databases used by different studies. The diversity of calibration databases by different studies lies in input parameters regarding traffic, climate, and materials.

This study also found that the nationally-calibrated IRI model only accurately predicted the IRI between 35 in./mile to 65 in./mile. Although the IRI prediction was improved through the local calibration (77.7% reduction in bias and 3.4% reduction in SEE), the improvement was not adequately validated (24.4% increase in bias and 2.4% increase in SEE).

Table 4.8 Local calibration coefficients for the NCAT Test Track

Prediction Models	Recommended Values
Rutting	$\beta_{r1} = 0.05$, $\beta_{r2} = 0.5$, $\beta_{r3} = 2$; $\beta_b = 0$; $\beta_s = 0$
Bottom-up Fatigue Cracking	$\beta_{f1} = 2.2$, $\beta_{f2} = 1$, $\beta_{f3} = 1$; $C_1 = 2.03$, $C_2 = 2.62$, $C_4 = 5729.28$
IRI	$C_1 = 40$ (default), $C_2 = 0.4$ (default), $C_3 = 0.008$ (default), $C_4 = 0.015$ (default)

Chapter 5 Automation

This chapter covers the concept of automation for the purpose of Pavement ME model calibration. The automation scheme was only integrated into the local calibration process due to repetitive work involved. The automation scheme was evaluated against human maneuver in time savings. Also, the time investment for developing automation macros is discussed.

5.1 Scheme of automation

The automation in this study was adopted in the rutting and bottom-up fatigue cracking model calibrations. The goal of automation was to reduce the labor and time for data entry, software runs, and data compilation. With the created pavement design projects, the automation can facilitate the coefficient optimization involving the Pavement ME Design software by using macro-based computer methods.

To explain the automation scheme, a flow chart of the bottom-up fatigue cracking model calibration is shown in Figure 5.1.

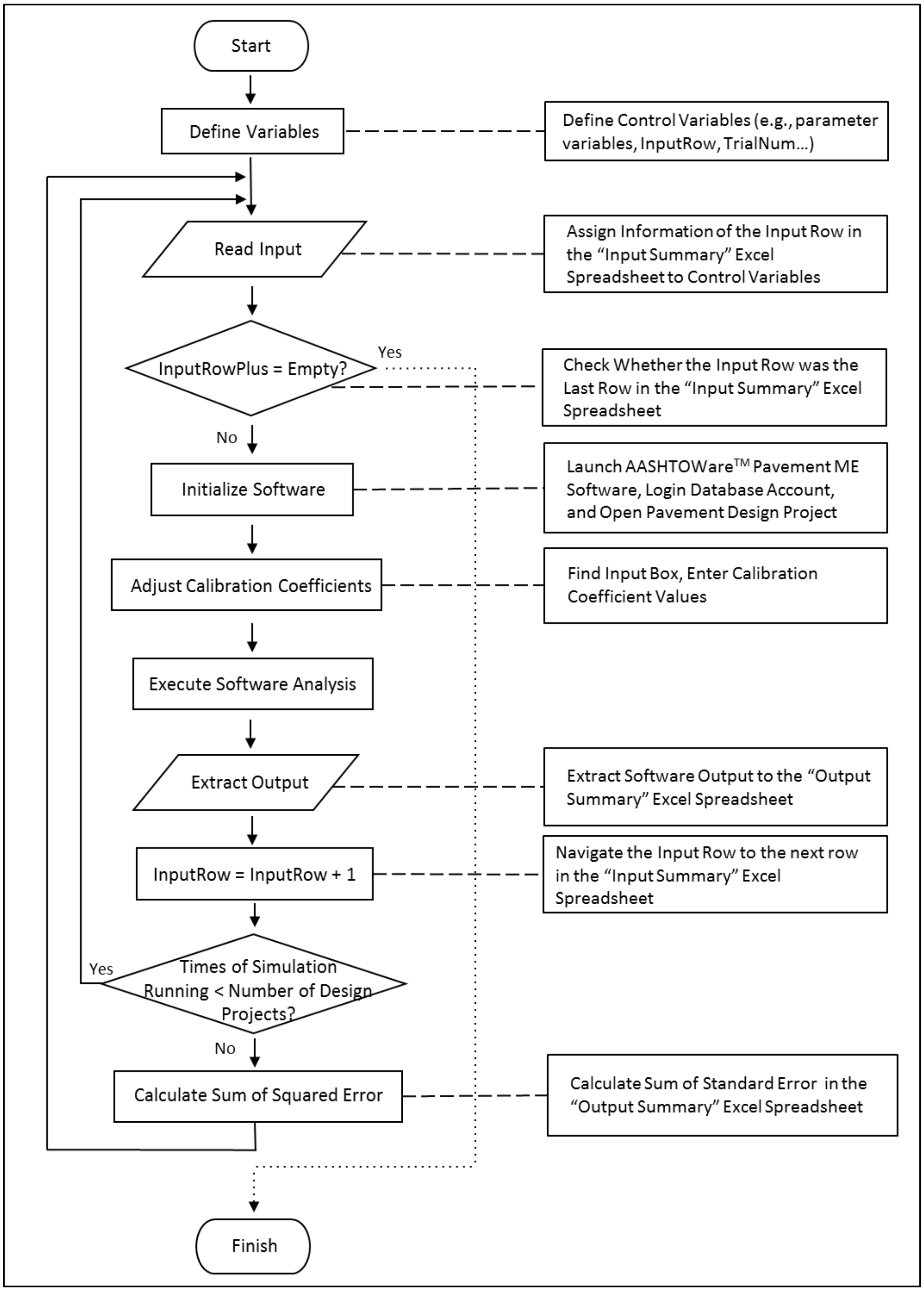

Figure 5.1 Flowchart of automation

The automation begins with creating or defining the control variables. For example, the parameter variables BF1, BF2, and BF3 were assigned with values of trial calibration coefficients β_{f1}, β_{f2}, and β_{f3}.

The variable InputRow was used for navigating the “Input Summary” spreadsheet (Figure 5.2). The variable TrialNum (or Trial #) was used for counting the loops. The “Input Summary” spreadsheet was used to store values of trial calibration coefficients (i.e., BF1, BF2, and BF3) and other identifiers (e.g., trial #, project, and project file path) for the purpose of executing loops.

	A	B	C	D	E	F	G
1	Trial #	Project	Project file name	BF1	BF2	BF3	Project file path
2	1	N1_2003	N1_2003.dgpx	1	1.2	2.1	E:\AASHTOWare Data\AASHTOWare Projects\N1_2003
3	2	N1_2006	N1_2006.dgpx	1	1.2	2.1	E:\AASHTOWare Data\AASHTOWare Projects\N1_2006
4	3	N2_2003	N2_2003.dgpx	1	1.2	2.1	E:\AASHTOWare Data\AASHTOWare Projects\N2_2003
5	4	N2_2006	N2_2006.dgpx	1	1.2	2.1	E:\AASHTOWare Data\AASHTOWare Projects\N2_2006
6	5	N3_2003	N3_2003.dgpx	1	1.2	2.1	E:\AASHTOWare Data\AASHTOWare Projects\N3_2003
7	1	N1_2003	N1_2003.dgpx	1	1.2	2.1	E:\AASHTOWare Data\AASHTOWare Projects\N1_2003
8	2	N1_2006	N1_2006.dgpx	1	1.2	2.1	E:\AASHTOWare Data\AASHTOWare Projects\N1_2006
9	3	N2_2003	N2_2003.dgpx	1	1.2	2.1	E:\AASHTOWare Data\AASHTOWare Projects\N2_2003
10	4	N2_2006	N2_2006.dgpx	1	1.2	2.1	E:\AASHTOWare Data\AASHTOWare Projects\N2_2006
11	5	N3_2003	N3_2003.dgpx	1	1.2	2.1	E:\AASHTOWare Data\AASHTOWare Projects\N3_2003
12	6	N3_2012	N3_2012.dgpx	1	1.2	2.1	E:\AASHTOWare Data\AASHTOWare Projects\N3_2012
13	7	N4_2003	N4_2003.dgpx	1	1.2	2.1	E:\AASHTOWare Data\AASHTOWare Projects\N4_2003
14	8	N4_2012	N4_2012.dgpx	1	1.2	2.1	E:\AASHTOWare Data\AASHTOWare Projects\N4_2012
15	9	N5_2003	N5_2003.dgpx	1	1.2	2.1	E:\AASHTOWare Data\AASHTOWare Projects\N5_2003
16	10	N5_2009	N5_2009.dgpx	1	1.2	2.1	E:\AASHTOWare Data\AASHTOWare Projects\N5_2009

Figure 5.2 “Input Summary” spreadsheet

After creating and defining the control variables, a loop containing repetitive actions was executed a number of times until all experimental sections (21 experimental sections for bottom-up fatigue cracking model calibration) have been run for simulations. In each loop, the control variables were assigned based on input information, which was stored in a formatted “Input Summary” spreadsheet. Then, the created pavement design project was opened up in the pavement ME design software followed by entering the calibration coefficients. Next, the software analysis was launched, and the automation suspends temporarily while the software simulation was running. When the Pavement ME Design software completed simulation runs, the automation continued to extract and transfer the output data to a formatted “Output Summary” spreadsheet (Figure 5.3). The “Output Summary” spreadsheet was used to compare the output data with the measurement data.

E	F	G	H	I	J	K	L	M	N	O	P	Q	R	S	T
heet								Hac	C1'	C2'	C1	C2	C4	Distress Measurement Summary	
Project	N2_2003	BF1	2.20	BF2	1.00	BF3	1.00	4.90	5.32	-2.66	2.03	2.62	5729.28	N2_2003	
Crack Spaci	Mean Predicted Distress					Predicted Distress @ Reliability								Month	Fatigue cracking
	IRI (in/mi)	Permanent def	AC thermal crac	Total Cracking	Reflective	IRI (in/mi)	Permanent deforn	AC thermal c	Bottom-Up Cracking (%)		Damage	Total Cracking			
500.00	70.70	0.35	0.00	1.13	0.00	95.50	0.44	27.17	3.69		2.0800	0.02		Oct-03	0
500.00	72.00	0.37	0.00	1.94	0.00	97.80	0.46	27.17	13.95		3.3400	0.08		Nov-03	0
500.00	72.50	0.38	0.00	2.39	0.00	98.90	0.47	27.17	18.13		4.0200	0.13		Dec-03	0
500.00	73.00	0.38	0.00	2.84	0.00	99.70	0.47	27.17	20.04		4.7000	0.21		Jan-04	0
500.00	73.60	0.39	0.00	3.36	0.00	100.60	0.48	27.17	21.12		5.4600	0.33		Feb-04	0
500.00	74.70	0.40	0.00	4.21	0.00	102.20	0.50	27.17	22.23		6.6800	0.61		Mar-04	0
500.00	77.00	0.43	0.00	5.73	0.00	105.40	0.53	27.17	23.83		8.8500	1.42		Apr-04	0
500.00	81.00	0.49	0.00	8.23	0.00	110.80	0.60	27.17	26.34		12.4000	3.84		May-04	0
500.00	85.10	0.54	0.00	11.3	0.00	116.50	0.66	27.17	29.41		16.8000	9.06		Jun-04	0
500.00	88.40	0.58	0.00	14.2	0.00	121.00	0.70	27.17	32.31		21.1000	16.48		Jul-04	19.52
500.00	90.70	0.60	0.00	16.6	0.00	124.00	0.73	27.17	34.71		24.7000	23.99		Aug-04	27.39
500.00	92.60	0.62	0.00								28.1000				
500.00	94.00	0.63	0.00	20.5	0.00	128.50	0.76	27.17	38.61		30.9000	37.96		Oct-04	37.53
500.00	94.50	0.63	0.00	21.2	0.00	129.10	0.76	27.17	39.31		32.0000	40.40		Nov-04	42.43
500.00	94.70	0.63	0.00								32.5000				
500.00	94.90	0.63	0.00								33.0000				
500.00	95.30	0.63	0.00								33.9000				
500.00	95.60	0.63	0.00	22.7	0.00	130.50	0.77	27.17	40.81		34.6000	45.97		Mar-05	43.85
500.00	96.00	0.63	0.00								35.5000				
500.00	96.50	0.64	0.00				Output data from				36.9000			Measured data	
500.00	97.00	0.64	0.00				software simulation				37.9000				
500.00	97.40	0.64	0.00								39.1000				
500.00	97.90	0.64	0.00								40.3000				
500.00	98.30	0.65	0.00								41.1000				

Figure 5.3 “Output Summary” spreadsheet

Once every 21 times of loop executions (because of 21 experimental sections used), Excel Solver was launched in the “Output Summary” spreadsheet to derive the calibration coefficients C_1, C_2, and C_4 and calculate the derived SSE. The software output files and “Output Summary” spreadsheets were saved after the calculation. The total number of loops required was equal to a product of the number of sets of trial calibration coefficients (i.e., 310) and the number of pavement design projects (i.e., 21).

The program selected for executing the automation was Automation Anywhere®. Several automation programs were reviewed and compared regarding advantages of implementing conceptual logic in Figure 5.1, such as AutoIt, AutoHotKey, Automation Anywhere®, Keyboard Maestro, Livrot Mic Command©, Macro Express®, Workspace Macro Pro, UBot Studio©, and GNU Xnee. Three criteria were used to select a suitable program based on the interaction needs of the Pavement ME Design software. First, the automation software must be capable of recording mouse movements and keyboard operations as these are integral to operating the Pavement ME Design software. All the programs listed above except AutoHotKey and UBot Studio have this capacity. Second, the capability of compilation to output/execute EXE files is a necessary function since the developed macro can be turned into an Executable program for other users. This function can be used to further develop self-contained programs. Only three programs, AutoIt, AutoHotKey, and Automation Anywhere® can compile the developed macro to EXE files, which satisfies the first criterion. Third, “smart” mouse recording (record the absolute and relative coordinate) is a required function for this study since the mouse macro can crash if the absolute coordinate is only used to locate the mouse pointer. Automation Anywhere was the software that has the function of smart mouse recording and the other features. Owing to stable and powerful functionality, Automation Anywhere® was selected for use (Guo and Timm, 2016).

5.2 Benefits of automation

One benefit of automation was labor savings, which refers to the amount of time commitment that was diminished by the automation. The unit of time (minutes or hours) was used to quantify the labor savings. Another benefit of automation was time savings, which referred to an amount of time required by a project that was shortened by the automation. By the same metric of time, the labor savings and time savings were evaluated and presented as follows. The labor savings were calculated as the time required for the optimization by human maneuver, and the time savings were calculated as the difference between the optimization time by human maneuver and the optimization time by automation.

5.2.1 Rutting model calibration

During the optimization, there were 65 sets of trial calibration coefficients (presented in Chapter 3), and thus, the loop was iterated 65 times. In each loop, the simulations of 25 experimental sections were run one by one. In total, 1,625 (65x25) times of simulation runs were required. Table 5.1 lists the time required for each step of optimization by both manual maneuver and automation. The labor savings was 87.21 hours. The time savings was 30.06 hours, which was a 34.4% reduction for the coefficient optimization. This calculation includes software running time. If only actions requiring human interaction are considered, a 64.5% time reduction was realized.

Table 5.1 Time required for rutting model optimization

Stepwise Work	Manual Maneuver Time per Run, mins	Automation Time per Run, mins	Time Savings per Run, mins	Number of Simulation Runs	Manual Maneuver Time for All Runs, hrs	Automation Time for All Runs, hrs	Time Savings for All Runs, hrs
Initialize Software	0.1	0.1	0	65*25	2.71	2.71	0
Enter Trial Values of Coefficients	0.5	0.25	0.25	65*25	13.54	6.77	6.77
Execute Software Simulation	1.5	1.5	0	65*25	40.63	40.63	0
Extract Output	1	0.25	0.75	65*25	27.08	6.77	20.31
SSE Calculation	3	0.25	2.75	65	3.25	0.27	2.98
Total	6.1	2.35	3.75	-	87.21	57.15	30.06

5.2.2 Bottom-up fatigue cracking model calibration

During the optimization, there were 310 sets of trial calibration coefficients (presented in Chapter 3), and thus, the loop was iterated 310 times. In each loop, the simulation of 21 experimental sections was run one by one. In total, 6,510 (310x21) times of simulation runs were required. Table 5.2 lists the time required for each step of optimization by both manual maneuver and automation. The labor savings was 351.85 hours, and the time savings was 122.708 hours, which was a 34.9% reduction for the coefficient optimization. This calculation includes Pavement ME Design software running time. If only actions requiring human interaction are considered, a 68.8% time reduction for the coefficient optimization was realized.

Table 5.2 Time required for bottom-up fatigue cracking model optimization

Stepwise Work	Manual Maneuver Time per Run, mins	Automation Time per Run, mins	Time Savings per Run, mins	Number of Simulation Runs	Manual Maneuver Time for All Runs, hrs	Automation Time for All Runs, hrs	Time Savings for All Runs, hrs
Initialize Software	0.1	0.1	0	310*21	10.85	10.85	0
Enter Trial Values of Coefficients	0.5	0.25	0.25	310*21	54.25	27.125	27.125
Execute Software Simulation	1.5	1.5	0	310*21	162.75	162.75	0
Extract Output	1	0.25	0.75	310*21	108.5	27.125	81.375
SSE Calculation	3	0.25	2.75	310	15.5	1.292	14.208
Total	6.1	2.35	3.75	-	351.85	229.142	122.708

In addition to time and labor savings, the benefits of automation include an extension of working hours and accuracy. On the one hand, the automation can be conducted within 24 hours of a day and 7 days of a week. The working hours are greatly extended. On the other hand, the automation generates accurate outcomes. The results from the automation were checked against the one from the manual maneuver. There was no error met during a total of 286.29 hours' automation.

5.3 Investment for automation

Though automation was very beneficial, basic programming knowledge and skills are required for its successful use. There was an initial commitment to developing the automation macros. As described below, three phases are needed to accomplish automation: learning the computer language, familiarization with automation software, and macro recording/programming (Guo and Timm, 2016).

- Phase I – Learning computer language:

  Basic concepts of computer languages are required to undertake any programming task. Sequences of commands, conditional structures, and looping structures underpin the logic of codes, and these might take a beginner a few weeks to learn (e.g., by through self-study or by training courses). Many computer users may have already possessed this knowledge (Guo and Timm, 2016).

- Phase II – Familiarization with automation software:

Central to this investigation was to utilize Automation Anywhere® for running the Pavement ME Design software. Automation Anywhere® is an object-oriented programming tool, which can equip users with user-friendly capabilities of organizing objects (i.e., interactive features) instead of actions (i.e., codes of commands). Thus, the familiarization of this software relies on the user guide and technical support videos associated with the software. Phase II may take developers several weeks, or even months, depending on what functionalities developers would adopt in their macros (Guo and Timm, 2016).

- Phase III – Macro recording/programming:

Once the language and automation software basics are learned, the actual recording/programming of macros, as well as debugging and macro testing, may only take users days or weeks (Guo and Timm, 2016).

In summary, the method of automation is an easy-to-use technique that can facilitate studies requiring repetitive human maneuvering on software runs and data compiling. The automation software, like Automation Anywhere®, can very well satisfy the need of users. Though there may be a time investment (e.g., a few months for beginners) in learning, the tremendous time savings (e.g., 34.4% or 34.9% reduction in the optimization time) and labor savings (i.e., 100% reduction in optimization labor) brought by automation can justify its adoption. The working hours can be greatly extended, and the accuracy of work is reliable. Based on these, the method of automation is recommended in future M-E design calibration studies.

Chapter 6 Comparison between Master's thesis and Ph.D. dissertation

This chapter summarizes the comparison between the author's Master's thesis and Ph.D. dissertation research. There were differences in design software versions, the calibration dataset size, and calibration results. The following are the discussion for the rutting, bottom-up fatigue cracking, and IRI model calibration.

6.1 Rutting model

Table 6.1 includes a comparison for the rutting model calibration. The number of sections for the evaluation and local calibration increased from 8 to 25, and the number of sections used by the dissertation meets the AASHTO guidance (i.e., more than 20) for the rutting model calibration (AASHTO, 2010). Although the number of trial sets decreased from 106 to 64, the ranges of trial values expanded from (0.05, 1.2) to (0.05, 8). More importantly, the ranges of trial values were able to reach the "boundary" condition, which increased the probability of successful searching for optimal coefficients. In addition, the searching for $\beta_{r1,}$ $\beta_{b,}$ and β_s was conducted through an optimization process by Excel Solver after attempting each trial set of β_{r2} and β_{r3} in the software runs for the dissertation, rather than attempting a very limited number of trial values as done for the thesis. For the achieved SSE reduction, the two studies had very similar outcomes (i.e., about 90% SSE reduction), which means both studies significantly improved the prediction accuracy of the rutting model.

Table 6.1 Differences of rutting model calibration between thesis and dissertation

	Design Software	Number of Calibration and Validation Sections	Number of Trial Sets and Range of Trial Values	Achieved SSE Reduction	Local Calibration Coefficients
Investigation in Thesis	MEPDG v1.1	8 sections for calibration (157 data points) and 6 sections for validation (136 data points)	106 sets of five-coefficient combination (coefficients range from 0.05 to 1.2)	98% (from 6644.36 to 114.05)	β_{r1} = 1, β_{r2} = 1, β_{r3} = 1; β_b = 0.05; β_s = 0.05
Investigation in Dissertation	AASHTOWare™ Pavement ME Design v2.0 (build 2.0.19)	25 sections for calibration (526 data points) and 6 sections for validation (120 data points)	64 sets for β_{r2} and β_{r3} combination (range from 0.05 to 8) coupled with Excel Solver solving for β_{r1}, β_b, and β_s	89% (from 28371.89 to 3139.15)	β_{r1} = 0.05, β_{r2} = 0.5, β_{r3} = 2; β_b = 0; β_s = 0

The findings are listed as follows:

- The thesis was based on the MEPDG v1.1. The design software MEPDG was commercialized by developers late 2013 after completion of the thesis. The dissertation was based on a newer AASHTOWare™ Pavement ME Design v2.0. Though it is widely believed that the simulation algorithms of the software are not altered between versions, Kim et al. (2014) found that the two versions (i.e., MEPDG v1.1 vs. Pavement ME Design v1.1) provided different performance predictions based on the same design inputs. In this study, the configuration of pavement structures was different from that of the thesis for some sections (e.g., N3_2003 and N4_2003) since the newer version only allows three lifts of AC at most. To account for this change, the original four-layer or five-layer AC structure was converted into a three-lift AC structure by combining adjacent AC lifts. This conversion required the input changes for these sections. For this reason, the direct comparison between the prediction results of two software versions was not feasible to achieve.

- The dissertation had a larger dataset than the thesis. The number of pavement sections for the local calibration was substantially increased, so the software models were examined within a larger range of materials. Meanwhile, the information contained in each experimental section accounted for a less portion of the entire dataset, and therefore, one single section exerted a smaller impact in the process of the evaluation and local calibration. As a result, the local calibration became less dictated by any single section. Thus, the calibration results of the dissertation represented the Test Track condition more comprehensively and generally.
- The coefficient optimization in the dissertation was better than that in the thesis regarding the exhaustiveness and effectiveness of the searching. The number of trial sets β_{r2} and β_{r3} for the software runs was reduced. However, the computational power of Excel Solver was taken advantage to optimize the coefficients $\beta_{r1,}$ $\beta_{b,}$ and β_s after attempting each trial set of β_{r2} and β_{r3} in the software run. The range of trial coefficients was expanded, which increased the probability of successful searching for optimal coefficients. Therefore, the optimization in the dissertation can be considered as an advanced strategy compared to that in the thesis.
- The local calibration coefficients for the dissertation were not the same as that of the thesis, but it can be found that their coefficients, β_b and β_s, were both close to zero. This similarity indicated that the local calibration could improve the rutting prediction by reducing the rutting proportion of base and subgrade, which has been corroborated by many other studies (i.e., Mallela et al., 2009; Li et al., 2009; Darter et al., 2014; Haider et al., 2016). The calibration coefficients derived from the dissertation should be given priority when considering adoption. Since trenching has not been extensively performed to investigate the rutting proportion of base and subgrade for the Test Track sections, the assumption of layer rutting was not validated, and the calibration was only limited to reach an agreement between the total rutting predictions with the total rutting measurements.

6.2 Bottom-up fatigue cracking model

Table 6.2 includes a comparison for the bottom-up fatigue cracking model calibration. The number of sections for the evaluation and calibration increased from 7 to 21, and the number of sections used by the dissertation became much closer to the AASHTO guidance (i.e., more than 30) for the load-related cracking model calibration (AASHTO, 2010). The number of trial sets for β_{f1}, β_{f2}, and β_{f3} increased from 66 to 310, and the ranges of these trial values expanded from (0.7, 1.5) to (0.25, 4). The searching for C_1, C_2, and C_4 was conducted through an optimization process by Excel Solver after attempting each trial set of β_{f1}, β_{f2}, and β_{f3} in the software runs for the Ph.D. dissertation, rather than through an optimization just for once after reaching the optimal values of β_{f1}, β_{f2}, and β_{f3} as done for the thesis. As for the achieved SSE reduction, the two studies did not have quite similar results (i.e., 75% versus 47%) but this could be due to the difference in the calibration dataset size and the coefficient optimization.

Table 6.2 Differences of bottom-up fatigue cracking model calibration between thesis and dissertation

	Design Software	**Number of Calibration and Validation Sections**	**Number of Trial Sets and Range of Trial Values**	**Achieved SSE Reduction**	**Local Calibration Coefficients**
Investigation in Thesis	MEPDG v1.1	7 sections for calibration (28 data points) and 4 sections for validation (10 data points)	66 sets for β_{f1}, β_{f2}, and β_{f3} combination (coefficients ranged from 0.7 to 1.5) coupled with Excel Solver solving for C_1, C_2, and C_4	75% (from 452.02 originally to 111.99)	β_{f1} = 1, β_{f2} = 1, β_{f3} = 1; C_1 = 2.06; C_2 = 2.09; C_4 = 10000;
Investigation in Dissertation	AASHTOWare Pavement ME Design v2.0 (build 2.0.19)	21 sections for calibration (394 data points) and 4 sections for validation (85 data points)	310 sets for β_{f1}, β_{f2}, and β_{f3} combination (ranged from 0.25 to 4) coupled with Excel Solver solving for C_1, C_2, and C_4	47% (from 15782.68 originally to 8317.852)	β_{f1} = 2.2, β_{f2} = 1, β_{f3} = 1; C_1 = 2.03; C_2 = 2.62; C_4 = 5729.28;

The findings are listed as follows:

- Regarding the measurement data, there was a difference between the two studies. The thesis included measurement data since the cracking appeared at the road surface, but the dissertation included measurement data of the entire testing phase, including the data of "zero" cracking. The latter was appropriate to evaluate the software model at a wider range of cracking development (i.e., AC fatigue and cracking occurrence).
- The calibration data was expanded in the dissertation as compared to the thesis. The number of pavement sections for calibration was significantly increased from 7 to 21. Thus, the evaluation and local calibration became more inclusive and comprehensive.
- The coefficient optimization in the dissertation was better than that in the thesis regarding the exhaustiveness and effectiveness of the searching. The searching range for calibration coefficients was expanded, which increased the probability of successful searching for optimal coefficients. The computational power of Excel Solver was taken advantage to optimize the coefficients $C_{1,}$ $C_{2,}$ and C_4 after attempting each trial set of β_{f1}, β_{f2}, and β_{f3} in the software run. Besides, it was found that the SSE reduction from just optimizing the β_{f1}, β_{f2}, and β_{f3} was more significant than the SSE reduction from just optimizing the $C_{1,}$ $C_{2,}$ and C_4 (See more explanation in Appendix C). The optimization in the dissertation can be considered as an advanced strategy compared to that in the thesis.
- The local calibration coefficients for the dissertation were not the same as that for the thesis, but this can be explained by the difference in the calibration dataset size and the coefficient optimization. The calibration coefficients derived from the dissertation should be given priority when considering adoption.

6.3 IRI model

Table 6.3 includes a comparison for the IRI model calibration. The number of sections for the evaluation and calibration increased from 7 to 21. The searching for C_1, C_2, C_3, and C_4 was performed by the Excel Solver. For both studies, there was no validated SSE reduction brought by the local calibration. For this reason, the local calibration coefficients were the default values for the two studies.

Table 6.3 Differences of bottom-up fatigue cracking model calibration between thesis and dissertation

	Design Software	Number of Calibration and Validation Sections	Number of Trial Sets and Range of Trial Values	Achieved SSE Reduction	Local Calibration Coefficients
Investigation in Thesis	MEPDG v1.1	7 sections for calibration (143 data points) and 4 sections for validation (88 data points)	Excel Solver solving for coefficients	No SSE reduction through IRI model calibration	C_1 = 40; C_2 = 0.4; C_3 = 0.08; C_4 = 0.015;
Investigation in Dissertation	AASHTOWare^{TM} Pavement ME Design v2.0 build 2.0.19	21 sections for calibration (445 data points) and 4 sections for validation (83 data points)	Excel Solver solving for coefficients	The SSE reduction is not seen in the validation.	C_1 = 40; C_2 = 0.4; C_3 = 0.08; C_4 = 0.015;

The findings are listed as follows:

- The local calibration was not able to improve the IRI predictions in both studies. However, it could be expected that the improvement in rutting and bottom-up fatigue cracking prediction could increase the accuracy of IRI prediction.

Chapter 7 Conclusion and Recommendation

Each of earlier chapters details a component of this study. To summarize them, the study was conceived when state agencies were putting efforts in the implementation of the M-E design approaches. A problem for the implementation was a lack of confidence in the adequacy of the performance prediction models for local design conditions, though these models have been nationally-calibrated. Faced with this problem, state agencies had conducted model evaluation and local calibration studies, but the data availability and accuracy for their studies were not necessarily ideal. As a result, the values and full potential of evaluation and calibration studies were not much ascertained. Motivated by realizing this uncertainty and following up an earlier relevant study (Guo, 2013), this study was organized to evaluate and calibrate the performance predictions models (i.e., rutting, bottom-up fatigue cracking, and IRI) in the AASHTOWare^{TM} Pavement ME Design v2.0 under the NCAT Test Track condition. The design input information, regarding materials, traffic, and climate, was formulated based on the Test Track research-grade database, which was relied on by the software to simulate the configuration and response (or performance) of pavement sections. Predictions from the nationally-calibrated models in the software were compared with the measured field data at the Test Track, and the local calibration was conducted by using the automation method. The conclusions of this study were as follows:

- Over-prediction of rutting was seen in most of 25 sections using the nationally-calibrated model. Local calibration significantly improved the rutting model as evident by a 98.6% reduction in bias and a 50.2% reduction in the SEE (standard error of the estimate). The local calibration coefficients are: $\beta_{r1} = 0.05$, $\beta_{r2} = 0.5$, $\beta_{r3} = 2$, $\beta_b = 0$, and $\beta_s = 0$. Six independent sections were used to validate the local-calibrated rutting model. It showed that the improved model reduced bias by 95.9% and reduced the SEE by 71.2%.
- Over-prediction of bottom-up fatigue cracking was seen in most of 21 sections. After calibration, the prediction of bottom-up fatigue cracking was improved (80.4% reduction in bias and 52.1% reduction in SEE). The local calibration coefficients are: $\beta_{f1} = 2.2$, $\beta_{f2} = 1$, $\beta_{f3} = 1$, $C_1 = 2.03$, $C_2 =$

2.62, and C_4= 5729.28. Four independent sections were used to validate the local-calibrated model, which suggested a fair effectiveness of local calibration (78.4% reduction in bias and 54.2% reduction in SEE).

- The nationally-calibrated model accurately predicted the IRI between 35 in./mile to 65 in./mile. However, the model could not predict the IRI above 65 in./mile. In this regards, the nationally-calibrated model could be of little value for future implementation. The local calibration improved the IRI model accuracy (77.7% reduction in bias and 3.4% reduction in SEE). Four sections were used to validate the local-calibrated model, which suggested no effectiveness of local calibration (24.4% increase in bias and 2.4% increase in SEE).
- Automation is an easy-to-use technique that can facilitate studies requiring repetitive human maneuvering during software runs and data compiling. Considerable labor savings (100% reduction in optimization labor) and time savings (nearly 35% reduction in optimization time) were gained. The working hours can be greatly extended, and the accuracy of work is reliable.

From the findings of this study, it can be seen that the nationally-calibrated rutting, bottom-up fatigue cracking, and IRI models were not ready for Test Track use. Local calibration can be considered to be a necessary measure for improving the prediction accuracy for the rutting and bottom-up fatigue cracking models. The nationally-calibrated IRI model was not recommended for use. The local calibration coefficients for rutting and bottom-up fatigue cracking were ready for Test Track use. However, if they are adopted for non-Test Track design conditions, the coefficients should be evaluated based on a local and reliable database to ensure its suitability. Automation is recommended for future evaluation and calibration studies because of its benefits for coefficient optimization.

Reference

AASHTO. "Memorandum - Distribution of the Recommended Mechanistic-Empirical Pavement Design Guide (NCHRP Project 1-37A)", 2004

AASHTO. Mechanistic-Empirical Pavement Design Guide, Interim Edition: A Manual of Practice. Washington, D.C., 2008.

Alabama Geography from Netstate (December 14th, 2016). Retrieved from http://www.netstate.com/states/geography/al_geography.htm

ARA. *AASHTOWare Pavement ME Design – Release Notes*, July 1st 2013.

ARA. *Release Notes Build 2.0.19*, January 22nd 2014.

Banerjee, Ambarish, Jose P. Aguiar-Moya, and Jorge A. Prozzi. Calibration of Mechanistic-Empirical Pavement Design Guide Permanent Deformation Models – Texas Experience with Long-Term Pavement Performance. *Transportation Research Record: Journal of the Transportation Research Board*. No. 2094, pp. 12-20, Washington, D.C., 2009.

Clark, Trenton M. "DARWin-ME Pavement Design Software. 2010." Accessed at <http://www.cpe.vt.edu/pavementevaluation/presentations/Clark.pdf>, May 26th, 2016.

Darter, Michael I., Leslie Titus-Glover, Harold L. Von Quintus, Biplab B. Bhattacharya, and Jagannath Mallela. *Calibration and Implementation of the AASHTO Mechanistic-Empirical Pavement*

Design Guide in Arizona. Publication FHWA-AZ-14-606, Applied Research Associates (ARA), Inc., Champaign, IL, September 2014.

Darter, Michael I., Jag Mallela, Leslie Titus-Glover, Chetana Rao, Gregg Larson, Alex Gotlif, Harold Von Quintus, Lev Khazanovich, Matthew Witczak, Mohamed EI-Basyouny, Sherif El-Badawy, Alexksander Zborowski, and Claudia Zapata. *Changes to the Mechanistic-Empirical Pavement Design Guide Software through Version 0.900 July 2006*, Research Results Digest 308, Transportation Research Board, Washington D.C., September 2006.

Guide for the Local Calibration of the Mechanistic-Empirical Pavement Design Guide. American Association of State Highway Transportation Officials (AASHTO), Washington, D.C., 2010.

Guide for Mechanistic-Empirical Pavement Design of New and Rehabilitated Pavement Structures. NCHRP 1-37A. Applied Research Associates (ARA), Inc., ERES Division, Champaign, IL, March 2004.

Guo, Xiaolong and David H. Timm. Automating Mechanistic-Empirical Pavement Design Calibration Studies. In a submission to the Accelerated Pavement Testing Conference, Costa Rica, 2016.

Guo, Xiaolong and David H. Timm. Mechanistic-Empirical Pavement Design Software Automation. *Proceedings of the 95th Annual Transportation Research Board*, Washington, D.C., 2016.

Guo, Xiaolong and David H. Timm. Local Calibration of MEPDG Using NCAT Test Track Data. *Proceedings of the 94th Annual Transportation Research Board*, Washington, D.C., 2015.

Guo, Xiaolong. Local Calibration of the MEPDG Using the NCAT Test Track Data. A Master's Thesis Submitted to the Graduate Faculty. Department of Civil Engineering, Auburn University, Auburn, Alabama, 2013.

Haider, Syed W., Wouter C. Brink, and Neeraj Buch. Local Calibration of the Pavement-ME Flexible Pavement Performance Models in Michigan. *Proceedings of the 95th Annual Transportation Research Board*. Washington, D.C., 2016.

Hall, Kevin D., Danny X. Xiao, and Kelvin C. P. Wang. Calibration of the Mechanistic-Empirical Pavement Design Guide for Flexible Pavement Design in Arkansas. *Transportation Research Record: Journal of the Transportation Research Board*, No. 2226, pp. 135-141, Washington, D.C., 2011.

Hall, Kevin D. and Steven Beam. Estimating the Sensitivity of Design Input Variables for Rigid Pavement Analysis with a Mechanistic-Empirical Design Guide. *Transportation Research Record: Journal of the Transportation Research Board*, No. 1919, pp. 65-73, Washington, D.C., 2005.

Hoegh, Kyle, Lev Khazanovich, and Maureen Jensen. Local Calibration of Mechanistic-Empirical Pavement Design Guide Rutting Model. *Transportation Research Record: Journal of the Transportation Research Board*, No.2180, pp. 130-141, Washington, D.C., 2010.

Hossain, Zahid, Musharraf Zaman, Curtis Doiron, and Steve Cross. *Development of Flexible Pavement Database for Local Calibration of MEPDG – Volume 1*. Publication FHWA-OK-11-06(1), Oklahoma City, OK, June 2011.

Jadoun, Fadi M. and Richard Y. Kim. Calibrating Mechanistic-Empirical Pavement Design Guide for North Carolina. *Transportation Research Record: Journal of the Transportation Research Board*, No. 2305, pp. 131-140, Washington, D.C., 2012.

Kim, Sunghwan, Halil Ceylan, Di Ma, and Kasthurirangan Gopalakrishnan. Calibration of Pavement ME Design and Mechanistic-Empirical Pavement Design Guide Performance Prediction Models for Iowa Pavement Systems. *Journal of Transportation Engineering*, Volume 140, Issue 10, Reston, VA, 2014.

Li, Jianhua, Linda M. Pierce, and Jeff Uhlmeyer. Calibration of Flexible Pavement in Mechanistic-Empirical Pavement Design Guide for Washington State. *Transportation Research Record: Journal of the Transportation Research Board*, No. 2095, pp. 73-83, Washington, D.C., 2009.

Li, Qiang, Danny X. Xiao, Kelvin C. P. Wang, Kevin D. Hall, and Yanjun Qiu. Mechanistic-Empirical Pavement Design Guide (MEPDG): a Bird's-eye view. *Journal of Modern Transportation*, Volume 19, pp. 114-133, Chengdu, Sichuan Province, P. R. China, January 2011.

Mallela, Jagannath, Leslie Titus-Glover, Harold L. Von Quintus, Michael I. Darter, Mark Stanley, and Chetana Rao. *Implementing the AASHTO Mechanistic-Empirical Pavement Design Guide in Missouri, Volume II: MEPDG Model Validation and Calibration*, Publication MoDOT Study RI04-002, Applied Research Associates (ARA), Inc., Champaign, IL, March 2009.

Muthadi, Naresh R. and Richard Y. Kim. Local Calibration of Mechanistic-Empirical Pavement Design Guide for Flexible Pavement Design. *Transportation Research Record: Journal of the Transportation Research Board*, No. 2087, pp. 131-141, Washington, D.C., 2008.

Nantung, Tommy E. Implementing the Mechanistic-Empirical Pavement Design Guide for Cost Savings in Indiana. *TR News Journal*, Number 271, pp. 34-36, Washington, D.C., November-December 2010.

Pierce, Linda M. and Ginger McGovern. *Implementation of the AASHTO Mechanistic-Empirical Pavement Design Guide and Software*. *NCHRP Synthesis 457*. Transportation Research Board of the National Academies, Washington, D.C., 2014.

Rahman, Md S. Local Calibration of the MEPDG Prediction Models for Pavement Rehabilitation and Evaluation of Top-down Cracking for Oregon Roadways. A Ph.D. Dissertation Submitted to the Graduate Faculty, Iowa State University, Ames, Iowa, 2014.

"Release Notes for MEPDG Version 1.1-September 2009." (May 26th, 2016) Retrieved from http://onlinepubs.trb.org/onlinepubs/archive/mepdg/mepdg_1100_releasenotes.pdf

Robbins, Mary R.. New Methods for Predicting Critical Tensile Strains in an M-E Framework. Doctoral Dissertation Submitted to the Graduate Faculty, Department of Civil Engineering, Auburn University, 2013.

Saeed, Athar and Jim W. Hall. Jr. *Mississippi DOT's Plan to Implement the 2002 Design Guide, Final Report*. Publication FHWA/MS-DOT-RD-03-163, Applied Research Associates (ARA), Inc., ERES Division, Champaign, IL, 2003.

Schram, Scott and Magdy Abdelrahman. Improving Prediction Accuracy in Mechanistic-Empirical Pavement Design Guide. *Transportation Research Record: Journal of the Transportation Research Board*, No. 1947, pp. 59-68, Washington, D.C., 2006.

Schwartz, Charles W. and Regis L. Carvalho. *Implementation of the NCHRP 1-37A Design Guide Final Report - Volume 2: Evalution of Mechanistic-Empirical Design Procedure*. Publication MDSHA Project No. SP0077B41, UMD FRS No. 430572. Lutherville, MD, 2007.

Sharpe, Gary W. *AASHTO Memorandum - Distribution of the Recommended Mechanistic-Empirical Pavement Design Guide (NCHRP Project 1-37A)*. American Association of State Highway Transportation Officials (AASHTO), June 2004.

Shen, Sijun and David M. Neyens. The effects of age, gender, and crash types on drivers' injury-related health care costs. *Accident Analysis & Prevention*, Volume 77, pp. 82-90, 2015.

Summary of ME Design Software Local Calibration Efforts. (December 9th, 2016). Retrieved from http://www.eng.auburn.edu/research/centers/ncat/newsroom/2016/local-calibration.html

Taylor, Adam J. and David H. Timm. *Mechanistic Characterization of Resilient Moduli for Unbound Pavement Layer Materials*. Report 09-06, National Center for Asphalt Technology, Auburn University, 2009.

Timm, David H., Mary M. Robbins, Nam Tran, and Carolina Rodezno. *Flexible Pavement Design – State of the Practice*. Report 14-04, National Center for Asphalt Technology, Auburn University, Auburn, AL, 2014.

Timm, David H. *Design, Construction, and Instrumentation of the 2006 Test Track Structural Study*. Report No. 09-01, National Center for Asphalt Technology, Auburn University, 2009.

Timm, David H. and Angela L. Priest. *Material Properties of the 2003 NCAT Test Track Structural Study*. Report No. 06-01, National Center for Asphalt Technology, Auburn University, 2006.

Titus-Glover, Leslie and Jagannath Mallela. *Guidelines for Implementing NCHRP 1-37A M-E Design Procedures in Ohio: Volume 4 – MEPDG Models Validation & Recalibration.* Publication FHWA/OH-2009/9D, Applied Research Associates (ARA), Inc., Champaign, IL, 2009.

Tran, Nam and Kevin D. Hall. Development and Influence of Statewide Axle Load Spectra on Flexible Pavement Performance. *Transportation Research Record: Journal of the Transportation Research Board*, No. 2037, pp. 106-114, Washington, D.C., 2007.

U.S. Climate Data (February 9th, 2017). Retrieved from http://www.usclimatedata.com/climate/opelika/alabama/united-states/usal0413

Velasquez, R., K. Hoegh, I. Yut, N. Funk, G. Cochran, M. Marasteanu, and L. Khazanovich. *Implementation of the MEPDG for New and Rehabilitated Pavement Structures for Design of Concrete and Asphalt Pavements in Minnesota*. Publication No. NM/RC 2009-06, Minnesota Department of Transportation, January 2009.

Von Quintus, Harold L. and James S. Moulthrop. *Mechanistic-Empirical Pavement Design Guide Flexible Pavement Performance Prediction Models for Montana: Volume I Executive Research Summary*. Publication FHWA/MT-07-008/8158-1, Helena, MT, August 2007.

Wang, Kelvin C. P., Qiang Li, Kevin D. Hall, Vu Nguyen, Weiguo Gong, and Zhiqiong Hou. Database Support for the New Mechanistic-Empirical Pavement Design Guide. *Transportation*

Research Record: Journal of the Transportation Research Board, No. 2087, pp. 109-119, Washington, D.C., 2008.

Appendix A

The content of Appendix A is a summary of design inputs for the AASHTOWare™ Pavement ME Design software and the measured performance data. For the design inputs, the highest level of detail was provided where possible (Table A.1).

Table A.1 Detail level of design inputs

<table>
<tr><th colspan="4">Input Category</th><th>Level Achieved</th></tr>
<tr><td rowspan="6">Traffic</td><td rowspan="4">Traffic Volume Adjustment Factors</td><td colspan="2">Monthly Adjustment</td><td>Level 1</td></tr>
<tr><td colspan="2">Vehicle Class Distribution</td><td>Level 1</td></tr>
<tr><td colspan="2">Hourly Truck Distribution</td><td>No level classifications</td></tr>
<tr><td colspan="2">Traffic Growth Factor</td><td>No level classifications</td></tr>
<tr><td colspan="3">Axle Load Distribution Factors</td><td>Level 1</td></tr>
<tr><td colspan="3">General Traffic Inputs</td><td>No level classifications</td></tr>
<tr><td rowspan="2">Climate</td><td colspan="3">Geographic Information</td><td>No level classifications</td></tr>
<tr><td colspan="3">Hourly Environmental Condition History</td><td>Self-collected</td></tr>
<tr><td rowspan="7">Material</td><td colspan="3">HMA Design Properties</td><td>No level classifications</td></tr>
<tr><td rowspan="5">Layer Properties</td><td rowspan="3">Asphalt Material Properties</td><td>Asphalt Mix</td><td>Level 1</td></tr>
<tr><td>Asphalt Binder</td><td>Level 1</td></tr>
<tr><td>Asphalt General</td><td>No level classifications</td></tr>
<tr><td colspan="2">Crushed Stone</td><td>Level 3</td></tr>
<tr><td colspan="2">Subgrade</td><td>Level 3</td></tr>
<tr><td colspan="3">Thermal Cracking Properties</td><td>Level 3 (Default)</td></tr>
</table>

The following are the traffic and climate inputs for sections of the four cycles (i.e., 2003, 2006, 2009, and 2012 cycle).

2003 Cycle

Traffic volume and axle configuration of the 2003 cycle

Two-way AADTT	2118
Number of Lanes	1
Percent Trucks in Design Direction, %	100
Percent Trucks in Design Lane, %	100
Operational Speed, mph	45
Average Axle Width, ft	8.5
Dual Tire Spacing, in.	13.5
Tire Pressure, psi	100
Tandem Axle Spacing, in.	51.6
Tridem Axle Spacing, in.	49.2
Quad Axle Spacing, in.	49.2
Mean Wheel Location, in.	18
Traffic Wander Standard Deviation, in.	10
Design Lane Width, ft	12
Average Spacing of Short Axle, ft	12
Average Spacing of Medium Axle, ft	15
Average Spacing of Long Axle, ft	18
Percent Trucks with Short Axles	33
Percent Trucks with Medium Axles	33
Percent Trucks with Long Axles	34

Vehicle class distribution and growth of the 2003 cycle

Vehicle Class	Distribution, %	Growth Rate, %
Class 4	0	0
Class 5	0	0
Class 6	0	0
Class 7	0	0
Class 8	0	0
Class 9	9	0
Class 10	0	0
Class 11	0	0
Class 12	45.5	0
Class 13	45.5	0

Monthly adjustment of the 2003 cycle

Month	Class 4	Class 5	Class 6	Class 7	Class 8	Class 9	Class 10	Class 11	Class 12	Class 13
January	1	1	1	1	1	1	1	1	1	1
February	1	1	1	1	1	1	1	1	1	1
March	1	1	1	1	1	1	1	1	1	1
April	1	1	1	1	1	1	1	1	1	1
May	1	1	1	1	1	1	1	1	1	1
June	1	1	1	1	1	1	1	1	1	1
July	1	1	1	1	1	1	1	1	1	1
August	1	1	1	1	1	1	1	1	1	1
September	1	1	1	1	1	1	1	1	1	1
October	1	1	1	1	1	1	1	1	1	1
November	1	1	1	1	1	1	1	1	1	1
December	1	1	1	1	1	1	1	1	1	1

Axles per truck of the 2003 cycle

Vehicle Class	Single	Tandem	Tridem	Quad
Class 4	0	0	0	0
Class 5	0	0	0	0
Class 6	0	0	0	0
Class 7	0	0	0	0
Class 8	0	0	0	0
Class 9	1	2	0	0
Class 10	0	0	0	0
Class 11	0	0	0	0
Class 12	1	0	0	0
Class 13	5	1	0	0

Single axle weight distribution of the 2003 cycle

Month	Class	Total	…	12000 lbs	…	21000 lbs	…
…	…	0	0	0	0	0	0
January	9	100	0	100	0	0	0
…	…	0	0	0	0	0	0
January	12	100	0	100	0	0	0
January	13	100	0	0	0	100	0
…	…	0	0	0	0	0	0
December	9	100	0	100	0	0	0
…	…	0	0	0	0	0	0
December	12	100	0	100	0	0	0
December	13	100	0	0	0	100	0

Tandem axle weight distribution of the 2003 cycle

Month	Class	Total	…	34000 lbs	…	42000 lbs	…
…	…	0	0	0	0	0	0
January	9	100	0	100	0	0	0
…	…	0	0	0	0	0	0
January	13	100	0	0	0	100	0
…	…	0	0	0	0	0	0
December	9	100	0	100	0	0	0
…	…	0	0	0	0	0	0
December	13	100	0	0	0	100	0

General climate information of the 2003 cycle

Longitude	-85.3
Latitude	32.6
Elevation	600
Depth of Water Table	Annual (60)
Climate Station	Opelika (Self-generated)
Start Time	2003100100
End Time	2009013123

2006 Cycle

Traffic volume and axle configuration of the 2006 cycle

Two-way AADTT	3082
Number of Lanes	1
Percent Trucks in Design Direction, %	100
Percent Trucks in Design Lane, %	100
Operational Speed, mph	45
Average Axle Width, ft	8.5
Dual Tire Spacing, in.	13.5
Tire Pressure, psi	100
Tandem Axle Spacing, in.	51.6
Tridem Axle Spacing, in.	49.2
Quad Axle Spacing, in.	49.2
Mean Wheel Location, in.	18
Traffic Wander Standard Deviation, in.	10
Design Lane Width, ft	12
Average Spacing of Short Axle, ft	12
Average Spacing of Medium Axle, ft	15
Average Spacing of Long Axle, ft	18
Percent Trucks with Short Axles	33
Percent Trucks with Medium Axles	33
Percent Trucks with Long Axles	34

Vehicle class distribution and growth of the 2006 cycle

Vehicle Class	Distribution, %	Growth Rate, %
Class 4	0	0
Class 5	0	0
Class 6	0	0
Class 7	0	0
Class 8	0	0
Class 9	0	0
Class 10	0	0
Class 11	0	0
Class 12	50	0
Class 13	50	0

Monthly adjustment of the 2006 cycle

Month	Class 4	Class 5	Class 6	Class 7	Class 8	Class 9	Class 10	Class 11	Class 12	Class 13
January	1	1	1	1	1	1	1	1	1	1
February	1	1	1	1	1	1	1	1	1	1
March	1	1	1	1	1	1	1	1	1	1
April	1	1	1	1	1	1	1	1	1	1
May	1	1	1	1	1	1	1	1	1	1
June	1	1	1	1	1	1	1	1	1	1
July	1	1	1	1	1	1	1	1	1	1
August	1	1	1	1	1	1	1	1	1	1
September	1	1	1	1	1	1	1	1	1	1
October	1	1	1	1	1	1	1	1	1	1
November	1	1	1	1	1	1	1	1	1	1
December	1	1	1	1	1	1	1	1	1	1

Axles per truck of the 2006 cycle

Vehicle Class	Single	Tandem	Tridem	Quad
Class 4	0	0	0	0
Class 5	0	0	0	0
Class 6	0	0	0	0
Class 7	0	0	0	0
Class 8	0	0	0	0
Class 9	0	0	0	0
Class 10	0	0	0	0
Class 11	0	0	0	0
Class 12	1	0	0	0
Class 13	5	1	0	0

Single axle weight distribution of the 2006 cycle

Month	Class	Total	…	10000 lbs	12000 lbs	…	21000 lbs	…
…	…	0	0	0	0	0	0	0
January	12	100	0	20	80	0	0	0
January	13	100	0	0	0	0	100	0
…	…	0	0	0	0	0	0	0
December	12	100	0	20	80	0	0	0
December	13	100	0	0	0	0	100	0

Tandem axle weight distribution of the 2006 cycle

Month	Class	Total	…	42000 lbs	…
…	…	0	0	0	0
January	13	100	0	100	0
…	…	0	0	0	0
December	13	100	0	100	0

General climate information of the 2006 cycle

Longitude	-85.3
Latitude	32.6
Elevation	600
Depth of Water Table	Annual (60)
Climate Station	Opelika (Self-generated)
Start Time	2003100100
End Time	2009013123

2009 Cycle

Traffic volume and axle configuration of the 2009 cycle

Two-way AADTT	3082
Number of Lanes	1
Percent Trucks in Design Direction, %	100
Percent Trucks in Design Lane, %	100
Operational Speed, mph	45
Average Axle Width, ft	8.5
Dual Tire Spacing, in.	13.5
Tire Pressure, psi	100
Tandem Axle Spacing, in.	51.6
Tridem Axle Spacing, in.	49.2
Quad Axle Spacing, in.	49.2
Mean Wheel Location, in.	18
Traffic Wander Standard Deviation, in.	10
Design Lane Width, ft	12
Average Spacing of Short Axle, ft	12
Average Spacing of Medium Axle, ft	15
Average Spacing of Long Axle, ft	18
Percent Trucks with Short Axles	33
Percent Trucks with Medium Axles	33
Percent Trucks with Long Axles	34

Vehicle class distribution and growth of the 2009 cycle

Vehicle Class	Distribution, %	Growth Rate, %
Class 4	0	0
Class 5	0	0
Class 6	0	0
Class 7	0	0
Class 8	0	0
Class 9	0	0
Class 10	0	0
Class 11	0	0
Class 12	50	0
Class 13	50	0

Monthly adjustment of the 2009 cycle

Month	Class 4	Class 5	Class 6	Class 7	Class 8	Class 9	Class 10	Class 11	Class 12	Class 13
January	1	1	1	1	1	1	1	1	1	1
February	1	1	1	1	1	1	1	1	1	1
March	1	1	1	1	1	1	1	1	1	1
April	1	1	1	1	1	1	1	1	1	1
May	1	1	1	1	1	1	1	1	1	1
June	1	1	1	1	1	1	1	1	1	1
July	1	1	1	1	1	1	1	1	1	1
August	1	1	1	1	1	1	1	1	1	1
September	1	1	1	1	1	1	1	1	1	1
October	1	1	1	1	1	1	1	1	1	1
November	1	1	1	1	1	1	1	1	1	1
December	1	1	1	1	1	1	1	1	1	1

Axles per truck of the 2009 cycle

Vehicle Class	Single	Tandem	Tridem	Quad
Class 4	0	0	0	0
Class 5	0	0	0	0
Class 6	0	0	0	0
Class 7	0	0	0	0
Class 8	0	0	0	0
Class 9	0	0	0	0
Class 10	0	0	0	0
Class 11	0	0	0	0
Class 12	1	0	0	0
Class 13	5	1	0	0

Single axle weight distribution of the 2009 cycle

Month	Class	Total	…	10000 lbs	12000 lbs	…	21000 lbs	…
…	…	0	0	0	0	0	0	0
January	12	100	0	20	80	0	0	0
January	13	100	0	0	0	0	100	0
…	…	0	0	0	0	0	0	0
December	12	100	0	20	80	0	0	0
December	13	100	0	0	0	0	100	0

Tandem axle weight distribution of the 2009 cycle

Month	Class	Total	…	42000 lbs	…
…	…	0	0	0	0
January	13	100	0	100	0
…	…	0	0	0	0
December	13	100	0	100	0

General climate information of the 2009 cycle

Longitude	-85.3
Latitude	32.6
Elevation	600
Depth of Water Table	Annual (60)
Climate Station	Opelika (Self-generated)
Start Time	2009011501
End Time	2011100315

2012 Cycle

Traffic volume and axle configuration of the 2012 cycle

Two-way AADTT	3082
Number of Lanes	1
Percent Trucks in Design Direction, %	100
Percent Trucks in Design Lane, %	100
Operational Speed, mph	45
Average Axle Width, ft	8.5
Dual Tire Spacing, in.	13.5
Tire Pressure, psi	100
Tandem Axle Spacing, in.	51.6
Tridem Axle Spacing, in.	49.2
Quad Axle Spacing, in.	49.2
Mean Wheel Location, in.	18
Traffic Wander Standard Deviation, in.	10
Design Lane Width, ft	12
Average Spacing of Short Axle, ft	12
Average Spacing of Medium Axle, ft	15
Average Spacing of Long Axle, ft	18
Percent Trucks with Short Axles	33
Percent Trucks with Medium Axles	33
Percent Trucks with Long Axles	34

Vehicle class distribution and growth of the 2012 cycle

Vehicle Class	Distribution, %	Growth Rate, %
Class 4	0	0
Class 5	0	0
Class 6	0	0
Class 7	0	0
Class 8	0	0
Class 9	0	0
Class 10	0	0
Class 11	0	0
Class 12	50	0
Class 13	50	0

Monthly adjustment of the 2012 cycle

Month	Class 4	Class 5	Class 6	Class 7	Class 8	Class 9	Class 10	Class 11	Class 12	Class 13
January	1	1	1	1	1	1	1	1	1	1
February	1	1	1	1	1	1	1	1	1	1
March	1	1	1	1	1	1	1	1	1	1
April	1	1	1	1	1	1	1	1	1	1
May	1	1	1	1	1	1	1	1	1	1
June	1	1	1	1	1	1	1	1	1	1
July	1	1	1	1	1	1	1	1	1	1
August	1	1	1	1	1	1	1	1	1	1
September	1	1	1	1	1	1	1	1	1	1
October	1	1	1	1	1	1	1	1	1	1
November	1	1	1	1	1	1	1	1	1	1
December	1	1	1	1	1	1	1	1	1	1

Axles per truck of the 2012 cycle

Vehicle Class	Single	Tandem	Tridem	Quad
Class 4	0	0	0	0
Class 5	0	0	0	0
Class 6	0	0	0	0
Class 7	0	0	0	0
Class 8	0	0	0	0
Class 9	0	0	0	0
Class 10	0	0	0	0
Class 11	0	0	0	0
Class 12	1	0	0	0
Class 13	5	1	0	0

Single axle weight distribution of the 2012 cycle

Month	Class	Total	…	10000 lbs	12000 lbs	…	21000 lbs	…
…	…	0	0	0	0	0	0	0
January	12	100	0	20	80	0	0	0
January	13	100	0	0	0	0	100	0
…	…	0	0	0	0	0	0	0
December	12	100	0	20	80	0	0	0
December	13	100	0	0	0	0	100	0

Tandem axle weight distribution of the 2012 cycle

Month	Class	Total	…	42000 lbs	…
…	…	0	0	0	0
January	13	100	0	100	0
…	…	0	0	0	0
December	13	100	0	100	0

General climate information of the 2012 cycle

Longitude	-85.3
Latitude	32.6
Elevation	600
Depth of Water Table	Annual (60)
Climate Station	Opelika (Self-generated)
Start Time	2012100100
End Time	2014110416

A summary of material inputs for 31 experimental sections is provided hereinafter. The design inputs, if not listed, were set as default values. The material inputs are compiled in the following order:

1. N1 through N8 of the 2003 cycle
2. N1, N2, N8 through N10, and S11 of the 2006 cycle
3. N5 through N7, N10, N11, and S8 through S12 of the 2009 cycle
4. N3 through N5, S5, S6, S12, and S13 of the 2012 cycle

N1_2003

Design Life	Base Construction	Pavement Construction	Traffic Opening	Initial IRI
2 yrs	Jun, 2003	Jul, 2003	Oct, 2003	57 in./mile

AC general information of N1_2003

Lift No.	Thickness, in.	Unit Weight, pcf	Binder Content, % by volume	Air Void, %	Poisson's Ratio	Reference Temperature, °F
1	1	143.73	13.37	7.2	0.35	70
2	1.7	149.11	9.73	7.2	0.35	70
3	2.2	150.07	9.22	7	0.35	70

E* data for lift No. 1 of N1_2003

Frequency, Hz → Dynamic Modulus, psi ↘ Temperature, °F ↓	0.1	0.5	1	5	10	25
14	2083358	2468142	2629424	2985601	3162982	3344061
40	974980	1241885	1362085	1656076	1793318	2000360
70	298959	436418	511874	732658	867760	1029622
100	85463	124986	147902	245658	310272	380289
130	41408	55332	63164	99387	124043	152833

G* data for lift No. 1 of N1_2003

Temperature, °F	Shear Modulus, Pa	Phase Angle, °
70	1881000	57.98
100	134200	60.55
130	22420	58.39

E* data for lift No. 2 of N1_2003

Frequency, Hz → Dynamic Modulus, psi ↘ Temperature, °F ↓	0.1	0.5	1	5	10	25
14	2277563	2725367	2907715	3304176	3502587	3689759
40	1153195	1474779	1623189	1988503	2148479	2404942
70	394829	565357	653141	913955	1061821	1243734
100	151383	214801	254106	404945	507342	614706
130	65267	83832	95036	142898	174009	218137

G* data for lift No. 2 of N1_2003

Temperature, °F	Shear Modulus, Pa	Phase Angle, °
70	1881000	57.98
100	134200	60.55
130	22420	58.39

E* data for lift No. 3 of N1_2003

Frequency, Hz → Dynamic Modulus, psi ↘ Temperature, °F ↓	0.1	0.5	1	5	10	25
14	2277563	2725367	2907715	3304176	3502587	3689759
40	1153195	1474779	1623189	1988503	2148479	2404942
70	394829	565357	653141	913955	1061821	1243734
100	151383	214801	254106	404945	507342	614706
130	65267	83832	95036	142898	174009	218137

G* data for lift No. 3 of N1_2003

Temperature, °F	Shear Modulus, Pa	Phase Angle, °
70	1881000	57.98
100	134200	60.55
130	22420	58.39

Unbound materials general information of N1_2003

	Thickness, in.	Resilient Modulus, psi	Coefficient of lateral pressure	Poisson's Ratio
Base	6	8219	0.357	0.4
Subbase	19	8219	0.357	0.4
Subgrade	∞	26958	0.357	0.45

Unbound materials gradation and Atterberg limits of N1_2003

Sieve Size	Base	Subbase	Subgrade
#200	10	48	48
#100	15	56	56
#50	23	61	61
#30	32	64	64
#16	40	66	66
#8	49	68	68
#4	59	71	71
3/8-in.	76	75	75
1/2-in.	80	78	78
3/4-in.	90	81	81
1-in.	96	83	83
$1\frac{1}{2}$-in.	100	100	100
Liquid Limit	6	21	21
Plastic Index	1	5	5

N2_2003

Design Life	Base Construction	Pavement Construction	Traffic Opening	Initial IRI
2 yrs	Jun, 2003	Jul, 2003	Oct, 2003	56 in./mile

AC general information of N2_2003

Lift No.	Thickness, in.	Unit Weight, pcf	Binder Content, % by volume	Air Void, %	Poisson's Ratio	Reference Temperature, °F
1	1.1	144.23	13.11	7.1	0.35	70
2	2	151.76	9.17	6.1	0.35	70
3	1.8	150.07	9.22	7	0.35	70

E* data for lift No. 1 of N2_2003

Frequency, Hz → Dynamic Modulus, psi ↘ Temperature, °F ↓	0.1	0.5	1	5	10	25
14	2029222	2417379	2581816	2944301	3101703	3271941
40	791507	1031399	1139742	1432827	1564304	1723628
70	288879	430798	508140	737843	859820	1031689
100	87639	123391	146234	235505	295514	382066
130	31256	39958	45397	64941	77414	97647

G* data for lift No. 1 of N2_2003

Temperature, °F	Shear Modulus, Pa	Phase Angle, °
70	2156000	55.8
100	241800	61.59
130	26710	70.67

E* data for lift No. 2 of N2_2003

Frequency, Hz → Dynamic Modulus, psi ↘ Temperature, °F ↓	0.1	0.5	1	5	10	25
14	2298485	2724243	2897164	3289201	3421801	3617276
40	1072481	1395625	1543418	1920335	2087564	2327093
70	378875	547046	643423	930961	1064722	1310597
100	139490	197650	233293	359657	445592	574095
130	63055	79553	89815	135103	167845	215345

G* data for lift No. 2 of N2_2003

Temperature, °F	Shear Modulus, Pa	Phase Angle, °
70	2156000	55.8
100	241800	61.59
130	26710	70.67

E* data for lift No. 3 of N2_2003

Frequency, Hz → Dynamic Modulus, psi ↘ Temperature, °F ↓	0.1	0.5	1	5	10	25
14	2277563	2725367	2907715	3304176	3502587	3689759
40	1153195	1474779	1623189	1988503	2148479	2404942
70	394829	565357	653141	913955	1061821	1243734
100	151383	214801	254106	404945	507342	614706
130	65267	83832	95036	142898	174009	218137

G* data for lift No. 3 of N2_2003

Temperature, °F	Shear Modulus, Pa	Phase Angle, °
70	2156000	55.8
100	241800	61.59
130	26710	70.67

Unbound materials general information of N2_2003

	Thickness, in.	Resilient Modulus, psi	Coefficient of lateral pressure	Poisson's Ratio
Base	6	10061	0.357	0.4
Subbase	19	10061	0.357	0.4
Subgrade	∞	27482	0.357	0.45

Unbound materials gradation and Atterberg limits of N2_2003

Sieve Size	Base	Subbase	Subgrade
#200	10	48	48
#100	15	56	56
#50	23	61	61
#30	32	64	64
#16	40	66	66
#8	49	68	68
#4	59	71	71
3/8-in.	76	75	75
1/2-in.	80	78	78
3/4-in.	90	81	81
1-in.	96	83	83
$1\frac{1}{2}$-in.	100	100	100
Liquid Limit	6	21	21
Plastic Index	1	5	5

N3_2003

Design Life	Base Construction	Pavement Construction	Traffic Opening	Initial IRI
2 yrs	Jun, 2003	Jul, 2003	Oct, 2003	35 in./mile

AC general information of N3_2003

Lift No.	Thickness, in.	Unit Weight, pcf	Binder Content, % by volume	Air Void, %	Poisson's Ratio	Reference Temperature, °F
1	1.2	144.07	13.09	7.2	0.35	70
2	1.8	150.79	9.12	6.7	0.35	70
3	6.1	150.12	9.97	6.35	0.35	70

E* data for lift No. 1 of N3_2003

Frequency, Hz → Dynamic Modulus, psi ↘ Temperature, °F ↓	0.1	0.5	1	5	10	25
14	2029222	2417379	2581816	2944301	3101703	3271941
40	791507	1031399	1139742	1432827	1564304	1723628
70	288879	430798	508140	737843	859820	1031689
100	87639	123391	146234	235505	295514	382066
130	31256	39958	45397	64941	77414	97647

G* data for lift No. 1 of N3_2003

Temperature, °F	Shear Modulus, Pa	Phase Angle, °
70	2156000	55.8
100	241800	61.59
130	26710	70.67

E* data for lift No. 2 of N3_2003

Frequency, Hz → Dynamic Modulus, psi ↘ Temperature, °F ↓	0.1	0.5	1	5	10	25
14	2298485	2724243	2897164	3289201	3421801	3617276
40	1072481	1395625	1543418	1920335	2087564	2327093
70	378875	547046	643423	930961	1064722	1310597
100	139490	197650	233293	359657	445592	574095
130	63055	79553	89815	135103	167845	215345

G* data for lift No. 2 of N3_2003

Temperature, °F	Shear Modulus, Pa	Phase Angle, °
70	2156000	55.8
100	241800	61.59
130	26710	70.67

E* data for lift No. 3 of N3_2003

Frequency, Hz → Dynamic Modulus, psi ↘ Temperature, °F ↓	0.1	0.5	1	5	10	25
14	2298485	2724243	2897164	3289201	3421801	3617276
40	1072481	1395625	1543418	1920335	2087564	2327093
70	378875	547046	643423	930961	1064722	1310597
100	139490	197650	233293	359657	445592	574095
130	63055	79553	89815	135103	167845	215345

G* data for lift No. 3 of N3_2003

Temperature, °F	Shear Modulus, Pa	Phase Angle, °
70	2156000	55.8
100	241800	61.59
130	26710	70.67

Unbound materials general information of N3_2003

	Thickness, in.	Resilient Modulus, psi	Coefficient of lateral pressure	Poisson's Ratio
Base	6	13083	0.357	0.4
Subbase	15	13083	0.357	0.4
Subgrade	∞	32516	0.357	0.45

Unbound materials gradation and Atterberg limits of N3_2003

Sieve Size	Base	Subbase	Subgrade
#200	10	48	48
#100	15	56	56
#50	23	61	61
#30	32	64	64
#16	40	66	66
#8	49	68	68
#4	59	71	71
3/8-in.	76	75	75
1/2-in.	80	78	78
3/4-in.	90	81	81
1-in.	96	83	83
$1\frac{1}{2}$-in.	100	100	100
Liquid Limit	6	21	21
Plastic Index	1	5	5

N4_2003

Design Life	Base Construction	Pavement Construction	Traffic Opening	Initial IRI
2 yrs	Jun, 2003	Jul, 2003	Oct, 2003	48 in./mile

AC general information of N4_2003

Lift No.	Thickness, in.	Unit Weight, pcf	Binder Content, % by volume	Air Void, %	Poisson's Ratio	Reference Temperature, °F
1	1	145.35	12.98	6.6	0.35	70
2	4	149.22	9.82	6.9	0.35	70
3	3.8	148.41	10.1	7.25	0.35	70

E* data for lift No. 1 of N4_2003

Frequency, Hz → Dynamic Modulus, psi ↘ Temperature, °F ↓	0.1	0.5	1	5	10	25
14	2083358	2468142	2629424	2985601	3162982	3344061
40	974980	1241885	1362085	1656076	1793318	2000360
70	298959	436418	511874	732658	867760	1029622
100	85463	124986	147902	245658	310272	380289
130	41408	55332	63164	99387	124043	152833

G* data for lift No. 1 of N4_2003

Temperature, °F	Shear Modulus, Pa	Phase Angle, °
70	1881000	57.98
100	134200	60.55
130	22420	58.39

E* data for lift No. 2 of N4_2003

Frequency, Hz → Dynamic Modulus, psi ↘ Temperature, °F ↓	0.1	0.5	1	5	10	25
14	2277563	2725367	2907715	3304176	3502587	3689759
40	1153195	1474779	1623189	1988503	2148479	2404942
70	394829	565357	653141	913955	1061821	1243734
100	151383	214801	254106	404945	507342	614706
130	65267	83832	95036	142898	174009	218137

G* data for lift No. 2 of N4_2003

Temperature, °F	Shear Modulus, Pa	Phase Angle, °
70	1881000	57.98
100	134200	60.55
130	22420	58.39

E* data for lift No. 3 of N4_2003

Frequency, Hz → Dynamic Modulus, psi ↘ Temperature, °F ↓	0.1	0.5	1	5	10	25
14	2277563	2725367	2907715	3304176	3502587	3689759
40	1153195	1474779	1623189	1988503	2148479	2404942
70	394829	565357	653141	913955	1061821	1243734
100	151383	214801	254106	404945	507342	614706
130	65267	83832	95036	142898	174009	218137

G* data for lift No. 3 of N4_2003

Temperature, °F	Shear Modulus, Pa	Phase Angle, °
70	1881000	57.98
100	134200	60.55
130	22420	58.39

Unbound materials general information of N4_2003

	Thickness, in.	Resilient Modulus, psi	Coefficient of lateral pressure	Poisson's Ratio
Base	6	11717	0.357	0.4
Subbase	15	11717	0.357	0.4
Subgrade	∞	33889	0.357	0.45

Unbound materials gradation and Atterberg limits of N4_2003

Sieve Size	Base	Subbase	Subgrade
#200	10	48	48
#100	15	56	56
#50	23	61	61
#30	32	64	64
#16	40	66	66
#8	49	68	68
#4	59	71	71
3/8-in.	76	75	75
1/2-in.	80	78	78
3/4-in.	90	81	81
1-in.	96	83	83
$1\frac{1}{2}$-in.	100	100	100
Liquid Limit	6	21	21
Plastic Index	1	5	5

N5_2003

Design Life	Base Construction	Pavement Construction	Traffic Opening	Initial IRI
2 yrs	Jun, 2003	Jul, 2003	Oct, 2003	59 in./mile

AC general information of N5_2003

Lift No.	Thickness, in.	Unit Weight, pcf	Binder Content, % by volume	Air Void, %	Poisson's Ratio	Reference Temperature, °F
1	1	145.2	12.97	6.7	0.35	70
2	3.9	148.89	9.77	7.15	0.35	70
3	2	148.71	10.52	6.8	0.35	70

E* data for lift No. 1 of N5_2003

Frequency, Hz → Dynamic Modulus, psi ↘ Temperature, °F ↓	0.1	0.5	1	5	10	25
14	2083358	2468142	2629424	2985601	3162982	3344061
40	974980	1241885	1362085	1656076	1793318	2000360
70	298959	436418	511874	732658	867760	1029622
100	85463	124986	147902	245658	310272	380289
130	41408	55332	63164	99387	124043	152833

G* data for lift No. 1 of N5_2003

Temperature, °F	Shear Modulus, Pa	Phase Angle, °
70	1881000	57.98
100	134200	60.55
130	22420	58.39

E* data for lift No. 2 of N5_2003

Frequency, Hz → Dynamic Modulus, psi ↘ Temperature, °F ↓	0.1	0.5	1	5	10	25
14	2277563	2725367	2907715	3304176	3502587	3689759
40	1153195	1474779	1623189	1988503	2148479	2404942
70	394829	565357	653141	913955	1061821	1243734
100	151383	214801	254106	404945	507342	614706
130	65267	83832	95036	142898	174009	218137

G* data for lift No. 2 of N5_2003

Temperature, °F	Shear Modulus, Pa	Phase Angle, °
70	1881000	57.98
100	134200	60.55
130	22420	58.39

E* data for lift No. 3 of N5_2003

Frequency, Hz → Dynamic Modulus, psi ↘ Temperature, °F ↓	0.1	0.5	1	5	10	25
14	2277563	2725367	2907715	3304176	3502587	3689759
40	1153195	1474779	1623189	1988503	2148479	2404942
70	394829	565357	653141	913955	1061821	1243734
100	151383	214801	254106	404945	507342	614706
130	65267	83832	95036	142898	174009	218137

G* data for lift No. 3 of N5_2003

Temperature, °F	Shear Modulus, Pa	Phase Angle, °
70	1881000	57.98
100	134200	60.55
130	22420	58.39

Unbound materials general information of N5_2003

	Thickness, in.	Resilient Modulus, psi	Coefficient of lateral pressure	Poisson's Ratio
Base	6	7852	0.357	0.4
Subbase	17	7852	0.357	0.4
Subgrade	∞	30564	0.357	0.45

Unbound materials gradation and Atterberg limits of N5_2003

Sieve Size	Base	Subbase	Subgrade
#200	10	48	48
#100	15	56	56
#50	23	61	61
#30	32	64	64
#16	40	66	66
#8	49	68	68
#4	59	71	71
3/8-in.	76	75	75
1/2-in.	80	78	78
3/4-in.	90	81	81
1-in.	96	83	83
$1\frac{1}{2}$-in.	100	100	100
Liquid Limit	6	21	21
Plastic Index	1	5	5

N6_2003

Design Life	Base Construction	Pavement Construction	Traffic Opening	Initial IRI
2 yrs	Jun, 2003	Jul, 2003	Oct, 2003	52 in./mile

AC general information of N6_2003

Lift No.	Thickness, in.	Unit Weight, pcf	Binder Content, % by volume	Air Void, %	Poisson's Ratio	Reference Temperature, °F
1	1.1	145	13.56	6.3	0.35	70
2	4.1	150.41	10.04	6.21	0.35	70
3	2	153.23	11.07	4	0.35	70

E* data for lift No. 1 of N6_2003

Frequency, Hz → Dynamic Modulus, psi ↘ Temperature, °F ↓	0.1	0.5	1	5	10	25
14	2029222	2417379	2581816	2944301	3101703	3271941
40	791507	1031399	1139742	1432827	1564304	1723628
70	288879	430798	508140	737843	859820	1031689
100	87639	123391	146234	235505	295514	382066
130	31256	39958	45397	64941	77414	97647

G* data for lift No. 1 of N6_2003

Temperature, °F	Shear Modulus, Pa	Phase Angle, °
70	2156000	55.8
100	241800	61.59
130	26710	70.67

E* data for lift No. 2 of N6_2003

Frequency, Hz → Dynamic Modulus, psi ↘ Temperature, °F ↓	0.1	0.5	1	5	10	25
14	2298485	2724243	2897164	3289201	3421801	3617276
40	1072481	1395625	1543418	1920335	2087564	2327093
70	378875	547046	643423	930961	1064722	1310597
100	139490	197650	233293	359657	445592	574095
130	63055	79553	89815	135103	167845	215345

G* data for lift No. 2 of N6_2003

Temperature, °F	Shear Modulus, Pa	Phase Angle, °
70	2156000	55.8
100	241800	61.59
130	26710	70.67

E* data for lift No. 3 of N6_2003

Frequency, Hz → Dynamic Modulus, psi ↘ Temperature, °F ↓	0.1	0.5	1	5	10	25
14	2298485	2724243	2897164	3289201	3421801	3617276
40	1072481	1395625	1543418	1920335	2087564	2327093
70	378875	547046	643423	930961	1064722	1310597
100	139490	197650	233293	359657	445592	574095
130	63055	79553	89815	135103	167845	215345

G* data for lift No. 3 of N6_2003

Temperature, °F	Shear Modulus, Pa	Phase Angle, °
70	2156000	55.8
100	241800	61.59
130	26710	70.67

Unbound materials general information of N6_2003

	Thickness, in.	Resilient Modulus, psi	Coefficient of lateral pressure	Poisson's Ratio
Base	6	11153	0.357	0.4
Subbase	17	11153	0.357	0.4
Subgrade	∞	34682	0.357	0.45

Unbound materials gradation and Atterberg limits of N6_2003

Sieve Size	Base	Subbase	Subgrade
#200	10	48	48
#100	15	56	56
#50	23	61	61
#30	32	64	64
#16	40	66	66
#8	49	68	68
#4	59	71	71
3/8-in.	76	75	75
1/2-in.	80	78	78
3/4-in.	90	81	81
1-in.	96	83	83
$1\frac{1}{2}$-in.	100	100	100
Liquid Limit	6	21	21
Plastic Index	1	5	5

N7_2003

Design Life	Base Construction	Pavement Construction	Traffic Opening	Initial IRI
2 yrs	Jun, 2003	Jul, 2003	Oct, 2003	44 in./mile

AC general information of N7_2003

Lift No.	Thickness, in.	Unit Weight, pcf	Binder Content, % by volume	Air Void, %	Poisson's Ratio	Reference Temperature, °F
1	1	141.63	13.72	6.9	0.35	70
2	4.1	150.52	10.05	6.14	0.35	70
3	2	151.64	10.96	5	0.35	70

E* data for lift No. 1 of N7_2003

Frequency, Hz → Dynamic Modulus, psi ↘ Temperature, °F ↓	0.1	0.5	1	5	10	25
14	2298485	2724243	2897164	3289201	3421801	3617276
40	1072481	1395625	1543418	1920335	2087564	2327093
70	378875	547046	643423	930961	1064722	1310597
100	139490	197650	233293	359657	445592	574095
130	63055	79553	89815	135103	167845	215345

G* data for lift No. 1 of N7_2003

Temperature, °F	Shear Modulus, Pa	Phase Angle, °
70	2156000	55.8
100	241800	61.59
130	26710	70.67

E* data for lift No. 2 of N7_2003

Frequency, Hz → Dynamic Modulus, psi ↘ Temperature, °F ↓	0.1	0.5	1	5	10	25
14	2298485	2724243	2897164	3289201	3421801	3617276
40	1072481	1395625	1543418	1920335	2087564	2327093
70	378875	547046	643423	930961	1064722	1310597
100	139490	197650	233293	359657	445592	574095
130	63055	79553	89815	135103	167845	215345

G* data for lift No. 2 of N7_2003

Temperature, °F	Shear Modulus, Pa	Phase Angle, °
70	2156000	55.8
100	241800	61.59
130	26710	70.67

E* data for lift No. 3 of N7_2003

Frequency, Hz → Dynamic Modulus, psi ↘ Temperature, °F ↓	0.1	0.5	1	5	10	25
14	2298485	2724243	2897164	3289201	3421801	3617276
40	1072481	1395625	1543418	1920335	2087564	2327093
70	378875	547046	643423	930961	1064722	1310597
100	139490	197650	233293	359657	445592	574095
130	63055	79553	89815	135103	167845	215345

G* data for lift No. 3 of N7_2003

Temperature, °F	Shear Modulus, Pa	Phase Angle, °
70	2156000	55.8
100	241800	61.59
130	26710	70.67

Unbound materials general information of N7_2003

	Thickness, in.	Resilient Modulus, psi	Coefficient of lateral pressure	Poisson's Ratio
Base	6	12243	0.357	0.4
Subbase	17	12243	0.357	0.4
Subgrade	∞	33817	0.357	0.45

Unbound materials gradation and Atterberg limits of N7_2003

Sieve Size	Base	Subbase	Subgrade
#200	10	48	48
#100	15	56	56
#50	23	61	61
#30	32	64	64
#16	40	66	66
#8	49	68	68
#4	59	71	71
3/8-in.	76	75	75
1/2-in.	80	78	78
3/4-in.	90	81	81
1-in.	96	83	83
$1\frac{1}{2}$-in.	100	100	100
Liquid Limit	6	21	21
Plastic Index	1	5	5

N8_2003

Design Life	Base Construction	Pavement Construction	Traffic Opening	Initial IRI
2 yrs	Jun, 2003	Jul, 2003	Oct, 2003	42 in./mile

AC general information of N8_2003

Lift No.	Thickness, in.	Unit Weight, pcf	Binder Content, % by volume	Air Void, %	Poisson's Ratio	Reference Temperature, °F
1	1.1	141.58	13.75	6.9	0.35	70
2	3.9	149.12	9.97	7	0.35	70
3	2	148.92	10.94	6.7	0.35	70

E* data for lift No. 1 of N8_2003

Frequency, Hz → Dynamic Modulus, psi ↘ Temperature, °F ↓	0.1	0.5	1	5	10	25
14	2501030	3002969	3219256	3670070	3851331	4038067
40	1271183	1639905	1818265	2239708	2427604	2700312
70	378222	526886	602668	840348	962434	1150910
100	136843	192356	227383	354291	434497	536096
130	54679	71504	82128	132746	166975	203415

G* data for lift No. 1 of N8_2003

Temperature, °F	Shear Modulus, Pa	Phase Angle, °
70	1881000	57.98
100	134200	60.55
130	22420	58.39

E* data for lift No. 2 of N8_2003

Frequency, Hz → Dynamic Modulus, psi ↘ Temperature, °F ↓	0.1	0.5	1	5	10	25
14	2298485	2724243	2897164	3289201	3421801	3617276
40	1072481	1395625	1543418	1920335	2087564	2327093
70	378875	547046	643423	930961	1064722	1310597
100	139490	197650	233293	359657	445592	574095
130	63055	79553	89815	135103	167845	215345

G* data for lift No. 2 of N8_2003

Temperature, °F	Shear Modulus, Pa	Phase Angle, °
70	2156000	55.8
100	241800	61.59
130	26710	70.67

E* data for lift No. 3 of N8_2003

Frequency, Hz → Dynamic Modulus, psi ↘ Temperature, °F ↓	0.1	0.5	1	5	10	25
14	2761276	3333933	3219220	3974323	4214904	4448777
40	1157219	1588235	1796618	2290544	2514047	2828271
70	366474	537292	639000	954565	1119401	1364623
100	127959	177671	209543	324123	403205	533630
130	52540	66536	75637	116139	142935	180318

G* data for lift No. 3 of N8_2003

Temperature, °F	Shear Modulus, Pa	Phase Angle, °
70	2156000	55.8
100	241800	61.59
130	26710	70.67

Unbound materials general information of N8_2003

	Thickness, in.	Resilient Modulus, psi	Coefficient of lateral pressure	Poisson's Ratio
Base	6	10258	0.357	0.4
Subbase	17	10258	0.357	0.4
Subgrade	∞	30859	0.357	0.45

Unbound materials gradation and Atterberg limits of N8_2003

Sieve Size	Base	Subbase	Subgrade
#200	10	48	48
#100	15	56	56
#50	23	61	61
#30	32	64	64
#16	40	66	66
#8	49	68	68
#4	59	71	71
3/8-in.	76	75	75
1/2-in.	80	78	78
3/4-in.	90	81	81
1-in.	96	83	83
$1\frac{1}{2}$-in.	100	100	100
Liquid Limit	6	21	21
Plastic Index	1	5	5

N1_2006

Design Life	Base Construction	Pavement Construction	Traffic Opening	Initial IRI
2 yrs	Aug, 2006	Sep, 2006	Nov, 2006	115.01 in./mile

AC general information of N1_2006

Lift No.	Thickness, in.	Unit Weight, pcf	Binder Content, % by volume	Air Void, %	Poisson's Ratio	Reference Temperature, °F
1	2.2	147.52	10.38	5.4	0.35	70
2	1.9	143.14	10.55	7.8	0.35	70
3	3.3	147.53	9.7	7.9	0.35	70

E* data for lift No. 1 of N1_2006

Frequency, Hz → Dynamic Modulus, psi ↘ Temperature, °F ↓	0.5	1	2	5	10	20
15	2157627	2410856	2693804	3119436	3485547	3894627
40	1046350	1173742	1313558	1501575	1649804	1805284
70	331943	399192	477657	597217	701644	821300
100	101212	123625	157849	214849	268658	334312
130	69097	77207	86268	99899	111624	124724

G* data for lift No. 1 of N1_2006

Temperature, °F	Shear Modulus, Pa	Phase Angle, °
70	2053000	55.59
100	225900	62.21
130	28460	69.96

E* data for lift No. 2 of N1_2006

Frequency, Hz → Dynamic Modulus, psi ↘ Temperature, °F ↓	0.5	1	2	5	10	20
15	2157627	2410856	2693804	3119436	3485547	3894627
40	1046350	1173742	1313558	1501575	1649804	1805284
70	331943	399192	477657	597217	701644	821300
100	101212	123625	157849	214849	268658	334312
130	69097	77207	86268	99899	111624	124724

G* data for lift No. 2 of N1_2006

Temperature, °F	Shear Modulus, Pa	Phase Angle, °
70	2053000	55.59
100	225900	62.21
130	28460	69.96

E* data for lift No. 3 of N1_2006

Frequency, Hz → Dynamic Modulus, psi ↘ Temperature, °F ↓	0.5	1	2	5	10	20
15	2458627	2750572	3077182	3569202	3993019	4467161
40	1157594	1304856	1459611	1676636	1848167	2021584
70	362401	438207	526632	662194	779674	910982
100	101227	123137	155480	210643	263824	330154
130	70623	79009	88391	102524	114698	128318

G* data for lift No. 3 of N1_2006

Temperature, °F	Shear Modulus, Pa	Phase Angle, °
70	2156000	55.8
100	241800	61.59
130	26710	70.67

Unbound materials general information of N1_2006

	Thickness, in.	Resilient Modulus, psi	Coefficient of lateral pressure	Poisson's Ratio
Base	10	23597	0.357	0.4
Subgrade	∞	29701	0.357	0.45

Unbound materials gradation and Atterberg limits of N1_2006

Sieve Size	Base	Subgrade
#200	18.8	48
#100	21	56
#50	23	61
#30	26	64
#16	32	66
#8	44	68
#4	61	71
3/8-in.	81	75
1/2-in.	88	78
3/4-in.	100	81
1-in.	100	83
$1\frac{1}{2}$-in.	100	100
Liquid Limit	6	21
Plastic Index	1	5

N2_2006

Design Life	Base Construction	Pavement Construction	Traffic Opening	Initial IRI
2 yrs	Aug, 2006	Sep, 2006	Nov, 2006	105.8 in./mile

AC general information of N2_2006

Lift No.	Thickness, in.	Unit Weight, pcf	Binder Content, % by volume	Air Void, %	Poisson's Ratio	Reference Temperature, °F
1	2	148.14	10.33	5	0.35	70
2	2	145.48	11.3	5.8	0.35	70
3	3.1	152.01	10.08	5.1	0.35	70

E* data for lift No. 1 of N2_2006

Frequency, Hz → Dynamic Modulus, psi ↘ Temperature, °F ↓	0.5	1	2	5	10	20
15	2164720	2404672	2671222	3069457	3409696	3787650
40	1055004	1178044	1307756	1483590	1622101	1763900
70	349879	417370	494772	613171	715519	829761
100	99167	118974	149824	201119	249852	309317
130	71687	79633	88460	101648	112916	125432

G* data for lift No. 1 of N2_2006

Temperature, °F	Shear Modulus, Pa	Phase Angle, °
70	2177000	55.88
100	267400	59.63
130	37560	65.3

E* data for lift No. 2 of N2_2006

Frequency, Hz → Dynamic Modulus, psi ↘ Temperature, °F ↓	0.5	1	2	5	10	20
15	2164720	2404672	2671222	3069457	3409696	3787650
40	1055004	1178044	1307756	1483590	1622101	1763900
70	349879	417370	494772	613171	715519	829761
100	99167	118974	149824	201119	249852	309317
130	71687	79633	88460	101648	112916	125432

G* data for lift No. 2 of N2_2006

Temperature, °F	Shear Modulus, Pa	Phase Angle, °
70	2177000	55.88
100	267400	59.63
130	37560	65.3

E* data for lift No. 3 of N2_2006

Frequency, Hz → Dynamic Modulus, psi ↘ Temperature, °F ↓	0.5	1	2	5	10	20
15	2458627	2750572	3077182	3569202	3993019	4467161
40	1157594	1304856	1459611	1676636	1848167	2021584
70	362401	438207	526632	662194	779674	910982
100	101227	123137	155480	210643	263824	330154
130	70623	79009	88391	102524	114698	128318

G* data for lift No. 3 of N2_2006

Temperature, °F	Shear Modulus, Pa	Phase Angle, °
70	2156000	55.8
100	241800	61.59
130	26710	70.67

Unbound materials general information of N2_2006

	Thickness, in.	Resilient Modulus, psi	Coefficient of lateral pressure	Poisson's Ratio
Base	10	25605	0.357	0.4
Subgrade	∞	29638	0.357	0.45

Unbound materials gradation and Atterberg limits of N2_2006

Sieve Size	Base	Subgrade
#200	18.8	48
#100	21	56
#50	23	61
#30	26	64
#16	32	66
#8	44	68
#4	61	71
3/8-in.	81	75
1/2-in.	88	78
3/4-in.	100	81
1-in.	100	83
$1\frac{1}{2}$-in.	100	100
Liquid Limit	6	21
Plastic Index	1	5

N8_2006

Design Life	Base Construction	Pavement Construction	Traffic Opening	Initial IRI
2 yrs	Aug, 2006	Oct, 2006	Nov, 2006	94.56 in./mile

AC general information of N8_2006

Lift No.	Thickness, in.	Unit Weight, pcf	Binder Content, % by volume	Air Void, %	Poisson's Ratio	Reference Temperature, °F
1	2.3	137.31	10.91	8.2	0.35	70
2	5.75	145.45	7.52	6.74	0.35	70
3	2	147.02	11.16	2.8	0.35	70

E* data for lift No. 1 of N8_2006

Frequency, Hz → Dynamic Modulus, psi ↘ Temperature, °F ↓	0.5	1	2	5	10	20
15	2703490	2994983	3317905	3798828	4208421	4662178
40	1184842	1321351	1464910	1663524	1818250	1972919
70	321868	385365	460930	575335	675179	785611
100	97097	119862	152214	205185	256073	317038
130	55862	61885	68558	78495	86959	96335

G* data for lift No. 1 of N8_2006

Temperature, °F	Shear Modulus, Pa	Phase Angle, °
70	2672000	54.25
100	344800	57.77
130	34410	59.23

E* data for lift No. 2 of N8_2006

Frequency, Hz → Dynamic Modulus, psi ↘ Temperature, °F ↓	0.5	1	2	5	10	20
15	2748833.3	3026427	3332146	3784343	4166888	4588228
40	1415287.6	1563867	1715773	1917402	2072983	2227840
70	492710.7	585286.8	688849.4	843313.6	974041.2	1115902
100	144072.9	177377.8	224644	300840.9	372337.5	459446.4
130	114671.4	126141.5	138762.7	157412	173172.7	190516.4

G* data for lift No. 2 of N8_2006

Temperature, °F	Shear Modulus, Pa	Phase Angle, °
70	2397819	55.21
100	288259	60.03
130	31814	66.10

E* data for lift No. 3 of N8_2006

Frequency, Hz → Dynamic Modulus, psi ↘ Temperature, °F ↓	0.5	1	2	5	10	20
15	1852345	2088949	2355775	2761508	3114241	3512029
40	862249	983597	1112197	1289095	1427703	1565150
70	249030	311686	385075	499075	599924	712618
100	61936	79263	102812	146749	190434	245404
130	50456	56901	64169	75221	84829	95664

G* data for lift No. 3 of N8_2006

Temperature, °F	Shear Modulus, Pa	Phase Angle, °
70	768800	57.77
100	183600	62.92
130	25920	68.94

Unbound materials general information of N8_2006

	Thickness, in.	Resilient Modulus, psi	Coefficient of lateral pressure	Poisson's Ratio
Base	6.4	26020	0.357	0.4
Subgrade	∞	9801	0.357	0.45

Unbound materials gradation and Atterberg limits of N8_2006

Sieve Size	Base	Subgrade
#200	48	57.7
#100	56	82
#50	61	92
#30	64	98
#16	66	99
#8	68	100
#4	71	100
3/8-in.	75	100
1/2-in.	78	100
3/4-in.	81	100
1-in.	83	100
$1\frac{1}{2}$-in.	100	100
Liquid Limit	21	51
Plastic Index	5	30

N9_2006

Design Life	Base Construction	Pavement Construction	Traffic Opening	Initial IRI
2 yrs	Aug, 2006	Oct, 2006	Nov, 2006	104.9 in./mile

AC general information of N9_2006

Lift No.	Thickness, in.	Unit Weight, pcf	Binder Content, % by volume	Air Void, %	Poisson's Ratio	Reference Temperature, °F
1	2	139.1	11.14	7	0.35	70
2	9.2	146.61	7.38	6.08	0.35	70
3	3.2	142.79	10.74	5.6	0.35	70

E* data for lift No. 1 of N9_2006

Frequency, Hz → Dynamic Modulus, psi ↘ Temperature, °F ↓	0.5	1	2	5	10	20
15	2703490	2994983	3317905	3798828	4208421	4662178
40	1184842	1321351	1464910	1663524	1818250	1972919
70	321868	385365	460930	575335	675179	785611
100	97097	119862	152214	205185	256073	317038
130	55862	61885	68558	78495	86959	96335

G* data for lift No. 1 of N9_2006

Temperature, °F	Shear Modulus, Pa	Phase Angle, °
70	2672000	54.25
100	344800	57.77
130	34410	59.23

E* data for lift No. 2 of N9_2006

Frequency, Hz → Dynamic Modulus, psi ↘ Temperature, °F ↓	0.5	1	2	5	10	20
15	2748833.3	3026427	3332146	3784343	4166888	4588228
40	1415287.6	1563867	1715773	1917402	2072983	2227840
70	492710.7	585286.8	688849.4	843313.6	974041.2	1115902
100	144072.9	177377.8	224644	300840.9	372337.5	459446.4
130	114671.4	126141.5	138762.7	157412	173172.7	190516.4

G* data for lift No. 2 of N9_2006

Temperature, °F	Shear Modulus, Pa	Phase Angle, °
70	2397819	55.21
100	288259	60.03
130	31814	66.10

E* data for lift No. 3 of N9_2006

Frequency, Hz → Dynamic Modulus, psi ↘ Temperature, °F ↓	0.5	1	2	5	10	20
15	1852345	2088949	2355775	2761508	3114241	3512029
40	862249	983597	1112197	1289095	1427703	1565150
70	249030	311686	385075	499075	599924	712618
100	61936	79263	102812	146749	190434	245404
130	50456	56901	64169	75221	84829	95664

G* data for lift No. 3 of N9_2006

Temperature, °F	Shear Modulus, Pa	Phase Angle, °
70	768800	57.77
100	183600	62.92
130	25920	68.94

Unbound materials general information of N9_2006

	Thickness, in.	Resilient Modulus, psi	Coefficient of lateral pressure	Poisson's Ratio
Base	8.4	24155	0.357	0.4
Subgrade	∞	14804	0.357	0.45

Unbound materials gradation and Atterberg limits of N9_2006

Sieve Size	Base	Subgrade
#200	48	57.7
#100	56	82
#50	61	92
#30	64	98
#16	66	99
#8	68	100
#4	71	100
3/8-in.	75	100
1/2-in.	78	100
3/4-in.	81	100
1-in.	83	100
$1\frac{1}{2}$-in.	100	100
Liquid Limit	21	51
Plastic Index	5	30

N10_2006

Design Life	Base Construction	Pavement Construction	Traffic Opening	Initial IRI
2 yrs	Aug, 2006	Oct, 2006	Nov, 2006	65.33 in./mile

AC general information of N10_2006

Lift No.	Thickness, in.	Unit Weight, pcf	Binder Content, % by volume	Air Void, %	Poisson's Ratio	Reference Temperature, °F
1	1	139.92	10.79	8.7	0.35	70
2	3.4	143.9	8.83	7.5	0.35	70
3	2.2	144.73	9.58	6.7	0.35	70

E* data for lift No. 1 of N10_2006

Frequency, Hz → Dynamic Modulus, psi ↘ Temperature, °F ↓	0.5	1	2	5	10	20
15	2533492	2807917	3112066	3565268	3951453	4379469
40	1158174	1292866	1432586	1622391	1768444	1914739
70	318793	386332	466538	588273	691588	809649
100	92713	117891	153005	212238	268803	337889
130	61988	68702	76144	87233	96682	107154

G* data for lift No. 1 of N10_2006

Temperature, °F	Shear Modulus, Pa	Phase Angle, °
70	2413000	60.11
100	223600	65.73
130	21580	70.63

E* data for lift No. 2 of N10_2006

Frequency, Hz → Dynamic Modulus, psi ↘ Temperature, °F ↓	0.01	0.1	0.5	1	5
15	1872962	2673802	3429180	3817066	4895428
40	868486	1325886	1703564	1872146	2268873
70	171773	385317	615540	732199	1066414
115	20494	42032	75492	98775	192078
130	58961	84171	107950	120161	154108

G* data for lift No. 2 of N10_2006

Temperature, °F	Shear Modulus, Pa	Phase Angle, °
70	2413000	60.11
100	223600	65.73
130	21580	70.63

E* data for lift No. 3 of N10_2006

Frequency, Hz → Dynamic Modulus, psi ↘ Temperature, °F ↓	0.5	1	2	5	10	20
15	2399518	2670238	2971501	3422533	3808672	4238377
40	1181658	1322744	1468724	1669420	1824538	1982448
70	371840	449218	539721	675912	792885	923382
100	110254	139298	179593	246419	307842	382392
130	81342	90519	100732	116022	129112	143678

G* data for lift No. 3 of N10_2006

Temperature, °F	Shear Modulus, Pa	Phase Angle, °
70	2066000	56.25
100	220100	62.21
130	24310	70.56

Unbound materials general information of N10_2006

	Thickness, in.	Resilient Modulus, psi	Coefficient of lateral pressure	Poisson's Ratio
Base	5	16752	0.357	0.4
Subgrade	∞	28174	0.357	0.45

Unbound materials gradation and Atterberg limits of N10_2006

Sieve Size	Base	Subgrade
#200	25.1	48
#100	36	56
#50	49	61
#30	58	64
#16	64	66
#8	71	68
#4	79	71
3/8-in.	88	75
1/2-in.	92	78
3/4-in.	97	81
1-in.	99	83
$1\frac{1}{2}$-in.	100	100
Liquid Limit	6	21
Plastic Index	1	5

S11_2006

Design Life	Base Construction	Pavement Construction	Traffic Opening	Initial IRI
2 yrs	Aug, 2006	Oct, 2006	Nov, 2006	67.38 in./mile

AC general information of S11_2006

Lift No.	Thickness, in.	Unit Weight, pcf	Binder Content, % by volume	Air Void, %	Poisson's Ratio	Reference Temperature, °F
1	1	143.3	14.18	6.8	0.35	70
2	2.1	150.36	10.92	5.8	0.35	70
3	4.5	147.3	8.38	8.22	0.35	70

E* data for lift No. 1 of S11_2006

Frequency, Hz → Dynamic Modulus, psi ↘ Temperature, °F ↓	0.5	1	2	5	10	20
15	1756400	1968603	2206444	2565513	2875471	3222877
40	835804	944340	1058002	1218220	1344113	1472277
70	259521	313185	377436	476981	563375	660985
100	77489	94120	119100	163573	205132	259472
130	52461	58799	65903	76628	85886	96262

G* data for lift No. 1 of S11_2006

Temperature, °F	Shear Modulus, Pa	Phase Angle, °
70	1881000	57.98
100	134200	60.55
130	22420	58.39

E* data for lift No. 2 of S11_2006

Frequency, Hz → Dynamic Modulus, psi ↘ Temperature, °F ↓	0.01	0.1	0.5	1	5
15	1458885	2126002	2766145	3098177	4031043
40	726107	1094986	1438870	1595850	1977347
70	171483	385317	595186	701402	990559
130	59497	86704	112811	126352	164397

G* data for lift No. 2 of S11_2006

Temperature, °F	Shear Modulus, Pa	Phase Angle, °
70	1881000	57.98
100	134200	60.55
130	22420	58.39

E* data for lift No. 3 of S11_2006

Frequency, Hz → Dynamic Modulus, psi ↘ Temperature, °F ↓	0.5	1	2	5	10	20
15	2458627	2750572	3077182	3569202	3993019	4467161
40	1157594	1304856	1459611	1676636	1848167	2021584
70	362401	438207	526632	662194	779674	910982
100	101227	123137	155480	210643	263824	330154
130	70623	79009	88391	102524	114698	128318

G* data for lift No. 3 of S11_2006

Temperature, °F	Shear Modulus, Pa	Phase Angle, °
70	2156000	55.8
100	134200	60.55
130	22420	58.39

Unbound materials general information of S11_2006

	Thickness, in.	Resilient Modulus, psi	Coefficient of lateral pressure	Poisson's Ratio
Base	6.1	12530	0.357	0.4
Subgrade	∞	28873	0.357	0.45

Unbound materials gradation and Atterberg limits of S11_2006

Sieve Size	Base	Subgrade
#200	10.2	48
#100	15	56
#50	23	61
#30	31	64
#16	39	66
#8	47	68
#4	57	71
3/8-in.	78	75
1/2-in.	83	78
3/4-in.	88	81
1-in.	95	83
$1\frac{1}{2}$-in.	100	100
Liquid Limit	6	21
Plastic Index	1	5

N5_2009

Design Life	Base Construction	Pavement Construction	Traffic Opening	Initial IRI
2 yrs	Jun, 2009	Jul, 2009	Aug, 2009	69.8 in./mile

AC general information of N5_2009

Lift No.	Thickness, in.	Unit Weight, pcf	Binder Content, % by volume	Air Void, %	Poisson's Ratio	Reference Temperature, °F
1	1.3	145.15	12.39	5.9	0.35	70
2	4.8	148.12	11.30	7.04	0.35	70
3	2.9	147.07	12.99	6.4	0.35	70

E* data for lift No. 1 of N5_2009

Frequency, Hz → Dynamic Modulus, psi ↘ Temperature, °F ↓	0.1	0.5	1	5	10	25
14	1709153	1996679	2108132	2334691	2418300	2516474
40	789039.2	1091271	1229417	1551924	1686462	1856134
70	202318	333991.7	409128.3	629085.9	742301.4	906129.1
100	50873.3	83264.98	103989.8	175512.9	219340.7	292233.9
130	19428.17	27555.57	32705.36	50906.75	62626.51	83324.41

G* data for lift No. 1 of N5_2009

Temperature, °F	Shear Modulus, Pa	Phase Angle, °
70	1881000	57.98
100	134200	60.55
130	22420	58.39

E* data for lift No. 2 of N5_2009

Frequency, Hz → Dynamic Modulus, psi ↘ Temperature, °F ↓	0.1	0.5	1	5	10	25
14	2419001	2613685	2681676	2808171	2851051	2898839
40	1565154	1908913	2044251	2319713	2420595	2537808
70	592054.5	880655.1	1023551	1379228	1535074	1736273
100	173808.4	279703	343507.8	543254.5	652756.8	818029.3
130	66410.55	95833.07	114506.7	179482.5	220068.2	289065.6

G* data for lift No. 2 of N5_2009

Temperature, °F	Shear Modulus, Pa	Phase Angle, °
70	1881000	57.98
100	134200	60.55
130	22420	58.39

E* data for lift No. 3 of N5_2009

Frequency, Hz → Dynamic Modulus, psi ↘ Temperature, °F ↓	0.1	0.5	1	5	10	25
14	2063399	2312172	2403525	2580770	2643324	2714777
40	1136149	1476950	1621597	1936371	2059169	2207527
70	349866	553775.8	662983.4	959139.3	1100251	1293224
100	92897.48	152598.7	190027.4	314348.3	387078.5	502972.1
130	34882.7	50349.05	60223.18	95159.77	117514.3	156526.9

G* data for lift No. 3 of N5_2009

Temperature, °F	Shear Modulus, Pa	Phase Angle, °
70	1881000	57.98
100	134200	60.55
130	22420	58.39

Unbound materials general information of N5_2009

	Thickness, in.	Resilient Modulus, psi	Coefficient of lateral pressure	Poisson's Ratio
Base	5.67	11376	0.357	0.4
Subgrade	∞	25516	0.357	0.45

Unbound materials gradation and Atterberg limits of N5_2009

Sieve Size	Base	Subgrade
#200	10.2	48
#100	15	56
#50	23	61
#30	31	64
#16	39	66
#8	47	68
#4	57	71
3/8-in.	78	75
1/2-in.	83	78
3/4-in.	88	81
1-in.	95	83
$1\frac{1}{2}$-in.	100	100
Liquid Limit	6	21
Plastic Index	1	5

N6_2009

Design Life	Base Construction	Pavement Construction	Traffic Opening	Initial IRI
2 yrs	Jun, 2009	Jul, 2009	Aug, 2009	58.1 in./mile

AC general information of N6_2009

Lift No.	Thickness, in.	Unit Weight, pcf	Binder Content, % by volume	Air Void, %	Poisson's Ratio	Reference Temperature, °F
1	1.1	144.34	12.55	6.2	0.35	70
2	2.8	148.05	11.32	7.1	0.35	70
3	3.1	147.4	12.83	6.3	0.35	70

E* data for lift No. 1 of N6_2009

Frequency, Hz → Dynamic Modulus, psi ↘ Temperature, °F ↓	0.1	0.5	1	5	10	25
14	1709153	1996679	2108132	2334691	2418300	2516474
40	789039.2	1091271	1229417	1551924	1686462	1856134
70	202318	333991.7	409128.3	629085.9	742301.4	906129.1
100	50873.3	83264.98	103989.8	175512.9	219340.7	292233.9
130	19428.17	27555.57	32705.36	50906.75	62626.51	83324.41

G* data for lift No. 1 of N6_2009

Temperature, °F	Shear Modulus, Pa	Phase Angle, °
70	1881000	57.98
100	134200	60.55
130	22420	58.39

E* data for lift No. 2 of N6_2009

Frequency, Hz → Dynamic Modulus, psi ↘ Temperature, °F ↓	0.1	0.5	1	5	10	25
14	2419001	2613685	2681676	2808171	2851051	2898839
40	1565154	1908913	2044251	2319713	2420595	2537808
70	592054.5	880655.1	1023551	1379228	1535074	1736273
100	173808.4	279703	343507.8	543254.5	652756.8	818029.3
130	66410.55	95833.07	114506.7	179482.5	220068.2	289065.6

G* data for lift No. 2 of N6_2009

Temperature, °F	Shear Modulus, Pa	Phase Angle, °
70	1881000	57.98
100	134200	60.55
130	22420	58.39

E* data for lift No. 3 of N6_2009

Frequency, Hz → Dynamic Modulus, psi ↘ Temperature, °F ↓	0.1	0.5	1	5	10	25
14	2063399	2312172	2403525	2580770	2643324	2714777
40	1136149	1476950	1621597	1936371	2059169	2207527
70	349866	553775.8	662983.4	959139.3	1100251	1293224
100	92897.48	152598.7	190027.4	314348.3	387078.5	502972.1
130	34882.7	50349.05	60223.18	95159.77	117514.3	156526.9

G* data for lift No. 3 of N6_2009

Temperature, °F	Shear Modulus, Pa	Phase Angle, °
70	1881000	57.98
100	134200	60.55
130	22420	58.39

Unbound materials general information of N6_2009

	Thickness, in.	Resilient Modulus, psi	Coefficient of lateral pressure	Poisson's Ratio
Base	4.8	14222	0.357	0.4
Subgrade	∞	26405	0.357	0.45

Unbound materials gradation and Atterberg limits of N6_2009

Sieve Size	Base	Subgrade
#200	10.2	48
#100	15	56
#50	23	61
#30	31	64
#16	39	66
#8	47	68
#4	57	71
3/8-in.	78	75
1/2-in.	83	78
3/4-in.	88	81
1-in.	95	83
$1\frac{1}{2}$-in.	100	100
Liquid Limit	6	21
Plastic Index	1	5

N7_2009

Design Life	Base Construction	Pavement Construction	Traffic Opening	Initial IRI
2 yrs	Jun, 2009	Jul, 2009	Aug, 2009	125.2 in./mile

AC general information of N7_2009

Lift No.	Thickness, in.	Unit Weight, pcf	Binder Content, % by volume	Air Void, %	Poisson's Ratio	Reference Temperature, °F
1	1.1	144.3	12.64	6.3	0.35	70
2	2.1	147.45	10.51	7.3	0.35	70
3	2.5	147.37	10.65	7.2	0.35	70

E* data for lift No. 1 of N7_2009

Frequency, Hz → Dynamic Modulus, psi ↘ Temperature, °F ↓	0.1	0.5	1	5	10	25
14	2038637	2246074	2325276	2486024	2545748	2616562
40	1222522	1498604	1615079	1871824	1974537	2101727
70	453831	651473.8	749735.3	1001884	1117814	1274482
100	129166	204147.5	247302.8	377709.6	447945	554079.4
130	40583	62218.99	75456.84	119405.2	145685.3	189052.7

G* data for lift No. 1 of N7_2009

Temperature, °F	Shear Modulus, Pa	Phase Angle, °
70	1881000	57.98
100	134200	60.55
130	22420	58.39

E* data for lift No. 2 of N7_2009

Frequency, Hz → Dynamic Modulus, psi ↘ Temperature, °F ↓	0.1	0.5	1	5	10	25
14	2116670	2372648	2467291	2652261	2718066	2793657
40	1147699	1493310	1640788	1963957	2091047	2245519
70	340639.7	541494.4	649456.1	943973.5	1085331	1279858
100	85474.34	141790.1	177204.3	295380.8	364902.5	476278.1
130	30389.43	44353.99	53284.78	84967.02	105302.5	140904.6

G* data for lift No. 2 of N7_2009

Temperature, °F	Shear Modulus, Pa	Phase Angle, °
70	1881000	57.98
100	134200	60.55
130	22420	58.39

E* data for lift No. 3 of N7_2009

Frequency, Hz → Dynamic Modulus, psi ↘ Temperature, °F ↓	0.1	0.5	1	5	10	25
14	2116670	2372648	2467291	2652261	2718066	2793657
40	1147699	1493310	1640788	1963957	2091047	2245519
70	340639.7	541494.4	649456.1	943973.5	1085331	1279858
100	85474.34	141790.1	177204.3	295380.8	364902.5	476278.1
130	30389.43	44353.99	53284.78	84967.02	105302.5	140904.6

G* data for lift No. 3 of N7_2009

Temperature, °F	Shear Modulus, Pa	Phase Angle, °
70	1881000	57.98
100	134200	60.55
130	22420	58.39

Unbound materials general information of N7_2009

	Thickness, in.	Resilient Modulus, psi	Coefficient of lateral pressure	Poisson's Ratio
Base	5.52	16336	0.357	0.4
Subgrade	∞	26483	0.357	0.45

Unbound materials gradation and Atterberg limits of N7_2009

Sieve Size	Base	Subgrade
#200	10.2	48
#100	15	56
#50	23	61
#30	31	64
#16	39	66
#8	47	68
#4	57	71
3/8-in.	78	75
1/2-in.	83	78
3/4-in.	88	81
1-in.	95	83
$1\frac{1}{2}$-in.	100	100
Liquid Limit	6	21
Plastic Index	1	5

N10_2009

Design Life	Base Construction	Pavement Construction	Traffic Opening	Initial IRI
2 yrs	Jun, 2009	Jul, 2009	Aug, 2009	61.7 in./mile

AC general information of N10_2009

Lift No.	Thickness, in.	Unit Weight, pcf	Binder Content, % by volume	Air Void, %	Poisson's Ratio	Reference Temperature, °F
1	1.4	141.57	11.58	7.4	0.35	70
2	2.7	147.94	8.79	7.1	0.35	70
3	3	150.39	9.77	5	0.35	70

E* data for lift No. 1 of N10_2009

Frequency, Hz → Dynamic Modulus, psi ↘ Temperature, °F ↓	0.1	0.5	1	5	10	25
14	2132430	2357911	2441843	2607728	2667617	2737217
40	1257813	1575901	1708423	1994988	2106966	2243099
70	424244.5	649312.2	763632.6	1059329	1195045	1377092
100	101353.8	176691.7	222665	368741.7	450286.2	575653.4
130	27007.48	45255.43	57229.12	100116.9	127475.3	174602.5

G* data for lift No. 1 of N10_2009

Temperature, °F	Shear Modulus, Pa	Phase Angle, °
70	1881000	57.98
100	134200	60.55
130	22420	58.39

E* data for lift No. 2 of N10_2009

Frequency, Hz → Dynamic Modulus, psi ↘ Temperature, °F ↓	0.1	0.5	1	5	10	25
14	2613570	2782722	2841441	2950476	2987449	3028722
40	1835301	2157906	2281088	2526570	2615033	2717067
70	799582.8	1133045	1288328	1653858	1806429	1997919
100	244374.8	395987.8	483220	740061.4	872402.8	1063248
130	82195.05	127107.8	155557.8	252767.1	311763.7	409027.7

G* data for lift No. 2 of N10_2009

Temperature, °F	Shear Modulus, Pa	Phase Angle, °
70	1881000	57.98
100	134200	60.55
130	22420	58.39

E* data for lift No. 3 of N10_2009

Frequency, Hz → Dynamic Modulus, psi ↘ Temperature, °F ↓	0.1	0.5	1	5	10	25
14	2613570	2782722	2841441	2950476	2987449	3028722
40	1835301	2157906	2281088	2526570	2615033	2717067
70	799582.8	1133045	1288328	1653858	1806429	1997919
100	244374.8	395987.8	483220	740061.4	872402.8	1063248
130	82195.05	127107.8	155557.8	252767.1	311763.7	409027.7

G* data for lift No. 3 of N10_2009

Temperature, °F	Shear Modulus, Pa	Phase Angle, °
70	1881000	57.98
100	134200	60.55
130	22420	58.39

Unbound materials general information of N10_2009

	Thickness, in.	Resilient Modulus, psi	Coefficient of lateral pressure	Poisson's Ratio
Base	3.98	9960	0.357	0.4
Subgrade	∞	24987	0.357	0.45

Unbound materials gradation and Atterberg limits of N10_2009

Sieve Size	Base	Subgrade
#200	10.2	48
#100	15	56
#50	23	61
#30	31	64
#16	39	66
#8	47	68
#4	57	71
3/8-in.	78	75
1/2-in.	83	78
3/4-in.	88	81
1-in.	95	83
$1\frac{1}{2}$-in.	100	100
Liquid Limit	6	21
Plastic Index	1	5

N11_2009

Design Life	Base Construction	Pavement Construction	Traffic Opening	Initial IRI
2 yrs	Jun, 2009	Jul, 2009	Aug, 2009	34.4 in./mile

AC general information of N11_2009

Lift No.	Thickness, in.	Unit Weight, pcf	Binder Content, % by volume	Air Void, %	Poisson's Ratio	Reference Temperature, °F
1	1.2	140.75	11.64	7.9	0.35	70
2	3	147.62	9.44	6.9	0.35	70
3	2.9	149.54	9.36	5.8	0.35	70

E* data for lift No. 1 of N11_2009

Frequency, Hz → Dynamic Modulus, psi ↘ Temperature, °F ↓	0.1	0.5	1	5	10	25
14	2063790	2312228	2404803	2587405	2653069	2729089
40	1160471	1494410	1635561	1943405	2064291	2211400
70	363754.2	579076.6	691807.6	990904.2	1130938	1320747
100	83784.5	149912.7	191509.6	328162.6	406704.3	529797.3
130	22997.82	38543.06	48918.86	86988.99	111866.1	155550.4

G* data for lift No. 1 of N11_2009

Temperature, °F	Shear Modulus, Pa	Phase Angle, °
70	1881000	57.98
100	134200	60.55
130	22420	58.39

E* data for lift No. 2 of N11_2009

Frequency, Hz → Dynamic Modulus, psi ↘ Temperature, °F ↓	0.1	0.5	1	5	10	25
14	2452784	2650328	2720597	2853871	2900025	2952236
40	1605805	1942347	2075272	2348278	2449580	2568596
70	621588	918565.3	1062524	1415353	1568497	1765787
100	167001	283414.8	352755.6	565348.4	679340.6	848674.3
130	49857.39	80749.84	100820.9	171618.7	215960.3	290955.7

G* data for lift No. 2 of N11_2009

Temperature, °F	Shear Modulus, Pa	Phase Angle, °
70	1881000	57.98
100	134200	60.55
130	22420	58.39

E* data for lift No. 3 of N11_2009

Frequency, Hz → Dynamic Modulus, psi ↘ Temperature, °F ↓	0.1	0.5	1	5	10	25
14	2452784	2650328	2720597	2853871	2900025	2952236
40	1605805	1942347	2075272	2348278	2449580	2568596
70	621588	918565.3	1062524	1415353	1568497	1765787
100	167001	283414.8	352755.6	565348.4	679340.6	848674.3
130	49857.39	80749.84	100820.9	171618.7	215960.3	290955.7

G* data for lift No. 3 of N11_2009

Temperature, °F	Shear Modulus, Pa	Phase Angle, °
70	1881000	57.98
100	134200	60.55
130	22420	58.39

Unbound materials general information of N11_2009

	Thickness, in.	Resilient Modulus, psi	Coefficient of lateral pressure	Poisson's Ratio
Base	4.22	12089	0.357	0.4
Subgrade	∞	26194	0.357	0.45

Unbound materials gradation and Atterberg limits of N11_2009

Sieve Size	Base	Subgrade
#200	10.2	48
#100	15	56
#50	23	61
#30	31	64
#16	39	66
#8	47	68
#4	57	71
3/8-in.	78	75
1/2-in.	83	78
3/4-in.	88	81
1-in.	95	83
$1\frac{1}{2}$-in.	100	100
Liquid Limit	6	21
Plastic Index	1	5

S8_2009

Design Life	Base Construction	Pavement Construction	Traffic Opening	Initial IRI
2 yrs	Jun, 2009	Jul, 2009	Aug, 2009	125.9 in./mile

AC general information of S8_2009

Lift No.	Thickness, in.	Unit Weight, pcf	Binder Content, % by volume	Air Void, %	Poisson's Ratio	Reference Temperature, °F
1	1.3	116.16	7.42	25	0.35	70
2	3	149.45	10.39	6.3	0.35	70
3	2.6	144.88	11.19	8.3	0.35	70

E* data for lift No. 1 of S8_2009

Frequency, Hz → Dynamic Modulus, psi ↘ Temperature, °F ↓	0.1	0.5	1	5	10	25
14	2186687	2419474	2505967	2676407	2737703	2808718
40	1295743	1621364	1757461	2052191	2167382	2307312
70	458621.6	686248.7	802014.4	1102416	1240772	1426770
100	128558.5	208746.6	256675.4	406879.1	490096.9	617735.6
130	43892.89	66274.05	80328.95	128592.3	158406.9	208801.7

G* data for lift No. 1 of S8_2009

Temperature, °F	Shear Modulus, Pa	Phase Angle, °
70	1881000	57.98
100	134200	60.55
130	22420	58.39

E* data for lift No. 2 of S8_2009

Frequency, Hz → Dynamic Modulus, psi ↘ Temperature, °F ↓	0.1	0.5	1	5	10	25
14	2186687	2419474	2505967	2676407	2737703	2808718
40	1295743	1621364	1757461	2052191	2167382	2307312
70	458621.6	686248.7	802014.4	1102416	1240772	1426770
100	128558.5	208746.6	256675.4	406879.1	490096.9	617735.6
130	43892.89	66274.05	80328.95	128592.3	158406.9	208801.7

G* data for lift No. 2 of S8_2009

Temperature, °F	Shear Modulus, Pa	Phase Angle, °
70	1881000	57.98
100	134200	60.55
130	22420	58.39

E* data for lift No. 3 of S8_2009

Frequency, Hz → Dynamic Modulus, psi ↘ Temperature, °F ↓	0.1	0.5	1	5	10	25
14	1946534	2242233	2353081	2571382	2649390	2739073
40	1020629	1378295	1534272	1881067	2018821	2186903
70	307798.9	508777	618962.7	923734.1	1071232	1274704
100	80092.84	139868.1	178316.1	308755.4	386130.1	510178.9
130	27979.87	43636.44	53995.91	91999.48	116994.4	161298.4

G* data for lift No. 3 of S8_2009

Temperature, °F	Shear Modulus, Pa	Phase Angle, °
70	1881000	57.98
100	134200	60.55
130	22420	58.39

Unbound materials general information of S8_2009

	Thickness, in.	Resilient Modulus, psi	Coefficient of lateral pressure	Poisson’s Ratio
Base	5.51	14440	0.357	0.4
Subgrade	∞	26335	0.357	0.45

Unbound materials gradation and Atterberg limits of S8_2009

Sieve Size	Base	Subgrade
#200	10.2	48
#100	15	56
#50	23	61
#30	31	64
#16	39	66
#8	47	68
#4	57	71
3/8-in.	78	75
1/2-in.	83	78
3/4-in.	88	81
1-in.	95	83
$1\frac{1}{2}$-in.	100	100
Liquid Limit	6	21
Plastic Index	1	5

S9_2009

Design Life	Base Construction	Pavement Construction	Traffic Opening	Initial IRI
2 yrs	Jun, 2009	Jul, 2009	Aug, 2009	65.2 in./mile

AC general information of S9_2009

Lift No.	Thickness, in.	Unit Weight, pcf	Binder Content, % by volume	Air Void, %	Poisson's Ratio	Reference Temperature, °F
1	1.2	143.61	12.26	6.9	0.35	70
2	2.8	147.72	10.28	7.2	0.35	70
3	3	146.77	10.87	7.4	0.35	70

E* data for lift No. 1 of S9_2009

Frequency, Hz → Dynamic Modulus, psi ↘ Temperature, °F ↓	0.1	0.5	1	5	10	25
14	1709153	1996679	2108132	2334691	2418300	2516474
40	789039.2	1091271	1229417	1551924	1686462	1856134
70	202318	333991.7	409128.3	629085.9	742301.4	906129.1
100	50873.3	83264.98	103989.8	175512.9	219340.7	292233.9
130	19428.17	27555.57	32705.36	50906.75	62626.51	83324.41

G* data for lift No. 1 of S9_2009

Temperature, °F	Shear Modulus, Pa	Phase Angle, °
70	1881000	57.98
100	134200	60.55
130	22420	58.39

E* data for lift No. 2 of S9_2009

Frequency, Hz → Dynamic Modulus, psi ↘ Temperature, °F ↓	0.1	0.5	1	5	10	25
14	2186687	2419474	2505967	2676407	2737703	2808718
40	1295743	1621364	1757461	2052191	2167382	2307312
70	458621.6	686248.7	802014.4	1102416	1240772	1426770
100	128558.5	208746.6	256675.4	406879.1	490096.9	617735.6
130	43892.89	66274.05	80328.95	128592.3	158406.9	208801.7

G* data for lift No. 2 of S9_2009

Temperature, °F	Shear Modulus, Pa	Phase Angle, °
70	1881000	57.98
100	134200	60.55
130	22420	58.39

E* data for lift No. 3 of S9_2009

Frequency, Hz → Dynamic Modulus, psi ↘ Temperature, °F ↓	0.1	0.5	1	5	10	25
14	1946534	2242233	2353081	2571382	2649390	2739073
40	1020629	1378295	1534272	1881067	2018821	2186903
70	307798.9	508777	618962.7	923734.1	1071232	1274704
100	80092.84	139868.1	178316.1	308755.4	386130.1	510178.9
130	27979.87	43636.44	53995.91	91999.48	116994.4	161298.4

G* data for lift No. 3 of S9_2009

Temperature, °F	Shear Modulus, Pa	Phase Angle, °
70	1881000	57.98
100	134200	60.55
130	22420	58.39

Unbound materials general information of S9_2009

	Thickness, in.	Resilient Modulus, psi	Coefficient of lateral pressure	Poisson's Ratio
Base	5.8	13404	0.357	0.4
Subgrade	∞	26070	0.357	0.45

Unbound materials gradation and Atterberg limits of S9_2009

Sieve Size	Base	Subgrade
#200	10.2	48
#100	15	56
#50	23	61
#30	31	64
#16	39	66
#8	47	68
#4	57	71
3/8-in.	78	75
1/2-in.	83	78
3/4-in.	88	81
1-in.	95	83
$1\frac{1}{2}$-in.	100	100
Liquid Limit	6	21
Plastic Index	1	5

S10_2009

Design Life	Base Construction	Pavement Construction	Traffic Opening	Initial IRI
2 yrs	Jun, 2009	Jul, 2009	Aug, 2009	58.6 in./mile

AC general information of S10_2009

Lift No.	Thickness, in.	Unit Weight, pcf	Binder Content, % by volume	Air Void, %	Poisson's Ratio	Reference Temperature, °F
1	1.3	142.32	12.18	7.7	0.35	70
2	2.7	147.82	10.58	7.1	0.35	70
3	3	147.04	10.42	7.7	0.35	70

E* data for lift No. 1 of S10_2009

Frequency, Hz → Dynamic Modulus, psi ↘ Temperature, °F ↓	0.1	0.5	1	5	10	25
14	1784082	2086064	2201212	2431033	2514137	2610318
40	808239.6	1134534	1283744	1629873	1772718	1951047
70	198794	334090.9	412912.3	647699.1	769941.7	947547.6
100	51343.58	82795.59	103218.4	175177.9	220177.2	296150.8
130	21519.44	29384.74	34377.29	52128.6	63659.5	84216.79

G* data for lift No. 1 of S10_2009

Temperature, °F	Shear Modulus, Pa	Phase Angle, °
70	1881000	57.98
100	134200	60.55
130	22420	58.39

E* data for lift No. 2 of S10_2009

Frequency, Hz → Dynamic Modulus, psi ↘ Temperature, °F ↓	0.1	0.5	1	5	10	25
14	2049583	2326361	2429592	2632549	2705092	2788606
40	1069001	1419975	1572226	1910225	2044598	2208882
70	305788	496338.2	600719.9	890797	1032298	1228996
100	76323.44	128158.1	161182	273114.2	339925.2	448092.1
130	27347.44	40208.16	48500.34	78229.62	97509.74	131543.3

G* data for lift No. 2 of S10_2009

Temperature, °F	Shear Modulus, Pa	Phase Angle, °
70	1881000	57.98
100	134200	60.55
130	22420	58.39

E* data for lift No. 3 of S10_2009

Frequency, Hz → Dynamic Modulus, psi ↘ Temperature, °F ↓	0.1	0.5	1	5	10	25
14	1917037	2244845	2367209	2605996	2690259	2786153
40	956146	1338208	1507435	1885869	2036111	2218651
70	269416.7	465921.4	577659.1	896102.7	1053477	1272534
100	69512.99	123738.3	159814.4	287094.3	365188.6	493160.7
130	25677.6	39636.44	49048	84535.77	108537.2	152060.3

G* data for lift No. 3 of S10_2009

Temperature, °F	Shear Modulus, Pa	Phase Angle, °
70	1881000	57.98
100	134200	60.55
130	22420	58.39

Unbound materials general information of S10_2009

	Thickness, in.	Resilient Modulus, psi	Coefficient of lateral pressure	Poisson's Ratio
Base	6.35	10571	0.357	0.4
Subgrade	∞	26158	0.357	0.45

Unbound materials gradation and Atterberg limits of S10_2009

Sieve Size	Base	Subgrade
#200	10.2	48
#100	15	56
#50	23	61
#30	31	64
#16	39	66
#8	47	68
#4	57	71
3/8-in.	78	75
1/2-in.	83	78
3/4-in.	88	81
1-in.	95	83
$1\frac{1}{2}$-in.	100	100
Liquid Limit	6	21
Plastic Index	1	5

S11_2009

Design Life	Base Construction	Pavement Construction	Traffic Opening	Initial IRI
2 yrs	Jun, 2009	Jul, 2009	Aug, 2009	84.4 in./mile

AC general information of S11_2009

Lift No.	Thickness, in.	Unit Weight, pcf	Binder Content, % by volume	Air Void, %	Poisson's Ratio	Reference Temperature, °F
1	1.5	144.07	12.86	6.3	0.35	70
2	2.8	148.11	10.34	7.1	0.35	70
3	2.6	147.77	11.87	6.1	0.35	70

E* data for lift No. 1 of S11_2009

Frequency, Hz → Dynamic Modulus, psi ↘ Temperature, °F ↓	0.1	0.5	1	5	10	25
14	1704030	2025299	2148012	2392218	2480007	2581046
40	697627.3	1020738	1172992	1533879	1685089	1875027
70	150574.9	261113.7	328547.4	539843	654919.7	827067.1
100	39274.71	61745.39	76611.13	130730.7	165848.5	227097.9
130	18200.79	23693.4	27170.06	39555.91	47659.71	62265.57

G* data for lift No. 1 of S11_2009

Temperature, °F	Shear Modulus, Pa	Phase Angle, °
70	1881000	57.98
100	134200	60.55
130	22420	58.39

E* data for lift No. 2 of S11_2009

Frequency, Hz → Dynamic Modulus, psi ↘ Temperature, °F ↓	0.1	0.5	1	5	10	25
14	1842698	2177770	2304012	2552029	2640037	2740478
40	842821.7	1208841	1375809	1758897	1914452	2105921
70	211545.3	368846.9	461764.9	739332.5	882960.4	1089424
100	55176.16	92894.14	118099.2	209167.1	266977.3	364960.9
130	23006.67	32528.19	38773.93	61834.14	77304.94	105482.6

G* data for lift No. 2 of S11_2009

Temperature, °F	Shear Modulus, Pa	Phase Angle, °
70	1881000	57.98
100	134200	60.55
130	22420	58.39

E* data for lift No. 3 of S11_2009

Frequency, Hz → Dynamic Modulus, psi ↘ Temperature, °F ↓	0.1	0.5	1	5	10	25
14	2061333	2339974	2443102	2644237	2715508	2797065
40	1041943	1400302	1556241	1902364	2039652	2207025
70	273618.2	454769.5	556128	843292.5	985546.9	1184971
100	64323.58	108445.7	137100.8	236752.4	297749.1	398405
130	23381.57	33670.77	40333.26	64462.16	80320.85	108698.3

G* data for lift No. 3 of S11_2009

Temperature, °F	Shear Modulus, Pa	Phase Angle, °
70	1881000	57.98
100	134200	60.55
130	22420	58.39

Unbound materials general information of S11_2009

	Thickness, in.	Resilient Modulus, psi	Coefficient of lateral pressure	Poisson's Ratio
Base	6.17	13033	0.357	0.4
Subgrade	∞	25794	0.357	0.45

Unbound materials gradation and Atterberg limits of S11_2009

Sieve Size	Base	Subgrade
#200	10.2	48
#100	15	56
#50	23	61
#30	31	64
#16	39	66
#8	47	68
#4	57	71
3/8-in.	78	75
1/2-in.	83	78
3/4-in.	88	81
1-in.	95	83
$1\frac{1}{2}$-in.	100	100
Liquid Limit	6	21
Plastic Index	1	5

S12_2009

Design Life	Base Construction	Pavement Construction	Traffic Opening	Initial IRI
2 yrs	Jun, 2009	Jul, 2009	Aug, 2009	127.3 in./mile

AC general information of S12_2009

Lift No.	Thickness, in.	Unit Weight, pcf	Binder Content, % by volume	Air Void, %	Poisson's Ratio	Reference Temperature, °F
1	1.4	145.83	12.34	5.5	0.35	70
2	2.9	150.53	11.68	4.8	0.35	70
3	2.6	148.42	11.43	6.1	0.35	70

E* data for lift No. 1 of S12_2009

Frequency, Hz → Dynamic Modulus, psi ↘ Temperature, °F ↓	0.1	0.5	1	5	10	25
14	1940483	2238283	2347691	2558599	2632223	2715506
40	947418.7	1318937	1482008	1843598	1986019	2158213
70	236017.4	415139.9	518486.8	817283.1	966784.2	1176477
100	53304.02	95037.5	123293.2	225692.4	290314.9	398685.1
130	18987.36	28428.31	34783.69	58901.4	75424.77	105878

G* data for lift No. 1 of S12_2009

Temperature, °F	Shear Modulus, Pa	Phase Angle, °
70	1881000	57.98
100	134200	60.55
130	22420	58.39

E* data for lift No. 2 of S12_2009

Frequency, Hz → Dynamic Modulus, psi ↘ Temperature, °F ↓	0.1	0.5	1	5	10	25
14	2293718	2531552	2615887	2774427	2828622	2889272
40	1325949	1700707	1854167	2176035	2296935	2439324
70	407162.6	655116.8	786464.8	1134780	1296123	1511586
100	100209.3	170899.6	216164.2	368634.9	458233.2	600472
130	35606.16	52509.17	63596.62	104056.1	130632.9	177811.4

G* data for lift No. 2 of S12_2009

Temperature, °F	Shear Modulus, Pa	Phase Angle, °
70	1881000	57.98
100	134200	60.55
130	22420	58.39

E* data for lift No. 3 of S12_2009

Frequency, Hz → Dynamic Modulus, psi ↘ Temperature, °F ↓	0.1	0.5	1	5	10	25
14	2293718	2531552	2615887	2774427	2828622	2889272
40	1325949	1700707	1854167	2176035	2296935	2439324
70	407162.6	655116.8	786464.8	1134780	1296123	1511586
100	100209.3	170899.6	216164.2	368634.9	458233.2	600472
130	35606.16	52509.17	63596.62	104056.1	130632.9	177811.4

G* data for lift No. 3 of S12_2009

Temperature, °F	Shear Modulus, Pa	Phase Angle, °
70	1881000	57.98
100	134200	60.55
130	22420	58.39

Unbound materials general information of S12_2009

	Thickness, in.	Resilient Modulus, psi	Coefficient of lateral pressure	Poisson's Ratio
Base	5.27	12685	0.357	0.4
Subgrade	∞	25910	0.357	0.45

Unbound materials gradation and Atterberg limits of S12_2009

Sieve Size	Base	Subgrade
#200	10.2	48
#100	15	56
#50	23	61
#30	31	64
#16	39	66
#8	47	68
#4	57	71
3/8-in.	78	75
1/2-in.	83	78
3/4-in.	88	81
1-in.	95	83
$1\frac{1}{2}$-in.	100	100
Liquid Limit	6	21
Plastic Index	1	5

N3_2012

Design Life	Base Construction	Pavement Construction	Traffic Opening	Initial IRI
2 yrs	Jul, 2012	Aug, 2012	Oct, 2012	70 in./mile

AC general information of N3_2012

Lift No.	Thickness, in.	Unit Weight, pcf	Binder Content, % by volume	Air Void, %	Poisson's Ratio	Reference Temperature, °F
1	2.1	160.49	13.36	4.3	0.35	70
2	4	152.03	8.33	6.76	0.35	70
3	3.65	152.03	8.33	6.76	0.35	70

E* data for lift No. 1 of N3_2012

Frequency, Hz → Dynamic Modulus, psi ↘ Temperature, °F ↓	0.1	0.5	1	5	10	25
14	1831321	2092077	2191372	2390654	2463441	2548470
40	926534	1235531	1371736	1680003	1805198	1960672
70	257178	416778	504449	750212	871608	1042376
100	61344	103759	130669	221635	275942	364118
130	20467	30727	37328	60910	76150	102992

G* data for lift No. 1 of N3_2012

Temperature, °F	Shear Modulus, Pa	Phase Angle, °
70	1881000	57.98
100	134200	60.55
130	22420	58.39

E* data for lift No. 2 of N3_2012

Frequency, Hz → Dynamic Modulus, psi ↘ Temperature, °F ↓	0.1	0.5	1	5	10	25
14	2562216	2726344	2783439	2889774	2925969	2966490
40	1729021	2054198	2179136	2429635	2520487	2625737
70	638087	951194	1101376	1464155	1619104	1816364
100	141770	252093	319514	530717	645684	817689
130	34881	58463	74305	132521	170386	236246

G* data for lift No. 2 of N3_2012

Temperature, °F	Shear Modulus, Pa	Phase Angle, °
70	2156000	55.8
100	241800	61.59
130	26710	70.67

E* data for lift No. 3 of N3_2012

Frequency, Hz → Dynamic Modulus, psi ↘ Temperature, °F ↓	0.1	0.5	1	5	10	25
14	2562216	2726344	2783439	2889774	2925969	2966490
40	1729021	2054198	2179136	2429635	2520487	2625737
70	638087	951194	1101376	1464155	1619104	1816364
100	141770	252093	319514	530717	645684	817689
130	34881	58463	74305	132521	170386	236246

G* data for lift No. 3 of N3_2012

Temperature, °F	Shear Modulus, Pa	Phase Angle, °
70	2156000	55.8
100	241800	61.59
130	26710	70.67

Unbound materials general information of N3_2012

	Thickness, in.	Resilient Modulus, psi	Coefficient of lateral pressure	Poisson's Ratio
Base	6.22	10876	0.357	0.4
Subgrade	∞	24491	0.357	0.45

Unbound materials gradation and Atterberg limits of N3_2012

Sieve Size	Base	Subgrade
#200	10	48
#100	15	56
#50	23	61
#30	32	64
#16	40	66
#8	49	68
#4	59	71
3/8-in.	76	75
1/2-in.	80	78
3/4-in.	90	81
1-in.	96	83
$1\frac{1}{2}$-in.	100	100
Liquid Limit	6	21
Plastic Index	1	5

N4_2012

Design Life	Base Construction	Pavement Construction	Traffic Opening	Initial IRI
2 yrs	Jul, 2012	Aug, 2012	Oct, 2012	71.8 in./mile

AC general information of N4_2012

Lift No.	Thickness, in.	Unit Weight, pcf	Binder Content, % by volume	Air Void, %	Poisson's Ratio	Reference Temperature, °F
1	1.97	161.12	12.8	4.7	0.35	70
2	1.94	154.75	7.28	7.4	0.35	70
3	4.23	154.75	7.28	7.4	0.35	70

E* data for lift No. 1 of N4_2012

Frequency, Hz → Dynamic Modulus, psi ↘ Temperature, °F ↓	0.1	0.5	1	5	10	25
14	1831321	2092077	2191372	2390654	2463441	2548470
40	926534	1235531	1371736	1680003	1805198	1960672
70	257178	416778	504449	750212	871608	1042376
100	61344	103759	130669	221635	275942	364118
130	20467	30727	37328	60910	76150	102992

G* data for lift No. 1 of N4_2012

Temperature, °F	Shear Modulus, Pa	Phase Angle, °
70	1881000	57.98
100	134200	60.55
130	22420	58.39

E* data for lift No. 2 of N4_2012

Frequency, Hz → Dynamic Modulus, psi ↘ Temperature, °F ↓	0.1	0.5	1	5	10	25
14	2562216	2726344	2783439	2889774	2925969	2966490
40	1729021	2054198	2179136	2429635	2520487	2625737
70	638087	951194	1101376	1464155	1619104	1816364
100	141770	252093	319514	530717	645684	817689
130	34881	58463	74305	132521	170386	236246

G* data for lift No. 2 of N4_2012

Temperature, °F	Shear Modulus, Pa	Phase Angle, °
70	2156000	55.8
100	241800	61.59
130	26710	70.67

E* data for lift No. 3 of N4_2012

Frequency, Hz → Dynamic Modulus, psi ↘ Temperature, °F ↓	0.1	0.5	1	5	10	25
14	2562216	2726344	2783439	2889774	2925969	2966490
40	1729021	2054198	2179136	2429635	2520487	2625737
70	638087	951194	1101376	1464155	1619104	1816364
100	141770	252093	319514	530717	645684	817689
130	34881	58463	74305	132521	170386	236246

G* data for lift No. 3 of N4_2012

Temperature, °F	Shear Modulus, Pa	Phase Angle, °
70	2156000	55.8
100	241800	61.59
130	26710	70.67

Unbound materials general information of N4_2012

	Thickness, in.	Resilient Modulus, psi	Coefficient of lateral pressure	Poisson's Ratio
Base	6.08	11087	0.357	0.4
Subgrade	∞	25328	0.357	0.45

Unbound materials gradation and Atterberg limits of N4_2012

Sieve Size	Base	Subgrade
#200	10	48
#100	15	56
#50	23	61
#30	32	64
#16	40	66
#8	49	68
#4	59	71
3/8-in.	76	75
1/2-in.	80	78
3/4-in.	90	81
1-in.	96	83
$1\frac{1}{2}$-in.	100	100
Liquid Limit	6	21
Plastic Index	1	5

N5_2012

Design Life	Base Construction	Pavement Construction	Traffic Opening	Initial IRI
2 yrs	Jul, 2012	Aug, 2012	Oct, 2012	56.8 in./mile

AC general information of N5_2012

Lift No.	Thickness, in.	Unit Weight, pcf	Binder Content, % by volume	Air Void, %	Poisson's Ratio	Reference Temperature, °F
1	1.42	150.63	5.86	8.4	0.35	70
2	1.67	152.76	6.19	6.9	0.35	70
3	3.02	152.69	7.83	6.5	0.35	70

E* data for lift No. 1 of N5_2012

Frequency, Hz → Dynamic Modulus, psi ↘ Temperature, °F ↓	0.1	0.5	1	5	10	25
14	2200766	2448923	2538906	2711722	2772144	2840784
40	1245093	1608096	1759020	2081307	2204832	2352462
70	373478	608165	732467	1063241	1217507	1425071
100	83121	149728	192655	337424	422394	557123
130	24354	39287	49334	86832	111826	156485

G* data for lift No. 1 of N5_2012

Temperature, °F	Shear Modulus, Pa	Phase Angle, °
70	2156000	55.8
100	241800	61.59
130	26710	70.67

E* data for lift No. 2 of N5_2012

Frequency, Hz → Dynamic Modulus, psi ↘ Temperature, °F ↓	0.1	0.5	1	5	10	25
14	2574207	2764159	2829078	2947630	2987079	3030537
40	1692351	2060685	2201762	2481554	2581416	2695558
70	596426	931835	1096489	1498227	1669913	1887261
100	132075	244527	315816	546355	674511	867774
130	34921	59142	75894	139657	182385	258147

G* data for lift No. 2 of N5_2012

Temperature, °F	Shear Modulus, Pa	Phase Angle, °
70	2156000	55.8
100	241800	61.59
130	26710	70.67

E* data for lift No. 3 of N5_2012

Frequency, Hz → Dynamic Modulus, psi ↘ Temperature, °F ↓	0.1	0.5	1	5	10	25
14	2574207	2764159	2829078	2947630	2987079	3030537
40	1692351	2060685	2201762	2481554	2581416	2695558
70	596426	931835	1096489	1498227	1669913	1887261
100	132075	244527	315816	546355	674511	867774
130	34921	59142	75894	139657	182385	258147

G* data for lift No. 3 of N5_2012

Temperature, °F	Shear Modulus, Pa	Phase Angle, °
70	2156000	55.8
100	241800	61.59
130	26710	70.67

Unbound materials general information of N5_2012

	Thickness, in.	Resilient Modulus, psi	Coefficient of lateral pressure	Poisson's Ratio
Base	5.6	19286	0.357	0.4
Subgrade	∞	26505	0.357	0.45

Unbound materials gradation and Atterberg limits of N5_2012

Sieve Size	Base	Subgrade
#200	10	48
#100	15	56
#50	23	61
#30	32	64
#16	40	66
#8	49	68
#4	59	71
3/8-in.	76	75
1/2-in.	80	78
3/4-in.	90	81
1-in.	96	83
$1\frac{1}{2}$-in.	100	100
Liquid Limit	6	21
Plastic Index	1	5

S5_2012

Design Life	Base Construction	Pavement Construction	Traffic Opening	Initial IRI
2 yrs	Jul, 2012	Aug, 2012	Oct, 2012	105.2 in./mile

AC general information of S5_2012

Lift No.	Thickness, in.	Unit Weight, pcf	Binder Content, % by volume	Air Void, %	Poisson's Ratio	Reference Temperature, °F
1	1	145.39	11.08	6.5	0.35	70
2	2.56	152.19	9.02	4.2	0.35	70
3	2.69	152.01	6.24	7.2	0.35	70

E* data for lift No. 1 of S5_2012

Frequency, Hz → Dynamic Modulus, psi ↘ Temperature, °F ↓	0.1	0.5	1	5	10	25
14	2175580	2408234	2493447	2659030	2717712	2785032
40	1213242	1553929	1696434	2003842	2123185	2267275
70	345323	556954	669221	970408	1112600	1306106
100	70861	126234	161756	281733	352642	466155
130	19470	30975	38619	66841	85542	118950

G* data for lift No. 1 of S5_2012

Temperature, °F	Shear Modulus, Pa	Phase Angle, °
70	2156000	55.8
100	241800	61.59
130	26710	70.67

E* data for lift No. 2 of S5_2012

Frequency, Hz → Dynamic Modulus, psi ↘ Temperature, °F ↓	0.1	0.5	1	5	10	25
14	2460684	2659786	2730457	2864237	2910478	2962724
40	1562784	1908469	2045526	2327692	2432569	2555866
70	543219	830079	972262	1327405	1484019	1687629
100	123457	219150	278291	466976	571820	731378
130	32495	53915	68232	120698	154835	214379

G* data for lift No. 2 of S5_2012

Temperature, °F	Shear Modulus, Pa	Phase Angle, °
70	2156000	55.8
100	241800	61.59
130	26710	70.67

E* data for lift No. 3 of S5_2012

Frequency, Hz → Dynamic Modulus, psi ↘ Temperature, °F ↓	0.1	0.5	1	5	10	25
14	2424119	2635937	2711515	2855057	2904794	2961044
40	1498465	1850311	1991795	2286281	2396751	2527262
70	512586	783043	919515	1266994	1423034	1628272
100	127054	215286	269583	443698	541447	691804
130	40031	61463	75369	125016	156781	211806

G* data for lift No. 3 of S5_2012

Temperature, °F	Shear Modulus, Pa	Phase Angle, °
70	1881000	57.98
100	134200	60.55
130	22420	58.39

Unbound materials general information of S5_2012

	Thickness, in.	Resilient Modulus, psi	Coefficient of lateral pressure	Poisson's Ratio
Base	6.09	13050	0.357	0.4
Subgrade	∞	25658	0.357	0.45

Unbound materials gradation and Atterberg limits of S5_2012

Sieve Size	Base	Subgrade
#200	10	48
#100	15	56
#50	23	61
#30	32	64
#16	40	66
#8	49	68
#4	59	71
3/8-in.	76	75
1/2-in.	80	78
3/4-in.	90	81
1-in.	96	83
$1\frac{1}{2}$-in.	100	100
Liquid Limit	6	21
Plastic Index	1	5

S6_2012

Design Life	Base Construction	Pavement Construction	Traffic Opening	Initial IRI
2 yrs	Jul, 2012	Aug, 2012	Oct, 2012	61.5 in./mile

AC general information of S6_2012

Lift No.	Thickness, in.	Unit Weight, pcf	Binder Content, % by volume	Air Void, %	Poisson's Ratio	Reference Temperature, °F
1	1.32	148.7	7.66	7.9	0.35	70
2	2.38	153.94	7.49	6	0.35	70
3	2.32	155.19	9.72	3.5	0.35	70

E* data for lift No. 1 of S6_2012

Frequency, Hz → Dynamic Modulus, psi ↘ Temperature, °F ↓	0.1	0.5	1	5	10	25
14	2262436	2478537	2557256	2709681	2763558	2825298
40	1384390	1715010	1850030	2135929	2245202	2376015
70	488704	738737	864342	1184442	1328892	1520053
100	125699	212893	265711	432177	524297	664822
130	38112	60466	74912	125951	158174	213313

G* data for lift No. 1 of S6_2012

Temperature, °F	Shear Modulus, Pa	Phase Angle, °
70	2156000	55.8
100	241800	61.59
130	26710	70.67

E* data for lift No. 2 of S6_2012

Frequency, Hz → Dynamic Modulus, psi ↘ Temperature, °F ↓	0.1	0.5	1	5	10	25
14	2545262	2703800	2760951	2871220	2910209	2955006
40	1771675	2057385	2169277	2399512	2485657	2587828
70	768456	1055826	1189133	1506401	1641634	1814942
100	224718	355551	428803	640722	749259	906459
130	66078	103649	126862	204018	249822	324452

G* data for lift No. 2 of S6_2012

Temperature, °F	Shear Modulus, Pa	Phase Angle, °
70	2156000	55.8
100	241800	61.59
130	26710	70.67

E* data for lift No. 3 of S6_2012

Frequency, Hz → Dynamic Modulus, psi ↘ Temperature, °F ↓	0.1	0.5	1	5	10	25
14	2379161	2588771	2662644	2801211	2848577	2901652
40	1396683	1758472	1904661	2208797	2322461	2456148
70	403612	648082	776865	1117142	1274532	1484834
100	85988	148283	188425	324930	406009	535958
130	27556	40565	49099	80355	101026	138033

G* data for lift No. 3 of S6_2012

Temperature, °F	Shear Modulus, Pa	Phase Angle, °
70	1881000	57.98
100	134200	60.55
130	22420	58.39

Unbound materials general information of S6_2012

	Thickness, in.	Resilient Modulus, psi	Coefficient of lateral pressure	Poisson's Ratio
Base	6.04	15690	0.357	0.4
Subgrade	∞	26931	0.357	0.45

Unbound materials gradation and Atterberg limits of S6_2012

Sieve Size	Base	Subgrade
#200	10	48
#100	15	56
#50	23	61
#30	32	64
#16	40	66
#8	49	68
#4	59	71
3/8-in.	76	75
1/2-in.	80	78
3/4-in.	90	81
1-in.	96	83
$1\frac{1}{2}$-in.	100	100
Liquid Limit	6	21
Plastic Index	1	5

S12_2012

Design Life	Base Construction	Pavement Construction	Traffic Opening	Initial IRI
2 yrs	Jul, 2012	Aug, 2012	Oct, 2012	150.7 in./mile

AC general information of S12_2012

Lift No.	Thickness, in.	Unit Weight, pcf	Binder Content, % by volume	Air Void, %	Poisson's Ratio	Reference Temperature, °F
1	2.04	160.56	13.4	4.2	0.35	70
2	1.88	152.07	8.07	6.7	0.35	70
3	5.14	155.2	9.72	3.5	0.35	70

E* data for lift No. 1 of S12_2012

Frequency, Hz → Dynamic Modulus, psi ↘ Temperature, °F ↓	0.1	0.5	1	5	10	25
14	1831321	2092077	2191372	2390654	2463441	2548470
40	926534	1235531	1371736	1680003	1805198	1960672
70	257178	416778	504449	750212	871608	1042376
100	61344	103759	130669	221635	275942	364118
130	20467	30727	37328	60910	76150	102992

G* data for lift No. 1 of S12_2012

Temperature, °F	Shear Modulus, Pa	Phase Angle, °
70	1881000	57.98
100	134200	60.55
130	22420	58.39

E* data for lift No. 2 of S12_2012

Frequency, Hz → Dynamic Modulus, psi ↘ Temperature, °F ↓	0.1	0.5	1	5	10	25
14	2562216	2726344	2783439	2889774	2925969	2966490
40	1729021	2054198	2179136	2429635	2520487	2625737
70	638087	951194	1101376	1464155	1619104	1816364
100	141770	252093	319514	530717	645684	817689
130	34881	58463	74305	132521	170386	236246

G* data for lift No. 2 of S12_2012

Temperature, °F	Shear Modulus, Pa	Phase Angle, °
70	2156000	55.8
100	241800	61.59
130	26710	70.67

E* data for lift No. 3 of S12_2012

Frequency, Hz → Dynamic Modulus, psi ↘ Temperature, °F ↓	0.1	0.5	1	5	10	25
14	2562216	2726344	2783439	2889774	2925969	2966490
40	1729021	2054198	2179136	2429635	2520487	2625737
70	638087	951194	1101376	1464155	1619104	1816364
100	141770	252093	319514	530717	645684	817689
130	34881	58463	74305	132521	170386	236246

G* data for lift No. 3 of S12_2012

Temperature, °F	Shear Modulus, Pa	Phase Angle, °
70	2156000	55.8
100	241800	61.59
130	26710	70.67

Unbound materials general information of S12_2012

	Thickness, in.	Resilient Modulus, psi	Coefficient of lateral pressure	Poisson's Ratio
Base	5.87	12685	0.357	0.4
Subgrade	∞	25910	0.357	0.45

Unbound materials gradation and Atterberg limits of S12_2012

Sieve Size	Base	Subgrade
#200	10	48
#100	15	56
#50	23	61
#30	32	64
#16	40	66
#8	49	68
#4	59	71
3/8-in.	76	75
1/2-in.	80	78
3/4-in.	90	81
1-in.	96	83
$1\frac{1}{2}$-in.	100	100
Liquid Limit	6	21
Plastic Index	1	5

S13_2012

Design Life	Base Construction	Pavement Construction	Traffic Opening	Initial IRI
2 yrs	Jul, 2012	Aug, 2012	Oct, 2012	81 in./mile

AC general information of S13_2012

Lift No.	Thickness, in.	Unit Weight, pcf	Binder Content, % by volume	Air Void, %	Poisson's Ratio	Reference Temperature, °F
1	1.21	148.2	8.23	7.1	0.35	70
2	3.2	152.57	8.19	5.6	0.35	70
3	2.02	149.07	11.68	7.7	0.35	70

E* data for lift No. 1 of S13_2012

Frequency, Hz → Dynamic Modulus, psi ↘ Temperature, °F ↓	0.1	0.5	1	5	10	25
14	1708803	1967069	2069480	2283723	2365488	2463939
40	851301	1121736	1243609	1528177	1648065	1801240
70	250773	387998	461953	668103	770475	916137
100	64180	104198	128533	207443	253082	325953
130	21102	31627	38171	60568	74464	98201

G* data for lift No. 1 of S13_2012

Temperature, °F	Shear Modulus, Pa	Phase Angle, °
70	1881000	57.98
100	134200	60.55
130	22420	58.39

E* data for lift No. 2 of S13_2012

Frequency, Hz → Dynamic Modulus, psi ↘ Temperature, °F ↓	0.1	0.5	1	5	10	25
14	2257586	2477697	2559198	2719546	2777182	2843977
40	1376142	1696419	1828878	2113579	2224218	2358265
70	503862	741064	859740	1163159	1301161	1485332
100	141863	228777	280063	438396	524893	656264
130	47167	71518	86726	138517	170225	223417

G* data for lift No. 2 of S13_2012

Temperature, °F	Shear Modulus, Pa	Phase Angle, °
70	1881000	57.98
100	134200	60.55
130	22420	58.39

E* data for lift No. 3 of S13_2012

Frequency, Hz → Dynamic Modulus, psi ↘ Temperature, °F ↓	0.1	0.5	1	5	10	25
14	1494374	1749036	1852322	2072668	2158304	2262570
40	712789	950935	1061228	1325862	1440306	1589061
70	217161	328100	388534	560122	647175	773213
100	65540	99260	119333	183556	220513	279624
130	26651	36784	42845	62786	74772	94853

G* data for lift No. 3 of S13_2012

Temperature, °F	Shear Modulus, Pa	Phase Angle, °
70	1881000	57.98
100	134200	60.55
130	22420	58.39

Unbound materials general information of S13_2012

	Thickness, in.	Resilient Modulus, psi	Coefficient of lateral pressure	Poisson's Ratio
Base	5.81	14149	0.357	0.4
Subgrade	∞	26134	0.357	0.45

Unbound materials gradation and Atterberg limits of S13_2012

Sieve Size	Base	Subgrade
#200	10	48
#100	15	56
#50	23	61
#30	32	64
#16	40	66
#8	49	68
#4	59	71
3/8-in.	76	75
1/2-in.	80	78
3/4-in.	90	81
1-in.	96	83
$1\frac{1}{2}$-in.	100	100
Liquid Limit	6	21
Plastic Index	1	5

The measurement data was summarized regarding rutting, bottom-up fatigue cracking, and IRI as below. Outliers were removed.

Measurement data for evaluation and local calibration

N2_2003			
Month	Rutting	Bottom-up cracking	IRI
Oct-03	0.84	0.00	54.6
Nov-03	1.04	0.00	52.5
Dec-03	1.11	0.00	52.3
Jan-04	1.26	0.00	53.4
Feb-04	1.54	0.00	54.3
Mar-04	1.78	0.00	51.6
Apr-04	2.20	0.00	93.5
May-04	3.62	0.00	80
Jun-04	4.37	0.00	73.5
Jul-04	5.44	19.52	74.9
Aug-04	6.00	27.39	84.3
Sep-04	6.87		93.8
Oct-04	7.19	37.53	102.7
Nov-04	9.02	42.43	
Dec-04			156.7
Jan-05			
Feb-05	4.41		
Mar-05	4.55	43.85	
Apr-05	4.31		
May-05	4.20		
Jun-05	3.98		
Jul-05	3.79		
Aug-05	3.92		
Sep-05	3.67		
N3_2003			
Month	Rutting	Bottom-up cracking	IRI
Oct-03	0.51	0.00	34.2
Nov-03	0.67	0.00	33.7
Dec-03	0.58	0.00	33
Jan-04	0.70	0.00	33
Feb-04	0.83	0.00	33.7
Mar-04	0.91	0.00	34.3
Apr-04	1.36	0.00	34.5
May-04	2.42	0.00	33.2

Jun-04	3.03	0.00	32.4
Jul-04	3.88	0.00	33.1
Aug-04	4.32	0.00	33.4
Sep-04	4.34	0.00	32.1
Oct-04	4.48	0.00	31.8
Nov-04	4.41	0.00	34
Dec-04		0.00	32.4
Jan-05		0.00	34.3
Feb-05	4.41	0.00	35.2
Mar-05	4.55	0.00	33.9
Apr-05	4.31		41.2
May-05	4.20		35.2
Jun-05	3.98		37.1
Jul-05	3.79		36.6
Aug-05	3.92		36.9
Sep-05	3.67		37.5
N5_2003			
Month	Rutting	Bottom-up cracking	IRI
Oct-03	0.19	0.00	59.7
Nov-03	0.31	0.00	59.3
Dec-03	0.27	0.00	60
Jan-04	0.34	0.00	59.8
Feb-04	0.44	0.00	59.8
Mar-04	0.57	0.00	63.1
Apr-04	0.85	0.00	60.4
May-04	1.42	0.00	60.6
Jun-04	1.82	0.00	59.2
Jul-04	2.46	0.00	59.3
Aug-04	2.56	0.00	59.7
Sep-04	2.74	0.00	60.3
Oct-04	2.98	0.00	58.7
Nov-04	2.90	0.00	59.1
Dec-04		0.00	60.1
Jan-05		0.00	62.4
Feb-05	2.93	0.00	62.5
Mar-05	2.92	0.00	64.4
Apr-05	2.90	0.00	66.3
May-05	2.93	0.00	64.9
Jun-05	3.01		65.3
Jul-05	3.16	0.14	65.1

Aug-05	3.49		67.7
Sep-05	3.34	0.38	70.9
N6_2003			
Month	Rutting	Bottom-up cracking	IRI
Oct-03	0.15	0.00	50.7
Nov-03	0.30	0.00	46.6
Dec-03	0.26	0.00	49.3
Jan-04	0.34	0.00	50.5
Feb-04	0.42	0.00	43
Mar-04	0.43	0.00	41.4
Apr-04	1.06	0.00	42.8
May-04	2.28	0.00	44.9
Jun-04	3.03	0.00	47.8
Jul-04	4.04	0.00	50.3
Aug-04	4.65	0.00	49.2
Sep-04	4.85	0.00	49.8
Oct-04	4.77	0.00	52
Nov-04	4.79	0.96	50.1
Dec-04			49.7
Jan-05			50.2
Feb-05	4.83		51.3
Mar-05	4.82	1.04	50
Apr-05	4.80		52
May-05	4.95	1.06	48.3
Jun-05	5.09		49.9
Jul-05	5.05	2.03	46.9
Aug-05	5.22		49.6
Sep-05	5.22	2.73	52.4
N7_2003			
Month	Rutting	Bottom-up cracking	IRI
Oct-03	0.26	0.00	43.1
Nov-03	0.40	0.00	40.1
Dec-03	0.39	0.00	41.5
Jan-04	0.47	0.00	41
Feb-04	0.50	0.00	42.7
Mar-04	0.61	0.00	43.4
Apr-04	1.06	0.00	41.9
May-04	2.13	0.00	41.6
Jun-04	2.77	0.00	40.7

Jul-04	3.69	0.00	41.2
Aug-04	4.17	0.00	41.5
Sep-04	4.33	0.00	40.2
Oct-04	4.36	0.00	42.3
Nov-04	4.28	0.00	40.8
Dec-04			41.7
Jan-05			40.4
Feb-05	4.31		42.7
Mar-05	4.34	0.16	42
Apr-05	4.34		42.2
May-05	4.39		40.6
Jun-05	4.26		42.2
Jul-05	3.98	0.41	44
Aug-05	4.28		44.3
Sep-05	4.11	1.98	46.9
N8_2003			
Month	Rutting	Bottom-up cracking	IRI
Nov-06	0.42		
Dec-06	0.57		
Jan-07	0.59		
Feb-07	0.66		
Mar-07	0.78		
Apr-07	1.02		
May-07	1.28		
Jun-07	2.24		
Jul-07	2.96		
Aug-07	3.83		
Sep-07	4.36		
Oct-07	4.56	Layer slippage	Section N8_2003 was not in the calibration dataset for Bottom-up cracking model calibration
Nov-07	4.99		
Dec-07	4.51		
Jan-08			
Feb-08			
Mar-08	3.90		
Apr-08	4.23		
May-08	4.16		
Jun-08	3.60		
Jul-08	2.93		
Aug-08	2.40		
Sep-08	2.15		

Oct-08	2.46		
N1_2006			
Month	Rutting	Bottom-up cracking	IRI
Nov-06	0.50	Top-down cracking	Section N1_2006 was not in the calibration dataset for Bottom-up cracking model calibration
Dec-06	0.40		
Jan-07	0.50		
Feb-07	0.50		
Mar-07	0.30		
Apr-07	0.50		
May-07	0.50		
Jun-07	0.50		
Jul-07	1.20		
Aug-07	1.90		
Sep-07	0.70		
Oct-07	1.30		
Nov-07	1.30		
Dec-07	1.40		
Jan-08	2.50		
Feb-08	0.90		
Mar-08			
Apr-08	2.10		
May-08	1.40		
Jun-08	3.10		
Jul-08	3.20		
Aug-08	3.40		
Sep-08	3.60		
Oct-08	3.30		
N2_2006			
Month	Rutting	Bottom-up cracking	IRI
Nov-06	0.40	Top-down cracking	Section N2_2006 was not in the calibration dataset for Bottom-up cracking model calibration
Dec-06	0.30		
Jan-07	0.60		
Feb-07	0.60		
Mar-07	0.30		
Apr-07	0.80		
May-07	0.70		
Jun-07	0.00		
Jul-07	0.80		
Aug-07	1.60		

Sep-07	0.80	Top-down cracking	Section N2_2006 was not in the calibration dataset for Bottom-up cracking model calibration
Oct-07	1.90		
Nov-07	1.20		
Dec-07	1.50		
Jan-08	1.50		
Feb-08	0.20		
Mar-08			
Apr-08	1.40		
May-08	1.50		
Jun-08	2.20		
Jul-08	2.90		
Aug-08	2.50		
Sep-08	3.50		
Oct-08	3.00		
N8_2006			
Month	Rutting	Bottom-up cracking	IRI
Nov-06	1.20	0.00	94.5
Dec-06	1.20	0.00	88.8
Jan-07	1.10	0.00	91.0
Feb-07	2.30	0.00	93.1
Mar-07	1.20	0.00	93.6
Apr-07	1.50	0.00	96.1
May-07	1.40	0.00	100.5
Jun-07	1.60	0.00	101.7
Jul-07	2.80	0.00	105.3
Aug-07	4.40	0.00	109.2
Sep-07	4.30	0.00	113.7
Oct-07	4.60	0.00	113.4
Nov-07	4.80	0.00	114.6
Dec-07	4.40	0.00	115.6
Jan-08	4.70	0.00	119.0
Feb-08	4.50	0.00	120.9
Mar-08		0.00	115.4
Apr-08	5.90	0.00	123.4
May-08	5.30	0.00	131.3
Jun-08	5.60	0.00	130.1
Jul-08	6.80	4.00	142.5
Aug-08	7.50	6.54	148.3
Sep-08	7.10		157.2
Oct-08	8.20	14.69	

N9_2006			
Month	Rutting	Bottom-up cracking	IRI
Sep-09	0.70	0.00	110.7
Oct-09	1.00	0.00	107.3
Nov-09	1.10	0.00	106.5
Dec-09	1.80	0.00	102.2
Jan-10	0.90	0.00	106.4
Feb-10	0.90	0.00	110.2
Mar-10	0.50	0.00	111.1
Apr-10	0.20	0.00	113.5
May-10	0.60	0.00	114.4
Jun-10	1.60	0.00	116.1
Jul-10	0.70	0.00	114.1
Aug-10	2.00	0.00	120.3
Sep-10	1.70		118.5
Oct-10	2.00		118.5
Nov-10	1.30		114.2
Dec-10	1.70		114.7
Jan-11			116.4
Feb-11	3.20		111.8
Mar-11	1.70		120.8
Apr-11	2.80		124.1
May-11	2.00		125.3
Jun-11	1.90		122.1
Jul-11	2.00		123.8
Aug-11	2.00		119
N10_2006			
Month	Rutting	Bottom-up cracking	IRI
Nov-06	0.40	0.00	66.9
Dec-06	0.50	0.00	64.6
Jan-07	0.60	0.00	63.2
Feb-07	0.70	0.00	61
Mar-07	0.00	0.00	60
Apr-07	0.00	0.00	68.6
May-07	0.50	0.00	80.9
Jun-07	1.40	0.00	77.6
Jul-07	4.70	0.00	89.4
Aug-07	6.50	0.00	103.6
Sep-07	7.20	0.00	127

Oct-07	7.70	0.00	106.7
Nov-07	7.50	0.00	106.1
Dec-07	8.30	0.00	106.9
Jan-08	7.80	0.00	125.6
Feb-08	7.90	0.00	105.8
Mar-08		0.00	118.8
Apr-08	9.20	0.00	118.7
May-08	8.30	0.00	113.9
Jun-08	8.00	0.00	122.1
Jul-08	10.40	2.26	139
Aug-08	11.90		157.3
Sep-08	11.30		
Oct-08	11.40	10.48	
S11_2006			
Month	Rutting	Bottom-up cracking	IRI
Sep-09	0.00	0.00	67.7
Oct-09	0.00	0.00	66.1
Nov-09	0.00	0.00	67.3
Dec-09	0.52	0.00	65.4
Jan-10	0.16	0.00	67.9
Feb-10	0.41	0.00	68.9
Mar-10	1.05	0.00	71.6
Apr-10	1.84	0.00	73.3
May-10	3.90	0.00	75.1
Jun-10	5.84	0.00	74.5
Jul-10	6.10	0.00	73.8
Aug-10	6.72	0.00	74.3
Sep-10	7.08	0.00	74.6
Oct-10	6.81	0.00	75.6
Nov-10	6.59	0.00	76.2
Dec-10	7.04		74.2
Jan-11			73.9
Feb-11	8.70		75.7
Mar-11	6.99		78.6
Apr-11	8.85		80.8
May-11	9.97	9.72	80.8
Jun-11	10.71		84.0
Jul-11	10.77		85.5
Aug-11	10.67	10.48	87.3

N5_2009			
Month	Rutting	Bottom-up cracking	IRI
Aug-09	0.00	0.00	69.8
Sep-09	1.30	0.00	63.6
Oct-09	1.90	0.00	64.6
Nov-09	2.50	0.00	67.1
Dec-09		0.00	67.2
Jan-10	3.00	0.00	
Feb-10		0.00	68.8
Mar-10	3.10	0.00	66.9
Apr-10	3.50	0.00	64.5
May-10	3.90	0.00	65.2
Jun-10	5.40	0.00	65.3
Jul-10	6.90	0.00	67.4
Aug-10		0.00	72.0
Sep-10	7.00	0.00	68.4
Oct-10		0.00	71.2
Nov-10	6.30	0.00	71.2
Dec-10		0.00	72.7
Jan-11		0.00	
Feb-11	6.30	0.00	72.6
Mar-11	5.90	0.00	73.0
Apr-11	7.00	0.00	74.3
May-11	6.70	0.00	74.2
Jun-11	7.20	0.00	74.5
Jul-11	7.30	0.00	75.9
N7_2009			
Month	Rutting	Bottom-up cracking	IRI
Aug-09	0.00	0.00	125.2
Sep-09	0.10	0.00	121.1
Oct-09	1.40	0.00	111.8
Nov-09	1.80	0.00	117.4
Dec-09		0.00	117.8
Jan-10	2.10	0.00	
Feb-10		0.00	120.8
Mar-10	2.30	0.00	115.1
Apr-10	2.50	0.00	118.4
May-10	2.40	0.00	114.3
Jun-10	2.50	0.00	111.7
Jul-10	2.30	0.00	113.6

Aug-10		0.00	117.4
Sep-10	1.30	0.00	115.3
Oct-10		0.00	115.2
Nov-10	1.10	0.00	113.2
Dec-10		0.00	107.4
Jan-10		0.00	
Feb-11	1.10	0.00	108.9
Mar-11	1.70	0.00	109.5
Apr-11	1.20	0.00	110.2
May-11	1.70	0.00	112.5
Jun-11	1.20	0.00	110.2
Jul-11	1.40	0.00	105.3
N11_2009			
Month	Rutting	Bottom-up cracking	IRI
Sep-09	0.00	0.00	34.4
Oct-09	0.00	0.00	34.9
Nov-09	0.90	0.00	35.9
Dec-09	1.50	0.00	35.7
Jan-10		0.00	35.7
Feb-10	1.90	0.00	
Mar-10		0.00	35.9
Apr-10	2.10	0.00	35.6
May-10	2.20	0.00	36.1
Jun-10	1.90	0.00	36.8
Jul-10	2.90	0.00	38.7
Aug-10	3.70	0.00	38.6
Sep-10		0.00	42.2
Oct-10	2.80	0.00	39.1
Nov-10		0.00	38.4
Dec-10	1.90	0.00	39.1
Jan-11		0.00	39.1
Feb-11		0.00	
Mar-11	2.60	0.00	39.8
Apr-11	2.50	0.00	37.9
May-11	3.30	0.00	38.2
Jun-11	3.50	0.00	38.8
Jul-11	2.80	0.00	40.2
Aug-11	2.70	0.00	39.5

S8_2009			
Month	Rutting	Bottom-up cracking	IRI
Aug-09	0.30	0.00	125.9
Sep-09	1.30	0.00	108.0
Oct-09	1.70	0.00	104.6
Nov-09	2.60	0.00	106.3
Dec-09		0.00	105.0
Jan-10	3.50	0.00	
Feb-10		0.00	111.1
Mar-10	3.70	0.00	100.3
Apr-10	3.80	0.00	98.2
May-10	3.10	0.00	96.8
Jun-10	4.10	0.00	98.1
Jul-10	4.50	0.00	101.9
Aug-10		0.00	104.3
Sep-10	4.30	0.00	105.7
Oct-10		0.00	109.8
Nov-10	4.20	0.00	112.1
Dec-10		0.00	105.4
Jan-11		0.00	
Feb-11	3.50	0.00	103.6
Mar-11	4.60	0.00	104.8
Apr-11	4.80	0.00	102.1
May-11	5.20	0.00	105.2
Jun-11	4.00	0.00	106.1
Jul-11	4.40	0.00	105.4
S9_2009			
Month	Rutting	Bottom-up cracking	IRI
Sep-09	0.00	0.00	65.2
Oct-09	0.50	0.00	59.7
Nov-09	1.50	0.00	59.2
Dec-09	2.10	0.00	58.6
Jan-10		0.00	59.3
Feb-10	2.50	0.00	
Mar-10		0.00	60.2
Apr-10	2.60	0.00	58.7
May-10	2.50	0.00	58.7
Jun-10	3.00	0.00	56.6
Jul-10	4.30	0.00	54.4
Aug-10	5.40	0.00	58.8

Sep-10		0.00	60.4
Oct-10	4.90	0.00	59.1
Nov-10		0.00	59.9
Dec-10	4.60	0.00	58.4
Jan-11		0.00	59.0
Feb-11		0.00	
Mar-11	4.40	0.00	59.0
Apr-11	5.00	0.00	59.5
May-11	5.40	0.00	57.9
Jun-11	6.10	0.00	58.3
Jul-11	4.70	0.00	58.7
Aug-11	5.40	0.00	59.5
S10_2009			
Month	Rutting	Bottom-up cracking	IRI
Sep-09	0.00	0.00	58.6
Oct-09	0.60	0.00	64.8
Nov-09	1.60	0.00	63.7
Dec-09	2.20	0.00	65.2
Jan-10		0.00	66.5
Feb-10	2.50	0.00	
Mar-10		0.00	62.7
Apr-10	2.60	0.00	64.3
May-10	3.00	0.00	64.3
Jun-10	4.10	0.00	65.5
Jul-10	5.30	0.00	66.1
Aug-10	6.60	0.00	68.1
Sep-10		0.00	70.3
Oct-10	5.60	0.00	68.2
Nov-10		0.00	67.4
Dec-10	6.30	0.00	67.6
Jan-11		0.00	67.6
Feb-11		0.00	
Mar-11	5.80	0.00	67.8
Apr-11	6.40	0.00	67.4
May-11	7.20	0.00	68.6
Jun-11	7.20	0.00	68.1
Jul-11	6.40	0.00	68.9
Aug-11	7.00	0.00	69.7
S11_2009			

Month	Rutting	Bottom-up cracking	IRI
Sep-09	0.00	0.00	84.4
Oct-09	0.90	0.00	63.6
Nov-09	1.90	0.00	58.8
Dec-09	2.30	0.00	60.4
Jan-09		0.00	60.9
Feb-10	2.60	0.00	
Mar-10		0.00	61.9
Apr-10	2.70	0.00	57.6
May-10	3.10	0.00	60.1
Jun-10	4.40	0.00	64.7
Jul-10	5.50	0.00	69.9
Aug-10	7.00	0.00	73.7
Sep-10		0.00	79.8
Oct-10	6.90	0.00	78.8
Nov-10		0.00	80.2
Dec-10	6.40	0.00	78.5
Jan-11		0.00	78.7
Feb-11		0.00	
Mar-11	6.30	0.00	78.5
Apr-11	6.80	0.00	73.0
May-11	8.00	0.00	76.2
Jun-11	8.20	0.00	79.3
Jul-11	7.00	0.00	81.0
Aug-11	7.70	0.00	82.1
S12_2009			
Month	Rutting	Bottom-up cracking	IRI
Sep-09	0.00	0.00	127.3
Oct-09	0.20	0.00	103.2
Nov-09	1.20	0.00	98.5
Dec-09	1.80	0.00	100.2
Jan-10		0.00	98.4
Feb-10	2.30	0.00	
Mar-10		0.00	100.8
Apr-10	2.30	0.00	95.7
May-10	2.10	0.00	94.4
Jun-10	2.40	0.00	91.4
Jul-10	3.00	0.00	93.1
Aug-10	4.20	0.00	96.2
Sep-10		0.00	98.5

Oct-10	3.70	0.00	95.8
Nov-10		0.00	96.3
Dec-10	3.40	0.00	95.3
Jan-11		0.00	91.8
Feb-11		0.00	
Mar-11	3.20	0.00	91.8
Apr-11	3.90	0.00	95.1
May-11	4.50	0.00	94.4
Jun-11	4.50	0.00	94.0
Jul-11	3.50	0.00	91.2
Aug-11	3.70	0.00	90.1
N4_2012			
Month	Rutting	Bottom-up cracking	IRI
Oct-12	2.15	Lack of data	Section N4_2012 was not in the calibration dataset for Bottom-up cracking model calibration
crNov-12	2.77		
Dec-12	2.35		
Jan-13	2.46		
Feb-13	2.52		
Mar-13	2.39		
Apr-13	2.00		
May-13	2.39		
Jun-13	2.06		
Jul-13	3.86		
Aug-13	4.54		
Sep-13	3.70		
Oct-13	4.50		
Nov-13	4.62		
Dec-13	3.91		
Jan-14	4.25		
Feb-14	4.26		
Mar-14	3.76		
Apr-14	3.77		
May-14	5.48		
Jun-14	6.39		
Jul-14	6.99		
Aug-14	6.21		
Sep-14	6.20		
N5_2012			
Month	Rutting	Bottom-up cracking	IRI

Oct-12	1.55	0.00	55.5
Nov-12	1.83	0.00	55.2
Dec-12	1.79	0.00	54.9
Jan-13	2.03	0.00	52.5
Feb-13	1.89	0.00	53.3
Mar-13	1.85	0.00	54.0
Apr-13	1.81	2.00	58.0
May-13	2.55		71.1
Jun-13	2.70		80.0
Jul-13	5.95	6.00	91.6
Aug-13	9.03	32.00	115.2
Sep-13	5.46		137.9
Oct-13	5.95		125.3
Nov-13	5.32		117.3
Dec-13	4.63		
Jan-14	4.34		
Feb-14	5.46	39.00	
Mar-14	5.73		
Apr-14	0.42		
May-14	4.17		
Jun-14	11.53		
Jul-14	18.16		
Aug-14	19.09		
Sep-14	19.84		
S5_2012			
Month	Rutting	Bottom-up cracking	IRI
Oct-12	1.38	0.00	105.5
Nov-12	1.99	0.00	98.7
Dec-12	1.92	0.00	103.4
Jan-13	1.93	0.00	103.7
Feb-13	1.79	0.00	99.1
Mar-13	1.98	33.00	98.0
Apr-13	3.19		98.5
May-13	4.59		97.8
Jun-13	3.02		59.7
Jul-13	4.79		61.8
Aug-13	5.62		61.7
Sep-13	4.47		62.7
Oct-13	5.68		60.9
Nov-13	5.60		61.5

Dec-13	4.77		64.3
Jan-14	5.15		61.2
Feb-14	4.97		60.6
Mar-14	4.30		62.0
Apr-14	4.45		68.9
May-14	6.64		
Jun-14	7.82		60.5
Jul-14	7.87		61.3
Aug-14	7.17		69.8
Sep-14	6.99		61.5
S6_2012			
Month	Rutting	Bottom-up cracking	IRI
Oct-12	1.30	0.00	58.1
Nov-12	1.90	0.00	56.3
Dec-12	1.80	0.00	53.5
Jan-13	1.90	0.00	55.6
Feb-13	1.80	0.00	56.5
Mar-13	1.80	0.00	65.5
Apr-13	2.10	0.00	62.8
May-13	2.30	1.00	69.3
Jun-13	2.70		69.1
Jul-13	6.30	1.00	89.5
Aug-13	9.30		112.3
Sep-13	10.00	14.00	128.5
Oct-13	10.50		122.2
Nov-13	8.80		123.0
Dec-13	8.00		
Jan-14	9.40		
Feb-14	10.20	39.00	
Mar-14	10.30		
Apr-14	0.70		
May-14	3.20		
Jun-14	7.40		
Jul-14	13.70		
Aug-14	13.90		
Sep-14	15.30		
S13_2012			
Month	Rutting	Bottom-up cracking	IRI
Oct-12	2.00	0.00	75.0

Nov-12	1.80	0.00	70.3
Dec-12	1.90	0.00	70.2
Jan-13	2.00	0.00	66.8
Feb-13	1.90	0.00	67.2
Mar-13	2.00	0.00	70.1
Apr-13	2.10	0.00	69.4
May-13	2.50	0.00	74.1
Jun-13	3.30	1.00	71.8
Jul-13	5.70	2.00	83.7
Aug-13	6.70		92.3
Sep-13	6.40	22.00	107.4
Oct-13	7.70		114.0
Nov-13	7.20		143.9
Dec-13	6.80		145.9
Jan-14	7.20		
Feb-14	7.40	42.00	
Mar-14	7.40		
Apr-14	0.40		
May-14	6.30		
Jun-14	12.30		
Jul-14	14.50		
Aug-14	15.70		
Sep-14	17.50		
Number of data points	526	394	445

Measurement data for validation

N1_2003			
Month	Rutting	Bottom-up cracking	IRI
Oct-03	0.66	0	55.7
Nov-03	0.82	0	53
Dec-03	0.82	0	52.1
Jan-04	1.04	0	53.7
Feb-04	1.20	0	46.5
Mar-04	1.31	0	44.4
Apr-04	1.86	0	65.3
May-04	2.62	0	91.7
Jun-04	3.47	0	112.7
Jul-04	4.35	19.20	158.4
Aug-04	4.80	22.18	129.4
Sep-04	5.57		161.8

Oct-04	6.18	28.83	181.2
Nov-04	8.19		381.7
Dec-04		31.54	482
Jan-05			
Feb-05			
Mar-05			
Apr-05			
May-05			
Jun-05			
Jul-05			
Aug-05			
Sep-05			
N4_2003			
Month	Rutting	Bottom-up cracking	IRI
Oct-03	0.54	0	46.8
Nov-03	0.60	0	44.9
Dec-03	0.56	0	46.8
Jan-04	0.71	0	50.2
Feb-04	0.83	0	43.2
Mar-04	0.67	0	43.1
Apr-04	1.15	0	44.3
May-04	1.72	0	44.3
Jun-04	2.19	0	48.8
Jul-04	2.73	0	48.7
Aug-04	3.18	0	48.1
Sep-04	3.32	0	52
Oct-04	3.25	0	47.1
Nov-04	3.22	0	49.8
Dec-04		0	46.2
Jan-05		0	48.3
Feb-05	3.15	0	48.8
Mar-05	3.18	0	48.9
Apr-05	3.09	0	49
May-05	3.12	0	48.1
Jun-05	3.21	0	48.5
Jul-05	3.01	0	46.6
Aug-05	3.14	0	46.8
Sep-05	3.11	0	49.9

N6_2009			
Month	Rutting	Bottom-up cracking	IRI
Oct-03	0.00	0	58.1
Nov-03	1.14	0	58.7
Dec-03	2.12	0	57.2
Jan-04	2.46	0	58.4
Feb-04		0	59.1
Mar-04	3.09	0	
Apr-04		0	58.7
May-04	3.05	0	57.4
Jun-04	3.39	0	57.1
Jul-04	3.73	0	56
Aug-04	5.12	0	55.9
Sep-04	6.48	0	58.2
Oct-04		0	62.2
Nov-04	6.22	0	59.3
Dec-04		0	60.2
Jan-05	5.93	0	60.4
Feb-05		0	59.9
Mar-05		0	
Apr-05	5.97	0	59.2
May-05	5.59	0	59.5
Jun-05	6.63	0	59.4
Jul-05	6.78	0	58.9
Aug-05	7.03	0	60.4
Sep-05	7.58	0	60.7
N10_2009			
Month	Rutting	Bottom-up cracking	IRI
Oct-03	0.00	0	61.7
Nov-03	0.00	0	53.6
Dec-03	0.34	0	48.3
Jan-04	1.12	0	50.2
Feb-04		0	51.1
Mar-04	1.40	0	
Apr-04		0	53.8
May-04	1.61	0	49.5
Jun-04	1.61	0	49.8
Jul-04	1.06	0	47
Aug-04	1.69	0	46.1
Sep-04	2.26	0	49.4

Oct-04		0	52.6
Nov-04	1.10	0	51
Dec-04		0	51.5
Jan-05	0.85	0	51.8
Feb-05		0	48.5
Mar-05		0	
Apr-05	1.10	0	48.9
May-05	0.93	0	48.7
Jun-05	1.21	0	49.3
Jul-05	2.00	0	49.1
Aug-05	1.16	0	48.6
Sep-05	1.37	0	47.1
N3_2012			
Month	Rutting	Bottom-up cracking	IRI
Oct-12	1.66	Lack of data	Section N3_2012 was not in the validation dataset for Bottom-up cracking model validation
Nov-12	2.43		
Dec-12	2.66		
Jan-13	2.72		
Feb-13	2.60		
Mar-13	2.74		
Apr-13	1.70		
May-13	1.78		
Jun-13	1.71		
Jul-13	3.37		
Aug-13	4.15		
Sep-13	3.39		
Oct-13	4.12		
Nov-13	4.15		
Dec-13	3.42		
Jan-14	4.01		
Feb-14	3.81		
Mar-14	3.43		
Apr-14	3.37		
May-14	4.63		
Jun-14	5.58		
Jul-14	6.24		
Aug-14	5.39		
Sep-14	5.63		

S12_2012			
Month	Rutting	Bottom-up cracking	IRI
Nov-06	2.76	Lack of data	Section S12_2012 was not in the validation dataset for Bottom-up cracking model validation
Dec-06	2.83		
Jan-07	2.89		
Feb-07	2.79		
Mar-07	2.51		
Apr-07	2.56		
May-07	2.81		
Jun-07	2.97		
Jul-07	2.49		
Aug-07	4.57		
Sep-07	5.17		
Oct-07	4.68		
Nov-07	5.42		
Dec-07	5.12		
Jan-08	4.54		
Feb-08	4.76		
Mar-08	4.88		
Apr-08	4.28		
May-08	4.14		
Jun-08	3.99		
Jul-08	4.68		
Aug-08	5.57		
Sep-08	5.46		
Oct-08	5.53		
Number of data points	120	85	83

Appendix B

The random selection was conducted for determining how to use experimental sections. Each of 31 experimental sections was assigned a random number between 0 and 1. The six sections with the lowest random number were selected for validation group, while the other 25 sections were for the evaluation and calibration group. The two groups of sections were summarized in Table B.1.

Table B.1 Two groups of sections

	Evaluation and Calibration	Validation
Group Percent	80%	20%
Number of Sections	25 (rounded)	6 (rounded)
Section_Year	N2_2003, N3_2003, N5_2003, N6_2003, N7_2003, N8_2003, N1_2006, N2_2006, N8_2006, N9_2006, N10_2006, S11_2006, N5_2009, N7_2009, N11_2009, S8_2009, S9_2009, S10_2009, S11_2009, S12_2009, N4_2012, N5_2012, S5_2012, S6_2012, S13_2012.	N1_2003, N4_2003, N6_2009, N10_2009, N3_2012, S12_2012.

For the rutting model calibration, the 25 experimental sections (80%) shown in Table B.5 were used for the evaluation and calibration, and the remaining six (20%) sections were used for the validation. For the bottom-up fatigue cracking model calibration, due to premature failure or lack of measurement data for the four sections (i.e., N8_2003, N1_2006, N2_2006, and N4_2012), 21 of the 25 sections were used for evaluation and calibration. For the same reason, N3_2012 and S12_2012 were not available for use, so four of the six remaining sections (20%) shown in Table B.1 were used for the validation.

Section Use: Rutting model calibration				
SN	Cycle	Sectio	Use	Project
1	2003	N2	Evaluation & Calibration	N2_2003.dgpx
2	2003	N3	Evaluation & Calibration	N3_2003.dgpx
3	2003	N5	Evaluation & Calibration	N5_2003.dgpx
4	2003	N6	Evaluation & Calibration	N6_2003.dgpx
5	2003	N7	Evaluation & Calibration	N7_2003.dgpx
6	2003	N8	Evaluation & Calibration	N8_2003.dgpx
7	2006	N1	Evaluation & Calibration	N1_2006.dgpx
8	2006	N2	Evaluation & Calibration	N2_2006.dgpx
9	2006	N8	Evaluation & Calibration	N8_2006.dgpx
10	2006	N9	Evaluation & Calibration	N9_2006.dgpx
11	2006	N10	Evaluation & Calibration	N10_2006.dgpx
12	2006	S11	Evaluation & Calibration	S11_2006.dgpx
13	2009	N5	Evaluation & Calibration	N5_2009.dgpx
14	2009	N7	Evaluation & Calibration	N7_2009.dgpx
15	2009	N11	Evaluation & Calibration	N11_2009.dgpx
16	2009	S8	Evaluation & Calibration	S8_2009.dgpx
17	2009	S9	Evaluation & Calibration	S9_2009.dgpx
18	2009	S10	Evaluation & Calibration	S10_2009.dgpx
19	2009	S11	Evaluation & Calibration	S11_2009.dgpx
20	2009	S12	Evaluation & Calibration	S12_2009.dgpx
21	2012	N4	Evaluation & Calibration	N4_2012.dgpx
22	2012	N5	Evaluation & Calibration	N5_2012.dgpx
23	2012	S5	Evaluation & Calibration	S5_2012.dgpx
24	2012	S6	Evaluation & Calibration	S6_2012.dgpx
25	2012	S13	Evaluation & Calibration	S13_2012.dgpx
1	2003	N1	Validation	N1_2003.dgpx
2	2003	N4	Validation	N4_2003.dgpx
3	2009	N6	Validation	N6_2009.dgpx
4	2009	N10	Validation	N10_2009.dgpx
5	2012	N3	Validation	N3_2012.dgpx
6	2012	S12	Validation	S12_2012.dgpx

Section Use: Fatigue cracking and IRI model calibration					
SN	Cycle	Sectio	Use	Project	Reason to Cancel
1	2003	N2	Evaluation & Calibration	N2_2003.dgpx	
2	2003	N3	Evaluation & Calibration	N3_2003.dgpx	
3	2003	N5	Evaluation & Calibration	N5_2003.dgpx	
4	2003	N6	Evaluation & Calibration	N6_2003.dgpx	
5	2003	N7	Evaluation & Calibration	N7_2003.dgpx	
~~6~~	~~2003~~	~~N8~~	~~Evaluation & Calibration~~	~~N8_2003.dgpx~~	Layer slippage
~~7~~	~~2006~~	~~N1~~	~~Evaluation & Calibration~~	~~N1_2006.dgpx~~	Top-down cracking
~~8~~	~~2006~~	~~N2~~	~~Evaluation & Calibration~~	~~N2_2006.dgpx~~	Top-down cracking
9	2006	N8	Evaluation & Calibration	N8_2006.dgpx	
10	2006	N9	Evaluation & Calibration	N9_2006.dgpx	
11	2006	N10	Evaluation & Calibration	N10_2006.dgpx	
12	2006	S11	Evaluation & Calibration	S11_2006.dgpx	
13	2009	N5	Evaluation & Calibration	N5_2009.dgpx	
14	2009	N7	Evaluation & Calibration	N7_2009.dgpx	
15	2009	N11	Evaluation & Calibration	N11_2009.dgpx	
16	2009	S8	Evaluation & Calibration	S8_2009.dgpx	
17	2009	S9	Evaluation & Calibration	S9_2009.dgpx	
18	2009	S10	Evaluation & Calibration	S10_2009.dgpx	
19	2009	S11	Evaluation & Calibration	S11_2009.dgpx	
20	2009	S12	Evaluation & Calibration	S12_2009.dgpx	
~~21~~	~~2012~~	~~N4~~	~~Evaluation & Calibration~~	~~N4_2012.dgpx~~	lack of data
22	2012	N5	Evaluation & Calibration	N5_2012.dgpx	
23	2012	S5	Evaluation & Calibration	S5_2012.dgpx	
24	2012	S6	Evaluation & Calibration	S6_2012.dgpx	
25	2012	S13	Evaluation & Calibration	S13_2012.dgpx	
1	2003	N1	Validation	N1_2003.dgpx	
2	2003	N4	Validation	N4_2003.dgpx	
3	2009	N6	Validation	N6_2009.dgpx	
4	2009	N10	Validation	N10_2009.dgpx	
~~5~~	~~2012~~	~~N3~~	~~Validation~~	~~N3_2012.dgpx~~	lack of data
~~6~~	~~2012~~	~~S12~~	~~Validation~~	~~S12_2012.dgpx~~	lack of data

Appendix C

As mentioned earlier, the trial values of calibration coefficients and the derived SSE were tabulated herein (for rutting and bottom-up fatigue cracking calibration). For the rutting model calibration, the SSE under the default coefficients was 28371.89. The SSE under the optimal calibration coefficients (i.e., β_{r1}= 0.05; β_{r2}= 0.5; β_{r3}= 2; β_b= 0; β_s= 0;) was 3139.15, meaning an 89% improvement.

Table C.1 Trial values of coefficients (rutting) and SSE (1)

Trial #	Number of Sections	β_{r2}	β_{r3}	β_{r1}	β_b	β_s	SSE
Default	25	1	1	1	1	1	28371.89
1	25	0.05	0.05	1	0.50	0.67	4437.73
2	25	0.05	0.1	1	0.50	0.67	4437.73
3	25	0.05	0.25	1	0.50	0.67	4437.73
4	25	0.05	0.5	1	0.50	0.67	4437.73
5	25	0.05	1	420.34	0	0.31	3772.46
6	25	0.05	2	0.40	0	0.31	3293.37
7	25	0.05	4	0	0.50	0.67	4437.73
8	25	0.05	8	0	0.50	0.67	4437.73
9	25	0.1	0.05	0	0.50	0.67	4437.73
10	25	0.1	0.1	0	0.50	0.67	4437.73
11	25	0.1	0.25	0	0.50	0.67	4437.73
12	25	0.1	0.5	0	0.50	0.67	4437.73
13	25	0.1	1	340.33	0	0.24	3679.65
14	25	0.1	2	0.28	0	0.31	3298.72
15	25	0.1	4	0	0.50	0.67	4437.73
16	25	0.1	8	0	0.50	0.67	4437.73
17	25	0.25	0.05	0	0.50	0.67	4437.73
18	25	0.25	0.1	0	0.50	0.67	4437.73
19	25	0.25	0.25	0	0.50	0.67	4437.73
20	25	0.25	0.5	0	0.50	0.67	4437.73
21	25	0.25	1	117.42	0	0.26	3731.32
22	25	0.25	2	0.10	0	0.32	3314.54
23	25	0.25	4	0	0.50	0.67	4437.73
24	25	0.25	8	0	0.50	0.67	4437.73
25	25	0.5	0.05	0	0.50	0.67	4437.73
26	25	0.5	0.1	0	0.50	0.67	4437.73
27	25	0.5	0.25	283.42	0.35	0.65	4381.20
28	25	0.5	0.5	394.91	0	0.39	4083.17
29	25	0.5	1	19.89	0	0.27	3744.74

Table C.2 Trial values of coefficients (rutting) and SSE (2)

Trial #	Number of Sections	β_{r2}	β_{r3}	β_{r1}	βb	βs	SSE
30	25	0.5	2	0.05	0	0	3139.15
31	25	0.5	4	0	0.50	0.67	4437.73
32	25	0.5	8	0	0.50	0.67	4437.73
33	25	1	0.05	35.06	0.33	0.59	4413.88
34	25	1	0.1	29.41	0.32	0.59	4412.01
35	25	1	0.25	27.62	0.13	0.52	4342.06
36	25	1	0.5	10.57	0	0.41	4151.66
37	25	1	1	0.55	0	0.32	3785.30
38	25	1	2	0	0.44	0.69	4438.97
39	25	1	4	0	0.50	0.67	4437.73
40	25	1	8	0	0.50	0.67	4437.73
41	25	2	0.05	0.03	0.30	0.58	4391.54
42	25	2	0.1	0.02	0.28	0.57	4381.72
43	25	2	0.25	0.03	0	0.43	4230.78
44	25	2	0.5	0.04	0	0.05	4119.95
45	25	2	1	0	0.50	0.67	4437.73
46	25	2	2	0	0.50	0.67	4437.73
47	25	2	4	0	0.50	0.67	4437.73
48	25	2	8	0	0.50	0.67	4437.73
49	25	4	0.05	0	0.50	0.67	4437.73
50	25	4	0.1	0	0.50	0.67	4437.73
51	25	4	0.25	0	0.50	0.67	4437.73
52	25	4	0.5	0	0.50	0.67	4437.73
53	25	4	1	0	0.50	0.67	4437.73
54	25	4	2	0	0.50	0.67	4437.73
55	25	4	4	0	0.50	0.67	4437.73
56	25	4	8	0	0.50	0.67	4437.73
57	25	8	0.05	0	0.50	0.67	4437.73
58	25	8	0.1	0	0.50	0.67	4437.73
59	25	8	0.25	0	0.50	0.67	4437.73
60	25	8	0.5	0	0.50	0.67	4437.73
61	25	8	1	0	0.50	0.67	4437.73
62	25	8	2	0	0.50	0.67	4437.73
63	25	8	4	0	0.50	0.67	4437.73
64	25	8	8	0	0.50	0.67	4437.73

Secondly, for the bottom-up cracking model calibration, the SSE under the default calibration coefficients was 15782.68, and the SSE under the optimal calibration coefficients (i.e., β_{f1}= 2.2; β_{f2}= 1; β_{f3}= 1; C_1= 2.03; C_2= 2.62; C_4= 5729.28) was 8315.841, meaning 47.3% for the former.

Table C.3 Trial values of coefficients (bottom-up cracking) and SSE – round 1

Trial #	Number of Sections	β_{f1}	β_{f2}	β_{f3}	SSE1*	C_1	C_2	C_4	SSE2*
Default	21	1	1	1	15782.68	1	1	6000	-
1	21	0.25	0.25	0.25	3859664	2.3	0.38	5999.91	2017443
2	21	0.25	1	0.25	2511801	0	2.04	6.51E+10	2506609
3	21	0.25	4	0.25	3859763	1	1	6000	3859763
4	21	0.25	0.25	1	3859763	1	1	6000	3859763
5	21	0.25	1	1	125534.4	3.21	2.56	6078.35	8318.933
6	21	0.25	4	1	3859763	1	1	6000	3859763
7	21	0.25	0.25	4	3859763	1	1	6000	3859763
8	21	0.25	1	4	3859763	1	1	6000	3859763
9	21	0.25	4	4	3859763	1	1	6000	3859763
10	21	1	0.25	0.25	3859297	6.34	1.62	6000.48	388500.1
11	21	1	1	0.25	3757949	0	0.18	6000.16	3755274
12	21	1	4	0.25	3859763	1	1	6000	3859763
13	21	1	0.25	1	3859763	1	1	6000	3859763
14	21	1	1	1	15782.68	2.46	2.59	5833.38	8317.974
15	21	1	4	1	3859763	1	1	6000	3859763
16	21	1	0.25	4	3859763	1	1	6000	3859763
17	21	1	1	4	3859763	1	1	6000	3859763
18	21	1	4	4	3859763	1	1	6000	3859763
19	21	4	0.25	0.25	3857686	16.3	5.21	317.96	12963.46
20	21	4	1	0.25	3859763	1	1	6000	3859763
21	21	4	4	0.25	3859763	1	1	6000	3859763
22	21	4	0.25	1	3859763	1	1	6000	3859763
23	21	4	1	1	11199.92	1.67	2.56	6067.79	8315.974
24	21	4	4	1	3859763	1	1	6000	3859763
25	21	4	0.25	1	3859763	1	1	6000	3859763
26	21	4	1	4	3859763	1	1	6000	3859763
27	21	4	4	4	3859763	1	1	6000	3859763

*SSE1 represents the calculated Sum of Squared Error just after attempting the coefficients β_{f1}, β_{f2}, and β_{f3} (in the fatigue accumulation model) in the software runs.
*SSE2 represents the calculated Sum of Squared Error after attempting the three coefficients and optimizing the C_1, C_2, and C_4 (in the cracking conversion model) by the Excel Solver.

Table C.4 Trial values of coefficients (bottom-up cracking) and SSE – round 2 a(1)

Trial #	Number of Sections	β_{f1}	β_{f2}	β_{f3}	SSE1*	C_1	C_2	C_4	SSE2*
28	21	0.5	0.5	0.5	3813403.1	1.62	0.36	3562.19	223625.1
29	21	0.5	0.7	0.5	702118.11	2.26	2.17	243.7	13410.86
30	21	0.5	0.9	0.5	20693.544	0.81	0.11	6000.01	13976.69
31	21	0.5	1.1	0.5	2341801.5	0.79	0	5999.97	2341304
32	21	0.5	1.3	0.5	3859762.6	1	1	6000	3859763
33	21	0.5	1.5	0.5	3859762.6	1	1	6000	3859763
34	21	0.7	0.5	0.5	3795587	55.22	20.71	941	212111.1
35	21	0.7	0.7	0.5	560757.72	2.11	2.18	243.77	13410.4
36	21	0.7	0.9	0.5	27872.27	0.79	0.11	5365.15	23974.43
37	21	0.7	1.1	0.5	2503801.5	0.75	0.03	5999.96	2503388
38	21	0.7	1.3	0.5	3859762.6	1	1	6000	3859763
39	21	0.7	1.5	0.5	3859762.6	1	1	6000	3859763
40	21	0.9	0.5	0.5	3778430.8	1.28	0.25	2605.43	193770.7
41	21	0.9	0.7	0.5	475225.64	1.99	2.18	243.94	13410.18
42	21	0.9	0.9	0.5	26595.647	0	0.24	273.59	23801.59
43	21	0.9	1.1	0.5	2753401.5	0.75	0	5999.96	2752904
44	21	0.9	1.3	0.5	3859762.6	1	1	6000	3859763
45	21	0.9	1.5	0.5	3859762.6	1	1	6000	3859763
46	21	1.1	0.5	0.5	3761864.1	1.24	0.21	3569.4	173840
47	21	1.1	0.7	0.5	419145.86	1.89	2.18	243.78	13410.59
48	21	1.1	0.9	0.5	45918.795	0.51	0.13	1617.77	43932.9
49	21	1.1	1.1	0.5	3033401.5	0.69	0	5964.13	3032726
50	21	1.1	1.3	0.5	3859762.6	1	1	6000	3859763
51	21	1.1	1.5	0.5	3859762.6	1	1	6000	3859763
52	21	1.3	0.5	0.5	3745889.2	1.27	0.19	5950.16	163873.7
53	21	1.3	0.7	0.5	380020.84	1.81	2.18	243.99	13410.12
54	21	1.3	0.9	0.5	45515.782	0.02	0.24	343.47	43828.38
55	21	1.3	1.1	0.5	3190497.1	0.71	0	5999.92	3190046
56	21	1.3	1.3	0.5	3859762.6	1	1	6000	3859763
57	21	1.3	1.5	0.5	3859762.6	1	1	6000	3859763

*SSE1 represents the calculated Sum of Squared Error just after attempting the coefficients β_{f1}, β_{f2}, and β_{f3} (in the fatigue accumulation model) in the software runs.
*SSE2 represents the calculated Sum of Squared Error after attempting the three coefficients and optimizing the C_1, C_2, and C_4 (in the cracking conversion model) by the Excel Solver.

Table C.5 Trial values of coefficients (bottom-up cracking) and SSE – round 2 a(2)

Trial #	Number of Sections	β_{f1}	β_{f2}	β_{f3}	SSE1*	C_1	C_2	C_4	SSE2*
58	21	1.5	0.5	0.5	3730387.1	1.06	0.17	2286.03	153864.7
59	21	1.5	0.7	0.5	351638.33	1.75	2.18	243.83	13410.08
60	21	1.5	0.9	0.5	65264.987	0.78	0.11	5982.2	63974.38
61	21	1.5	1.1	0.5	3257949.3	0.7	0	5999.96	3257515
62	21	1.5	1.3	0.5	3859762.6	1	1	6000	3859763
63	21	1.5	1.5	0.5	3859762.6	1	1	6000	3859763
64	21	0.5	0.5	0.9	3859734.7	4.19	0.93	6000.26	3224791
65	21	0.5	0.7	0.9	3776163.9	9.55	3.33	5001.76	248283
66	21	0.5	0.9	0.9	665774.16	1.86	1.76	264.12	13403.06
67	21	0.5	1.1	0.9	247310.74	0	0.19	211.73	43861.98
68	21	0.5	1.3	0.9	2351622.2	0.68	0	3560.66	2351088
69	21	0.5	1.5	0.9	3619762.6	1.6	1.6	6000	3619763
70	21	0.7	0.5	0.9	3859721.4	2.34	0.36	5999.73	3084799
71	21	0.7	0.7	0.9	3748598.4	9.7	3.49	4482.64	248266.1
72	21	0.7	0.9	0.9	535646.47	0.92	0.04	6000.02	14040.51
73	21	0.7	1.1	0.9	255368.33	0.76	0.05	3879.71	64015.8
74	21	0.7	1.3	0.9	2533411.5	0.68	0	3330.23	2532972
75	21	0.7	1.5	0.9	3619762.6	1	1	6000	3619763
76	21	0.9	0.5	0.9	3859707.6	1.74	0.17	5999.63	2944801
77	21	0.9	0.7	0.9	3723309.4	10.82	4.01	3613.8	248228.4
78	21	0.9	0.9	0.9	458091.54	1.64	1.76	264.08	13403.5
79	21	0.9	1.1	0.9	264771.63	0.71	0.05	2994.77	84006.55
80	21	0.9	1.3	0.9	2813407.3	2.6	1.01	6000	2813402
81	21	0.9	1.5	0.9	3619762.6	1	1	6000	3619763
82	21	1.1	0.5	0.9	3859693.5	1.48	0.09	5999.64	2815002
83	21	1.1	0.7	0.9	3699821.1	18.65	7.13	2643.95	248163.2
84	21	1.1	0.9	0.9	407753.37	1.56	1.76	264.06	13403.43
85	21	1.1	1.1	0.9	275278.44	0.85	0.04	5999.8	104024
86	21	1.1	1.3	0.9	3050605.2	2.6	1.08	6000	3050602
87	21	1.1	1.5	0.9	3619762.6	1	1	6000	3619763

*SSE1 represents the calculated Sum of Squared Error just after attempting the coefficients β_{f1}, β_{f2}, and β_{f3} (in the fatigue accumulation model) in the software runs.
*SSE2 represents the calculated Sum of Squared Error after attempting the three coefficients and optimizing the C_1, C_2, and C_4 (in the cracking conversion model) by the Excel Solver.

Table C.6 Trial values of coefficients (bottom-up cracking) and SSE – round 2 a(3)

Trial #	Number of Sections	β_{f1}	β_{f2}	β_{f3}	SSE1*	C_1	C_2	C_4	SSE2*
88	21	1.3	0.5	0.9	3859679.2	1.39	0.06	5999.68	2705394
89	21	1.3	0.7	0.9	3677805.3	8.69	3.24	5980.46	248307.7
90	21	1.3	0.9	0.9	373047.71	1.49	1.76	263.98	13403.87
91	21	1.3	1.1	0.9	266715.09	0.85	0.04	5998.29	104024.1
92	21	1.3	1.3	0.9	3227951.9	2.6	1.13	6000	3227949
93	21	1.3	1.5	0.9	3619762.6	1	1	6000	3619763
94	21	1.5	0.5	0.9	3859664.5	2.17	0.32	5999.89	2598393
95	21	1.5	0.7	0.9	3657005.9	17.7	6.94	2641.51	248164
96	21	1.5	0.9	0.9	348071.85	66.9	92.79	188.99	13352.71
97	21	1.5	1.1	0.9	268907.21	0.81	0.04	4825.66	114019.2
98	21	1.5	1.3	0.9	3277951.2	0.6	0	3352.61	3277478
99	21	1.5	1.5	0.9	3619762.6	1	1	6000	3619763
100	21	0.5	0.5	1.3	3859762.6	1	1	6000	3859763
101	21	0.5	0.7	1.3	3859693.7	1.72	0.18	5999.84	3124799
102	21	0.5	0.9	1.3	3717108.1	7.11	2.38	6553.08	248293.5
103	21	0.5	1.1	1.3	639146.93	3.84	2.52	6067.8	248356.4
104	21	0.5	1.3	1.3	333847.28	0.87	0.02	5999.99	94040.87
105	21	0.5	1.5	1.3	2431948.5	0.72	0	4172.68	2381084
106	21	0.7	0.5	1.3	3859762.6	1	1	6000	3859763
107	21	0.7	0.7	1.3	3859662.7	1.34	0.05	5999.78	2974801
108	21	0.7	0.9	1.3	3679978.5	6.78	2.32	7074.85	248294.9
109	21	0.7	1.1	1.3	518472.72	0.86	0.16	3581.74	243743.7
110	21	0.7	1.3	1.3	363724.72	0.87	0.02	5999.99	124037.2
111	21	0.7	1.5	1.3	2658076.7	0.69	0	3708.62	2622943
112	21	0.9	0.5	1.3	3859762.6	1	1	6000	3859763
113	21	0.9	0.7	1.3	3859630.7	1.2	0	5999.8	2795002
114	21	0.9	0.9	1.3	3647612.3	6.72	2.35	7002.12	248293.2
115	21	0.9	1.1	1.3	446842.78	0.85	0.15	3586.17	243746.5
116	21	0.9	1.3	1.3	373563.01	0.87	0.02	5963.86	134035.9
117	21	0.9	1.5	1.3	2955869.1	0.6	0	2200.18	2930257

*SSE1 represents the calculated Sum of Squared Error just after attempting the coefficients β_{f1}, β_{f2}, and β_{f3} (in the fatigue accumulation model) in the software runs.
*SSE2 represents the calculated Sum of Squared Error after attempting the three coefficients and optimizing the C_1, C_2, and C_4 (in the cracking conversion model) by the Excel Solver.

Table C.7 Trial values of coefficients (bottom-up cracking) and SSE – round 2 a(4)

Trial #	Number of Sections	β_{f1}	β_{f2}	β_{f3}	SSE1*	C_1	C_2	C_4	SSE2*
118	21	1.1	0.5	1.3	3859762.6	1	1	6000	3859763
119	21	1.1	0.7	1.3	3859597.9	1.22	0	5999.83	2615394
120	21	1.1	0.9	1.3	3618662.1	6.69	2.38	6631.42	248293
121	21	1.1	1.1	1.3	400488.39	0.93	0.15	5988.52	243766.6
122	21	1.1	1.3	1.3	393382.97	0.87	0.02	5999.99	154033.4
123	21	1.1	1.5	1.3	3134443.3	3.97	2.78	6008.3	3071917
124	21	1.3	0.5	1.3	3859762.6	1	1	6000	3859763
125	21	1.3	0.7	1.3	3859564.9	1.57	0.13	5999.88	2498396
126	21	1.3	0.9	1.3	3592136.8	6.58	2.37	6623.19	248294.3
127	21	1.3	1.1	1.3	368452.21	0.83	0.12	3564	233829.9
128	21	1.3	1.3	1.3	403191.62	0.87	0.02	5999.99	164032
129	21	1.3	1.5	1.3	3272918.3	0.61	0	3593.61	3257484
130	21	1.5	0.5	1.3	3859762.6	1	1	6000	3859763
131	21	1.5	0.7	1.3	3859530.9	1.39	0.07	5999.84	2309014
132	21	1.5	0.9	1.3	3567616	6.31	2.28	7417.77	248295.2
133	21	1.5	1.1	1.3	345404.54	49.35	42.62	1514.64	230330.7
134	21	1.5	1.3	1.3	422992.9	0.86	0.02	6000	184029.1
135	21	1.5	1.5	1.3	3325906.1	0.64	0	4339.82	3313519
136	21	0.5	0.5	1.7	3859762.6	1	1	6000	3859763
137	21	0.5	0.7	1.7	3859762.6	1	1	6000	3859763
138	21	0.5	0.9	1.7	3859581.1	1.21	0.01	5999.85	3014801
139	21	0.5	1.1	1.7	3644368	6.95	2.27	6634.62	248393.2
140	21	0.5	1.3	1.7	620640.5	4.49	2.85	4979.93	248374.1
141	21	0.5	1.5	1.7	414172.84	5.85	18.32	0	284522.6
142	21	0.7	0.5	1.7	3859762.6	1	1	6000	3859763
143	21	0.7	0.7	1.7	3859762.6	1	1	6000	3859763
144	21	0.7	0.9	1.7	3859501.5	1.21	0	5999.88	2794803
145	21	0.7	1.1	1.7	3601943.1	6.84	2.29	6690.27	248396.5
146	21	0.7	1.3	1.7	508721.26	4.44	2.95	5104.5	248371.5
147	21	0.7	1.5	1.7	424280.35	2.33	71.27	3267.7	279225

*SSE1 represents the calculated Sum of Squared Error just after attempting the coefficients β_{f1}, β_{f2}, and β_{f3} (in the fatigue accumulation model) in the software runs.
*SSE2 represents the calculated Sum of Squared Error after attempting the three coefficients and optimizing the C_1, C_2, and C_4 (in the cracking conversion model) by the Excel Solver.

Table C.8 Trial values of coefficients (bottom-up cracking) and SSE – round 2 a(5)

Trial #	Number of Sections	β_{f1}	β_{f2}	β_{f3}	SSE1*	C_1	C_2	C_4	SSE2*
148	21	0.9	0.5	1.7	3859762.6	1	1	6000	3859763
149	21	0.9	0.7	1.7	3859762.6	1	1	6000	3859763
150	21	0.9	0.9	1.7	3859420	1.23	0	5999.91	2565195
151	21	0.9	1.1	1.7	3566235.5	6.45	2.19	6887.78	248395.2
152	21	0.9	1.3	1.7	442551.44	4.33	2.99	4879.64	248370
153	21	0.9	1.5	1.7	434337.13	1.97	0.91	0.01	194522.6
154	21	1.1	0.5	1.7	3859762.6	1	1	6000	3859763
155	21	1.1	0.7	1.7	3859762.6	1	1	6000	3859763
156	21	1.1	0.9	1.7	3859337.9	1.24	0	5999.92	2425603
157	21	1.1	1.1	1.7	3534903.8	6.66	2.3	6874.94	248393.8
158	21	1.1	1.3	1.7	399558.68	4.24	3.01	5064.7	248371.3
159	21	1.1	1.5	1.7	434371.5	1.71	2.52	0.03	194522.6
160	21	1.3	0.5	1.7	3859762.6	1	1	6000	3859763
161	21	1.3	0.7	1.7	3859762.6	1	1	6000	3859763
162	21	1.3	0.9	1.7	3859254.9	1.28	0.03	5999.9	2279014
163	21	1.3	1.1	1.7	3506648.2	6.54	2.29	6668.62	248394.9
164	21	1.3	1.3	1.7	369756.67	3.98	2.89	5155.56	248373.3
165	21	1.3	1.5	1.7	444394.14	0.19	0.02	274.23	203937.8
166	21	1.5	0.5	1.7	3859762.6	1	1	6000	3859763
167	21	1.5	0.7	1.7	3859762.6	1	1	6000	3859763
168	21	1.5	0.9	1.7	3859171.9	1.29	0.04	5999.91	2199560
169	21	1.5	1.1	1.7	3480808.4	6.08	2.14	7615.85	248392.5
170	21	1.5	1.3	1.7	348163.89	3.94	2.94	4874.68	248371.3
171	21	1.5	1.5	1.7	444409.83	0	0.06	173.96	203908.8
172	21	0.5	0.5	2.1	3859762.6	1	1	6000	3859763
173	21	0.5	0.7	2.1	3859762.6	1	1	6000	3859763
174	21	0.5	0.9	2.1	3859762.6	1	1	6000	3859763
175	21	0.5	1.1	2.1	3859254.4	1.22	0	5999.91	2844802
176	21	0.5	1.3	2.1	3574322.5	8.3	2.66	5965.88	248430.9
177	21	0.5	1.5	2.1	608182.07	4.66	2.8	5064.61	248376.9

*SSE1 represents the calculated Sum of Squared Error just after attempting the coefficients β_{f1}, β_{f2}, and β_{f3} (in the fatigue accumulation model) in the software runs.
*SSE2 represents the calculated Sum of Squared Error after attempting the three coefficients and optimizing the C_1, C_2, and C_4 (in the cracking conversion model) by the Excel Solver.

Table C.9 Trial values of coefficients (bottom-up cracking) and SSE – round 2 a(6)

Trial #	Number of Sections	β_{f1}	β_{f2}	β_{f3}	SSE1*	C_1	C_2	C_4	SSE2*
178	21	0.7	0.5	2.1	3859762.6	1	1	6000	3859763
179	21	0.7	0.7	2.1	3859762.6	1	1	6000	3859763
180	21	0.7	0.9	2.1	3859762.6	1	1	6000	3859763
181	21	0.7	1.1	2.1	3859035.8	1.24	0	5999.94	2644803
182	21	0.7	1.3	2.1	3530368.7	9.27	3.06	5233.66	248428.9
183	21	0.7	1.5	2.1	504487.95	4.55	2.86	5241.25	248375.2
184	21	0.9	0.5	2.1	3859762.6	1	1	6000	3859763
185	21	0.9	0.7	2.1	3859762.6	1	1	6000	3859763
186	21	0.9	0.9	2.1	3859762.6	1	1	6000	3859763
187	21	0.9	1.1	2.1	3858814.8	1.25	0	5999.95	2455196
188	21	0.9	1.3	2.1	3493556.8	8.54	2.87	5203.33	248425.2
189	21	0.9	1.5	2.1	443191.63	4.49	2.92	5143.52	248373
190	21	1.1	0.5	2.1	3859762.6	1	1	6000	3859763
191	21	1.1	0.7	2.1	3859762.6	1	1	6000	3859763
192	21	1.1	0.9	2.1	3859762.6	1	1	6000	3859763
193	21	1.1	1.1	2.1	3858590.8	1.18	0	5999.89	2308609
194	21	1.1	1.3	2.1	3461375.3	7.83	2.66	5825.67	248433.3
195	21	1.1	1.5	2.1	403264.52	4.55	3.06	4829.26	248368.6
196	21	1.3	0.5	2.1	3859762.6	1	1	6000	3859763
197	21	1.3	0.7	2.1	3859762.6	1	1	6000	3859763
198	21	1.3	0.9	2.1	3859762.6	1	1	6000	3859763
199	21	1.3	1.1	2.1	3858366.7	1.25	0.03	5999.91	2209560
200	21	1.3	1.3	2.1	3859762.6	1	1	6000	3859763
201	21	1.3	1.5	2.1	3855750.8	1.17	0	6000.06	2119592
202	21	1.5	0.5	2.1	3859763	1	1	6000	3859763
203	21	1.5	0.7	2.1	3859762.6	1	1	6000	3859763
204	21	1.5	0.9	2.1	3859762.6	1	1	6000	3859763
205	21	1.5	1.1	2.1	3858139.7	1.18	0	5999.89	2129592
206	21	1.5	1.3	2.1	3858135	1	1	6000	2129592
207	21	1.5	1.5	2.1	3858125	1	1	6000	2129592

*SSE1 represents the calculated Sum of Squared Error just after attempting the coefficients β_{f1}, β_{f2}, and β_{f3} (in the fatigue accumulation model) in the software runs.
*SSE2 represents the calculated Sum of Squared Error after attempting the three coefficients and optimizing the C_1, C_2, and C_4 (in the cracking conversion model) by the Excel Solver.

Table C.10 Trial values of coefficients (bottom-up cracking) and SSE – round 2 a(7)

Trial #	Number of Sections	β_{f1}	β_{f2}	β_{f3}	SSE1*	C_1	C_2	C_4	SSE2*
208	21	0.5	0.5	2.5	3859762.6	1	1	6000	3859763
209	21	0.5	0.7	2.5	3859763		1	6000	3859763
210	21	0.5	0.9	2.5	3859762.6	1	1	6000	3859763
211	21	0.5	1.1	2.5	3859763	1	1	6000	3859763
212	21	0.5	1.3	2.5	3858273.2	1.27	0.01	5999.94	2724803
213	21	0.5	1.5	2.5	3512811	9.41	2.95	5347.13	248427.6
214	21	0.7	0.5	2.5	3859763	1	1	6000	3859763
215	21	0.7	0.7	2.5	3859763	1	1	6000	3859763
216	21	0.7	0.9	2.5	3859763	1	1	6000	3859763
217	21	0.7	1.1	2.5	3859762	4.39	0	5998.55	3849763
218	21	0.7	1.3	2.5	3857647	1.31	0.02	5999.95	2535004
219	21	0.7	1.5	2.5	3467497	9.25	2.98	5096.45	248424.4
220	21	0.9	0.5	2.5	3859762.6	1	1	6000	3859763
221	21	0.9	0.7	2.5	3859763	1	1	6000	3859763
222	21	0.9	0.9	2.5	3859762.6	1	1	6000	3859763
223	21	0.9	1.1	2.5	3859762	4.4	0	5998.87	3849763
224	21	0.9	1.3	2.5	3857017.3	1.28	0.01	5999.94	2375603
225	21	0.9	1.5	2.5	3429808	8.47	2.76	5688.52	248432.2
226	21	1.1	0.5	2.5	3859763	1	1	6000	3859763
227	21	1.1	0.7	2.5	3859763	1	1	6000	3859763
228	21	1.1	0.9	2.5	3859763	1	1	6000	3859763
229	21	1.1	1.1	2.5	3859762	4.41	0	5999.07	3849763
230	21	1.1	1.3	2.5	3856387	1.35	0.06	6000.01	2209560
231	21	1.1	1.5	2.5	3397032	8.92	2.96	5401.91	248427.9
232	21	1.3	0.5	2.5	3859762.6	1	1	6000	3859763
233	21	1.3	0.7	2.5	3859763	1	1	6000	3859763
234	21	1.3	0.9	2.5	3859762.6	1	1	6000	3859763
235	21	1.3	1.1	2.5	3859762	4.41	0	5998.94	3839763
236	21	1.3	1.3	2.5	3855750.8	1.17	0	6000.06	2119592
237	21	1.3	1.5	2.5	3367790	8.34	2.79	5583.76	248433.6

*SSE1 represents the calculated Sum of Squared Error just after attempting the coefficients β_{f1}, β_{f2}, and β_{f3} (in the fatigue accumulation model) in the software runs.
*SSE2 represents the calculated Sum of Squared Error after attempting the three coefficients and optimizing the C_1, C_2, and C_4 (in the cracking conversion model) by the Excel Solver.

Table C.11 Trial values of coefficients (bottom-up cracking) and SSE – round 2 a(8)

Trial #	Number of Sections	β_{f1}	β_{f2}	β_{f3}	SSE1*	C_1	C_2	C_4	SSE2*
238	21	1.5	0.5	2.5	3859763	1	1	6000	3859763
239	21	1.5	0.7	2.5	3859763	1	1	6000	3859763
240	21	1.5	0.9	2.5	3859763	1	1	6000	3859763
241	21	1.5	1.1	2.5	3859762	4.42	0	5999.08	3839763
242	21	1.5	1.3	2.5	3855126	2.53	0.46	6000.57	2027823
243	21	1.5	1.5	2.5	3340963	8.31	2.81	5574.38	248431.9

*SSE1 represents the calculated Sum of Squared Error just after attempting the coefficients β_{f1}, β_{f2}, and β_{f3} (in the fatigue accumulation model) in the software runs.
*SSE2 represents the calculated Sum of Squared Error after attempting the three coefficients and optimizing the C_1, C_2, and C_4 (in the cracking conversion model) by the Excel Solver.

Table C.12 Trial values of coefficients (bottom-up cracking) and SSE – round 2 b(1)

Trial #	Number of Sections	β_{f1}	β_{f2}	β_{f3}	SSE1*	C_1	C_2	C_4	SSE2*
244	21	0.5	0.25	0.25	3859545	1.16	0.01	5999.67	1078854
245	21	0.5	1	0.25	3293297	0	0.4	17383.83	3291740
246	21	0.5	4	0.25	3859763	1	1	6000	3859763
247	21	0.5	0.25	1	3859763	1	1	6000	3859763
248	21	0.5	1	1	43187.95	2.84	2.57	6000.81	8315.974
249	21	0.5	4	1	3859763	1	1	6000	3859763
250	21	0.5	0.25	4	3859763	1	1	6000	3859763
251	21	0.5	1	4	3859763	1	1	6000	3859763
252	21	0.5	4	4	3859763	1	1	6000	3859763
253	21	2	0.25	0.25	3858776	35.66	10.91	261.05	29073.9
254	21	2	1	0.25	3843909	0.12	0	6000.01	3838079
255	21	2	4	0.25	3859763	1	1	6000	3859763
256	21	2	0.25	1	3859763	1	1	6000	3859763
257	21	2	1	1	10403.32	2.08	2.61	5709.24	8315.841
258	21	2	4	1	3859763	1	1	6000	3859763
259	21	2	0.25	4	3859763	1	1	6000	3859763
260	21	2	1	4	3859763	1	1	6000	3859763
261	21	2	4	4	3859763	1	1	6000	3859763

*SSE1 represents the calculated Sum of Squared Error just after attempting the coefficients β_{f1}, β_{f2}, and β_{f3} (in the fatigue accumulation model) in the software runs.
*SSE2 represents the calculated Sum of Squared Error after attempting the three coefficients and optimizing the C_1, C_2, and C_4 (in the cracking conversion model) by the Excel Solver.

Table C.13 Trial values of coefficients (bottom-up cracking) and SSE – round 2 b(2)

Trial #	Number of Sections	β_{f1}	β_{f2}	β_{f3}	SSE1*	C_1	C_2	C_4	SSE2*
262	21	3	0.25	0.25	3858238	16.49	5.16	318.27	12964.15
263	21	3	1	0.25	3854526	0.07	0	6000	3849416
264	21	3	4	0.25	3859763	1	1	6000	3859763
265	21	3	0.25	1	3859763	1	1	6000	3859763
266	21	3	1	1	10625	1.84	2.58	5837.23	8318.703
267	21	3	4	1	3859763	1	1	6000	3859763
268	21	3	0.25	4	3859763	1	1	6000	3859763
269	21	3	1	4	3859763	1	1	6000	3859763
270	21	3	4	4	3859763	1	1	6000	3859763
271	21	2.1	0.25	0.25	3858724	389.82	119.14	273.48	28977.63
272	21	2.1	1	0.25	3850005	0.09	0	6000	3844289
273	21	2.1	4	0.25	3859763	1	1	6000	3859763
274	21	2.1	0.25	1	3859763	1	1	6000	3859763
275	21	2.1	1	1	249996.9	42.04	65.86	353.23	13517.46
276	21	2.1	4	1	3859763	1	1	6000	3859763
277	21	2.1	0.25	4	3859763	1	1	6000	3859763
278	21	2.1	1	4	3859763	1	1	6000	3859763
279	21	2.1	4	4	3629763	1	1	6000	3629763

*SSE1 represents the calculated Sum of Squared Error just after attempting the coefficients β_{f1}, β_{f2}, and β_{f3} (in the fatigue accumulation model) in the software runs.
*SSE2 represents the calculated Sum of Squared Error after attempting the three coefficients and optimizing the C_1, C_2, and C_4 (in the cracking conversion model) by the Excel Solver.

Table C.14 Trial values of coefficients (bottom-up cracking) and SSE – round 2 c

Trial #	Number of Sections	β_{f1}	β_{f2}	β_{f3}	SSE1*	C_1	C_2	C_4	SSE2*
280	21	2.5	1	1	10396.72	1.94	2.58	5902.61	8319.011
281	21	1.5	1	1	11298.72	2.24	2.61	5720.85	8317.996
282	21	2.2	1	1	10349	2.03	2.62	5729.28	8317.852
283	21	1.8	1	1	11098.32	2.13	2.59	5837.87	8,318.15

*SSE1 represents the calculated Sum of Squared Error just after attempting the coefficients β_{f1}, β_{f2}, and β_{f3} (in the fatigue accumulation model) in the software runs.
*SSE2 represents the calculated Sum of Squared Error after attempting the three coefficients and optimizing the C_1, C_2, and C_4 (in the cracking conversion model) by the Excel Solver.

The following was a discussion about the recommended calibration coefficients. If reading the tables above shapely, you may find out that there were two similar sets of trial values resulting in very low SSEs, one in Table C.12 (i.e., β_{f1}= 2; β_{f2}= 1; β_{f3}= 1; C_1= 2.08; C_2= 2.61; C_4= 5709.24) and the other one in Table C.14 (i.e., βf_1= 2.2; β_{f2}= 1; β_{f3}= 1; C_1= 2.03; C_2= 2.62; C_4= 5729.28). It seemed that both can be identified as "inflection points."

Table C.15 shows the coefficient values of the trial #282 brought greater SSE reduction (SSE1 = 10349) than that of the trial #257 (SSE1 = 10403.32) by attempting the coefficients. However, the coefficient values of the trial #257 that generated a slightly lower ultimate SSE (SSE2 = 8315.841) after attempting the coefficients and optimizing by the Excel Solver than trial #282 (SSE2 = 8317.852). Though either set of coefficients can be the seen as optimal, we still determined the coefficient values of the trial #282 (i.e., β_{f1}= 2.2; β_{f2}= 1; β_{f3}= 1; C_1= 2.03; C_2= 2.62; C_4= 5729.28) to be the local calibration coefficients. The coefficient values of the trial #282 resulted in a greater reduction of SSE reduction (15782.68 – 10349 = 5433.68) by simply attempting the coefficients than the trial #257 (15782.68 – 10403.32 = 5379.36). Meanwhile, the SSE reduction brought simply by attempting the coefficients dominate the SSE reduction as compared with the SSE reduction simply by the Excel Solver, which can be seen from Table C.16. The set of trial coefficients, which maximize the impact on the dominant part of SSE reduction by attempting the coefficients, was expected to be the effective coefficients.

Table C.15 Comparison of two "inflection points"

Trial #	Number of Sections	β_{f1}	β_{f2}	β_{f3}	SSE1*	C_1	C_2	C_4	SSE2*
Default	21	1	1	1	15782.68	1	1	6000	-
257	21	2	1	1	10403.32	2.08	2.61	5709.24	8315.841
282	21	2.2	1	1	10349	2.03	2.62	5729.28	8317.852

*SSE1 represents the calculated Sum of Squared Error just after attempting the coefficients β_{f1}, β_{f2}, and β_{f3} (in the fatigue accumulation model) in the software runs.
*SSE2 represents the calculated Sum of Squared Error after attempting the three coefficients and optimizing the C_1, C_2, and C_4 (in the cracking conversion model) by the Excel Solver.

Table C.16 SSE changes affected by optimization

Round		Average of |SSE1*- SSEd*|	Average of |SSE2*-SSE1*|	Ratio between Average of |SSE1*- SSEd*|and Average of |SSE2*-SSE1*|
1		3367312.502	344191.572	9.8
2	(a)	2879199.198	791466.646	3.6
	(b)	3401345.375	404982.551	8.4
	(c)	4996.987	2467.437	2
3		480673.542	429885.836	1.1

*SSE1 represents the calculated Sum of Squared Error just after attempting the coefficients β_{f1}, β_{f2}, and β_{f3} (in the fatigue accumulation model) in the software runs.
*SSE2 represents the calculated Sum of Squared Error after attempting the three coefficients and optimizing the C_1, C_2, and C_4 (in the cracking conversion model) by the Excel Solver.
*SSEd is the calculated Sum of Squared Error using the default values of calibration coefficients.

Table C.17 Trial values of coefficients (bottom-up cracking) and SSE – round 3

Trial #	Number of Sections	β_{f1}	β_{f2}	β_{f3}	SSE1*	C_1	C_2	C_4	SSE2*
284	21	2.1	0.9	0.9	304520.35	59.75	92.11	189.33	13351.5
285	21	2.1	0.9	1	808204.85	0.93	0.06	6000.03	114003.6
286	21	2.1	0.9	1.1	1920933.6	4.87	2.57	6015.11	248305.6
287	21	2.1	1	1	249996.91	42.04	65.86	353.23	13517.46
288	21	2.1	1	0.9	248680.1	0.88	0.04	5999.98	14036.51
289	21	2.1	1	1.1	303985.5	54.55	86.96	181.87	13384.39
290	21	2.1	1.1	0.9	269146.13	0.84	0.04	5999.99	134021
291	21	2.1	1.1	1	264710.23	0.86	0.04	5615.94	34037.4
292	21	2.1	1.1	1.1	252584.93	0	1.37	264.04	13460.42
293	21	2.2	0.9	0.9	299934.5	0.91	0.04	5999.95	14040.49
294	21	2.2	0.9	1	784744.92	2.55	2.12	405.21	103103.9
295	21	2.2	0.9	1.1	1846618.8	1.58	0.63	4237.83	253595
296	21	2.2	1	0.9	248501.4	0	1.53	267.58	13459.16
297	21	2.2	1	1	10349	2.03	2.62	5729.28	8317.852
298	21	2.2	1	1.1	299556.5	52.76	85.57	181.58	13389.83
299	21	2.2	1.1	0.9	266296.9	0.84	0.04	6000	134020.9
300	21	2.2	1.1	1	264253.06	0	0.21	207.61	33868.81
301	21	2.2	1.1	1.1	252629.21	0.5	0.11	4926.25	27954.18
302	21	2.3	0.9	0.9	295839.32	58.21	92.61	189.07	13353.41
303	21	2.3	0.9	1	762851.17	2.53	2.12	405.12	103104.1
304	21	2.3	0.9	1.1	1858783.1	4.79	2.56	6109.2	248304.2
305	21	2.3	1	1	249987.8	40.28	65.43	353.19	13517.46
306	21	2.3	1	0.9	248329	0	1.55	272.24	13460.1

307	21	2.3	1	1.1	295572	1.16	1.59	267.51	13406.79
308	21	2.3	1.1	0.9	269146.13	0.84	0.04	5999.99	134021
309	21	2.3	1.1	1	264710.23	0.86	0.04	5615.94	34037.4
310	21	2.3	1.1	1.1	252584.93	0	1.37	264.04	13460.42

*SSE1 represents the calculated Sum of Squared Error just after attempting the coefficients β_{f1}, β_{f2}, and β_{f3} (in the fatigue accumulation model) in the software runs.
*SSE2 represents the calculated Sum of Squared Error after attempting the three coefficients and optimizing the C_1, C_2, and C_4 (in the cracking conversion model) by the Excel Solver.